Bjørn Eske Sørensen

Metamorphic refinement of quartz under influence of fluids during exhumation with reference to the metamorphic/metasomatic evolution observed in amphibolites

A detailed field, microtectonic and geochemical study from the Bamble sector, South Norway

Thesis for the degree philosophiae doctor

Trondheim, June 2007

Norwegian University of Science and Technology
Faculty of Engineering Science and Technology
Department of Geology and Mineral
Resources Engineering

NTNU
Innovation and Creativity

NTNU
Norwegian University of Science and Technology

Thesis for the degree philosophiae doctor

Faculty of Engineering Science and Technology
Department of Geology and Mineral Resources Engineering

ISBN 978-82-471-3196-1 (printed version)
ISBN 978-82-471-3201-2 (electronic version)
ISSN 1503-8181

Doctoral theses at NTNU, 2007:146

Printed by NTNU-trykk

Preface

The current PhD thesis is integrated in a larger project entitled "The value chain from mineral deposit to beneficiated product with emphasis on quartz". This thesis is dedicated to studies of quartz formed in a metamorphic environment with emphasis on the trace element evolution of quartz during prograde and retrograde recrystallisation processes. Quartz from quartzites and quartz veins from the Bamble sector was included in the study.

To understand the trace element behaviour in quartz in a metamorphic environment we had to address the more general issue of understanding the fate of quartz during multiple episodes of recrystallisation because we realised that not much was known regarding the behaviour of quartz in a complex shear zone environment such as the Bamble belt. Accordingly, the aim was enhanced to both document quartz purification and to understand more about the trace element behaviour of quartz in general in a metamorphic environment as a function of PT-X_{fluid} conditions. To place the quartz recrystallisation history and trace element evolution in a well constrained geological framework the study also include comprehensive studies of metamorphic petrology and fluid inclusions

Although the results of this thesis does show avenues to the genesis of high purity quartz, it is probably making more significant contributions to the importance of shearzone fluids and fluid-rock interaction processes, particularly in quartzites. The fluid evolution during cooling and exhumation of the Bamble sector is unravelled through fluid inclusion studies along with the construction of a new cooling and uplift path. Moreover the study of mineral equilibria in amphibolite demonstrates the importance of fluids on the composition of hydrous minerals and also suggests a genetic model for the formation of Fe-Cu deposits in the Bamble sector.

A vast amount of data was collected in connection with the thesis work. They are summarised in diagrams in each of the three papers, however, raw data were deliberately omitted from the thesis because of their voluminous character. An electronic file with raw data may be requested from the author or Rune B. Larsen.

All the data in this thesis, including the three papers were collected and processed by Bjørn Eske Sørensen. This is also the case with all of the calculations. First drafts of all the papers were written solely by Bjørn Eske Sørensen and then modified in accordance with comments and corrections given by the co-authors Rune B. Larsen and Håkon Austrheim.

Mineral abbreviations in this thesis follows the scheme given in Table 1.

Bjørn Eske Sørensen, Trondheim 2007

Table 1: Mineral abbreviations used in this thesis.

Mineral name	abbreviation
Actinolite	act
Albite	ab
Albite content	Ab_X, X_{ab}
Amphibole	amp
Andalusite	and
Anorthite content	An_X
Antarcticite	Ant
Apatite	ap
Apophyllite	apo
Biotite	bt
Calcite	cc
Chalcopyrite	cpy
Chlorite	chl
Clathrate	clath
Clinoziosite content in epidote	$EpCz_X$, e.g $EpCz_{65}$, X = Al/(Fe^{3+}+Al)
Clinozoisite	cz
Corundum	cor
Diopside	di
Dolomite	dol
Epidote	ep
Equivalent anorthite content in scapolite	EqAn = 100*(Al-3)/3
Garnet	grt
Hedenbergite	hed
Hematite	hem
Hydrohalite	HH
Ilmenite	ilm
K-feldspar	kfs
Kyanite	ky
Margarite	mrg
Margarite-paragonite solid solution	MaPa (Xma, (1-X)pa), pa(1-X) = X_{pa}= Na/(Na+Ca), maX = X_{ma} = Ca/(Ca + Na)
Microcline	mc
Muscovite	mu
Orthoclase	or
Orthoclase content	Or_X
Phlogopite	phl
Pistacite	ps
Pistacite content in epidote and clinozoisite	X_{Ps} = Fe^{3+}/(Fe^{3+}+Al)
Plagioclase	pl
Pyrite	py
Pyrrhotite	po
Quartz	qz
Rutile	ru
Sanidine	san
Scapolite	scp
Titanite	ttn
Tremolite	tr
Zircon	zr

Contents

Introduction

Background

Application of High Purity Quartz (HPQ)

High purity quartz (HPQ) owes its applicability and high demand to current expansions in the communication industry and other actors in the high technology sector. Some agencies forecast a solid 40 % annual growth in the demand for high purity granular quartz and even moderate estimates predicts a >25 % annual increase. By far the largest proportion of HPQ comes from granitic pegmatite in the Spruce Pine district, North Carolina. The quality of quartz from Spruce Pine is steadily decreasing and, having an arid climate with limited water supplies, the processing of quartz is difficult and costly.

The high purity silica glass industries may be divided in to the semi-conductor industry that requires very high chemical purity of HPQ and the lighting and fibre optical industries that accepts somewhat higher concentrations of impurities yet require excellent melting behaviour of HPQ and primarily are concerned with minimal bubble formation in the silica glass melts.

With these requirements in mind, it appears that HPQ at any time should contain very low concentrations of structural impurities and in particular for the lighting and optical fibre industries must have very low contents of fluid inclusions that, due to expansion during melting, will generate bubbles in the silica glass melt.

Trace elements in quartz

Quartz is a framework silicate comprising SiO_4 tetrahedrons that are corner linked in a network. Quartz is the most common SiO_2 polymorph in metamorphic environments. In the quartz structure, tetrahedra of SiO_2 are linked together in spirals (e.g. Heaney, 1994). Spirals are paired in groups that are related by a two fold rotation axis parallel to the c-axis (e.g. Heaney, 1994). Together six spirals produce helixes surrounding open channels running parallel to the c-axis. β-quartz is hexagonal with 6-fold symmetry in the helixes, whereas they have 3-fold symmetry in the trigonal α-quartz (Heaney, 1994). The α-quartz structure is more compact than the β-quartz structure hence is less open to the incorporation of trace elements.

Trace elements in quartz divides into two groups; lattice bound and not lattice bound. The lattice bound trace elements are related to substitutions in the quartz lattice and occurs along with defect in the lattice that do not relate to trace elements: NBOHC (Non Bridging Oxygen Hole Centres) (Griscom, 1985) silanol groups (Weil, 1984) or peroxy radicals and linkages (Friebele et al., 1979).

Substitution for Si^{4+} is seldom in quartz because of the small crystal radii (CR[1]) and high valence of Si^{4+} (0.40 Å Shannon, 1976). However trace amounts may be incorporated during crystal growth and recrystallisation in the cation site of quartz. The ionic potential (charge/ionic radius: Z/CR) and bonding type are the most important factors that control incorporation of trace elements. Al^{3+}(CR=0.53 Å), Ga^{3+}(CR=0.61 Å), Fe^{3+}(CR=0.63 Å), Ge^{4+}(CR=0.53 Å), Ti^{4+}(CR=0.56 Å) and P^{5+}(R=0.31 Å) were reported to substitute for Si^{4+} in quartz (see summary in Frondel (1962), Goetze et al. (2001) and Larsen et al. (2000). CR (CN=4) is from Shannon (1976).

Three main substitution modes govern the incorporation of lattice bound trace elements (e.g. Goetze et al., 2001 and Figure 1):

1) Single substitution. Corresponds to isoelectronic substitution of Si^{4+} by an other tetravalent cation, commonly Ti^{4+} or Ge^{4+}
2) Double substitution. Refers to $AlPO_4$ groups (Beck, 1949; Huttenlocher, 1935). Charge balance is maintained by direct replacement of two Si^{4+} atoms by one P^{5+} and one Al^{3+} cation.
3) Compensated substitution. Occurs when trivalent cations (Al^{3+}, Fe^{3+}) substitute for Si^{4+} to form [(Al, Fe)O_4/M^+] centres, in which M^+ represents a charge compensator alkali cation such as H^+, Li^+, Na^+ or K^+(Frondel, 1962; Goetze et al., 2004; Goetze et al., 2001; Mackey, 1963).

The small size of inter-atomic cavities in quartz prevents large cations from entering the lattice. The elasticity of the lattice and hence the available space for trace element incorporation varies as a function of pressure and temperature. Trace elements substituting for Si in the structure are strongly confined to the lattice defects. Trace elements incorporated along the channels running parallel to the c-axis are more mobile, because of the relative weakness of pure ionic bonds compared to ionic-covalent bonds. Accordingly, their abundance may be sensitive to remobilisation processes (Larsen et al., 2004). This has been extensively documented in sweeping experiments (solid state electrolysis). Na^+ and Li^+ in channels and lattice defects related to compensated substitution of Si^{4+} by Al^{3+} is replaced by Al-OH or Al-hole centres, whereas larger alkali ions (e.g. K^+) associated with compensated substitution of Al^{3+} for Si^{4+} appear to be less mobile, probably because they are too large to migrate along the channels (e.g. Armington, 1991).

Electron Paramagnetic Resonance (EPR) either alone or in combination with spectroscopic methods such as thermoluminescence (TL), cathodoluminescence (CL), infrared and atomic spectroscopy is the most efficient technique to identify point defects in quartz (Goetze and Ploetze, 1997; Goetze et al., 2001; Weil, 1984; Weil, 1993). Spectral CL-analysis in combination with spatially resolved trace element EPMA, SIMS or LA-ICP-MS analysis is an alternative technique to investigate and quantify point defects in quartz (Müller et al., 2003). Our study implement gray scale SEM-CL in combination with LA-ICP-MS and SEM-CL spectroscopy to quantify trace elements in quartz.

[1] CR = Crystal radii, states the actual size of the ion when the ion is tied in a lattice structure. The normal ionic radii in unrealistically large, because ions in the lattice share electrons and are partly drawn toward each other.

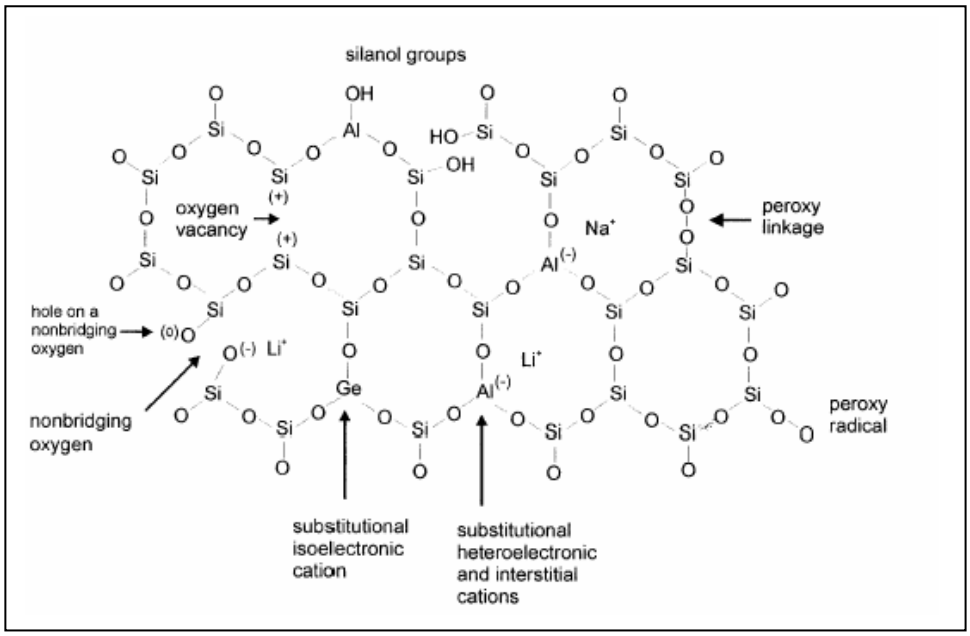

Figure 1: Schematic drawing of the quartz structure showing the most common intrinsic and extrinsic lattice defects. From Goetze et al. (2001). Note that the figure is highly schematic and that the quartz structure is drawn as a simple "ideal high quartz structure" projected along the c-axis as opposed to the true trigonal structure of low quartz.

Several studies document mobilisation of trace elements during recrystallisation. Larsen and co-workers (2004) documented sub solidus alteration of quartz leading to mobilisation of trace element in pegmatite quartz. Armington and Balascio (1984) documented that dislocation and trace element content of quartz was reduced through multiple recrystallisation events at conditions corresponding to the greenshist facies (Figure 2). Several SEM-CL studies document trace element mobilisation associated with textures related to sub solidus processes acting on magmatic quartz (e.g. Jacamon, 2006; Larsen et al., 2004; Müller et al., 2002) and on vein quartz (Landtwing and Pettke, 2005; Van den Kerkhof et al., 2004).

There is no general correlation between the hand-specimen colour of quartz and the trace element content. Clear apparently inclusion free quartz may be rich in trace elements whereas smoky quartz may have low trace elements contents i.e. <1 ppm. This is because a very small amount of colour centre related defects results in strong colouration of quartz. As an example the smoky colour in smoky quartz is due to ionising radiation from neighbouring minerals (Larsen et al., 1998) and minute concentrations of structurally bound elements in colour centres in the quartz lattice (Larsen et al., 2004). However, other colour variations are signs of high trace element abundance (Larsen et al., 2004). Amethyst owes its purple colour to structurally bound Fe (e.g. Aines and Rossman, 1986; Cohen and Makar, 1984; Cohen and Makar, 1985; Hassan and Cohen, 1974; Lehmann, 1975). Several explanations exist for the colour of rose quartz; structurally bound Fe and Ti (e.g.

Cohen and Makar, 1984; Cohen and Makar, 1985; Hassan and Cohen, 1974), by Al-P substitutions (Maschmeyer and Lehmann, 1983) or due to inclusions of microscopic rose coloured inclusions of dumortierite (e.g. Applin and Hicks, 1987; Goreva et al., 2001). The latter probably account for most occurrences of massive rose quartz (Goreva et al., 2001) and also seem to be the explanation in our study (paper 1, Sørensen and Larsen, 2007a). Most occurrences of blue quartz are explained by light scattering by tiny inclusions (Jayraman, 1939), which are commonly rutile (Postelmann, 1937; Vultée and Lietz, 1956) or ilmenite (Zolensky et al., 1988). The presence of tiny rutile needles explains the blue colour of quartz reported in our study.

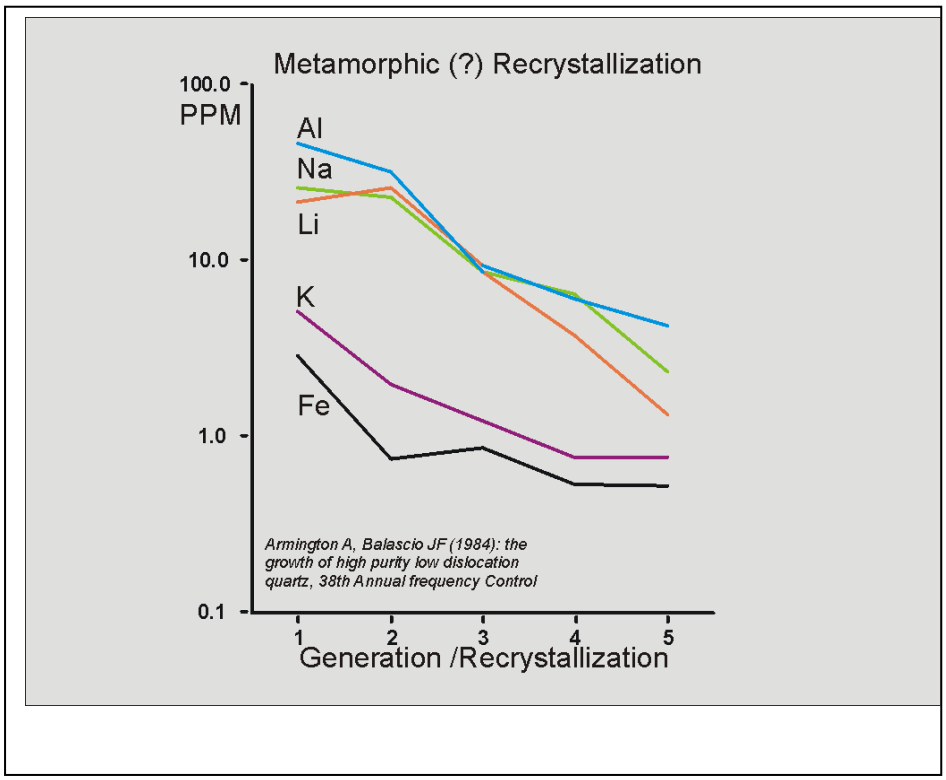

Figure 2: Experimental data by Armington and Balascio (1984) displaying the effect of multiple recrystallisation events on trace element content of quartz. Modified from Armington and Balascio (1984). Courtesy Rune B. Larsen.

Geological setting

The rocks included in this study comprise quartzites, amphibolites and calc-silicate lithologies from the Froland area, Bamble sector, South Norway (Figure 3). The Bamble sector is part of the South West Scandinavian domain (SSD) that is divided into a number of segments bounded by regional shear zones and thrusts that formed during the Sveconorwegian orogeny (Ahall and Gower, 1997; Bingen et al., 2002). The Bamble sector is interpreted as the mid-crustal part of a volcanic

arc complex (Knudsen and Andersen, 1999). The Bamble sector was accreted to the Telemark terrain during an early Sveconorwegian (1,15-1,10 Ga) event (Bingen et al., 2002; 2001).

Structurally, the Bamble sector comprises a SW to NE linear deformation belt with onshore dimensions of 20-40 km times 140-150 km (Figure 1).

Supracrustal lithologies of amphibolite to granulite facies metasedimentary and metavolcanic rocks dominate the belt and is intruded by numerous mafic stocks and dykes as well as granitiod plutons and pegmatites (Starmer, 1991; Starmer, 1993; Starmer, 1996). The Supracrustal suite was deposited in two inter-orogenic periods of the Gothian orogeny at 1,85-1,7 Ga (Knudsen et al., 1997) and 1,5-1,2 Ga (Bingen et al., 1998) respectively. Recent studies confirmed Sveconorwegian high-grade metamorphic overprint throughout the Bamble sector (Bingen et al., 1998; Bingen and Van-Breemen, 1998; Cosca et al., 1998; Johansson and Kullerud, 1993; Knudsen, 1996; Kullerud and Dahlgren, 1993; Kullerud and Machado, 1991).

Generally, the foliation trends NE-SW in the Bamble belt (Falkum and Petersen, 1980). Based on structural trends, the Bamble sector is divided in two main domains (Falkum and Petersen, 1980):

-*The eastern sub-region* (main zone) in the coastal area is dominated by intense shear folding with a NE-orientation, most other directions being rotated into parallelism by a dextral strike slip regime. The structural pattern is dominated by tight isoclinal folds and well developed mineral lineations. Older structures are preserved in rigid bodies.

- *The Northern border* constituting a transitional zone 10-15 km wide, is characterized by moderate shear folding where NE-SW trending structures of the Bamble sector are superimposed on former NW-SE trending folds of the Setesdal gneisses. The transition zone commonly shows interference between the two structural events.

The Bamble sector features well preserved granulite facies rocks and distinctive metamorphic zones gradually going from amphibolite facies in north to granulite facies along the coast. Peak metamorphic conditions are well constrained, both in terms of P, T and fluid evolution.

Traditionally the Bamble sector is divided into four coast parallel regions labelled A-D (Field et al., 1980; Lamb et al., 1986; Smalley et al., 1983):

A. Amphibolite facies, as defined by absence of metamorphic orthopyroxene in metabasite.
B. Granulite facies; primarily comprising acid to intermediate host gneisses with a broadly granitic mineralogy, separated from A by an orthopyroxene isograde in metabasites.
C. First occurrence of charnokitic gneiss (K-feldspar, plagioclase, orthopyroxene and quartz).
D. Region within the granulite facies area with low concentrations of potassium and low concentration of LILE, REE and chalcophile elements, especially Au, Sb, As and S.

Earlier studies of the Bamble sector placed the area of highest temperature in the coastal region near Arendal and Tromøy in region D which was thought to be LILE depleted during peak metamorphism. However recent studies imply that low LILE

concentration reflects the origin of the mafic gneisses rather than granulite facies depletion (Knudsen and Andersen, 1999). Furthermore, geothermobarometry show that the temperature in zones C and D are comparable (Harlov, 1992; Harlov, 2000a; Knudsen and Lidwin, 1996; Nijland and Maijer, 1993). Accordingly, zone D is not a separate metamorphic zone (Harlov, 2000b). Geothermobarometry of mineral equilibria imply that the highest temperatures probably were situated inland in a NW-SE oriented thermal dome with peak T at 830°C in the granulite facies area (Zones B and C) and peak T=750-700°C in the so called amphibolite facies area (zone A) (Nijland and Maijer, 1993). Obviously, given these temperatures the entire region was actually exposed to granulite facies metamorphism and the "amphibolite facies area" is a relic name from previous studies.

Metamorphic fluids developed from pure CO_2 +N_2 ±CH_4 inclusions in the granulite facies to mixed H_2O-CO_2 fluids in the amphibolite facies (Touret, 1971; Touret, 1972; Touret, 1985). Some authors suggest a magmatic origin of the CO_2 rich fluids (Knudsen and Lidwin, 1996; Van den Kerkhof et al., 1994). The presence of CO_2 rich fluids during peak granulite facies metamorphism is confirmed by titaniferous magnetite-ilmenite thermometry and titaniferous magnetite–ilmenite-orthopyroxene-quartz oxygen barometry, implying that the stable COH-fluid phase at $LOGfO_2$ = -11 to -14 estimated for the peak PT-conditions (800°C and 7.5 kbar) is CO_2 for both region C and D (Harlov, 2000b).

Given that the structures of the Setesdal district are rotated into the foliations of the Bamble belt, it is inferred that the structures in the Bamble belt comprise the youngest structural event in the evolution of the South Norwegian basement. Following the strike-slip deformation, the Bamble sector was thrust on top of the Setesdal sector. In many places, the main thrust zone follows the Porsgrund Kristiansand fault, but thrusts are also identified to the east of the fault (e.g Touret, 1968). Thrusting probably began in epidote-amphibolite facies and progressed through lower greenshist facies as exhumation proceeded (e.g Touret, 1968). Finally extensional tectonics depressed the SE Bamble block. Evidence of thrusting is indisputable, although the kinematic evolution during thrusting is poorly understood and mostly inferred from, mapping and large scale observations by Starmer (1987; 1991; 1993; 1996) (e.g. Henderson and Ihlen, 2004).

Thrust related greenshist facies deformation generated quartz mylonites (Morton et al., 1970), mainly comprising quartz and muscovite (Morton et al., 1970). Grain size reduction in the mylonites is considerable i.e. from cm-size to microns-size. Thrust related deformation terminated with brittle deformation, cataclasites and brecciation as exhumation proceeded and the temperatures lowered (e.g Touret, 1968).

Recently, Henderson & Ihlen (2004) documented ductile deformation of synkinematic pegmatites. They infer that thrust related deformation in the Bamble sector was incremental with long periods of ductile deformation interrupted by short periods of high strain rate leading to fracturing and injection of the syntectonic pegmatites.

Using the retrograde P-T path of Nijland et al. (1993b) the uplift and cooling rates were constrained to ~3°-8°C/Ma at 725-550°C, and cooling rates of ~2°-4°C/Ma in the interval 550-300°C (Cosca et al., 1998). Initial cooling of the

Bamble sector approached isobaric conditions (dP/dT=2bars/°C) from 725-550°C, but was followed by near isothermal uplift (dP/dT=30bars/°C) in the temperature interval 550-300°C (Cosca et al., 1998). Following the relatively fast exhumation path, the Bamble sector experienced near isobaric cooling from 300°C and onwards (Cosca et al., 1998). The very low temperature (<300°C) path is constrained by late prehnite and pumpelyite together with fluid inclusion data (Touret and Olsen, 1985).

Amphibolites are common in the Bamble sector. They feature four expressions (Nijland et al., 1993a):

1. Concordant amphibolite bands intercalated with gneisses (Brøgger, 1934; Starmer, 1985).
2. Entirely metamorphosed but discordant plutons like the Vimme amphibolite (Nijland, 1989)
3. Partly amphibolitised "hyperites" with cores of coronitic gabro, which are increasingly amphibolitised towards their margins (Brickwood and Craig, 1987; Brøgger, 1934; Bugge, 1940).

Nijland (1995) studied the geochemistry of the amphibolites in the Bamble sector and documented that the majority are of an igneous origin. The amphibolites are commonly subjected to significant metasomatic processes affecting the mineralogy (e.g. Brøgger, 1934; Frodesen, 1968).

The Bamble sector contains abundant coarse grained quartzites that experienced Sveconorwegian high grade metamorphism. This study concerns quartzites from the Nidelva Quartzite Complex close to Blakstad. Static high grade textures with cm-sized quartz grains formed at peak conditions (750°C/6-7 kbar (Nijland and Maijer, 1993)) and are cut by younger localized high-grade shear zones with mm-sized amoeboid quartz grains. Localized retrogression related to the formation of white mica occurs throughout the area, typically related to mm-thin fault zones with adjacent SGR (subgrain rotation recrystallisation) causing a reduction in grain size (50-200 microns).

There are several compositional and textural types including very pure and coarse-grained quartzite, quartzo-feldspatic gneiss and nodular gneiss/quartzite. The quartzose rocks contain variable amounts of tourmaline. Layers of stratabound tourmaline are locally observed (Nijland et al., 1993c). Black tourmaline frequently occur on the more Al-rich cleavage planes (Nijland et al., 1993c, this study). Red-brown transparent tourmaline (field colour, orange-red brown in thin section, dravitic) occurs in layers and lenses in quartz microcline and oligoclase and biotite at Grendal Tjern (Nijland et al., 1993c) and at Trevann (This study). Black tourmaline (field colour, green-brown pleocroic in thin section schorl-dravite) also occur as reaction zones bordering quartz veins in quartzites together with biotite and muscovite. In addition black (schorl rich) and brown (dravite rich) tourmaline together with biotite defines the foliation in some mylonitic gneisses. Occasionally rare sedimentary structures occur in the Nidelva Quartzite Complex (NQC), and well documented cases of cross beddings, mud cracks, ripple marks and strongly deformed meta-conglomerates imply a sedimentary origin (Nijland et al., 1993c).

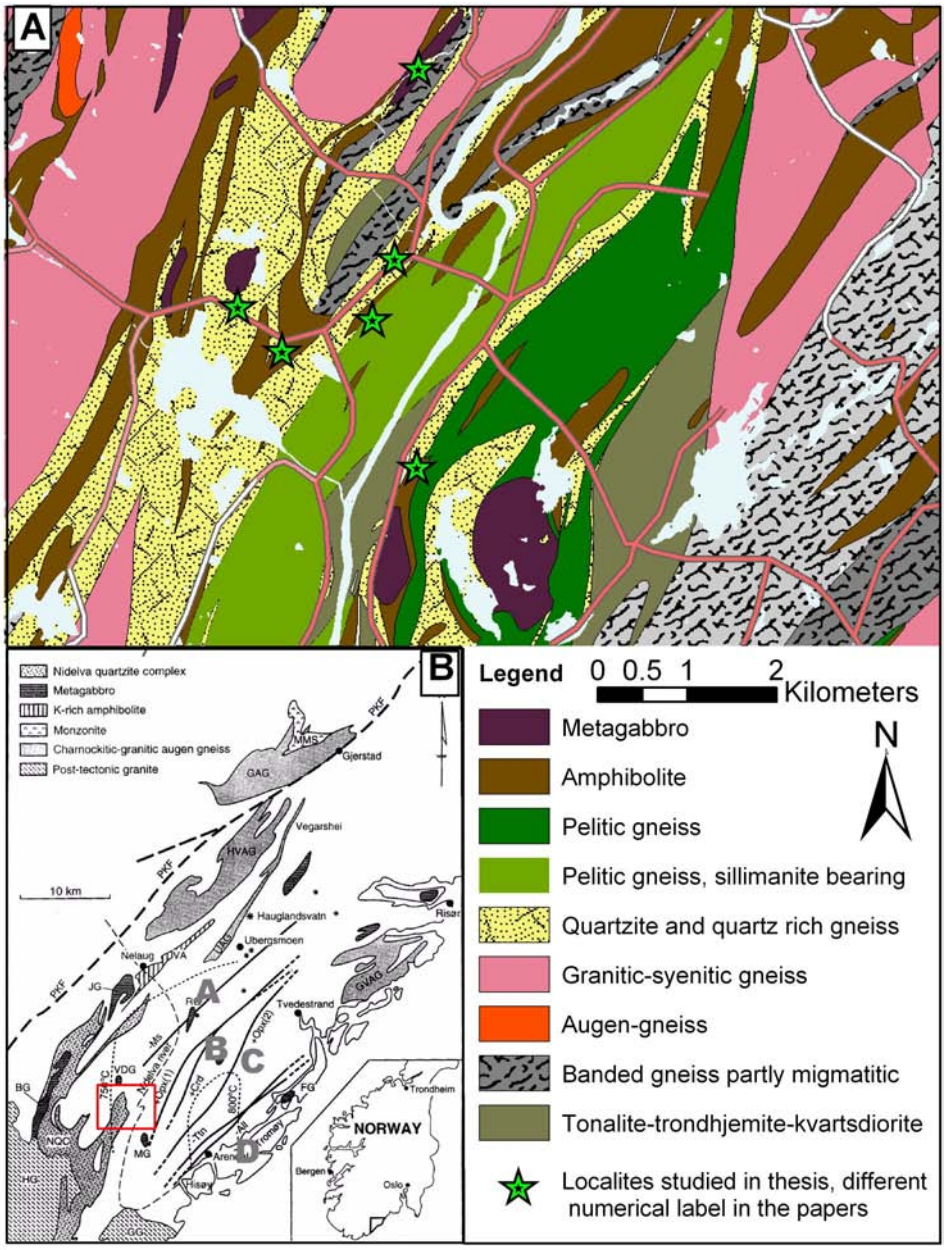

Figure 3: Geological maps. A) Detailed map of the investigated area. Modified from Geological Survey of Norway, N-50 berggrunnskart 16123 Nelaug and 16114 Arendal. Geographic data (roads, lakes and rivers) are added for easy orientation (source: www.geonorge.no). B) Overview map of the Bamble sector displaying the most important rock units (see legend on map). Insert shows the position of the Bamble Sector in South Norway. Red square denotes the position of the study area shown in A. From Nijland et al. (1998). Also shown in A are the metamorphic zones in the Bamble sector.

Objectives of the project

The aim of this thesis is to study the evolution of quartz from high T amphibolite/granulite facies conditions during multi stage retrogression induced by infiltrating fluids. The high grade quartzites are coarse-grained with cm sized quartz grains. They owe their blue colour to microscopic rutile needles. During the fist field season it was documented that the quartzites featured bleached zones, related to recrystallisation along narrow fault zones (mm-dm wide) formed during retrogression.

The results from this study were not expected to directly lead to the discovery of large resources of pure quartz. Instead we focussed on processes underlying quartz recrystallisation and the mobility of trace elements in association with metamorphic recrystallisation. From the fact that several studies had already documented trace element mobilisation through recrystallisation of quartz, we expected that the trace element concentration in the high grade blue quartz, was also lowered by retrograde metamorphic processes.

It was soon realised that the metasomatic processes in quartzites were much more complex than previously thought. Therefore, the main challenge was not to show that trace elements could be mobilised during retrogression, but how it happened. To pin down the important processes it was realised that one ought to improve our understanding of the relation between metamorphic/metasomatic processes and the observed quartz recrystallisation.

Accordingly, three main objectives crystallised from this realisation:

1: Document chronology and spatial relationships between quartz recrystallisation in veins, quartzites and quartz rich gneisses in the Froland area.

2: Document how the quartz chemistry related to recrystallisation events.

3: Understand the observed quartz recrystallisation and purification in the context of the regional P-T-X_{fluid} and tectonic evolution.

Although, quartz is the principal target of the present study, it is impossible to study and interpret the chemical alterations of quartz without also including chemical changes of other rock types and minerals to constrain the physiochemical framework.

As the quartzites are intimately associated with amphibolite/metagabbro that underwent the same metamorphic history it was natural to include the amphibolites in constraining the P-T-X conditions. Not least, because the amphibolites were intersected by and altered in association with the quartz veins.

Fluids are imperative in alteration processes and therefore, a fluid inclusion study was included as an important part of the thesis work. Main focus was on fluids that could be related to recrystallisation events in quartz. Calc-silicate rocks that were observed in close association with intense alteration of amphibolites, quartz veins and quartz rich gneisses were included as a supplement to the fluid inclusion study

because volatile dependant mineral equilibria in calc-silicates are highly sensitive to changes in P-T and fluid composition.

Based on the defined goals of the project, it was decided to combine a SEM-CL study with Laser ablation induced coupled mass spectroscopy (LA-ICP-MS) study to document the chemical evolution of quartz. To define the physiochemical framework underlying the observed quartz recrystallisation, a fluid inclusion study and metamorphic petrology study in amphibolites and calc-silicates, in which mineral equilibria are sensitive to fluid composition, was also initiated.

Outline of the thesis

This thesis is comprises three papers that are intended for journal publication. The version provided in the thesis is a bit longer than they will be at final publication. However it was the desire to include some additional documentation that may be omitted in the final versions. Each paper in the manuscript is written as an independent paper. Because all the papers are strongly tied together there is significant repetition partly because the documentation and interpretation of the results in on paper depends on the results documented in another paper. The essence of the three papers are summarised below:

Paper 1:
Sørensen, B.E. and Larsen R.B. 2007. "*Fluid induced multistage recrystallisation microstructures in Quartzites and Quartz veins from the Bamble shear zone complex*"

Paper 1 deduces basic principles of infiltration, physiochemical alteration processes and deformation mechanisms in quartzites and in quartz veins from the Froland area, the Bamble sector. SEM-CL is used to define generations of recrystallised quartz. A progressive quartz purification process ending with high purity quartz through recrystallisation is documented through LA-ICP-MS. The study demonstrates how fluids provokes recrystallisation and trace element mobilisation from the quartz lattice and at fluid-absent conditions, quartz is resistant to retrograde recrystallisation hence preserving its early high grade metamorphic trace element signature. Evidence of retrograde fluid flow is preserved in fluid channel textures intersecting quartz and documented by SEM-CL images as well as changes in the trace element distribution. Quartz recrystallisation is associated with metasomatic processes in the quartzites such as for example the replacement of ilmenite by rutile and replacement of biotite by muscovite. The strong focus of fluid flow along narrow pathways intersecting the quartzites generates mm-scale differences in the rheological properties of the quartz grains with increased ductility and recovery in recrystallised grains. Therefore, the study demonstrates a strong coupling between strain softening, fluid flow and mass transfer in shearzones in quartz rich rocks.

Paper 2:
Sørensen, B.E. and Larsen R.B. 2007. "*The fluid evolution of the Froland area in the Bamble sector from peak P-T through cooling and uplift: implications for retrograde mineral paragenesis and PT evolution of the Bamble sector*"

Paper 2 comprises a detailed characterisation of the fluid evolution during cooling and uplift through fluid inclusion studies compared with thermodynamic modelling of calc-silicate volatile dependant mineral equilibria. Fluids are documented to be brines throughout the cooling and uplift path. The paper also includes a detailed discussion of the chemical properties of the aggressive brines and their implications for mineral equilibria during cooling and exhumation. The study also document which fluids that were in equilibrium with quartz recrystallisation and purification. The study focussed on fluids that could be related to the quartz SEM-CL textures documented in Paper 1. Had the main purpose of this thesis been to understand calc-silicate equilibria in the Bamble sector fluid inclusions in the calc-silicates would have been in the focus.

Paper 3:
Sørensen, B.E, Larsen R.B. and Austrheim, H. 2007. "*Metasomatic evolution of the Froland amphibolites during cooling and uplift – textural observations and geochemical evolution of hydrous minerals*"

Paper 3 comprises a detailed study of alteration processes in amphibolites. The study focuses on the chemistry of amphiboles as a function P, T and the composition of the co-existing fluids. Amphibole and biotite undergo a co-genetic evolution both becoming more Mg-rich during cooling and exhumation. The chemical changes in biotite and amphibole reflects the interaction with the brines present throughout cooling and uplift. A relationship between element depletion in amphibolites and formation of Fe-Cu sulphides is observed.

As earlier stated the papers are strongly tied together. In conjunction with each other they deduce the metamorphic and metasomatic evolution of the area and put the observed quartz recrystallisation and purification into a physiochemical framework. The locality numbering varies between the papers because samples from different localities are included in each paper, accordingly a locality termed"1" in one of the papers may have a different number in the next paper. This was done because the papers are supposed to be independent research papers and the numbering logically relate to the context of the single papers and not the thesis as a whole.

In the next section the most important results that are deduced from the three papers are summarised.

Main results

Quartz recrystallisation during retrogression, implications for rheology and purification

Four main quartz types are documented in quartzites, quartz veins and quartz in leucosomes through SEM-CL (Paper 1, Sørensen and Larsen, 2007a) (Figure 4):

Qz1: Bright islands demarcated by darker cracks. Typically they are partially luminescence quenched. The bright islands in Qz1 relate to the high grade

history of the area, but the cracking relates to retrogression and formation of Qz2 (next). Qz1 is richer in B, Al and Ti than the other types.

Qz2: Light grey, sometimes featuring weak oscillatory zonation. Qz2 has brighter cores and darker rims approaching the luminescence of Qz3. The formation of the island texture in Qz1 and Qz2 are probably related, since Qz2 and the cracks in Qz1 has the same luminescence. Qz2 has low Al contents (<50 ppm) but variable Ti contents in quartz veins in amphibolite (210-10 ppm) due to inclusions of rutile needles and more consistent values in quartzites (peak value 32 ppm).

Qz3: Dark grey diffuse fluid channel texture, which follows grain boundaries or intersects grains. Qz3 relates to alteration of biotite to muscovite and SGR (Sub-Grain rotation Recrystallisation) in narrow fault zones. Qz3 has Ti< 5 ppm and Al contents below 10 ppm (≈LOD) and low B content (paper1, Sørensen and Larsen, 2007a). Therefore, the recrystallisation path documented by SEM-CL, lead to the formation of high purity quartz, represented by Qz3.

Qz4. Narrow cracks and pods of black quartz, intersecting the other types. Trace elements were not measured because Qz4 was too fine-grained

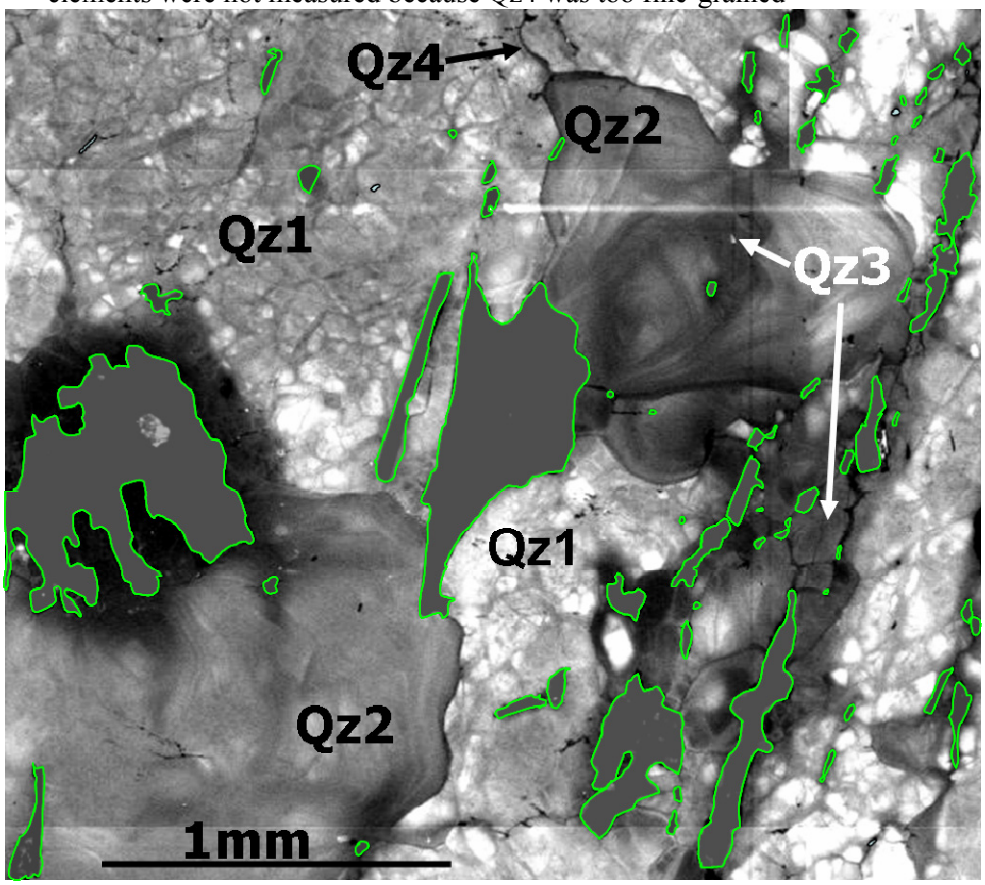

Figure 4: Definition of quartz types. SEM-CL image displays mica and quartz. Mica grains are given a green outline and uniform grey colour to enhance the quartz textures comprised by quartz types Qz1, Qz2, Qz3 and Qz4. See text for discussion.

The complex textures in quartz are explained by two major pulses of fluid in a genetic model related to deformation processes (Figure 5):

1. Homogeneous trace element rich quartz forms at high grade metamorphicconditions under relatively dry conditions.
2. Introduction of aqueous fluids under differential stress induced brecciation. Quartz dissolved during brecciation precipitates as Qz2, Qz1 is the brecciated old grains. Fluid inclusion studies (paper 2 Sørensen and Larsen, 2007b) document that Qz2 formed together with a mixture of low salinity CO_2-rich H_2O-CO_2 and H_2O-CO_2-NaCl-KCl brines with eutectic salinity (FIA2 see next section). Qz2 coexist with rutile and rutile quartz thermometry (Wark and Watson, 2006) on the typical Ti content in Qz2 in quartzites gives a formation temperature of 626°C in agreement with interpretation made from phase equilibria in calc-silicate rocks for the early stages of retrogression at 7kb, 626-640°C (Paper 2, Sørensen and Larsen, 2007b). Thus Qz2 formed during isobaric cooling stage of the Bamble sector. This agrees well with the decussate texture (static) in the alteration assemblages related to Qz2-rich quartz veins intersecting amphibolites (paper1, Sørensen and Larsen, 2007a).
3. Renewed deformation induces cracking. Infiltrating aqueous fluids move along the cracks causing recrystallisation (Qz3), and also increases crack mobility. The recrystallised quartz (Qz3) behaves more plastic than Qz1 and Qz2 and deform by SGR (subgrain rotation recrystallisation). Continuous fluid flow through the more fine-grained Qz3 domains increases recovery rates and reduce strain hardening. Crack propagation and recrystallisation still continue and the amount of Qz3 increase. Fluid composition in equilibrium with Qz3 is approximated by the H_2O-NaCl-$CaCl_2$ system with 25 wt% NaCl and 6 wt% $CaCl_2$ (FIA3)(paper 2, Sørensen and Larsen, 2007b). Textural observations demonstrate that not only was the quartz purified from structurally incorporated trace elements during the influx in FIA3, but rutile needles were also removed providing quartz that was also pure on the bulk scale (paper 2, Sørensen and Larsen, 2007b). The observation that Qz3 formed in relation with thrust related deformation in combination with the isochore of the fluid inclusions in Qz3 suggest formation conditions at 300-400°C, 4-6 kb. Exhumation occurred near the brittle–ductile transition as also suggested by the mix of plastic and cataclastic textures (paper 1, Sørensen and Larsen, 2007a). Qz1 experienced considerable strain hardening due to accumulation of dislocations as evidenced by increased SEM-intensity towards deformation zones comprising Qz3 (paper 1, Sørensen and Larsen, 2007a) (see Figure 4).

The relation between fluid infiltration, recrystallisation and change in rheology of quartz is supported by experiment in which the strength of quartz is an order of magnitude lower at water saturated than at dry conditions in experiments (e.g. Kronenberg, 1994). However, we suggest that other structural properties of the quartz may be equally as important as H_2O related defects. The presence of trace elements and other defects in the quartz structure may serve as obstacles for dislocation migration during deformation hence decrease the efficiency of both dislocation climb (recovery) and dislocation glide (plastic slip)

Grain boundary geometry is affected by the different defect structure of the quartz types. GBAR (Grain Bounday Area Reduction) facilitated straight boundaries and triple junctions between Qz2 grains whereas Qz2-Qz1 boundaries are lobate-interlobate with textures documenting consumption of Qz1 by Qz2 during GBM (high temperature Grain Boundary migration) (paper 1, Sørensen and Larsen, 2007a). The possibility exists that SEM-CL could be a vital tool to improve the understanding of the little understood GBM process in quartz tectonites (paper 1, Sørensen and Larsen, 2007a). In addition it is suspected that the trace elements may also contribute to the grain boundary migration processes.

Our results also demonstrate that quartz trace elements not only are structurally incorporated, but also exist as microscopic mineral inclusions (paper 1, Sørensen and Larsen, 2007a). A common example is rutile needles that are common in quartz types Qz1 and Qz2. They occur at two scales: in Qz1 they are comprised by crystallographically oriented needles only visible at 500 times magnification whereas in Qz2 are represented by coarser needles visible at 100 times magnification. In Qz2 in quartz veins in amphibolite the rutile needles are crystallographically oriented. The needles in Qz2 are inferred to have formed as intergrowths, whereas the needles in Qz1 are interpreted as exsolutions. The presence of rutile needles in Qz2 affects the measured Ti content, giving a wide Ti range in Qz2 in amphibolite, where the needles were too abundant to be completely avoided. In Qz2 in quartzites, rutile needles were less abundant and could be avoided. This resulted in a systematic Ti content characterised by a peak value at 32 ppm. The peak is asymmetric with a shoulder towards lower values probably reflecting partial recrystallisation towards Qz3. We did not find systematic variations in the Al content of quartz although high values measured during statistical analysis reveal that all quartz types have peaks close to the detection limit at 10 ppm. High values are inferred to be a result of sub microscopic inclusions of dumortierite $Al_{6.5\text{-}7}(BO_3)(SiO_4)_3(O, OH)_3$ as suggested by a strong correlation between B and Al. B content also reflect dumortierite inclusions. Qz3 has trace element contents close to or below the detection limits i.e. it has a very well defined chemical signature. In addition Qz3 almost has the same chemistry in both amphibolite and quartz veins and in quartz-muscovite veins, except for phosphorous which apparently is higher in the quartz-scapolite veins than in the quartzites.

The generally low trace element contents in Qz3 reflect quartz that is low in both trace elements associated with micro inclusions and structurally incorporated trace elements. The fine grain size of Qz3 and the localised nature of retrograde recrystallisation pose a challenge to the industrial applications because of the demand of bulk qualities. Three options are possible for the applications of quartz purified through metamorphic processes:

1: Quartz with a quality which was already close to the industrial standards, such as pegmatite quartz may be further refined through metamorphic processes.

2: Fine grained quartz bearing rocks with quartz of good quality may be crushed down and the quartz may be separated. This procedure requires aggregation after mineral separation. No technology is currently available for this at a commercial scale.

3: Multistage pervasive greenshist alteration under fluid saturated conditions may provide more homogeneous quartz qualities. Because fluids are expelled during high grade metamorphism and only locally reintroduced during retrogression quartz recrystallisation only occurs at localised scale. Prograde metamorphism of fluid saturated rocks to the greenshist grade is more promising in providing an environment in which fluids were constantly present facilitating more homogeneous quartz recrystallisation.

Fluid composition and growth rate may impose a control on the quartz chemistry. This study demonstrates that H_2O rich fluids facilitated the destabilisation of rutile thus preventing rutile quartz intergrowth. We do not report systematics in the structurally incorporated Al. In our study trace elements in quartz systematically decrease with decreasing temperature. This however, is not always the case because fluid properties impose an important control on the composition of quartz. As an example Al will be higher in quartz formed with a high pH fluid because of the association of Al with OH groups and the Al concentration in quartz will also be function of the Al-content of the fluid (Miyoshi et al., 2005). Studies of magmatic quartz display similar results suggesting that Al is buffered by the Al in the quartz forming environment (Jacamon and Larsen in Jacamon, 2006). Thus the trace elements cannot be directly associated with variations in PT-conditions. In our case a drop in PT conditions is probably responsible for the progressive drop in the Ti content of quartz during cooling and exhumation. This is in good agreement with recent experimental calibrations which predict that the Ti content of quartz in equilibrium with rutile decreases with temperature (Wark and Watson, 2006).

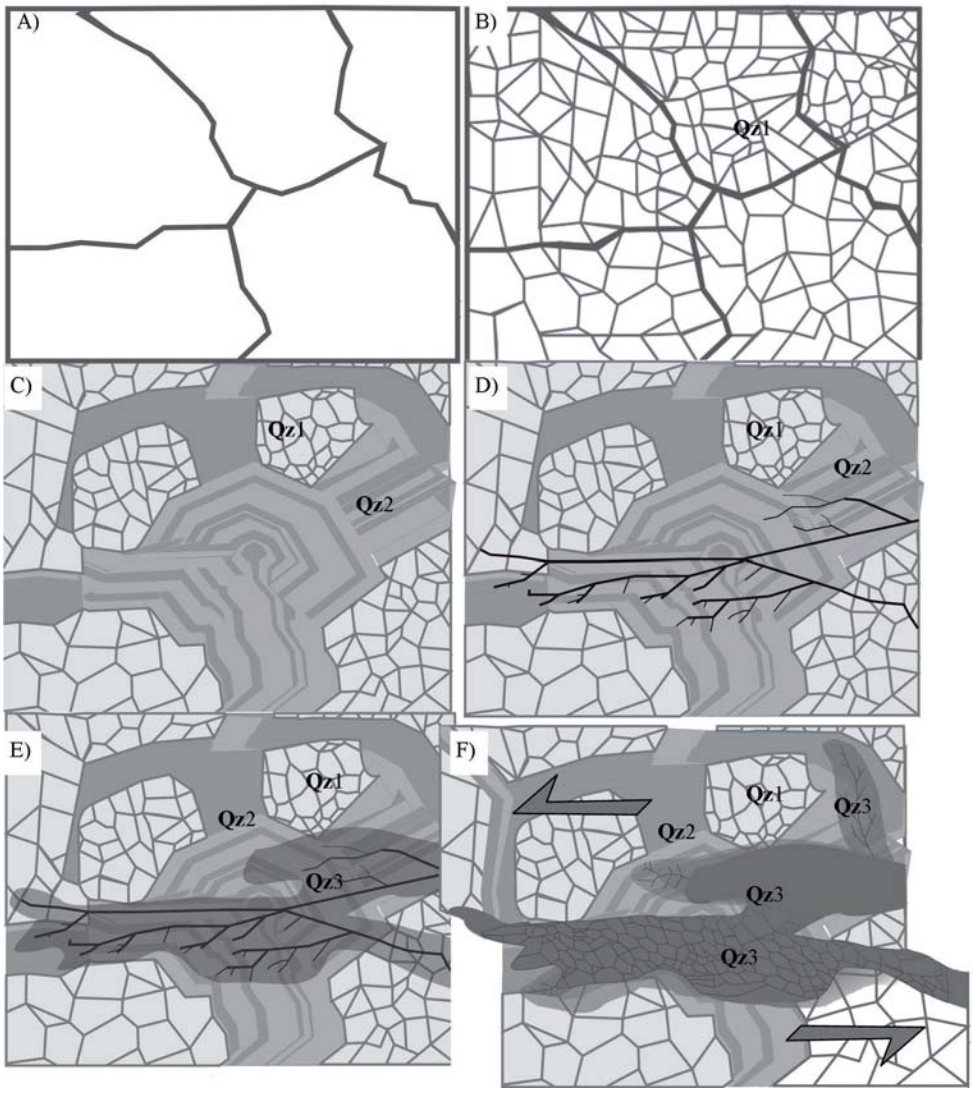

Figure 5: Patterns of recrystallisation of quartz in quartz rich rocks as revealed by SEM-CL and optical microscopy in paper 1. A) Homogeneous quartz at high grade conditions. B) Introduction of aqueous fluids under differential stress induces brecciation. C) Quartz dissolved during brecciation precipitates as Qz2, Qz1 is the brecciated old grains. D) Renewed deformation induce cracking E) Infiltrating aqueous fluids move along the cracks causing recrystallisation (Qz3), and increased crack mobility F) The recrystallised quartz (Qz3) behaves more plastic than Qz1 and Qz2 and deforms by SGR (subgrain rotation recrystallisation). Continuous fluid flow through the more fine-grained Qz3 domains increases recovery rates and reduces strain hardening. Crack propagation and recrystallisation still continue and the amount of Qz3 increases.

Retrograde P-T-X_{fluid} evolution of the Bamble sector

Fluid inclusion studies document a high salinity of about 30 wt% NaCl equivalent throughout cooling and uplift by four fluid inclusion assemblages (paper 2, Sørensen and Larsen, 2007b):

FIA1. Found in quartz (Qz1) in dm-sized garnet quartz symplectites, intersecting garnet amphibolite. Texturally correlated with high grade metamorphism of the area and comprising nearly pure CO_2-fluids co-existing with eutectic melts formed by partial melting of amphibolite. In agreement with studies of Fe-Ti oxides in the granulite facies area around Tromøy (2000b), CO_2 is the stable carbonic species at the ambient oxygen fugacities.

FIA2. Found in quartz (Qz2) in en echelon veins intersecting amphibolite. The earliest retrograde fluid and comprise mixtures of two fluid types: 1) low salinity CO_2-rich H_2O-CO_2 fluids, 2) H_2O-CO_2-NaCl-KCl brines with near eutectic compositions and low in CO_2. Thermodynamic modelling does not allow type 1 and 2 inclusions to be the result of in situ phase separation. Rather they represent fluid mixing of fluids derived from separate reservoirs.

FIA3. Found in recrystallised quartz (Qz3) in quartz-scapolite veins and in quartz-biotite-tourmaline gneiss in zones where biotite is partly replaced by chlorite and muscovite. Comprise LVS inclusions of aqueous brines and no carbonic fluids. The most important salts are NaCl (average 25 wt %) and $CaCl_2$ (average 6 wt%). The salinity is near constant and LV to L homogenisation occurs in a narrow range around 129 °C altogether giving dense brines following a steeply inclined isochore.

FIA4. Primary LV inclusions found in growth zones in calcite and in epidote in vug assemblages in calc-silicate rock. Comprises aqueous $CaCl_2$ (31-36 wt%) brines with no carbonic fluids. The degree of fill is high giving dense fluids following a steeply inclined isochore in P-T space. The final melting of antarcticite varies systematically along growth zones in calcite. Epidote grains are zoned with $EpCz_{71}$ in cores and $EpCz_{65}$ in rims. Amphibole display similar evolution with actinolite replacing tremolite in a fracture pattern recognised in backscatter images. FIA4 Fluid inclusions are only found in epidote cores. Fluid inclusions in the epidote cores correlate with fluid inclusions with the higher antarcticite melting temperatures in calcite, and with higher initial melting temperatures.

The salinity of the fluids has significant effects on the PT-position of dehydration and decarbonation reactions and was accounted for in phase diagram calculations of calc-silicate rocks observed in this study (paper 2, Sørensen and Larsen, 2007b) and in assemblages reported by Nijland and co-workers (1993b) using PERPLEX (Connolly, 1990; Connolly and Petrini, 2002).

The interpretation of the constructed phase diagrams lead to a redefinition of the cooling and uplift PT-X_{fluid} path of the Froland area (paper 2, Sørensen and Larsen, 2007b) (Figure 6). The retrograde fluids may partially be superimposed upon the PT-evolution of the Froland area (Figure 6). More details in (Sørensen and Larsen, 2007b, paper 2).

In summary, the cooling and uplift path begins by simultaneous formation of tremolite + sanidine and tremolite + sanidine + calcite assemblages at c. 626-636°C and 7 kb (Figure 6). The next stage agrees with MII (ky + chl + ms) and MIII (ma

+crn) of (Nijland et al., 1993b) (Figure 6). The pressure is uncertain although a path may be extended from this stage to the isochore of FIA3. Because the fluid inclusions in FIA3 are well preserved showing no evidence of post entrapment modification the exhumation path can not deviate more than 2 kb from the FIA3 isochore (Figure 6). The last part of the cooling and exhumation path is constrained by MV at 2-3 kb and 175-280°C (Nijland et al., 1993b; Touret, 1985) The PT-path preserves the main characteristics of the path published by Nijland et al.(1993b), but the uplift is shifted 100°C toward lower temperatures and is in better agreement with the dominance of cataclastic microstructures in thrust related structures. A shift between potassic and sodic-calcic alteration occurred between FIA2 and FIA3. The Shift between MII and MIII of Nijland et al. (1993b) probably correlates with the shift in alteration types (Figure 6).

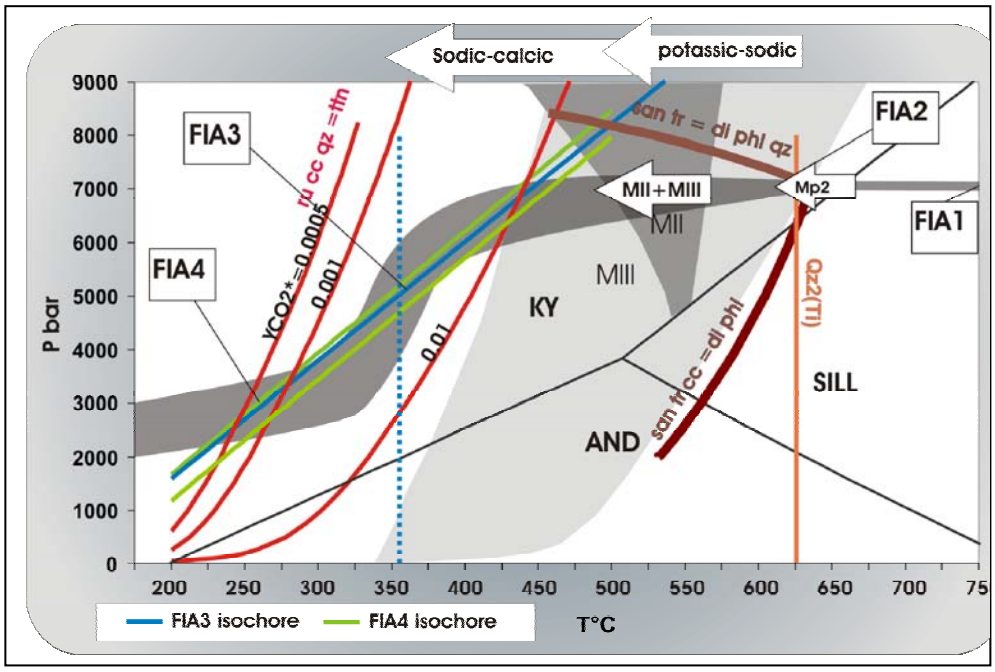

Figure 6: Tentative PT-Xfluid path of the study area, with possible implication for the uplift path of the Bamble sector. The PT-X_{fluid} path is assembled using a combination of mineral paragenetic and fluid inclusion data. Because fluid inclusions and mineral parageneses that are simple enough to be portrayed quantitatively in PT-space are not always present in "real life" the PT-path rely on textural correlations between assemblages in one rock type and fluid inclusions found in other rock types. Arrows on the top of the diagram indicate condition when alteration changed from potassic-sodic to sodic-calcic. From Sørensen (2007b, paper 2). For a more detailed discussion of the derivation of the PT-path see Sørensen (2007b, paper 2). Reactions are written such that the high temperature assemblage is to the right of the = sign. YCO2* denotes the CO_2 content compared to H_2O in a fluid with 30 wt% NaCl relative to H_2O.

Interaction between volatile bearing minerals and a coexisting fluid

Paper 3 (Sørensen et al., 2007) documents the complex interaction between hydrous minerals and a brine fluid during cooling and exhumation. Primary focus is on the chemistry of amphiboles, but chemistry of apatite, biotite and scapolite is also included.

Based on field and thin section observations the alteration of the amphibolites divides into three main alteration stages: Alt1 potassic alteration with biotite stable, Alt2 potassic alteration with K-feldspar stabilised over biotite and Alt3 scapolitisation. The most commonly observed alteration comprises overgrowth rims on amphibole associated with the introduction of biotite. The amphibole rims display a wide colour range from deep blue green to pale green reflecting a chemical variation from ferrotschermakite/ferropargasite rich in Al and Fe to actinolite (XMg = 0.9). Amphibole rims also commonly display outward zoning toward more Mg and Si and decreasing Fe, Al^{IV}, Al^{VI}, Cl, Ti, K and Na. Fe, Al, K and Na are positively correlated with Cl whereas Mg and Si are negatively correlated.

Coexisting biotite displays a similar chemical zonation of Mg and Fe, but Al does not show as clear a zonation as in amphibole. Neither biotite nor amphibole contain detectable amounts of F, but display variable Cl-contents. The Cl-content of coexisting biotite and amphibole is correlated in a trend which does not give a 1:1 correlation. In the most Cl rich compositions amphibole is richer in Cl than coexisting biotite whereas the opposite is the case at low Cl contents. A similar observation is seen in the Fe-content. A plot of KdFe biotite vs. amphibole results in a linear trend with a non zero intercept. We interpret the linear trend to reflect chemical equilibrium between the coexisting biotite and amphibole.

The compositional changes reflect the complex interaction between brine fluids and hydrous minerals during cooling and uplift, where the Fe and Mg contents of the silicates were changed. Accordingly, the brine fluids partly control the composition of Fe-Mg silicates. Hence the models arguing that the Cl content of biotite is a function of the Fe/Mg ratio of the mineral, fluid composition and PT-conditions (Munoz, 1992; Munoz and Swenson, 1981) can not explain the Froland amphiboles and biotites. The composition of the halogen bearing Fe-Mg silicates is partially controlled by the aqueous fluid composition along with P and T. Two models may explain the biotite and amphibole chemical zonation:

Model 1: zoning reflects interactions with a fluid of varying composition at fixed P and T. This model explains the compositional zoning observed by Kullerud and co-workers (1995; 1996; 1999), but cannot fully explain the compositional zoning observed in our study because the fluid salinity is constant.

Model 2: compositional zoning reflects interaction with a fluid having constant halogen contents during gradually changing PT-conditions.

Model 2 is preferred in the current study because fluid inclusion studies document constant salinities of the fluid during cooling and exhumation (Sørensen and Larsen, 2007b). This is in good agreement with the non zero intercept in the KdFe plot of amphibole inferred to indicate different temperature at each data point.

The difference in Cl, Fe and Al -contents of coexisting amphibole and biotite also probably reflect changes in the temperature and the different effects of the temperature upon the amphibole and biotite structures. Cl-incorporation increases the cell volume of amphibole and, therefore, it is expected that the Cl concentration is positively correlated with the temperature. Local ordering between Fe, Cl and K have been documented in amphibole (Oberti et al., 1993). This, together with the observation that the Al content in amphibole increases more than in biotite with increasing temperature, causes relatively higher Fe-content in amphibole at higher temperatures. Thus the change in KdFe and Cl content between amphibole and biotite is a function of temperature fluctuations. Accordingly, increasing temperature would cause increasing Fe in amphibole hence less Fe in biotite. This again would affect the Cl ratio amongst coexisting amphibole and biotite because Cl is attracted to Fe in the amphibole lattice.

Apatite features a halogen evolution that is the different from that of amphibole and biotite. Whereas F was not detected in the studied amphibole and biotite, apatite displays an evolution from Cl-OH apatite in the garnet quartz symplectites toward increasingly F-rich apatite parallel with amphiboles and biotites becoming Mg-rich and Cl poor. However, most hydrothermal apatite is F-rich due to the high partitioning of F into of apatite compared to the fluid. The $\log(aHCl/aH_2O)/\log(aHf/aH_2O)$ diagrams of Zhu and Sverjensky (1991) show that only small amounts of F ($\log(aF/aH_2O = 10^{-6})$ in the fluid would suffice to give F-apatite fractions of 0.9 in a 5 molal Cl- solution at 300°C. The stability field of F-apatite increase with decreasing temperature (Zhu and Sverjensky, 1991) Hence F-enrichment in the Froland-apatite most likely reflect dropping temperature and not F-enrichment in the fluid.

From our textural observations we infer that scapolite was late in the mineral assemblage. Although scapolite coexisted with CO_2-free fluids, scapolite formula recalculation shows that scapolite was meionite rich hence containing significant CO_3 and HCO_3. Accordingly, CO_2 did not come from the fluid. Textural observations imply that scapolitisation depended on the presence of calcite near plagioclase. Similar observations were done by Visser and co-workers (1999). Therefore, we suggest that scapolite formed by a reaction involving calcite as also suggested by Visser et al. (1999):

cc + NaCl+ pl = scp

The strongly variable composition is mostly a function of local chemical variations particularly in the amount of calcite, the composition of the replaced plagioclases and the Ca/Na ratio of the coexisting fluid. Given that the fluids maintained constant compositions (paper 2, Sørensen and Larsen, 2007b) it was primarily the local rock composition governed by plagioclase and calcite that buffered the scapolite composition.

Metasomatic evolution of the Bamble sector and formation ore deposits

The observation that both amphibole and biotite become increasingly Mg-rich during cooling and exhumation in combination with the observation that commonly the loss of Fe cannot be explained by other phases leads us to conclude that Fe was mobilised.

This is illustrated by mesoscale observations on cut and polished hand specimens and is particularly well illustrated by alteration patterns surrounding plagioclase-calcite veins:

The central zone1 is enriched in ilmenite, Ca CO_2 Fe and sulphur; this is followed by a zone free of biotite mainly comprising plagioclase and amphibole, followed by an amphibole free zone mainly comprising biotite and plagioclase. This local scale observation may possibly reflect what is going on at a larger scale in the Bamble sector. I.e. Fe and other elements are removed from the amphibolites which become increasingly Mg-rich and redeposited elsewhere giving rise to the numerous small Fe-Cu oxide/sulphide deposits scattered throughout the Bamble sector. This was also suggested by Brøgger (1934) for the breccia related deposits at Langøy in relation to the mafic rock that was altered by scapolitisation and albitisation processes and as a general genetic model by Korneliussen et al. (2000).

Genetic models of ore deposits will benefit from an increased understanding of the interaction of fluids with silicates in the wall rocks because fluid-rock interaction in the wall rock probably explain many element enrichments leading to ore formation. Bearing this in mind we find it peculiar that many studies of ore deposits use the (Munoz, 1992; Munoz and Swenson, 1981) model to calculate halogen activities in ore forming fluids because the model assumes that crystal chemical constraints are in control of the halogen contents of biotite and amphibole. Rather we suggest that the fluid phase pose a partial control on the mineral chemistry and that fluid rock interaction leads to changes in mineral and fluid composition in order to obtain equilibrium conditions. As parameters such as pressure, temperature, fluid composition and fluid-rock ratios changes the equilibrium also changes.

In our study the mineralogical changes are induced by fluid rock interaction with a fluid of constant salinity during cooling and exhumation, but different models explain similar mineral zonation elsewhere.

However, the understanding of the architecture and tectono-metamorphic evolution of the Bamble sector remain fragmentary. Partially because the importance of massive pulses of highly saline fluids were not fully appreciated. Our study concerns a rather limited portion of the Bamble sector, however, it is one of the few studies that documents the importance of highly saline aqueous fluids and demonstrates the implications for the mineralogy and metasomatic processes on micro as well as macro scale. Studies by Cameron (1993a; 1993b) and Cameron and co-workers (1993) document the mobilisation of Au and other chalcophile elements during high grade metamorphism and retrogression in the Bamble sector through analysis of the whole rock chemistry. Their results document how chalcophile elements are depleted through amphibolitisation of coronitic gabbro at

high f_{O2} (Cameron et al., 1993) and reintroduced in retrograde veins focused at higher crustal levels near the brittle-ductile transition (Cameron, 1993b).

Our work document details on the mineralogical, PT-X_{fluid} and metasomatic evolution of the Bamble sector. Although they represent a rather limited geographical area they confirm the main concept of the ore genetic model proposed by Cameron and co-workers. Further work should, on a much finer scale than done in this study, focus on the mineralogical evolution during cooling and uplift and compare that with the whole rock chemistry. In addition the study of fluid inclusions associated with the ore-forming process in amphibolite and in calc-silicates (Sørensen, 2006 unpublished data) will allow tighter constrains of the PT-X_{fluid} evolution associated with element mobilisation and re-deposition of ore deposits.

Publications and presentations during PhD work

Sørensen, B.E. and Larsen, R.B., 2007. Paper1 Fluid induced multistage recrystallisation microstructures in Quartzites and Quartz veins from the Bamble shear zone complex (in my PhD thesis)

Sørensen, B.E. and Larsen, R.B., 2007. Paper2: The fluid evolution of the Froland area in the Bamble sector from peak P-T through cooling and uplift: implications for retrograde mineral paragenesis and PT evolution of the Bamble sector.(in my PhD thesis)

Sørensen, B.E., Larsen, R.B. and Austrheim, H., 2007. Paper3: Metasomatic evolution of the Froland amphibolites during cooling and uplift - textural observations and geochemical evolution of hydrous minerals. (in my PhD thesis)

Sørensen, B.E. Quantitative interpretation of fluid dependant mineral equilibria in complex calc-silicate rocks. . In: Proceedings, 6th Annual Conference for Doctoral Candidates. NTNU: The Organization for Doctoral Candidates of Applied Earth Sciences (DIGOP) 2006. ISBN 82-92319-06-9.

Larsen, R.B.; Ihlen, P.; Jacamon, F.P.; Müller, A.; Sørensen, B.E. (2005). IGNEOUS REFINEMENT OF QUARTZ RAW-MATERIALS. GSA Abstracts with Programs 2005;37(7)

Sørensen, B.E.; Austrheim, H.; Larsen, R.B. (2005). Fluid-related recovery and deformation textures in quartz in partly retrogressed high-grade quartzites from the Bamble sector. Abstract to scientific lecture given at the mineral and rock physics session at the AGU fall meting 2005. Eos 2005;86(52)

Sørensen, B.E. (2005). Fluid related recovery and deformation textures in quartz in partly retro regressed high grade quartzites from the Bamble sector. In: Proceedings, 5th Annual Conference for Doctoral Candidates. NTNU: The Organization for Doctoral Candidates of Applied Earth Sciences (DIGOP) 2005. ISBN 82-92319-05-0.

Sørensen, B.E.; Austrheim, H.; Larsen, R.B. (2005). Fluid related recovery in partly retrogressed high-grade quartzites from the Bamble sector [Scientific lecture]. ECROFIXVIII; 06.07.2005 - 09.07.2005

Sørensen, B.E.; Larsen, R.B., Austrheim, H. (2005). Fluid versus strain-related recovery in quartz in partly retrogressed high-grade quartzites from the Bamble sector. Abstract to lecture given at Geologisk Vintermøte 2005 in Røros.

Sørensen, B.E. (2005). Fluid inclusions: Their significance, analysis and interpretation in metamorphic rocks. Detailed report focussing on thermodynamic interpretation of microthermometry data. 95 p.

Sørensen, B.E. (2003): Significance of Dauphiné twins in quartz tectonites- an EBSD study from the Norwegian Caledonides. The Alice Wain Memorial West Norway Eclogite Field Symposium. Abstract volume, p. 148.

Acknowledgements

Jamie Connolly (ETH, Zürich) patiently replied to numerous emails I sent to him concerning the PERPLEX package. I am especially grateful that he made me aware of the method of Trommsdorff & Connolly (1990), which is very useful for mixed volatile systems such as the calc-silicate rocks discussed in Paper 2.

Dennis Bird, Muriel Erambert (UIO, Oslo), **Roger Powell, Robert Frost and Daniel Harlov** replied to other emails provided thoughtful and helpful answers.

Arrild Monsøy, Kjetil Eriksen (IGB perparation lab) prepared more than 50 polished thin sections and doubly polished fluid inclusions sections. Their care in sample preparation and engagement in discussions of preparation qualities and technical improvements are highly appreciated. Their positive and cooperative spirits lead to continuous improvements in the quality of polished samples.

Filip Dal (SINTEFF Berg og Geoteknikk) instructed me with the rock cutting saw at NTNU. Many samples were cut and roughly polished to provide an overview of the textures. Observation done on polished rock slices is a corner stone in the scientific content of the papers in this thesis.

Ingrid Vokes, Kjell Kvamm assisted with XRD of mineral specimens, providing quick and easy classification of the metamorphic assemblages that were not easy to define optically.

Morten Peder Råness (NTNU, Department of Materials Science) assisted with the microprobe analyses and helped with optimisation of the standardisation methods.

Belinda Flem, Øyvin Skår (NGU) instructed me on the LA-ICP-MS at NGU used to trace elements analyse of quartz.

Axel Muller, Belinda Flem and Andreas Grimstvedt (NGU) and Rune Larsen (NTNU) instructed me with the calibration procedures for the translation LA-ICP-MS raw data to trace element concentrations.

Rune Larsen (NTNU) was my primary supervisor and somehow managed to survive throughout the long years of my PhD studies where he extremely patiently

listened to my endless monologues and prudishly waited for my return from yet a dry scientific path that I insisted on following. In the end he realised my ingenuity, accepted his inferior role, and took up new carrier path as a born again fundamentalist ale expert called to spend his early retirement in mikrobryggerriet (may he R.I.P.). Rune endured the proof reading of some of my intricate manuscripts. His suggestions and reformulations greatly improved the readability of this manuscript.

Håkon Austrheim (UIO) was my second supervisor. He joined us on a short notice during the first field season and greatly helped in organising the last paper. He also travelled to Trondheim to participate in meetings whenever called for. He also joined me in the last field season and helped to organise the main issues of the thesis.

Tore Prestvik (NTNU) stepped in as main supervisor when Rune Larsen was still at NGU. He provided help with various administrative tasks. In addition he proof read my project description and several meeting abstracts.

Lasse Telstø, Francois Jacamon, Kurt Aasly (NTNU) participated in many scientific discussions.

Lasse Telstø (NTNU) introduced me to fluid inclusion studies and to the microthermometric equipment at IGB.

Timo Nijland answered my emails concerning his papers and went back to his old notes and had a new look at his old samples and kindly answered my questions regarding his important Bamble papers.

Iain Henderson, Peter Ihlen and Are Korneliussen (NGU) introduced me to the geology of the Bamble Sector during a three day excursion in the beginning of my project.

Terje Malvik was the leader of the SUP project and arranged several seminars where we presented our results and discussed the further progress.

Jarle Hjelen, Jon Rasmus Leinum and Kari Moen introduced me to the impressive SEM instrument park at the department of materials science, NTNU. Free access to SEM equipped with grey scale SEM-Cl detector.

Finally I would like to thank friends and family for their patience and understanding during my thesis work.

References

Ahall, K.I. and Gower, C.F., 1997. The Gothian and Labradorian orogens; variations in accretionary tectonism along a late Paleoproterozoic Laurentia-Baltica margin. GFF, 119(2): 181-191.

Aines, R.D. and Rossman, G.R., 1986. Relationships between radiation-damage and trace water in zircon, quartz, and topaz. American Mineralogist, 71(9-10): 1186-1193.

Applin, K.R. and Hicks, B.D., 1987. Fibers of dumortierite in quartz. American Mineralogist, 71: 786-794.

Armington, A.F., 1991. Recent advances in the growth of high-quality quartz. Progress in Crystal Growth and Characterization of Materials, 21: 97-111.

Armington, A.F. and Balascio, J.F., 1984. The growth of high purity, low dislocation quartz, Proceedings of the 38th annual Frequency Control Symposium, USA, pp. 3-7.

Beck, W.R., 1949. Crystallographic inversions of the aluminum orthophosphate polymorphs and their relation to those of silica. Journal of the American Ceramic Society, 32(4): 147-151.

Bingen, B., Boven, A., Punzalan, L., Wijbrans, J.R. and Demaiffe, D., 1998. Hornblende (super 40) Ar/ (super 39) Ar geochronology across terrane boundaries in the Sveconorwegian Province of S. Norway. Precambrian Research, 90: 159-185.

Bingen, B., Mansfeld, J., Sigmond, E.M.O. and Stein, H., 2002. Baltica-Laurentia link during the Mesoproterozoic; 1.27 Ga development of continental basins in the Sveconorwegian Orogen, southern Norway. Canadian Journal of Earth Sciences = Revue Canadienne des Sciences de la Terre, 39(9): 1425-1440.

Bingen, B., Nordgulen, Ø. and Sigmond, E.M.O., 2001. Correlation of supracrustal sequences and origin of terranes in the Sveconorwegian orogen of SW Scandinavia: SIMS data on zircon in clastic metasediments. Precambran Research 108: 293-318.

Bingen, B. and Van-Breemen, O., 1998. Tectonic regimes and terrane boundaries in the high-grade Sveconorwegian Belt of SW Norway, inferred from U-Pb zircon geochronology and geochemical signature of augen gneiss suites. J. Geol. Soc. Lond. , 155: 143-154.

Brickwood, J.D. and Craig, J.W., 1987. Primary and reequilibrated mineral assemblages from the Kongsberg and Bamble areas, Norway. Norges Geologiske Undersøkelse, 410: 1-23.

Brøgger, W.C., 1934. On several Archean rocks from the south coast of Norway; II, The south Norwegian hyperites and their metamorphism. 1; 1, 421 pp.

Bugge, J.A.W., 1940. Geological and petrological investigations of the Arendal district. Norsk Geologisk Tidsskrift, 20: 71-112.

Cameron, E.M., 1993a. Precambrian gold - perspectives from the top and bottom of shear zones. Canadian Mineralogist, 31: 917-944.

Cameron, E.M., 1993b. Reintroduction of gold, other chalcophile elements and LILE during retrogression of depleted granulite, Tromoy, Norway. Lithos, 29(3-4): 303-309.

Cameron, E.M., Cogulu, E.H. and Stirling, J., 1993. Mobilization of gold in the deep crust - Evidence from mafic intrusions in the Bamble Belt, Norway. Lithos, 30(2): 151-166.

Cohen, A.J. and Makar, L.N., 1984. Differing effects of ionizing-radiation in massive and single-crystal rose quartz. Neues Jahrbuch Fur Mineralogie-Monatshefte(11): 513-521.

Cohen, A.J. and Makar, L.N., 1985. Dynamic biaxial absorption-spectra of Ti^{3+} and Fe^{2+} in a natural rose quartz crystal. Mineralogical Magazine, 49(354): 709-715.

Connolly, J.A.D., 1990. Multivariable phase-diagrams - An algorithm based on generalized thermodynamics. American Journal of Science, 290(6): 666-718.

Connolly, J.A.D. and Petrini, K., 2002. An automated strategy for calculation of phase diagram sections and retrieval of rock properties as a function of physical conditions. Journal of Metamorphic Geology, 20(7): 697-708.

Cosca, M.A., Mezger, K. and Essene, E.J., 1998. The Baltica-Laurentia connection Sveconorwegian (Grenvillian) metamorphism, cooling, and unroofing in the Bamble sector, Norway. Journal of Geology, 106: 539-552.

Falkum, T. and Petersen, J.S., 1980. The Sveconorwegian orogenic belt, a case of late-Proterozoic plate-collision. Geologische Rundshcau, 69: 622-647.

Field, D., Drury, S. and Cooper, D.C., 1980. Rare-earth and LIL element fractionation in high-grade charnockitic gneisses, South Norway. Lithos 13: 281-289.

Friebele, E.J., Griscom, D.L., Stapelbroek, M. and Weeks, R.A., 1979. Fundamental defect centers in glass - Peroxy radical in irradiated, high-purity, fused-silica. Physical Review Letters, 42(20): 1346-1349.

Frodesen, S., 1968. Petrographical and chemical investigations of a precambrian gabbro intrusion, Hiåsen, Bamble area, south Norway. Norsk Geologisk Tidsskrift, 48: 281-306.

Frondel, C., 1962. The system of mineralogy of James Dwight Dana and Edward Salisbury Dana, Yale University, Volume III Sillica Minerals. John Wiley and Sons, Inc., Newyourk and London, 334 pp.

Goetze, J. and Ploetze, M., 1997. Investigation of trace-element distribution in detrital quartz by Electron Paramagnetic Resonance (EPR). European Journal of Mineralogy, 9(3): 529-537.

Goetze, J., Ploetze, M., Graupner, T., Hallbauer, D.K. and Bray, C.J., 2004. Trace element incorporation into quartz; a combined study by ICP-MS, electron spin resonance, cathodoluminescence, capillary ion analysis, and gas chromatography. Geochimica et Cosmochimica Acta, 68(18): 3741-3759.

Goetze, J., Plotze, M. and Habermann, D., 2001. Origin, spectral characteristics and practical applications of the cathodolumimescence (CL) of quartz - a review. Mineralogy and Petrology, 71(3-4): 225-250.

Goreva, J.S., Ma, C. and Rossman, G.R., 2001. Fibrous nanoinclusions in massive rose quartz: The origin of rose coloration. American Mineralogist, 86: 466-472.

Griscom, D.L., 1985. Nature of defects and defect generation in optical-glasses. Proceedings of the Society of Photo-Optical Instrumentation Engineers, 541: 38-59.

Harlov, D.E., 1992. Comparative oxygen barometry in granulites, Bamble sector, SE Norway. Journal of Geology, 100: 447-464

Harlov, D.E., 2000a. Pressure-temperature estimation in orthopyroxene-garnet bearing granulite facies rocks, Bamble sector, Norway. Mineralogy and Petrology, 69: 11-33.

Harlov, D.E., 2000b. Titaniferous magnetite-ilmenite thermometry and titaniferous magnetite-ilmenite-orthopyroxene-quartz oxygen barometry in granulite facies gneisses, Bamble sector, SE Norway; implications for the role of high-grade CO_2-rich fluids during granulite genesis. Contributions to Mineralogy and Petrology 139: 180-197

Hassan, F. and Cohen, A.J., 1974. Biaxial color-centers in amethyst quartz. American Mineralogist, 59(7-8): 709-718.

Heaney, P.J., 1994. Structure and chemistry of the low-pressure silica polymorphs. In: C.T. Prewitt and G.V. Gibbs (Editors), Silica; physical behavior, geochemistry and materials applications. Reviews in Mineralogy. Mineralogical Society of America, Washington, DC, United States, pp. 123-176.

Henderson, I.H.C. and Ihlen, P.M., 2004. Emplacement of polygeneration pegmatites in relation to Sveco-Norwegian contractional tectonics; examples from southern Norway. Precambrian Research, 133(3-4): 207-222.

Huttenlocher, H.F., 1935. Kristalstruktur des aluminum -orthophosphates. Zeitshrift für Kristallographie, 90A: 508-516.

Jacamon, F., 2006. The significance of textures and trace element chemistry of quartz with regard to the petrogenesis of granitic rocks. Doctoral theses at NTNU 2006:155, PhD. Norwegian University of Science and Technology, Faculty of Engineering Science and Technology, Department of Geology and Mineral Resources Engineering, Trondheim.

Jayraman, N., 1939. The cause of the blue quartzes of the charnokites of soth India and of the champion gneiss and other related rocks of

Mysore. Proceedings of the Indian Academy of Science, A9: 265-285.

Johansson, L. and Kullerud, L., 1993. Late Sveconorwegian metamorphism and defromation in southwestern Sweden. Precambrain Research, 64: 347-360.

Knudsen, T.L., 1996. Petrology and geothermobarometry of granulite facies metapelites from the Hisøy-Torungen area, South Norway; new data on the Sveconorvegian P-T-t path of the Bamble sector. Journal of Metamorphic Geology, 14(3): 267-287.

Knudsen, T.L. and Andersen, T., 1999. Petrology and geochemistry of the Tromøy gneiss complex, South Norway; an alleged example of Proterozoic depleted lower continental crust. Journal of Petrology 40: 909-933.

Knudsen, T.L., Andersen, T., Maijer, C. and Verschure, R.H., 1997. Trace-element characteristics and Pb isotopic evolution of metasediments and associated Proterozoic rocks from the amphibolite- to granulite-facies Bamble sector, Southern Norway. Chemical Geology, 143(3-4): 145-169.

Knudsen, T.L. and Lidwin, A., 1996. Magmatic CO_2, brine and nitrogen inclusions in Sveconorwegian enderbitic dehydration veins and a gabbro from the Bamble sector, southern Norway. European Journal of Mineralogy, 8: 1041-1063.

Korneliussen, A., Dahlgren, S., Ihlen, P.M. and Sandstad, J.S., 2000. On the relationships between metasomatic processes (scapolitisation) at deep crustal levels and fracture-bound ore deposits in the Bamble sector of the Fennoscandian Shield, S. Norway. In: P. Weihed and O. Martinsson (Editors), 2nd annual GEODE-Fennoscandian shield workshop on Paleoproterozoic and Archean greenstone belts and VMS districts in the Fennoscandian Shield Luleå University of Technology Research Report Gällivare-Kiruna, Sweden, pp. 22-25.

Kronenberg, A.K., 1994. Hydrogen speciation and chemical weakening of quartz. In: P.J. Heaney, C.T. Prewitt and G.V. Gibbs (Editors), Silica; physical behavior, geochemistry and materials applications. Reviews in Mineralogy. Mineralogical Society of America, Washington, DC, United States, pp. 123-176.

Kullerud, K., 1995. Chlorine, titanium and barium-rich biotites - Factors controlling biotite composition and the Implications for garnet-biotite geothermometry. Contributions to Mineralogy and Petrology, 120(1): 42-59.

Kullerud, K., 1996. Chlorine-rich amphiboles: Interplay between amphibole composition and an evolving fluid. European Journal of Mineralogy, 8(2): 355-370.

Kullerud, K. and Erambert, M., 1999. Cl-scapolite, Cl-amphibole, and plagioclase equilibria in ductile shear zones at Nusfjord, Lofoten, Norway: Implications for fluid compositional evolution during fluid-mineral interaction in the deep crust. Geochimica et Cosmochimica Acta, 63: 3829-3844.

Kullerud, L. and Dahlgren, S., 1993. Sm-Nd geochronology of Sveconorwegian granulite facies mineral assemblages in the Bamble shear belt, South Norway. Precambrian Ressearch 64: 389-402.

Kullerud, L. and Machado, N., 1991. End of a controversy; U-Pb geochronological geochronological evidence for significant Grenvillian activity in the Bamble area, Norway., Sixth Meeting of the European Union of Geosciences. Terra Abstracts, pp. 504.

Lamb, R.C., Smalley, P.C. and Field, D., 1986. P-T conditions for the Arendal granulites, southern Norway; implications for the roles of P, T and CO_2 in deep crustal LILE-depletion. Journal of Metamorphic Geology 4: 143-160.

Landtwing, M.R. and Pettke, T., 2005. Relationships between SEM-cathodoluminescence response and trace-element composition of hydrothermal vein quartz. American Mineralogist, 90(1): 122-131.

Larsen, R.B., Henderson, I., Ihlen, P.M. and Jacamon, F., 2004. Distribution and petrogenetic behaviour of trace elements in granitic pegmatite quartz from South Norway. Contributions to Mineralogy and Petrology, 147(5): 615-628.

Larsen, R.B., Polvé, M. and Juve, G., 2000. Granite pegmatite quartz from Evje-Iveland: trace element chemistry and implications for high-purity quartz formation. Bulletin - Norges Geologiske Undersokelse, 437: 57-65.

Larsen, R.B., Polvé, M., Juve, G. and Poitrasson, F., 1998. Compostion of volatiles ahnd structural admixtures in quartz in granitic pegmatites, Evje-Iveland, South Norway (ext. abstr.). Bulletin - Norges Geologiske Undersokelse, 433: 38-39.

Lehmann, G., 1975. On the colour centres of iron in amethyst and synthetic quartz: a discussion. American Mineralogist, 86: 335-337.

Mackey, J.H., 1963. EPR study of impurity-related color centers in germanium-doped quartz. Journal of Chemical Physics, 39(1): 74-83.

Maschmeyer, D. and Lehmann, G., 1983. A trapped-hole center causing rose coloration of natural quartz. Zeitschrift Fur Kristallographie, 163(3-4): 181-196.

Miyoshi, N., Yamaguchi, Y. and Makino, K., 2005. Successive zoning of Al and H in hydrothermal vein quartz. American Mineralogist, 90(2-3): 310-315.

Morton, R.D., Batey, R. and O'Nions, R.K., 1970. Geological investigations in the Bamble sector of the Fennoscandian Shield south Norway. 1. The geology of eastern Bamble. Norges Geologiske Undersøkelse, 263, 61 pp.

Müller, A., Lennox, P. and Trzebski, R., 2002. Cathodoluminescence and microstructural evidence for crystallisation and deformation processes of granites in the eastern lachlan fold belt (se austia). Contributions to Mineralogy and Petrology, 143: 510-524.

Müller, A., Wiedenbeck, M., Van den Kerkhof, A.M., Kronz, A. and Simon, K., 2003. Trace elements in quartz; a combined electron microprobe, secondary ion mass spectrometry, laser-ablation ICP-MS, and cathodoluminescence study. European Journal of Mineralogy, 15(4): 747-763.

Munoz, J.L., 1992. Calculation of HF and HCl fugacites from biotite compositions; revised equations. Geological Society of America Abstracts with Programs, 24: 221.

Munoz, J.L. and Swenson, A., 1981. Chloride-hydroxyl exchange in biotite and estimation of relative HCl/HF activities in hydrothermal fluids. Economic Geology, 76(8): 2212-2221.

Nijland, T.G., 1989. De Geologie van het Nelaug gebeid, Bamble sector, Zuid Noorwegen. Unpublished Masters Degree Thesis, Utrecht university, Utrecht, 85 pp.

Nijland, T.G., Jansen, J.B.H. and Maijer, C., 1993a. Halogen geochemistry of fluid during amphibolite-granulite metamorphism as indicated by apatite and hydrous silicates in basic rocks from the Bamble sector, South Norway. Lithos, 30(2): 167-189.

Nijland, T.G., Liauw, F., Visser, D., Maijer, C. and Senior, A., 1993b. Metamorphic petrology of the Froland corundum-bearing rocks; the cooling and uplift history of the Bamble sector, South Norway. Bulletin - Norges Geologiske Undersokelse, 424: 51-63.

Nijland, T.G. and Maijer, C., 1993. The regional amphibolite to granulite facies transition at Arendal, Norway; evidence for a thermal dome. Neues Jahrbuch fuer Mineralogie Abhandlungen, 165: 191-221.

Nijland, T.G., Maijer, C., Senior, A. and Verschure, R.H., 1993c. Primary sedimentary structures and composition of the high-grade metamorphic Nivelda quartzite complex (Bamble, Norway), and the origin of nodular gneisses. Proceedings of the Koninklijke Nederlandse Akademie van Wetenschappen (1990), 96(2): 217-232.

Nijland, T.G., Touret, J.L.R. and Visser, D., 1998. Anomalously low temperature orthopyroxene, spinel, and sapphirine occurrences in metasediments from the Bamble amphibolite-to-granulite facies transition zone (South Norway); possible evidence for localized action of saline fluids. Journal of Geology, 106(5): 575-590.

Nijland, T.G. and Visser, D., 1995. The provenance of Bamble amphibolites, Norway. Proceedings of the Koninklijke Nederlandse Akademie Van Wetenschappen-Biological Chemical Geological Physical and Medical Sciences, 98(1): 69-88.

Oberti, R., Ungaretti, L., Cannillo, E. and Hawthorne, F.C., 1993. The mechanism of Cl incorporation in amphibole. American Mineralogist, 78(7-8): 746-752.

Postelmann, A., 1937. Die ursache der Blaufärbung gensteinbildender Quarze. Neues Jahrbuch fuer Mineralogie Abhandlungen, 72A: 401-440.

Shannon, R.D., 1976. Revised Effective Ionic-Radii and Systematic Studies of Interatomic Distances in Halides and Chalcogenides. Acta Crystallographica Section A, 32: 751-767.

Smalley, P.C., Field, D., Lamb, R.C. and Clough, P.W.L., 1983. Rare earth, Th-Hf-Ta and large-ion lithophile element variations in metabasites from the Proterozoic amphibolite-granulite transition zone at Arendal, South Norway. Earth Planet Scientiffic Letters, 63: 446-458.

Sørensen, B.E. and Larsen, R.B., 2007a. Paper1: Fluid induced multistage recrystallisation microstructures in quartzites and quartz veins from the Bamble shear zone complex. In: B.E. Sørensen (Editor), Metamorphic refinement of quartz under influence of fluids during exhumation with reference to the metamorphic/metasomatic evolution observed in amphibolites - a detailed field, microtectonic and geochemical study from the Bamble sector, South Norway. PhD Thesis, Department of Geology and Mineral Resources Engineering, NTNU Trondheim.

Sørensen, B.E. and Larsen, R.B., 2007b. Paper2: The fluid evolution of the Froland area in the Bamble sector from peak P-T through cooling and uplift: implications for retrograde mineral paragenesis and PT evolution of the Bamble sector. In: B.E. Sørensen (Editor), Metamorphic refinement of quartz under influence of fluids during exhumation with reference to the metamorphic/metasomatic evolution observed in amphibolites - a detailed field, microtectonic and geochemical study from the Bamble sector, South Norway. PhD Thesis, Department of Geology and Mineral Resources Engineering, NTNU Trondheim.

Sørensen, B.E., Larsen, R.B. and Austrheim, H., 2007. Paper3: Metasomatic evolution of the Froland amphibolites during cooling and uplift - textural observations and geochemical evolution of hydrous minerals. In: B.E. Sørensen (Editor), Metamorphic refinement of quartz under influence of fluids during exhumation with reference to the metamorphic/metasomatic evolution observed in amphibolites - a

detailed field, microtectonic and geochemical study from the Bamble sector, South Norway. PhD Thesis, Department of Geology and Mineral Resources Engineering, NTNU Trondheim.
Starmer, I.C., 1985. The evolution of the South Norwegian Proterozoic as revealed by major and mega-tectonics of the Kongsberg and Bamble sectors. In: J.L.R. Touret and A.C. Tobi (Editors), The deep Proterozoic crust of the North Atlantic Provinces. Reidel, Dordrecht, pp. 259-290.
Starmer, I.C., 1987. The geological map of the Bamble sector, South Norway, The geology of southernmost Norway: A geological excursion guide with thematic articles prepared for the NATO advanced study institute. Special Publication Geological Survey of Norway, pp. 25.
Starmer, I.C., 1991. The proterozoic evolution of the Bamble sector, Southern Norway; correlation across southern Scandinavia and the Grenvillian controversy. Precambrain Research, 49: 107-139.
Starmer, I.C., 1993. The Sweconorwegian orogeny in southern Norway, relative to deep crustal structures and events in the North Atlantic Proterozoic supercontinent. Norsk Geologisk Tidsskrift, 73: 109-132.
Starmer, I.C., 1996. Accretion, rifting, rotation and collision in the North Atlantic supercontinent, 1700-950 Ma. In: Precambrain crustal evolution in the North Atlantic Region. Geological Society of London Special Publications, 112: 219-248.
Touret, J., 1968. The Precambrian metamorphic rocks around the Lake Vegår (Aust-Agder, southern Norway). Norges Geologiske Undersøkelse, 257, 45 pp.
Touret, J., 1971. Le faciès granulite en Norvège méridionale II Les inclusions fluides. Lithos, 4: 423-436.
Touret, J., 1972. Le faciès granulite en Norvège méridionale et Les inclusions fluides. . Sci. Terre 17: 179-193.
Touret, J., 1985. Fluid regime in southern Norway: the record of fluid inclusions. In: A.C. Tobi and J. Touret (Editors), The deep Proterozoic crust in the North Atlantic Provinces NATO ASI Ser. Ser. C: Math. Phys. Sci., pp. 517-549.
Touret, J. and Olsen, S.N., 1985. Fluid inclusions in migmatites. In: J.R. Ashworth (Editor), Migmatites. Shiva, Glasgow, pp. 265-288.
Van den Kerkhof, A.M., Kreulen, R. and Touret, J.L.R., 1994. Juvenile CO_2 in enderbites of Tromøy near Arendal, southern Norway: a fluid inclusion and stable isotope study. Journal of Metamorphic Geology, 12: 301-310.
Van den Kerkhof, A.M., Kronz, A., Simon, K. and Scherer, T., 2004. Fluid-controlled quartz recovery in granulite as revealed by

cathodoluminescence and trace element analysis; Bamble sector, Norway. Contributions to Mineralogy and Petrology, 146(5): 637-652.

Visser, D., Nijland, T.G., Lieftink, D.J. and Maijer, C., 1999. The occurrence of preiswerkite in a tourmaline-biotite-scapolite rock from Blengsvatn, Norway. American Mineralogist, 84(5-6): 977-982.

Vultée, J.V. and Lietz, J., 1956. Über die rolle des titans als färbungsursache von blau- und rosenquarzen. Neues Jahrbuch fuer Mineralogie Monatshefte, 3: 49-58.

Wark, D. and Watson, E.B., 2006. TitaniQ: a titanium-in-quartz geothermometer Contributions to Mineralogy and Petrology, 152(6): 743-754.

Weil, J.A., 1984. A review of electron-spin spectroscopy and Its application to the study of paramagnetic defects in crystalline quartz. Physics and Chemistry of Minerals, 10(4): 149-165.

Weil, J.A., 1993. A review of the EPR spectroscopy of the point defects in α-quartz: the decade 1982-1992. In: C.R. Helms and B.E. Deal (Editors), Physics and chemistry of SiO_2 and the Si-SiO_2 interface 2. Plenum Press, New York, pp. 131-144.

Zhu, C. and Sverjensky, D.A., 1991. Partitioning of F-Cl-OH between minerals and hydrothermal fluids. Geochimica Et Cosmochimica Acta, 55(7): 1837-1858.

Zolensky, M.E., Sylvester, P.J. and Paces, J.B., 1988. Origin and significance of blue coloration in quartz from Llano Rhyolite (Llanite), North-Central Llano County, Texas. American Mineralogist, 73(3-4): 313-323.

Paper 1: Fluid induced multistage recrystallisation microstructures in Quartzites and Quartz veins from the Bamble shear zone complex

Bjørn Eske Sørensen
Department of Geology and Mineral Resources Engineering, Norwegian University of Science and Technology (NTNU), N7491 Trondheim, Norway
(bjorn.sorensen@ntnu.no)

Rune Berg Larsen
Department of Geology and Mineral Resources Engineering, Norwegian University of Science and Technology (NTNU), N7491 Trondheim, Norway
(rune.larsen@ntnu.no)

Abstract

The Bamble sector contains abundant coarse-grained quartzites that experienced Sveconorwegian high grade metamorphism. This study concerns quartzites from the Nidelva Quartzite Complex close to Blakstad. Static high grade textures formed at peak conditions (750°C/6-7 kbar (Nijland and Maijer, 1993)), are cut by younger localized high-grade shear zones with mm-sized amoeboid quartz grains. Localized retrogression related to the formation of white mica occurs throughout the area, typically related to mm-thin fault zones with adjacent SGR (subgrain rotation recrystallisation) causing a reduction in grain size (50-200 microns)

Four quartz types were defined with the SEM-CL technique:

Qz1: Bright islands demarcated by darker cracks. Typically they are partially luminescence quenched. The bright islands in Qz1 relate to the high grade history of the area, but the cracks relate to retrogression and formation of Qz2 (next).

Qz2: Light grey, sometimes featuring weak oscillatory zonation. Qz2 has brighter cores and darker rims approaching the luminescence of Qz3. The formation of the island texture in Qz1 and Qz2 are probably related, since Qz2 and the cracks in Qz1 has the same luminescence.

Qz3: Dark grey diffuse fluid channel textures, which follow grain boundaries or intersect grains. Qz3 relates to alteration of biotite to muscovite and SGR in narrow fault zones.

Qz4: Narrow cracks and pods of black quartz, intersecting all other qz-types.

Fluid inclusions related to Qz1, Qz2 and Qz3 are absent or very tiny in the quartzites, but quartz veins in amphibolite carry fluid inclusions that may be related to the same

quartz types as those found in the quartzites. The fluids follow the textural evolution of quartz. Qz1 relates to CO_2 rich LV fluids, Qz2 to potassic alteration of amphibolite and coexisting low salinity CO_2-rich H_2O-CO_2 and brine CO_2-H_2O-(Na,K)Cl LV fluids. Qz3 relates to brine (Na,Ca)Cl-H_2O LVS fluids and scapolitisation of amphibolite (see paper 2, Sørensen and Larsen, 2007).

Trace element contents in quartz measured by LA-HR-ICP-MS relate both to the textural and fluid evolution. Qz1 is enriched in B, Al and Ti when compared with the other types. Qz2 has low Al contents (<50 ppm) but variable Ti contents in quartz veins in amphibolite (210-10 ppm) due to inclusions of rutile needles and more consistent values in quartzites (peak value 32 ppm). Qz3 has Ti< 5 ppm and Al contents below 10 ppm and low B.

The textural and chemical evolution of quartz is explained by two major influxes of aqueous fluids during regional uplift and retrogression. They caused recrystallisation in the otherwise dry high grade quartzites. The first introduction of aqueous fluids was associated with brecciation of the high grade quartz (Qz1) and dissolution/precipitation of quartz (Qz2). Ti in quartz thermometry (Wark and Watson, 2006) of this stage gives 626°C in agreement with a retrograde PT-path deduced from phase diagrams (paper 2, Sørensen and Larsen, 2007). During subsequent deformation, Qz2 deformed more plastically than Qz1, probably due to an increase in the H_2O fugacity. Later fluid influx, related to scapolitisation of amphibolite was associated with localized recrystallisation (Qz3) and alteration of biotite to muscovite. During subsequent deformation, Qz3 deformed plastically and recovered by SGR, resulting in a reduction of grain size, whereas Qz1 quartz formed micro faults. Qz2 was plastic but did not experience SGR to the same degree as Qz3 quartz. Increased plasticity and recovery rates most likely relate to an increased water/rock ratio as also documented by fluid inclusions (paper 2, Sørensen and Larsen, 2007). However atomic lattice distortion by trace elements may also obstruct dislocation climb hence recovery and strain softening processes.

Key words:

Fluid migration patterns, shear zone fluids, quartz, retrograde recrystallisation of quartz, high purity quartz, metasomatism, Ti-mobilization, Hydrolytic weakening, scapolitisation, biotite-alteration, rose quartz, dumortierite

1 Introduction

The purpose of the current study was to improve the understanding of the retrograde behaviour of high grade quartz and quartzites, under the influence of infiltrating fluids and shear zone deformation. Furthermore, to study if quartzitic lithologies, due to their relatively simple chemistry and high preservation rate, may provide new information on fluid migration and regional mass balance properties during shear zone processes. Both chemical and rheological aspects were considered. In the literature a connection

between shear zones, fluids and regional mass transfer was often suggested, particularly in connection with auriferous ore deposits (e.g. Cameron, 1993; Cameron et al., 1993; Colivine et al., 1984; Groves et al., 1992; McCuaig and Kerrich, 1998; Nesbit and Muehlenbachs, 1989; Nesbit et al., 1986; Sibson et al., 1988). However the properties of fluid migration patterns are normally not explained in satisfactory detail.

In this paper we present documentation of fluid migration and fluid induced multi stage recrystallisation in quartzites from the Bamble sector. This mega shear zone is well known for its regional fluid infiltration phenomena, a process which is particularly well described for the early high grade part of the history (see geological setting in the next section.). In classic metamorphic petrology studies, quartzites are normally excluded, because they usually lack metamorphic index assemblages. However quartzite features some unique abilities that are not common in other metamorphic lithologies. Because quartzites comprise almost pure SiO_2 small proportions of added or removed material are easily recorded, for example in new mineral assemblages. Secondly quartz, the main mineral in quartzites is a good preservative for paleofluids in fluid inclusions, and is used to investigate fluids in many silica saturated rocks. Furthermore, quartz is stable throughout most crustal conditions whereas other minerals are stabilised/destabilised according to their thermodynamic properties. Accordingly early metamorphic/metasomatic events that are lost to decomposition of the index minerals may very well be preserved by remnants of quartz. Finally, quartz is an important commodity in the production of silica glasses and silicon product including high purity solar cell silicon that is currently in high demand by the world marked. The current study throws new light of natural refinement processes promoting the genesis of high purity quartz in the nature.

Our study relies on SEM-CL to interpret the complex recrystallisation behaviour observed in quartzites, quartz rich gneisses and quartz veins from the Bamble sector. The aim is to understand the parameters that control rheological and chemical behaviour of quartz during uplift and to understand their effects on lithological properties. SEM-CL has the advantage that it is imaging defect structures. However the intensity of the SEM-CL signal alone does not give direct evidence of the trace element concentrations because the CL signal reflects structural defects and not all defects are related to trace elements.

2 Previous work

Under upper crustal conditions, quartzites are some of the softest rocks in the continental crust hence acting as decollement zones during tectonic events (e.g. Tullis, 2002). However, contrary to the results of numerous quartz deformation experiments (e.g. Griggs and Blacic, 1965; Kronenberg, 1994; Kronenberg et al., 1986; Post and Tullis, 1998) it is often neglected, that different quartz types has different rheological properties. Tullis and Yund (1989) and Post et al. (1996) studied the effects of water and pressure on the recovery rate in deforming quartz aggregates and found a good

correlation between f_{H_2O} and the lowering of plastic strength. Post et al. (1996) evaluated several parameters in their experiments (a_{H^+}, f_{H_2O}; a_{OH^-}) and concluded that only H_2O had significant effects on creep strength as well as annealing rate. Both strain induced grain boundary migration and dislocation climb is enhanced by H_2O. Thus H_2O promotes recrystallisation accommodated dislocation creep as well as climb accommodated creep (Post et al., 1996). Kohlstedt and co-workers (1995) suggested the following formulation of the effect of H_2O in the flow law of quartz:

$$\dot{\varepsilon} = A\sigma^n f_{H_2O}{}^m e^{-(Q/RT)}$$

At constant strain rate and temperature the f_{H_2O} exponent can be determined from

$$\frac{d\log\sigma}{d\log(f_{H_2O})} = -\frac{m}{n}$$

$\dot{\varepsilon}$ is the strain rate, A a material constant, σ the differential stress, Q the activation energy, R the gas constant, T the temperature in K, m the f_{H_2O} fugacity exponent and n is the stress exponent.

The reliability of this expression was confirmed by Post and co-workers (1996), though the m exponent should be determined in steady state creep with free H_2O present and one deformation mechanism must dominate. Therefore, uncertainties may be introduced because the H_2O fugacity also increase climb rates significantly, causing deformation mechanism to change e.g. from dislocation glide to dislocation creep (Post and Tullis, 1998).

The rate of H_2O incorporation into quartz from a coexisting fluid is approximately an order of magnitude larger than the experimentally determined rate of oxygen diffusion (Post and Tullis, 1998). By assuming that the grain boundary diffusion is infinite Post & Tullis (1998) simulated the number of years it would take different grain sizes to re-equilibrate with the ambient H_2O fugacity. Their results imply that all grain sizes from 10 microns to 1 mm would re-equilibrate within 1 Ma at T>450°C, whereas at 300-350°C large grain sizes would require re-equilibration times >100 Ma., i.e. much longer than normally assumed residence times during uplift. Accordingly, in amphibolite facies, if fluids are present, quartzites should re-equilibrate at the cm-dm scale with the ambient water fugacity within some millions of years whereas quartzites, in the greenshist facies, would only re-equilibrate at the micrometer scale in the same time span. Because fluids migrate in pulses in the crust they are not residing throughout the metamorphic history. Accordingly, rocks in the amphibolite facies may be in disequilibrium at ambient H_2O fugacity.

The experimental results on hydrolytic weakening in quartzites correlate well with observations in natural quartz tectonites. Muto and co-workers (2004) showed that there was a good correlation between decreasing grain size in quartz in a natural shear zone and molecular H_2O, SiOH and SiH groups. The relation between H_2O fugacity and recrystallisation is complex. Muto and co-workers (2005), however, found that the

integrated H_2O IR spectra dropped along with increasing shear strain and recrystallisation in a high strain shear zone. This drop in the water content followed a drop in the SEM-CL intensity. It was concluded that dynamic recrystallisation lead to the removal of H_2O from quartz and that the main luminescence in the quartz comes from H_2O related defects (Muto et al., 2005). However numerous studies document a relation between CL and trace elements other than water in quartz hence contradicting the conclusions of Muto (2005) (e.g. .Goetze, 2000; Goetze et al., 2004; Goetze et al., 2005; Goetze et al., 2001; Müller et al., 2003). In these studies, colour CL and spectroscopy is used in combination with other analytical techniques documenting defect centres in the quartz lattice via e.g. EPR (electron paramagnetic resonance) and comparing with CL-spectra recorded under controlled conditions.

Landtwing and Pettke (2005) documented a positive correlation between TE content in hydrothermal quartz and the intensity in grey scale SEM-CL images. Van den Kerkhof et al (2004), documented fluid related recovery by SEM-CL imaging and spectroscopy in dispersed veins in enderbitic charnokite in the proximity of the area addressed in our study. They found a correlation between a drop in luminescence and mainly Ti-defects in the quartz.

3 Geological setting

The Bamble sector comprises exceptionally well preserved high grade amphibolite-granulite facies rocks. Most authors agree that the peak PT-conditions were approximately 850 °C in the HT granulite facies zone at Arendal, and tapering towards lower T in a thermal dome pattern (Figure 1). Peak P conditions were roughly 6-7 kb.

Fluid inclusion studies documented CO_2 dominated fluids in amphibolite lithologies, and CO_2 + brines in more siliceous gneisses (Touret, 1971). This COH fluid composition is matched by fluid modelling using the iron-titanium oxygen barometer (Harlov, 2000). The conditions during exhumation are far less constrained although the absence of retrograde aluminous silicate assemblages imply high alkali-chloride activities in the retrograde fluids (Touret, 1968). Knudsen (1996) summarise the available retrograde PT-paths of the Bamble sector and conclude that the PT-paths display systematic spatial variations characterised by a steep retrograde path in the southernmost part (Knudsen, 1996), followed by isobaric cooling in the southeast and a slight pressure increase in the north. However, it is also concluded that the P-T estimates are uncertain.

Sørensen and Larsen (2007, paper 2) used their observations in calc-silicate rocks along with fluid inclusion data and mineral paragenetic data of Nijland and co-workers (1993a) to redefine the cooling and uplift path of the Froland area. Their results imply a four stage PT-X_{fluid} cooling and uplift path:

1. Approximately at 626°C and 7 kb. The total fluid composition for this stage is in mole fractions: $XCO_2 = 0.30$, $XH_2O = 0.62$, $XNaCl = 0.08$ (30 wt% NaCl in the aqueous phase). Because sanidine + tremolite is not replaced by phlogopite + calcite

+ quartz during cooling and uplift it is inferred that XCO_2 decreased rapidly with falling temperatures.

2. Sørensen and Larsen (2007, paper 2) infer a shift from potassic-sodic and sodic-calcic alteration based on the assemblages documented by (Nijland et al., 1993a). MII (kyanite-chlorite-muscovite veins) and MIII (margarite + corundum) of (Nijland et al., 1993a) have overlapping PT stability fields. Both are alteration products of an assemblage originally comprising corundum + plagioclase. MII muscovite was stabilised by potassium rich fluids. Decreased potassium content/increased calcium content of the fluid stabilised margarite over muscovite and formed the margarite + corundum assemblage. P-T conditions of MII represent a relatively narrow temperature field from 450 to 550°C. Pressure is constrained by the stability of kyanite which defines the lower pressure limit to 4.5 kb.
3: The uplift path is constrained by the isochore of fluid inclusions in quartz (FIA3 of Sørensen and Larsen, (2007, paper 2). The well preserved fluid inclusions suggest an uplift path that was sub parallel with the isochore. Uplift occurred at 300 to 400°C. Accordingly, the Froland lithologies experienced a P-drop from 5-7 kb to 2-3 kb at 100 °C lower T than the interpretation provided by Nijland et al. (1993a).
4: Post kinematic alteration during final cooling after exhumation, including vug assemblages comprising epidote-calcite-actinolite-pyrite (paper 2, Sørensen and Larsen, 2007) and coexisting prehnite-pumpelyite + fluid inclusions at 2-3 kb and 175-280°C (Nijland et al., 1993a; Touret and Olsen, 1985).

Fluid related alteration follows a rhombohedral net work of shear zones and faults, associated with exhumation and possibly also extensional collapse of the Sweconorwegian mountain range. Brine-rich fluid inclusions are documented together with the alteration assemblages (e.g. Nijland and Touret, 2001; Nijland et al., 1998; Sørensen and Larsen, 2007; Touret, 1985).

Quartzites and quartz rich gneisses are abundant in the Bamble sector. Most of the work on Quartz rich rocks is focused on sedimentary structures and chemistry and not the metamorphic recrystallisation. There are several compositional and textural types including very pure and coarse-grained quartzite, quartzo-feldspatic gneiss and nodular gneiss/quartzite. The quartztose rocks contain variable amounts of tourmaline. Layers of stratabound tourmaline are locally observed (Nijland et al., 1993b). Black tourmaline frequently occur on the more Al-rich cleavage planes ((Nijland et al., 1993b); this study). Red-brown transparent tourmaline (field colour, orange-red brown in thin section, Dravitic) occurs in layers and lenses in quartz microcline and oligoclase and biotite at Grendal Tjern (Nijland et al., 1993b) and at Trevann (This study). Black tourmaline (field colour, green-brown pleocroic in thin section Schorl-Dravite) also occur as reaction zones bordering quartz veins in quartzites together with biotite and muscovite. In addition black (Schorl rich) and brown (Drawite rich) tourmaline together with biotite defines the foliation in some mylonitic gneisses. Rare sedimentary structures occur in the Nidelva Quartzite Complex (NQC), and well documented cases of cross beddings, mud cracks, ripple marks and strongly deformed meta-conglomerates imply a sedimentary origin (Nijland et al., 1993b).

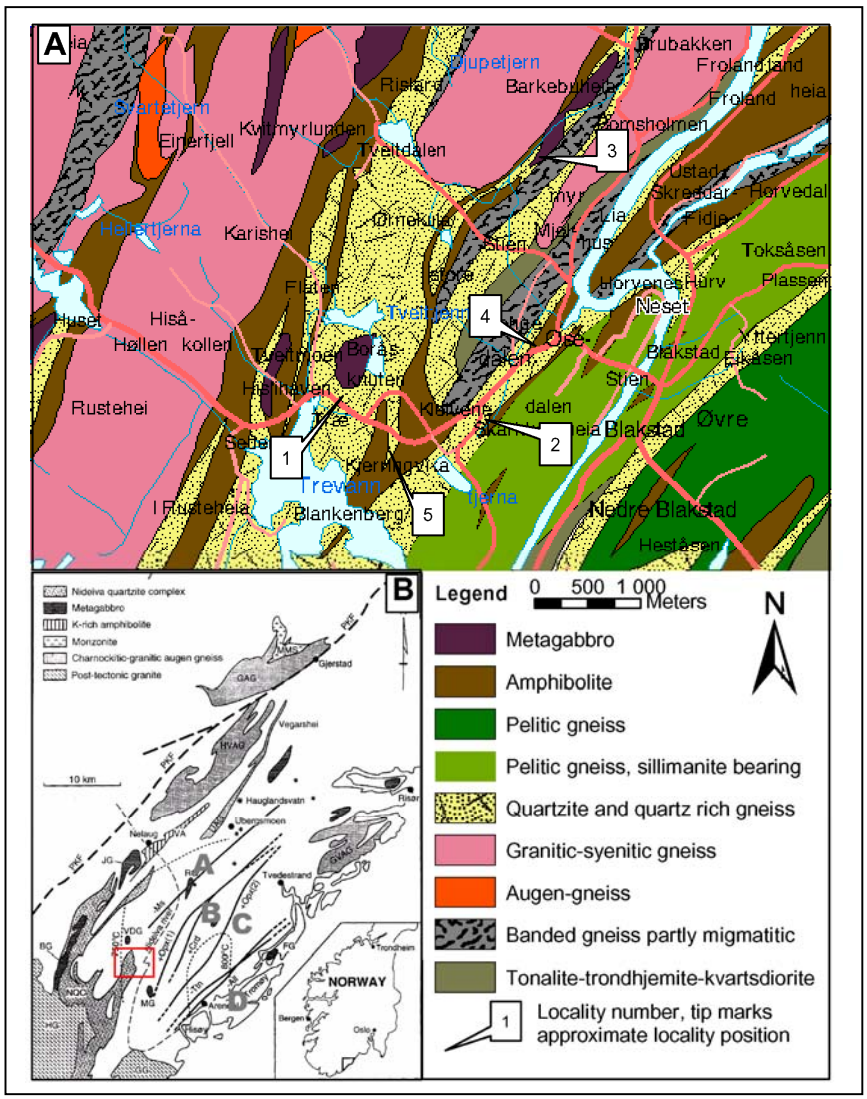

Figure 1: Geological maps. A) Detailed map of the investigated area. Modified from Geological Survey of Norway N-50 berggrunnskart 16123 Nelaug and 16114 Arendal. Geographic data (roads, lakes and rivers) are added for easy orientation (source: www.geonorge.no). B) Overview map of the Bamble sector displaying the most important rock units (see legend on map). Insert shows the position of the Bamble sector in South Norway. Red square denotes the position of the study area shown in A. From Nijland et al. (1998). Also shown in B are the metamorphic zones in the Bamble sector.

4 Methodology

4.1 Sample preparation

The textural relations between the different quartz types are typically found in a single hand specimen. Samples of quartzite, dominated by the individual texture types were also included, but samples displaying all types and textural relations were prioritised. Many samples were cut and polished roughly, before they were scanned on wet transparencies. Scanned pictures of rock slices of the selected hand specimens uncovered the timing and spatial relations between the different quartzite textures (see Figure 2 for an example). Based on these observations thin sections were prepared.

Thin and thick sections (for LA-ICP-MS) were prepared from the same block, in order to correlate common textures. Thick sections for LA-ICP-MS had to be 200 µm to accommodate the ablation craters for the ICP_MS analysis (up to 90 microns). Therefore, optical microstructures in the quartz were almost impossible to infer from the thick sections alone and were made in combination with observations in the thin sections. The quality of polishing is essential for the quality of SEM-CL imaging

4.2 SEM-CL methodology

SEM-CL was performed on a low vacuum SEM at the Department of Materials Sciences, NTNU. The luminescence signal was collected with a Robinson detector, giving a greyscale picture. Samples with much K-feldspar were avoided because high luminescence of the latter clouded the signal from quartz.

The absolute intensity could not be used as a criterion of distinction between quartz types because the contrast and intensity setting had to be changed continuously to enhance textural features. A mosaic of images was recovered and sampled in a single picture, in some cases covering the entire thin sections. In most cases the minimum working distance of 20 mm was chosen to achieve the best possible signal, but to take pictures at lower magnifications sometimes a working distance of 30 or 40 mm were used in combination with details from selected areas at 20 mm working distance. The acceleration voltage was also varied in order to optimise the image. For bigger working distances (20 or 40 mm) an acceleration voltage of 30 KV was optimal, whereas 15-25 KV was sufficient for working distance of 20 mm. Good polishing is essential to the quality of the SEM-CL imaging, and it is important that epoxy filled cavities are as few as possible because some epoxy types are strongly luminescent.

Several hundred SEM-CL pictures were investigated. The results included here characterize textures and relations that are general for all the investigated samples.

After definition of the different quartz types by greyscale SEM-CL some good quality CL-spectra of the main quartz types were achieved at the Department of Geology, University of Oslo, using a Mono-CL. Intensity was adjusted to a certain amount of counts per second (8000-9000), so the total intensity of the spectra can not be correlated with the trace element content. The relative intensity of the peaks does, however, give important additional information on the defect structure of the quartz.

4.3 LA-ICP-MS

The analyses of quartz were accomplished with a standard, double focusing sector field, ICP-MS (Finnigan MAT, ELEMENT1) instrument with a CD-1 option from Finnigan MAT and with an UV-laser from Finnigan MAT/Spectrum, Berlin, Germany.

The following elements are included in the analytical package: Al, B, Ba, Be, Cr, Fe, Ge, K, Li, Mg, Mn, Na, P, Pb, Rb, Sr, Th, Ti, U. Where ^{7}Li, ^{9}Be, ^{11}B, ^{27}Al, ^{55}Mn, ^{74}Ge, ^{85}Rb, ^{88}Sr, ^{137}Ba, ^{208}Pb, ^{232}Th, and ^{238}U were analysed at low resolution ($m/\Delta m=300$); ^{23}Na, ^{31}P, ^{25}Mg, ^{47}Ti, ^{52}Cr, and ^{56}Fe at medium resolution ($m/\Delta m\approx3500$) and ^{39}K at high resolution ($m/\Delta m>8000$). The isotope ^{29}Si was used as internal standard at low resolution and ^{30}Si was used at medium and high resolution. External calibration was done by using the international standards: NIST612, NIST614, NIST616, BCS313/1(BAS), RGM-1(USGS), SRM1830, Blank SiO_2 and BAM no.1 SiO_2 (Federal Institute for Material Research and Testing, Berlin, Germany). Blank SiO_2 was used to constrain the detection limits (LOD). LOD for most of the elements are between 0.2 and 0.01 ppm. To improve the lower limit of quantification and the analytical uncertainty at low concentrations, it is important to have calibration curves with well-defined intercepts. Laser ablation was accomplished in raster measuring 200x200 μm or less on 200 μm thick quartz wafers. Detailed information about the analytical conditions, recalculation and statistical treatment of the data is described elsewhere (Flem et al., 2002).

The selection of sampling spots in quartzite quartz is complicated by the high density of inclusions, such as muscovite, rutile needles, silimanite, biotite tourmaline and dumortierite. This fact complicated the analysis and many samples could not be ablated although, in the end, an appropriate number of representative quartz types were sampled.

5 Results

5.1 Field observations and Sampling

5.1.1 Quartzites

Fieldwork was done in the Arendal area, South Norway. Sampling was based on five different quartzite textures that were defined in the field: 1. High grade static, 2. High grade mylonitic gneisses, 3.Greyish quartzites, 4. Quartz muscovite veins, 5. Micro-faults *(*Table 1 *below)*

Table 1: Classification of quartz textures observed in the field

Type	Quartzite texture	Description
1	*High grade static*	Blue coarse-grained quartzite. Weakly foliated, Biotite SPO weak to absent, banding between dusty blue/whitish/purple quartz. The associated mineralogy typically comprise Quartz ± Bt± Kfs± Mt± Ilm/Hem and fibrolitic silimanite.
2	*High grade mylonitic gneisses*	Mm-sized amoeboid quartz grains, including grains of biotite ± Tourmaline, which define a continuous foliation
3	*Greyish quartzites*	*Greyish quartzites* with static textures
4	*Quartz muscovite veins*	Veins consisting of quartz and muscovite cutting through textures 1 and 2.
5	*Micro-faults*	separated by zones not affected by the retrogression and with blue type 1 quartzite lenses, crosscutting all other features except for late brittle cracks

Some of the quartzites appear pure and massive whereas more impure quartzites, show banding and lenticular structures. The mineralogy of the quartzites varies between K-feldspar-rich and biotite-rich parts. The content of other minerals than quartz also varies considerably. In effect more pure quartzites are coarser grained than impure varieties. In some places the quartzites feature a distinctively banded appearance, with cleavage domains rich in fibrolite and with white mica defining a disjunctive cleavage intersecting microlithons of quartz and biotite (Figure 2). The number of micro faults is generally higher in the cleavage domains. This may suggest that there is a genetic relation between the formation of the cleavage domains and the microfaults. However detailed field evidence document that the mineralogical variation between the quartzite matrix and the cleavage domains originates from pre-kinematic chemical variations. This is demonstrated by the transition between nodular quartzite and banded quartzite, which involves gradual shearing out of the nodules in the nodular quartzite to bands (Figure 2). The lensoid shape is usually completely obliterated (i.e. sheared out) in XZ sections (sections cut parallel to the lineation and perpendicular to the foliation), but subparallel to oblique in YZ sections (sections cut perpendicular to lineation and foliation) (Figure 2). In most samples they are oriented parallel with the foliation, but occasionally they are inclined to the foliation at a small angle (Figure 2).

The quartzites along the Frolands Verk road profile (locality 1, see Figure 1) are generally very coarse-grained, and have a bluish tint. Their purity varies significantly on m-dm scale between 99% quartz and 79-80% quartz. The main structural feature is narrow (mm-cm thick) cataclastic bands locally featuring a greenish colour probably

caused by micas. The mineral assemblage of the quartzites comprises variable amounts of microcline, biotite, and muscovite.

Biotite is normally present, either fresh or decomposed to a reddish alteration product or to muscovite. High–grade shear zones are common and in some cases may have a mineral assemblage comprising tourmaline and biotite.

Both static and dynamic high grade fabrics are cut by narrow faults predominantly cataclastic fault zones, with only limited dynamic recrystallisation of quartz.

The quartzites at Ovelands heia (locality 2, see figure 1) are generally more impure than the quartzites from locality 1. In fact the term quartzites only partially apply because the quartz content is usually to low (70-95%). The microcline content is considerably lower than at locality 1, whereas the biotite concentration is much higher. Accordingly the name quartz-biotite gneiss is preferred throughout this study. The quartz-biotite gneisses frequently have a banded appearance at locality 2 and more nodular textures are also found, gradually being sheared into bands (Figure 2). Similar textures are seen at locality 1 but are less common. Both bands and nodules are biotite free but rich in muscovite, and fibrolitic silimanite. More quartz rich parts are coarser grained and more bluish. On fresh surfaces local variations between bluish and more greyish quartz are observed (Figure 2). As with locality 1, there is a close relationship between an increase in grain size and purity of the quartzites.

At locality 2, centimetre- to metre scale en echelon quartz veins (see Figure 1) are surrounded by reaction zones of tourmaline, biotite and green muscovite (Figure 3). Gradual transitions from biotite tourmaline to muscovite tourmaline assemblages in the field and atoll textures of biotite within new muscovite grains document that the muscovite formed later at the expense of the biotite (Figure 3). Muscovite bearing quartz veins are also common and may be clearly distinguished from the former type. They occur at a much smaller scale (mm- to cm with) and form finger like structures.

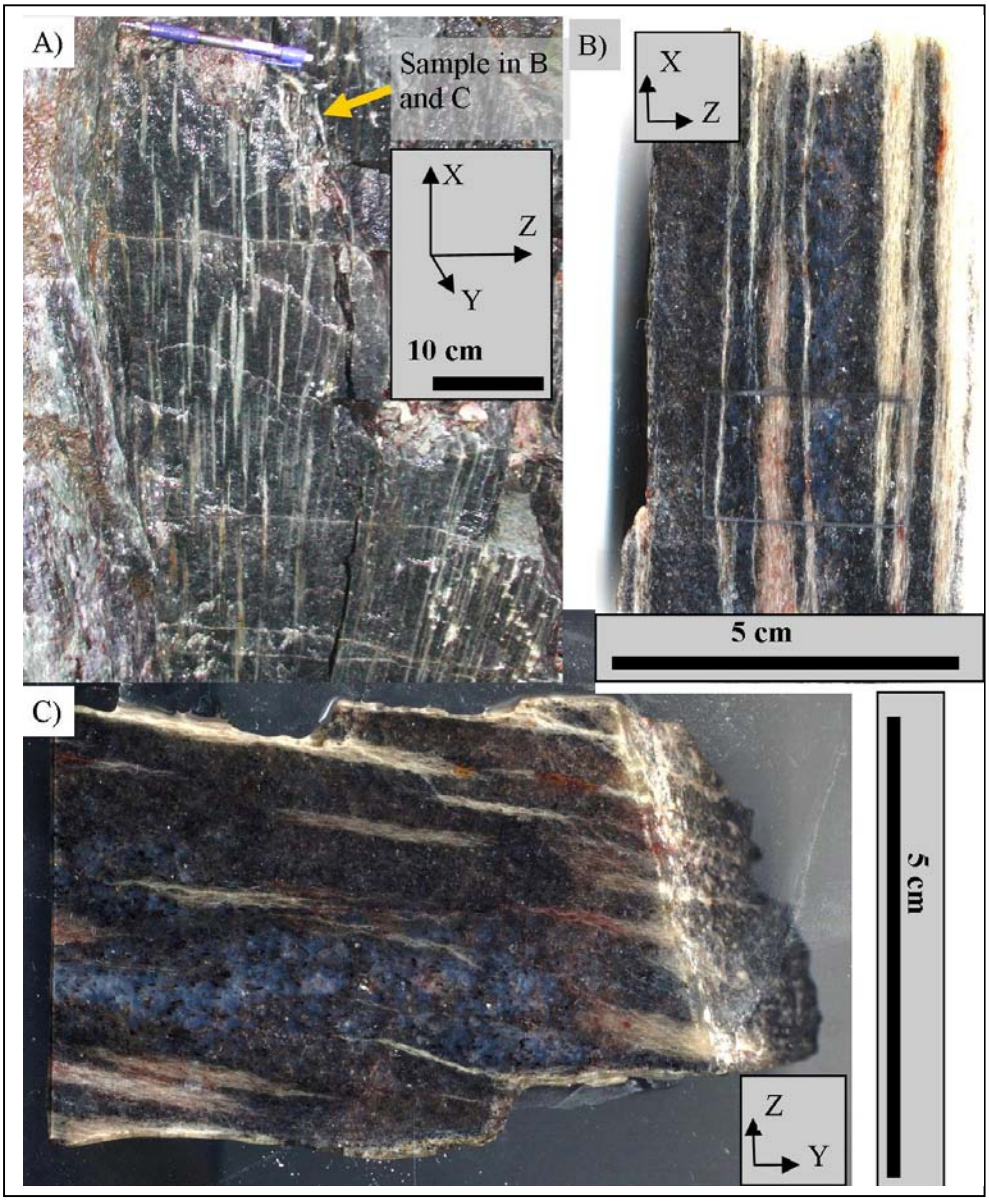

Figure 2: Transition from nodular to banded quartz-mica gneiss from locality 2. A) Field outcrop. Note the gradual change from lenticular structures (nodules) to the left to bands to the right. B) XZ section showing elongated lensoid structures, traces of the lensoid structures mostly parallel to foliation in sections of this orientation. C) ZY section showing the obliqueness of the lensoid structures with respect to the foliation (horizontal in picture). Note that the light coloured bands are present in both the greyish and the more bluish part of the quartz mica gneiss

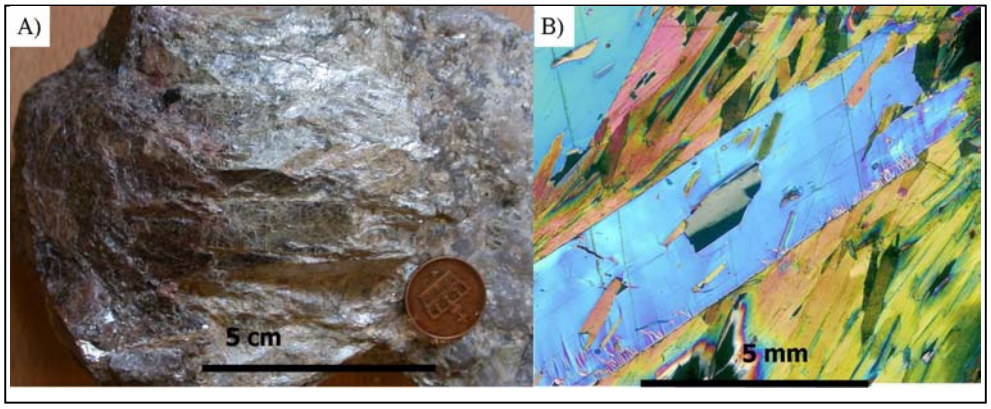

Figure 3: Alteration of biotite tourmaline reaction zone in quartz-mica gneiss at locality 2. A) Hand specimen displaying brown zone of biotite and tourmaline, altered to muscovite and tourmaline in the middle, closest to the contact with the quartz-mica gneiss (rightmost part of picture). B) Thin section image, polarized light, showing muscovite (blue) replacing biotite (greenish to pink). Note the atoll texture with biotite grains engulfed in a large grain of muscovite.

5.1.2 Quartz in amphibolite

The quartz evolution observed in quartzites inspired for a comparative study of quartz veins associated with the alteration of amphibolite. This was done in order to establish the chronology and relationship of the quartz alteration relative to regional metamorphic and metasomatic events. Quartz veins related to peak metamorphic conditions as well as quartz veins related to retrograde alteration were studied.

5.1.2.1 Quartz occurrences related to prograde metamorphism

Rose quartz veins and garnet quartz symplectites are common in amphibolites but are particularly well preserved at the Skytebanen locality (locality 3).

The rose quartz veins featuring shades of pink, violet and blue, are exposed in amphibolitised gabbro (Figure 8). They are in equilibrium with the prograde metamorphic assemblage in the amphibolites, including almandine rich garnet, tschermakitic hornblende and An_{30} plagioclase and ilmenite.

The garnet quartz symplectites occur in layers mostly comprising quartz, garnet and plagioclase intersecting the garnet amphibolite (see paper 3, Sørensen et al., 2007). Layers are boudinaged with pinches of plagioclase and quartz and swells of mainly garnet and bluish quartz.

5.1.2.2 Amphibolite alteration

En echelon quartz veins with reaction rims of biotite, black tourmaline apatite and actinolitic hornblende are commonly observed in amphibolite, but are especially well exposed at a road outcrop in Osedalen (locality 4).

At Heståsen (locality 5) the alteration phenomena in the amphibolites are particularly well displayed in relation to quartz veins. Three main types of amphibolite alteration were observed: 1. Potassic alteration with biotite introduced in the amphibolites, 2. Potassic alteration with K-feldspar replacing biotite, 3. Massive scapolitisation (Table 2). For more details on amphibolite alteration (see Sørensen et al., 2007, paper 3).

Table 2: Alteration types in amphibolite. From Sørensen and Larsen (2007, paper 2)

Alt1: Potassic alteration with biotite stable
Alt1a: Alteration of amphiboles associated with introduction of biotite. In thin sections amphibole cores are dark brownish green whereas rims vary from dark bluish green ferropargasite/ferrotschermakite (Amp3a) through light green magnesiohornblende (Amp3) to almost colourless actinolite (Amp4). **Alt1b:** Veins with a central assemblage comprising plagioclase, calcite, apatite, pyrrhotite, ilmenite/rutile and magnesiohornblende (Amp3). Surrounded by two successive alteration zones, the inner zone comprising amphibole, plagioclase and rutile/ilmenite and the outer zone comprising biotite, plagioclase and ilmenite/rutile. **Alt1c**: Alteration in relation to en-echelon quartz veins intersecting the foliation in the amphibolite. Alteration comprises biotite, amphibole and plagioclase and ilmenite. Alternating zonation with variation in the amount of biotite, plagioclase and amphibole. Ilmenite is partly replaced by titanite. **Alt1d**: biotite amphibole rock. Titanite most common, but ilmenite preserved as cores together with rutile. Similar to the alteration around the en-echelon quartz veins (Alt1c).
Alt2: Potassic alteration K-feldspar replacing plagioclase and biotite
Replacement of biotite by K-feldspar. Final alteration product is a light grey rock consisting of K-feldspar, and light green amphibole (Amp4). Titanite is very abundant in this rock type and almost no ilmenite/rutile is observed. Several types of replacements are seen replacing Alt1 assemblages.
Alt3: scapolitisation
Massive scapolitisation. Quartz veins surrounded by reaction rims of scapolite, but minor amounts of scapolite are also observed in many places in the amphibolite. The quartz veins with the reaction rim of scapolite have a different colouration than quartz veins with less scapolite. The scapolite has a white colour and is only distinguished from commonly occurring white feldspars by its characteristic cleavage.

5.2 SEM-CL/optical textures

Generally, four types of optical textures are observed in the quartzites. The coarse-grained quartzites with blue quartz typically show static textures, with undulose extinction being the only sign of deformation and with randomly oriented biotite. The high-grade quartzite textures are cut by high grade mylonitic gneisses with grain sizes of several mm's. These are again cut by lower grade cataclastic deformation and

occasionally subgrain rotation (SGR)-related deformation microstructures. The SGR relates to the formation of white mica and the breakdown of biotite to muscovite (Figure 5 and 6). Chess board textures are commonly observed in the more coarse-grained quartz, but are especially clear and well preserved in quartz veins in the amphibolites (Figure 10).

Four main types of quartz are defined by SEM-CL textures: Qz1: island channel texture, Qz2: light grey, Qz3 diffuse dark grey channels and Qz4: Narrow cracks and pods of non luminescent quartz (see Table 3 below and Figure 4).

Table 3: Quartz types defined by textures in SEM-CL images

Quartz type	Description
Qz1	Bright islands surrounded by darker cracks. Typically partially luminescence quenched.
Qz2	Light grey, sometimes with weak oscillatory zoning. Brighter cores and darker rims, approaching the luminescence of type 3.
Qz3	Dark grey diffuse fluid channel texture, which follows grain boundaries or cut through grains.
Qtz4	Narrow cracks and pods of black quartz, crosscutting the other types.

Fluid inclusions related to quartz types Qz1, Qz2 and Qz3 are absent in the quartzites, but occur in quartz veins in the amphibolites. These fluid inclusions were studied by Sørensen and Larsen (2007, paper 2) who defined a fluid evolution from CO_2 rich fluids (Qz1) through coexisting low salinity CO_2-rich H_2O-CO_2 fluids and eutectic salinity CO_2-H_2O-NaCl-KCl brines (Qz2) towards NaCl-$CaCl_2$-H_2O brines (Qz3) and ending with $CaCl_2$-H_2O fluids (calcite).

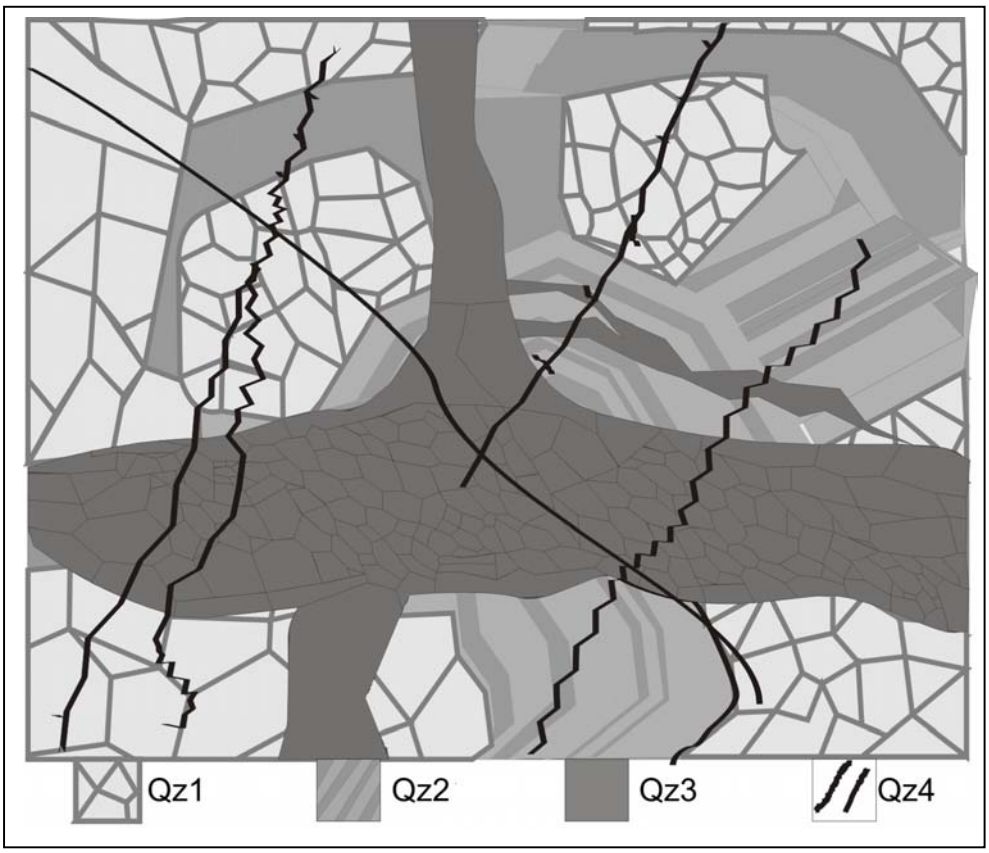

Figure 4: Schematic representation of the quartz textures observed in this study. See text and Table 3 for explanation.

5.2.1 Textural relations in quartzites

Generally there is a good correlation between the naked eye optical textures and the quartz evolution observed in the SEM-CL images. The coarse-grained bluish quartzites mainly consist of Qz1, whereas Qz2 dominates in the more greyish quartzites and in some mylonitic gneiss. Qz3 is the most rare quartz type and is typically related to localized SGR textures and alteration of biotite to muscovite,

Sample 03bes32 (Figure 5) demonstrates the relation between the quartz types and the transition from bluish quartzite to greyish quartzite (Figure 5). The more bluish part of the section is very coarse-grained. In the SEM-CL this corresponds to a mixture of (Qz1) and (Qz2). Of theses types, Qz2 dominate, followed by Qz1. Qz2-Qz2 grain boundaries are commonly straight with triple junctions, whereas Qz1-Qz2 grain boundaries are interlobate-lobate, with pinning, window, dragging and “left over grain”

microstructures (see e.g. Passchier and Trouw, 2005 for definition) implying the growth of Qz2 at the expense of Qz1 (Figure 5)

A distinct luminescence quenching (Qz3) affecting both Qz1 and Qz2 occurs where biotite grains are partly altered to muscovite, and inside quartz grains in channel like structures connecting muscovite grains (Figure 5). Biotite flanking these channels is partially or completely altered to poikiloblastic muscovite (Figure 5). Qz3 is also common next to sub-millimetre thin fault zones, where a smaller grain size is developed in Qz3 only. Qz1 is partially luminescence quenched, and based on luminescence, may be difficult to distinguish from Qz2. Preferably Qz1 and Qz2 are differentiated by recognition of the island channel texture. Notably the intensity of the CL-signal increase in Qz1 next to more deformed areas (Figure 5).

Alteration of ilmenite grains to rutile is seen in more coarse parts of the sample. The proportion of rutile formed at the expense of ilmenite correlates with the amount of Qz2 present (Figure 5). Locally weak SGR textures are observed, always in association with Qz3 (Figure 5).

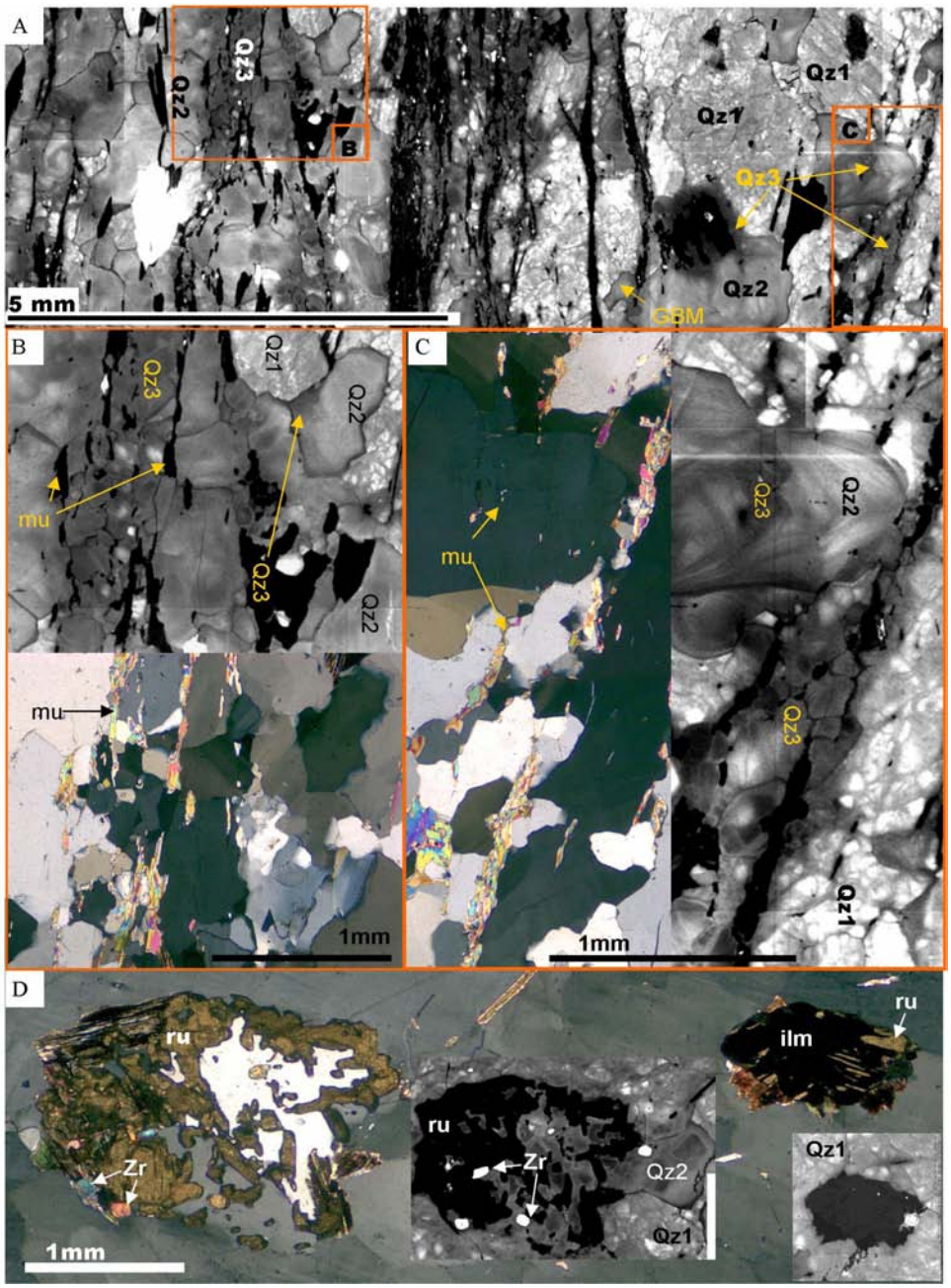

Figure 5: Optical and SEM-CL textures from 03bes32 (FRV-road profile, locality 1). A) Large scale SEM-Cl textures from part of 03bes32, showing relation between Qz1, Qz2 and Qz3. Note that the main proportion is Qz2. Note that Qz3 transects both types Qz1 and Qz2. B) Zoom on (A) and optical picture of the same area. Note the spatial

relationship to white mica, and grain size reduction of quartz in areas with Qz3. C) Zoom on (a). Qz3 cuts oscillatory zoning in Qz2 and relate to grain size reduction and formation of white mica. D) Ilmenite partly altered to rutile, most altered grain related to Qz2, whereas well preserved ilmenite grain relates to Qz1

In sample 03bes71, also from locality 1, the relations between Qz3 and deformation are better seen than in 03bes32, because the amount of Qz3 is larger. The sample was collected at the transition from coarse-grained bluish quartzite to pale quartzite with numerous narrow micro-faults (Figure 6). In the hand specimen, lenses of more bluish quartz occurs in strongly deformed and bleached domains (Figure 6). These domains are also recognized in optical and SEM-CL microscopy (Figure 6). Optically they are more coarse-grained and biotite is well preserved with only local alteration to muscovite. In the SEM-CL pictures it is evident that the coarse-grained lenses comprise Qz1 and Qz2. Places in the coarse-grained domains, where biotite is partly altered to muscovite are connected with luminescence quenching of Qz2 towards Qz3. Accordingly, both quartz types Qz1 and Qz2 coexist with biotite. Adjacent to the coarse-grained domains, the quartzites are more deformed in both cataclastic and plastic structures accompanied by dynamic recrystallisation dominated by SGR causing a reduction of the grain size to less than 200 microns and the formation of more polygonal grains, defining an oblique fabric, documenting a sinistral shear sense (Figure 6). This corresponds to relative upward movement of the SW block relative to the NE block in the direction of the oblique lineation observed in the field in agrrement with a N-S compressive stress-field. Deformation related to SGR textures continues as narrow cataclasite bands when entering other quartz types or disappear (Figure 6), suggesting different responses to deformation as a function of quartz types. The SEM-CL intensity of Qz1 increase towards zones where Qz3 is deformed by SGR compared to Qz1 in the less deformed areas.

In sample 04bes71 Qz3 is also common in coarse-grained parts of the sample as channel like structures commonly connecting grains of biotite that are partially altered to muscovite (Figure 6). Not only does the channel structures connect partially altered biotite grains, but the luminescence quenching textures also correlates with grain scale alteration textures in the individual biotite grains, such that biotite is exposed toward quartz types Qz1 and Qz2 whereas muscovite appear next to type 3 quartz (Figure 6).

Quartz muscovite veins are commonly observed. They are decussate with muscovite grains in a matrix of Qz3 (Figure 7). The formation of Qz3 in relation to the quartz muscovite veins is featured by sample 03bes103 (Figure 7). Dissolution of Qz1 relates to precipitation of Qz3 together with muscovite in veins fingering their way through the Qz1 and Qz2 matrix. Parallel cracks interpreted as microfaults are seen in a Qz1 grain (Figure 7). The microfaults are connected with luminescence quenching textures that tapers in to the quartz muscovite veins.

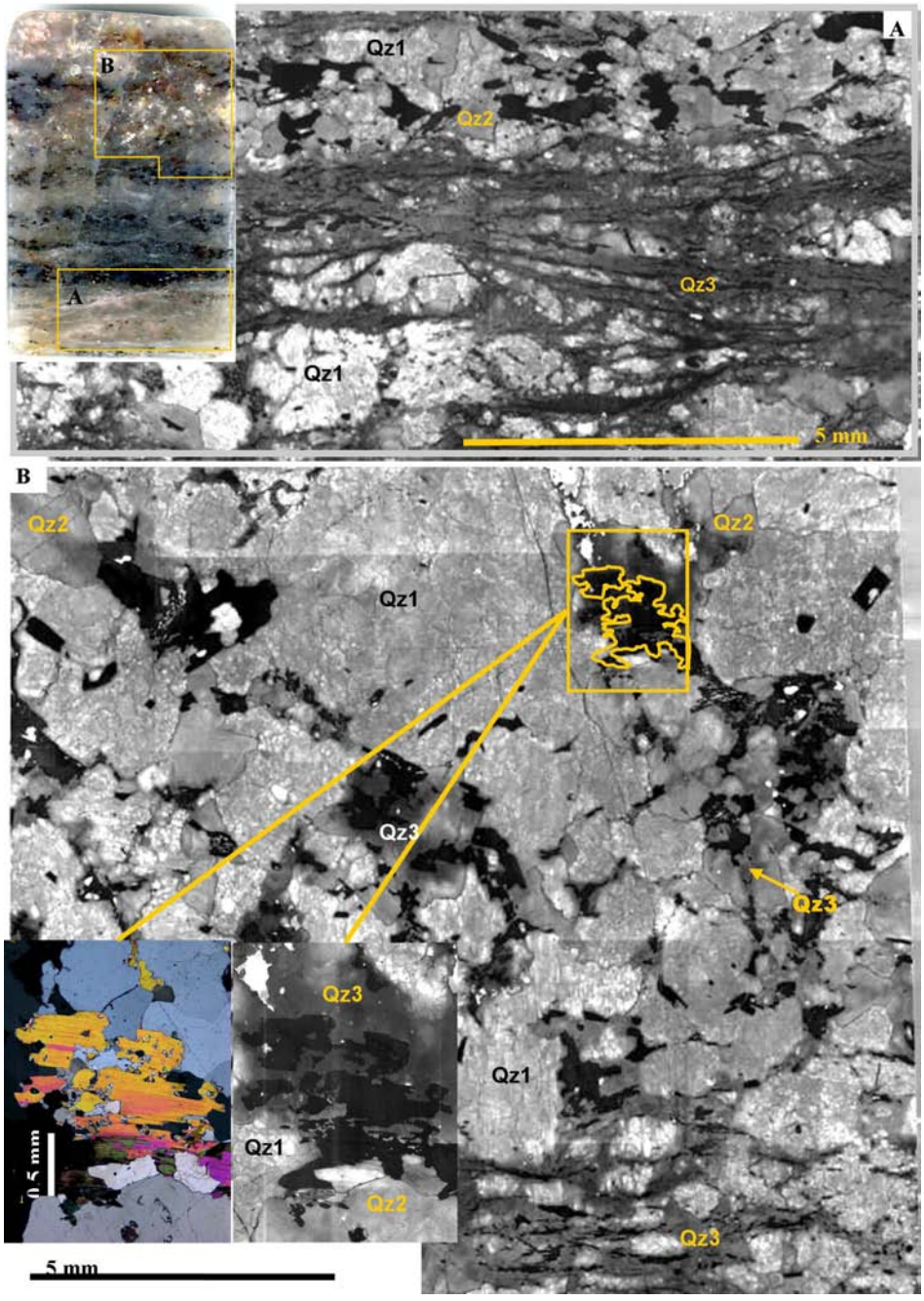

Figure 6: See caption on next page

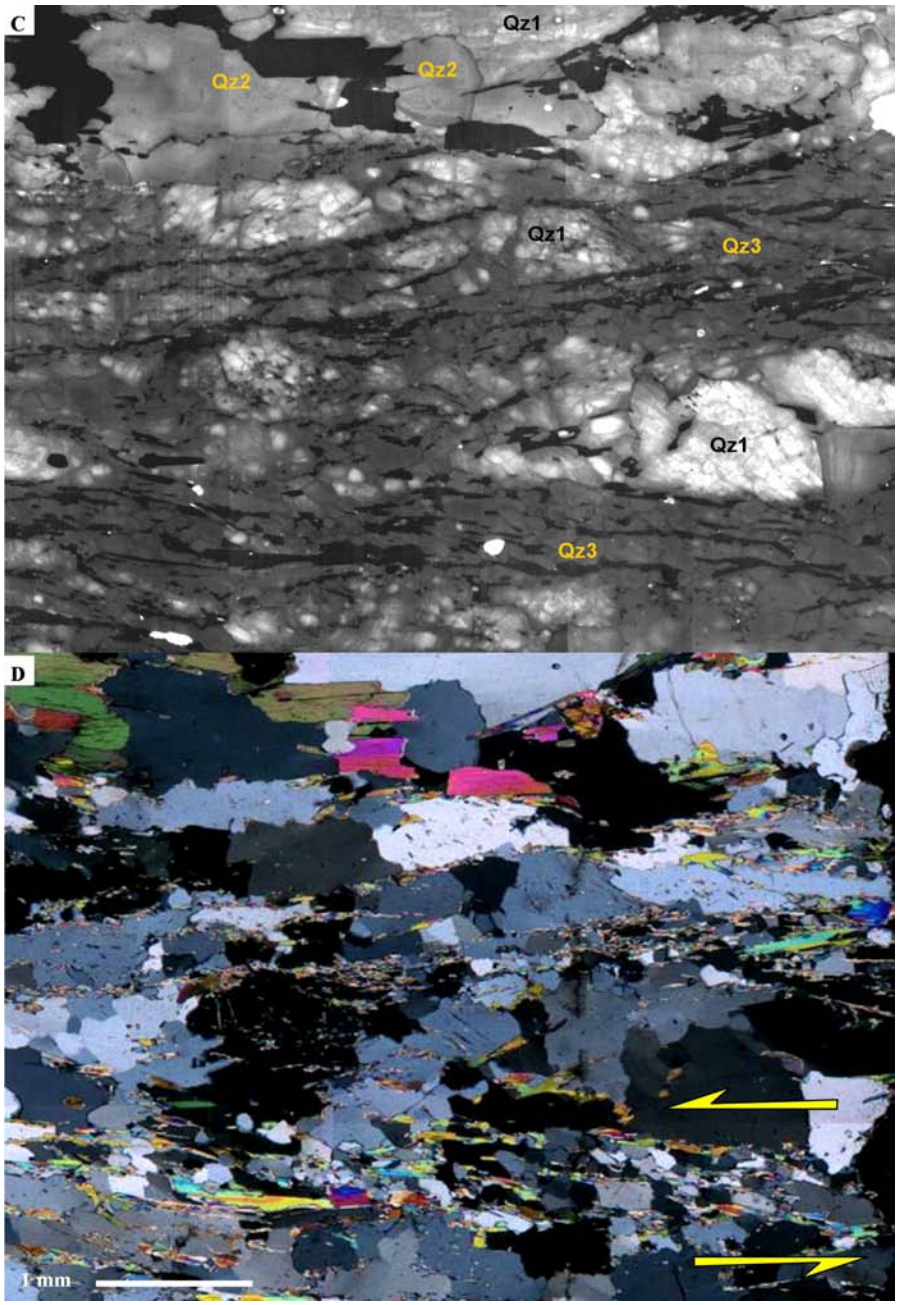

Figure 6: Optical and SEM-CL textures from 03bes71, insert shows the position of the large SEM-CL pictures (A &C) on the rock slab. Collected at locality 1, the FRV road profile A) Large SEM-CL picture of a deformed zone showing the distribution and textural relations amongst Qz1, Qz2 and Qz3. B) Image from a more coarse-grained part

of the sample dominated by luminescence quenched Qz1. Note however the network of Qz3 connecting mica grains. Zoom on (C) shows the spatial relationship between muscovite (bright interference colours), biotite relics and Qz1-3. Note how biotite relics in the optical picture correlates with Qz1, whereas the pure muscovite part of the grain is exposed against Qz3. C) Zoom on (A), showing the SEM-CL textures D) Optical image of the same region as in (C). Note that SGR optical textures in D between the yellow arrows occur only in connection with Qz3 in the SEM-CL image (C).

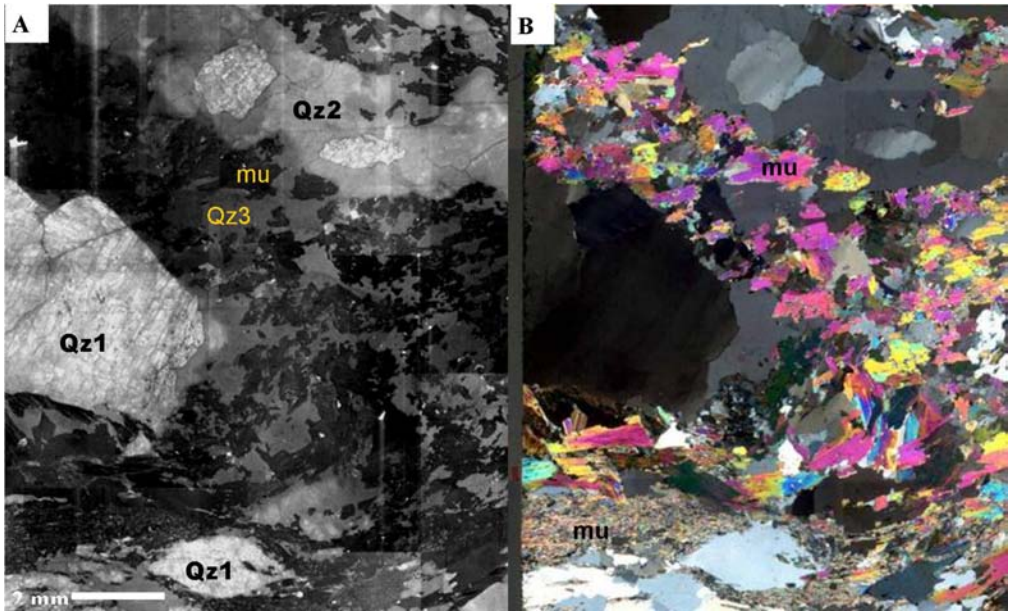

Figure 7: Optical and SEM-CL textures from 03bes103 quartz muscovite veins, showing optical and SEM-CL textures of quartz muscovite vein in quartzite. Sample collected at locality 2 A) SEM-CL image. B) Optical image. Same area displayed in both images. See text for discussion.

5.2.2 Textural relations in quartz in amphibolite

SEM-CL images of rose quartz veins in amphibolite have the highest luminescence of all the studied samples. Rose quartz is characterised by numerous crystallographically orientated needle-shaped inclusions. Luminescence quenching is weak and primarily occurs along grain boundaries (Figure 8). The island texture defining Qz1 is also present in this sample, but Qz2 is absent (Figure 8). The cracked grains of Qz1 are intersected by non luminescent quartz in few microns thick trans- and circum granular cracks (Figure 8). The latter quartz type was classified as Qz4 and was not analysed by LA-HR-ICP-MS because the high density of mineral and fluid inclusions would have interfered with the analysis.

Blue quartz similar to bluish quartz in the quartzites occurs in garnet quartz symplectites at the same locality as the rose quartz veins. However, the garnet is more almandine rich, and the amphiboles are more Al-rich and hastingsitic compared with the garnet amphibolite (see paper 3, Sørensen et al., 2007). Ilmenite and chlorapatite are also common in the garnet quartz symplectites. Unidentified prismatic solid inclusions in apatite contain CO_2 fluids at their tips. The texture of quartz in the garnet quartz symplectites consist of bright islands surrounded by cracks with less luminescent quartz (Qz1) (Figure 8). Some Qz2 is also present. Qz1 is brecciated and luminescence of the cracks in Qz1 is the same as in Qz2 (Figure 8). The brightest and least brecciated Qz1 is preserved as inclusions in garnet in the garnet quartz symplectites or as inclusions in tourmaline in quartz tourmaline leucosomes (Figure 8). The quartz in quartz-garnet leucosomes and in garnet quartz symplectites in other places show similar textures (Figure 8).

En echelon quartz veins at locality 4 are surrounded by a reaction zone comprising green acicular hornblende, biotite, ilmenite, apatite and plagioclase (Figure 9). Plagioclase is partially sausuritised and sericitised (Figure 9). Ilmenite is completely or partly replaced by titanite (Figure 9). The quartz within the quartz vein mostly consists of Qz2 with minor amounts of Qz1 (Figure 9). Both Qz2 and Qz1 are intersected by trans, inter, circum- and intragranular cracks that may only appear in the SEM-CL images as features belonging to Qz4 in sub-micron thick cracks with black CL (figure 9)

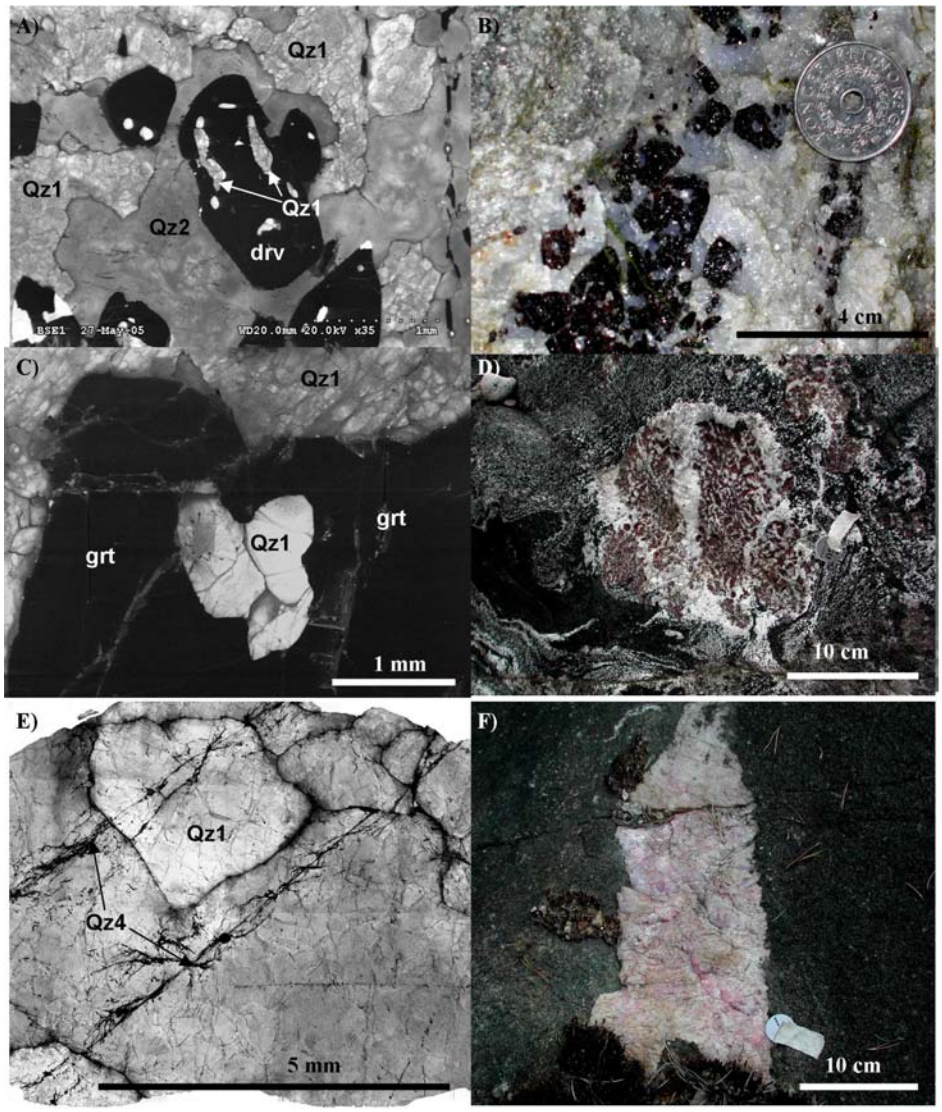

Figure 8: Optical and SEM-CL textures from garnet quartz symplectites (locality 3), rose quartz veins (locality 3), and intergrowths between quartz and tourmaline in quartz tourmaline gneiss (locality 5). A) SEM-CL image showing Qz1 inclusions in dravitic tourmaline (drv) in a matrix of Qz1 and Qz2 B) Field image showing the co-occurrence in leucosomes of dravitic tourmaline and blue Qz1. C) SEM-CL image showing bright Qz1 inclusions in garnet and more luminescence quenched Qz1 and Qz2 outside garnet. D) Field picture of garnet quartz symplectite. E) SEM-CL image of rose quartz vein, consisting of Qz1, cut by trans– and circumgranular cracks of Qz4. F) Field image of rose quartz vein in garnet amphibolite.

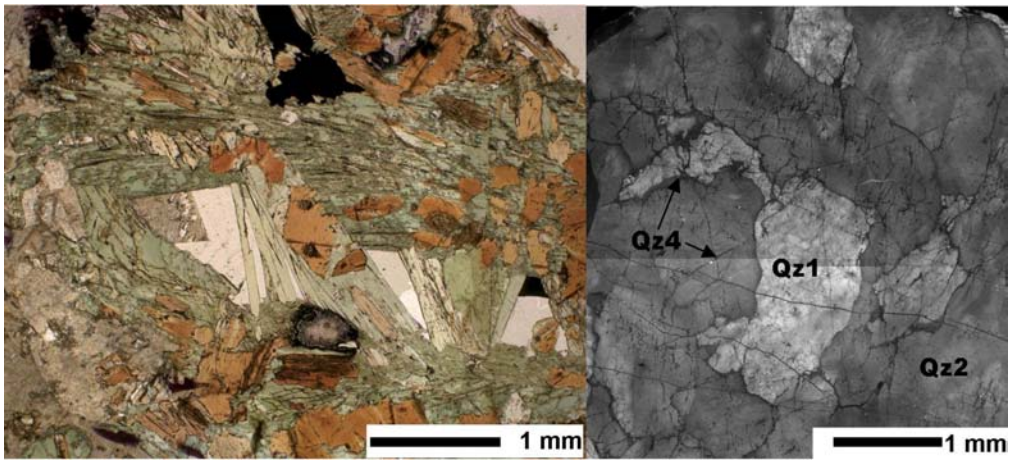

Figure 9: En-echelon quartz vein from locality 4. A) Decussate biotite-magnesiohornblende in a reaction texture enveloping the quartz vein. B) SEM-Cl image showing Qz1 and Qz2, both intersected by cracks with Qz4. See text for explanation

Quartz veins in amphibolites from locality 5 having the different alteration stages described in Table 2 (p.10) were also investigated by SEM-CL:

Quartz veins surrounded by alteration type 1 comprising greenish black amphibole (field colour) and biotite mainly consist of Qz1 and Qz2. Samples 04bes143, 04bes120 and 04bes121 are examples of such veins. They only contain minor amount of Qz3 (Figure 10). Qz2 in these samples is coarse-grained (Figure 10) and features a high density of coarse rutile. Qz1 also contain many needle shaped inclusions, but they are much finer. The optical microstructures of Qz1 and Qz2 are different; Qz1 comprises a chessboard texture of subgrains, whereas Qz2 has more even extinction pattern although it often display deformation lamellae (Figure 10). The chessboard microstructure is partly overprinted by basal subgrain microstructures, which relate to an increase in the luminescence intensity (Figure 10).

Quartz veins in alteration type 1 with lighter shades of green amphibole and lighter coloured biotite and alteration type 2 mostly consist of Qz1 and Qz2 (Figure 11), but both Qz1 and Qz2 have significantly lower luminescence intensity, when compared to quartz vein in alteration type 1 with darker amphibole and biotite (see Table 2 for definition). Qz3 is not very abundant in quartz veins in alteration types 2 and 3 but occurs as a diffuse channel system, altering the other quartz types (Figure 11).

The quartz-scapolite veins (Alt3) also consist of more than one quartz type (Figure 12), but the overall intensity is much lower than in the other samples, hence most of the quartz is classified as Qz3. However, some of the Qz3 appears homogeneous both in optical and SEM-Cl pictures, where subgrains are seen in both SEM-CL and optical images on the more luminescent Qz3 (Figure 12). Both Qz3 subtypes are intersected by micron thick irregular cracks of Qz4, which correlate with numerous solid inclusions of calcite and calcite bearing fluid inclusions (figure 12).

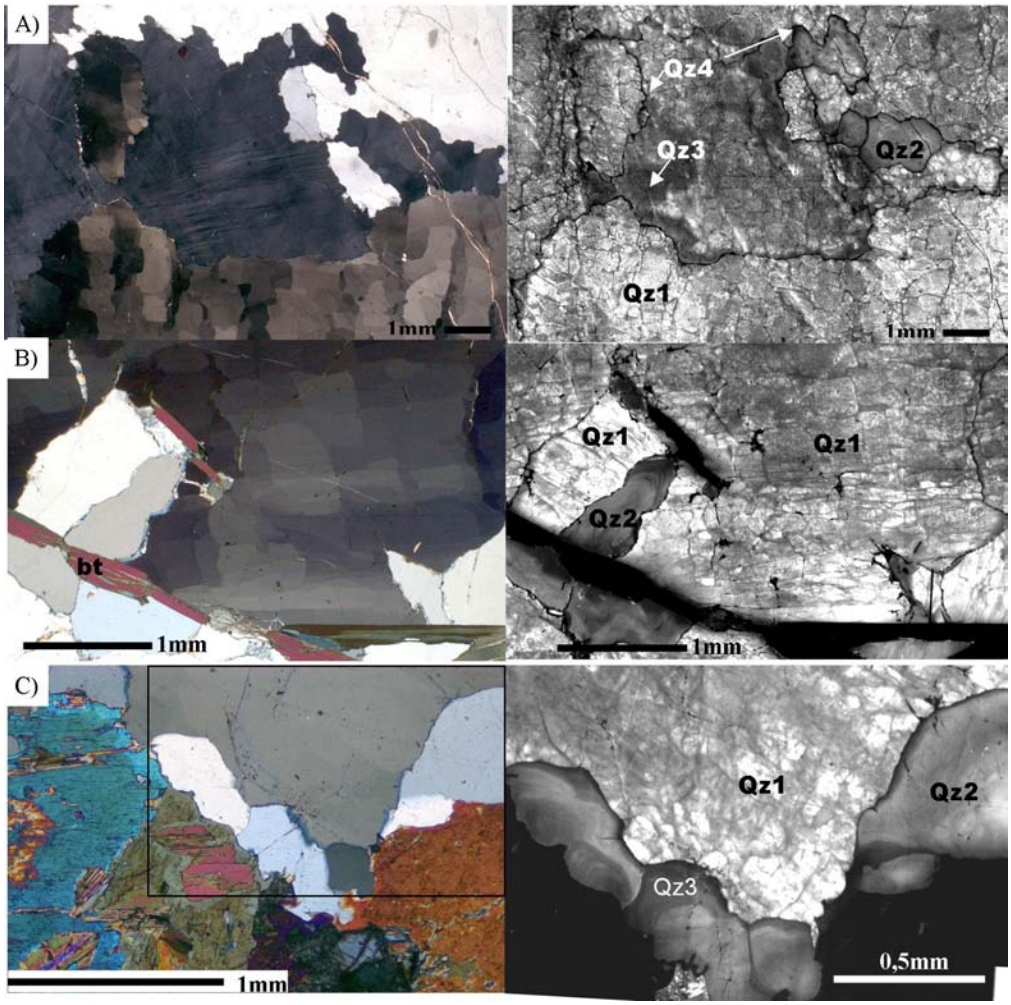

Figure 10: Comparison of optical and SEM-CL textures in quartz veins in amphibolite with alteration type 1, all from locality 5 (see text). A) 04bes121, the least altered sample, consisting of Qz1. Note the chessboard pattern in the optical microstructure coinciding with the island/channel texture (Qz1) in the SEM-CL image. Note also the deformation lamellae in the central luminescence quenched grain, consisting of both Qz1 and Qz2 and that the luminescence quenched grain consume the brighter grain (upper right). Note also that there are grain boundary textures at different scales; grain boundaries are lobate with Qz2 overgrowths consuming Qz1, but grain boundaries are also serrated at a finer scale with very dark to non luminescent quartz overgrowths consuming all other quartz types. B) 04bes120, mostly consisting of Qz1 with minor amounts of Qz2 and Qz3. Note chess board texture overprinted by elongated prismatic subgrains. In the lower part of the middle Qz1 grain, the prismatic subgrains override signs of the chess board texture, which is more pronounced in the upper part of the grain. In the corresponding SEM-CL

this shift in the microstructure is also detected. Note that the luminescence increases as the prismatic subgrains become more pronounced. C) 04bes120 polarised light micro photo showing the connection between amphibole alteration related to the introduction of biotite and formation of Qz2 in the lower part of the SEM-CL picture. Note also the dark grey Qz3 overgrowths on the Qz2 grains.

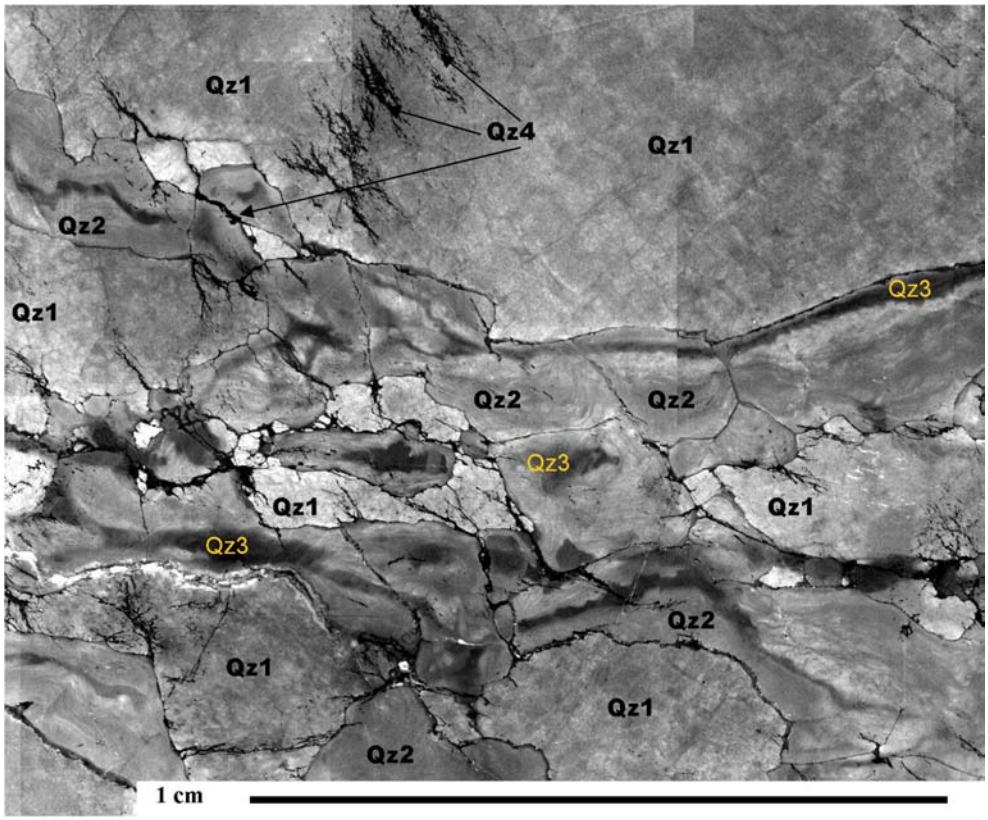

Figure 11: Optical and SEM-CL textures in quartz vein (04bes91, locality 5), surrounded by alteration type Alt1 with bleached actinolite and light brown biotite (se text and Table 2). Note that the contrast setting in the SEM was increased, compared to the other samples in this paper to see the textures in this sample, which generally are low luminescent. The difference between Qz1 and Qz2 is hardly recognised in this image, but may be differentiated by the barely recognisable cracked texture of Qz1 and the faint oscillatory zoning in Qz2. Qz3 in this sample display a partly connected channel network. Qz4 is seen as cracks in the large Qz1 grain to the right and along grain boundaries.

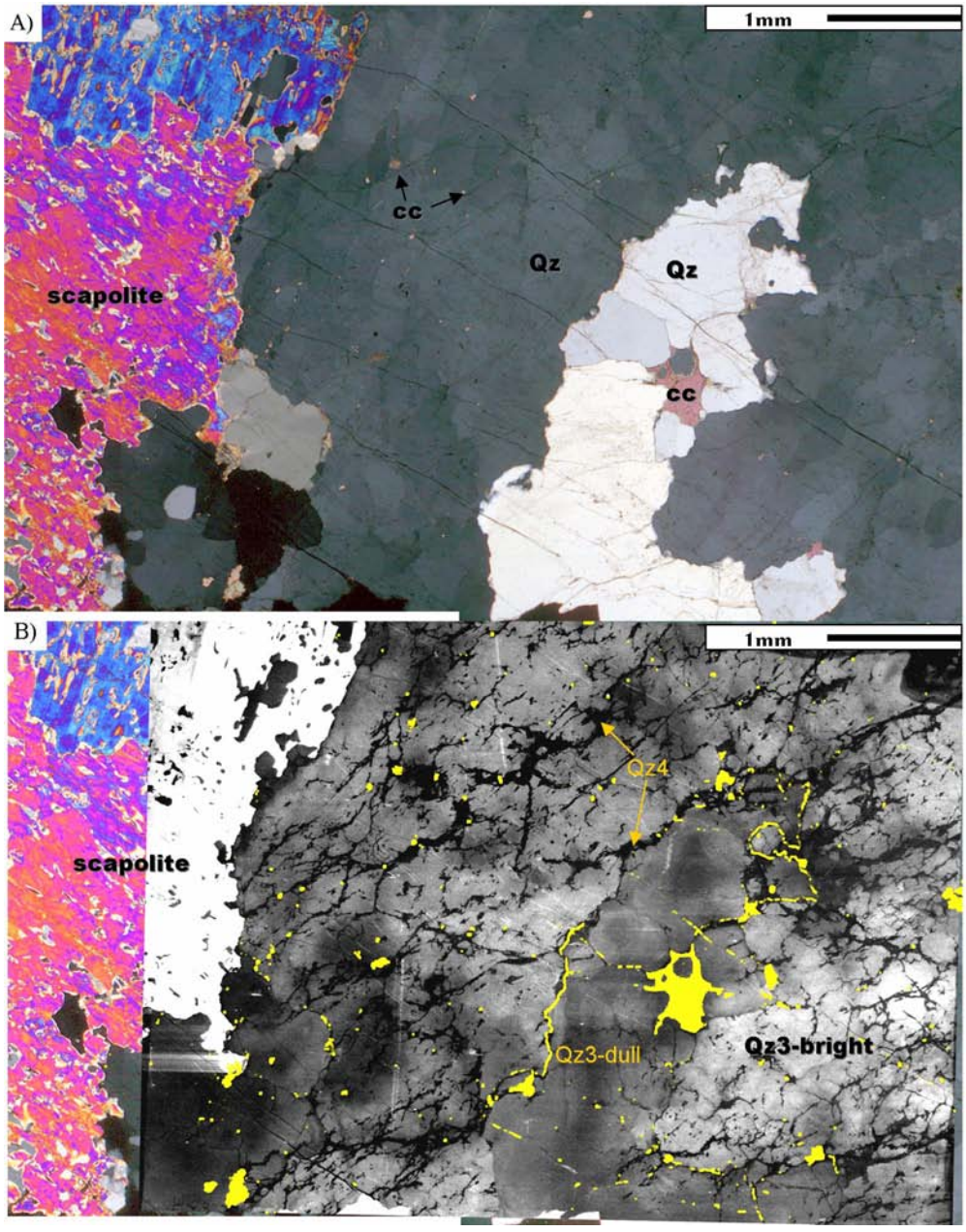

Figure 12: Optical and SEM-CL textures in quartz scapolite vein from locality 5 (04bes122, Alt3). A) Optical picture, showing scapolite to the left of the quartz vein consisting of two quartz types. One quartz types has a distinct subgrain texture whereas the other quartz has a more even optical extinction pattern. Note the many bright luminescent calcite inclusions in the quartz matrix. A larger calcite inclusion is seen in the

middle bright quartz grain. B) SEM-CL of the same area as in (A). Note that the contrast setting in the SEM was increased, compared to the other samples in this paper in order to image the textures in this sample which generally is low luminescent. The quartz with subgrains is higher and more unevenly luminescent than quartz with the even optical extinction pattern. Note luminescence quenching next to the Scapolite. Both the light grey and dark grey quartz in this image are classified as Qz3 by comparing with luminescence of other samples. Both light and dark grey Qz3 is cut by irregular trans and circumgranular cracks with Qz4. Yellow patches marking calcite inclusions detected by optical microscopy all correlate with Qz4 cracks

5.3 SEM Mono-CL spectra

Some samples were investigated by SEM-Mono-Cl to investigate the defect structures creating the contrast between the different quartz types. The results of the spectral analysis are shown in Figure 13. Because Qz1 had the largest variability in texture (degree of brecciation and luminescence quenching) and chemistry, Qz1 was investigated by SEM-mono-Cl in several samples. In most samples, Qz1 is dominated by at high peak at 350-470 nm, probably related to Ti defects in the quartz lattice and a peak at 500-670 nm probably related to H_2O and intrinsic defects (e.g. Goetze et al., 2001). The 500-670 nm peak is less dominant in bright Qz1. Rose quartz vein has a different spectra from that of the blue quartz with distinct peaks at 370 nm, 420 nm and 440 nm. Qz2 has the same peaks as Qz1, but the 500-670 nm peak is stronger when compared to the 350-470 nm peak. Qz3 only features the 500-670 nm peak indicating that H_2O related defects and intrinsic defects are the only significant defect in this quartz type.

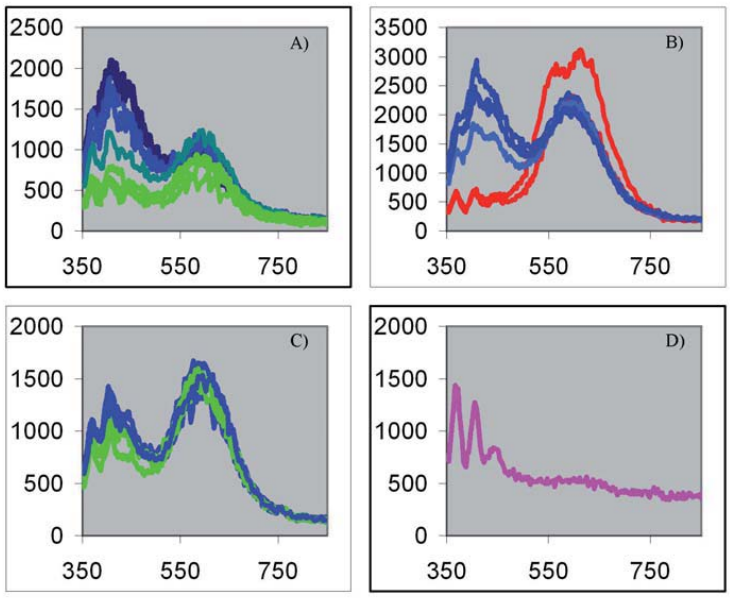

Figure 13: SEM-CL spectra of the studied quartz types, similar scales of wavelength in nm on the horizontal scale. Blue lines are Qz1, green Qz2, red Qz3 and the pink is Qz1 in rose quartz veins. Y-Scale is intensity (cps). A) Qz1 and Qz2 in garnet quartz symplectite, darkest blue represent bright well preserved Qz1 included in garnet,

blue bright Qz1 outside garnet and greenish blue duller Qz1. B) Qz1 same colour scheme as in A. Qz3 red C) Qz2 and dull Qz1 from quartzite (04bes32). D) Bright Qz1 in rose quartz vein (04bes99).

5.4 Quartz chemistry vs. texture

A wide range of trace elements were measured in the three quartz types Qz1, Qz2 and Qz3. Figure 14a show the mean value and standard deviation of each element in the quartz types. Only Ti, Al, K, and P occur in significant amounts (Figure 14a). All other elements are either below detection limits or in sub-ppm concentrations (Figure 14a). Ti is the most significant discriminator between the quartz types, both in quartz veins and quartzites (Figure 14a). The average Al content is higher in Qz1 than in the other qz-types, and is also higher in quartz veins in amphibolites than in quartzites (Figure 14a).

A plot of Ti versus Al shows that quartz from the study area represents a wide compositional range (Figure 14b). Qz1 shows the widest compositional range and is the only quartz type featuring considerable Al contents. Al in Qz1 varies from 50 to several hundred ppm (Figure 14b). At closer inspection, Qz1 falls in two groups, when B, Ti and Al contents are also considered (Figure 14b). High Al contents only occur in rose quartz (Figure 14b), whereas garnet quartz symplectites has much lower contents of both B and Al (Figure 14b). There is no systematic variation in the typical Al content between the qz-types (Figure 14e), although Qz1 has larger variation than the other qz-types.

At Ti contents below 100 ppm, the Al contents are relatively low and constant, but at higher Ti contents Al increase dramatically (Figure 14b). There is a strong correlation between Al and B especially at High Al concentrations i.e. the linear trend in Figure 14c. This linear trend is followed by Qz1 in amphibolites but not by Qz1 in quartzites (Figure 14c). The inclination of the trend line in Figure 14c matches the B/Al ratio in dumortierite ($Al_{6.5\text{-}7}(BO_3)(SiO_4)_3(O, OH)_3$). Accordingly the large variations in the Al content in Qz1 in Qz in amphibolite, do not relate to structurally incorporated Al, but rather is the result of micro-inclusions. All qz-types have the same distribution of Al content, with a typical average at 15 ppm (Figure 14e).

Qz2 shows considerable variation in the Ti content (from 20-100 ppm) but generally has Al contents below 50 ppm (Figure 14b). This is also reflected in the boron content which is also low in type 2 quartz as seen in the trend between B and Al for higher Al concentrations (Figure 14b). The variations in the Ti content of Qz2 are much larger for the quartz veins in amphibolite than for Qz2 in quartzite (Figure 14d). A frequency plot suggests that the variation in the Ti content in Qz2 in quartz veins in the amphibolites is random (Figure 14d), whereas the Ti content in Qz2 in quartzites varies systematically around a type value of c. 22 ppm (Figure 14d). Partially this could be the result of rutile needles that vary in density between the samples. However, Qz2 also formed during fluctuating conditions as demonstrated by oscillatory zoning and edge ward decreasing luminescence possibly associated with the formation of Qz3

(Figures 5-11). Qz3 sometimes follows the grain boundaries of Qz2 (Figures 5-11). In relation to darker rims on Qz2 the alteration of biotite to muscovite is common (Figures 5 and 6). Accordingly the dark rims on Qz2 probably are overgrowths of Qz3.

Apparently, Ti is easily leached from Qz1 whereas Al and B rarely are lower than 50 ppm. Conversely Qz2 and Qz3 consistently show low Al below 50 ppm (Figure 14b). Even in samples where the Qz1 is so luminescence quenched that it is almost indistinguishable from Qz2 and Qz3 it still contains significant amounts of Al and B (Figure 14d).

Qz3 has trace element content close to or below the detection limits i.e. it has a very well defined chemical signature (Figure 14a-d). In addition Qz3 features almost the same chemistry in both amphibolite and quartz veins and in quartz-muscovite veins, except for phosphorous which apparently is higher in the quartz-scapolite veins than in the quartzites (figure 14a).

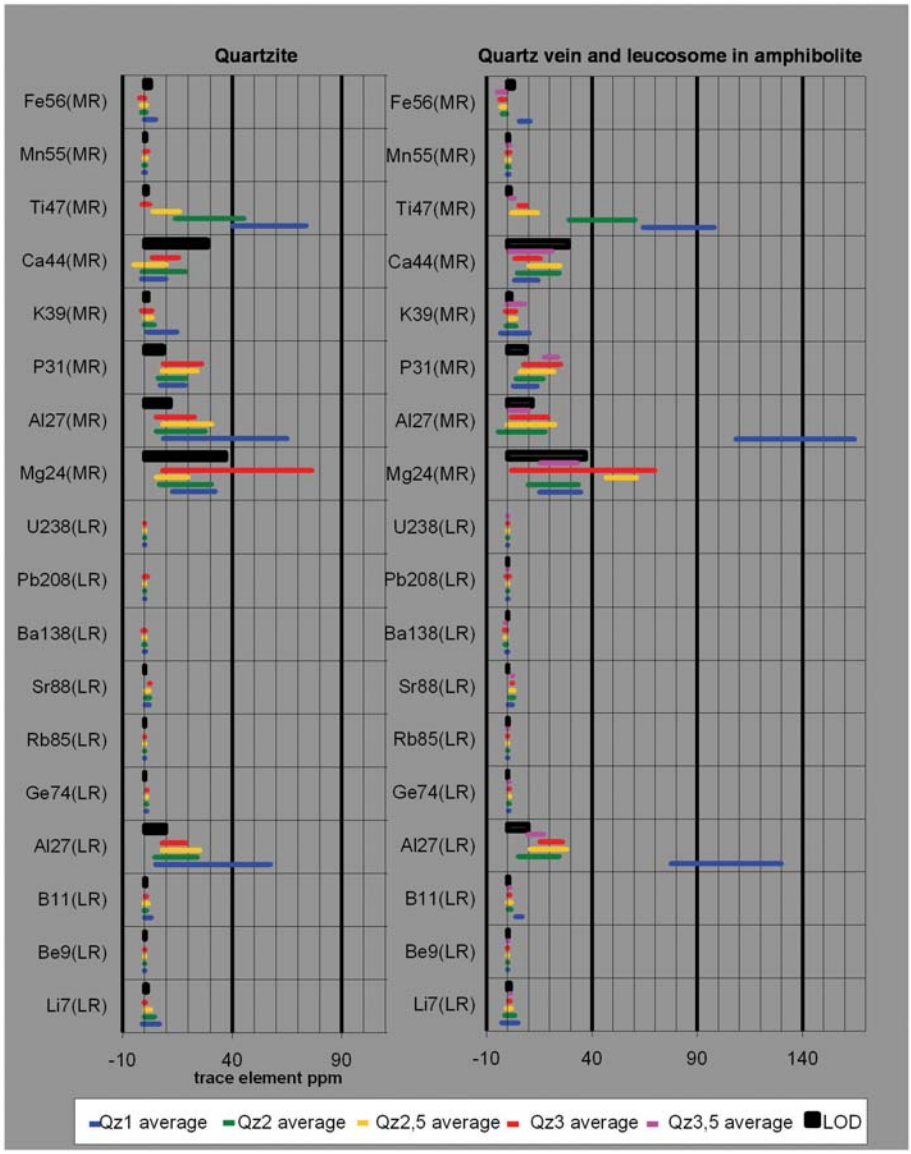

Figure 14: See caption on next page.

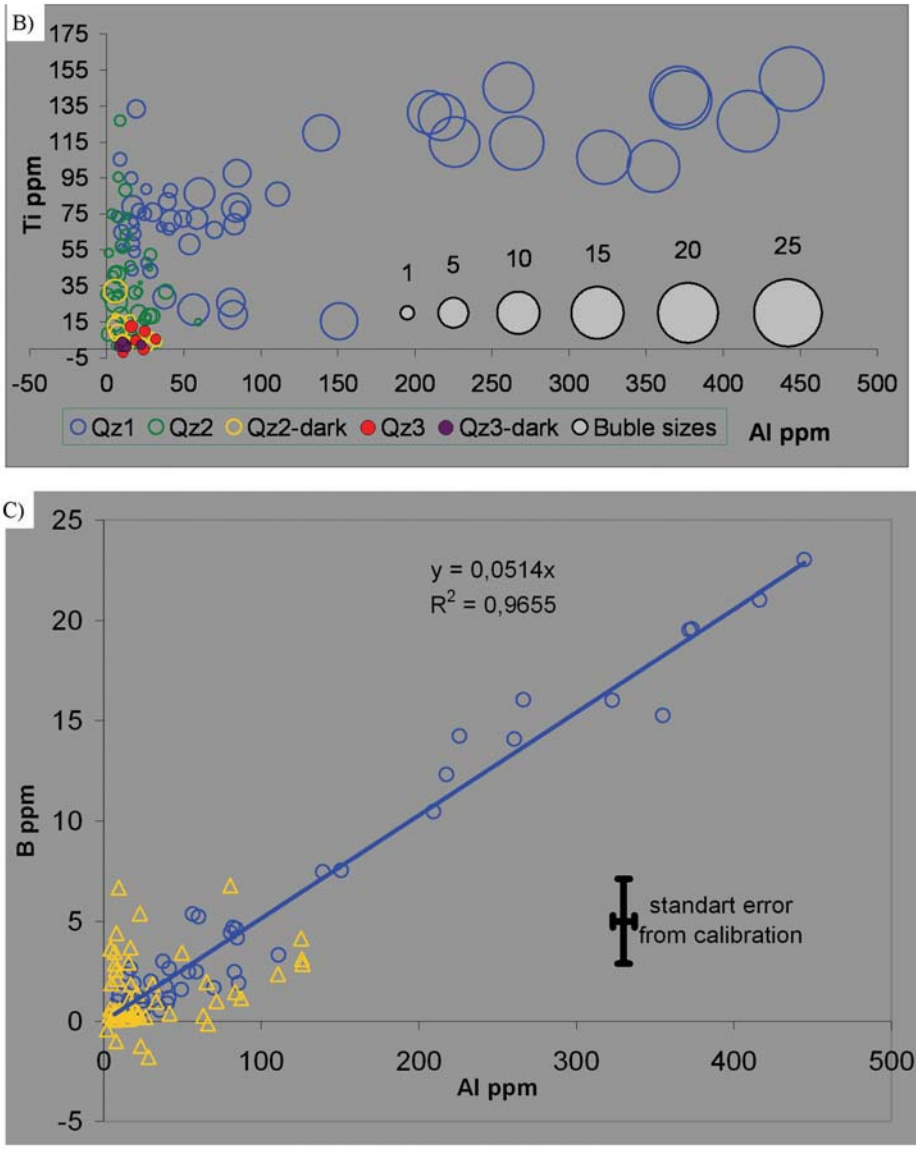

Figure 14: Continued. See caption on next page.

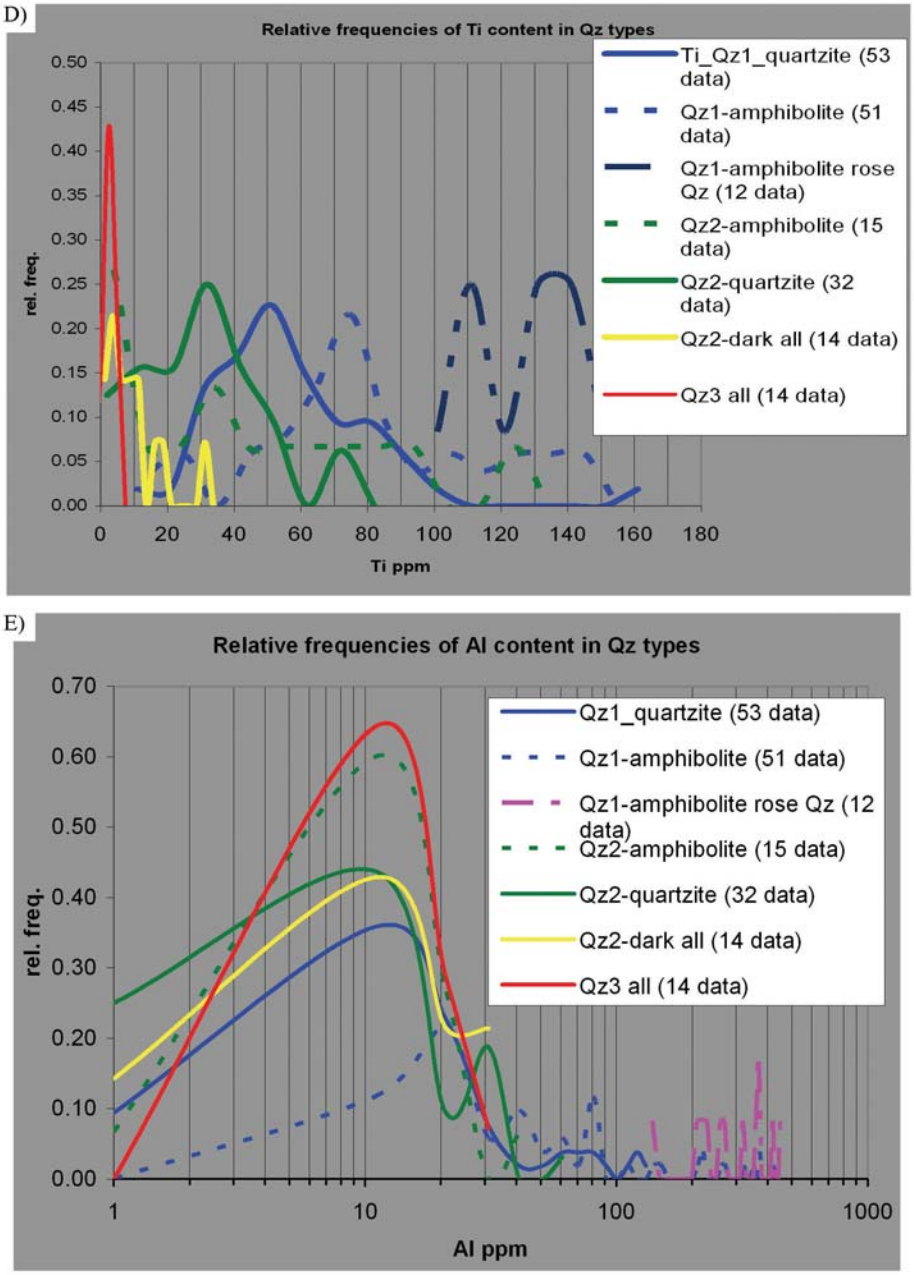

Figure 14: Trace element distribution in quartz. A) All elements shown as bars with mean value ± σ for quartzites (left) and quartz veins and leucosomes in amphibolite (right). B) Plot of Ti vs. Al with bubble size from boron. C) Linear correlation between Al and B, followed by quartz veins and leucosomes in amphibolite (blue symbols), but not by Qz1 in quartzite (yellow symbols) . D) Relative frequencies of Ti content in the different quartz types. E) Relative frequencies of Al content in the different quartz types.

6 Discussion

This paper focuses on the formation of complex recrystallisation textures in quartz and their relation to fluid flow and deformation. It is demonstrated that the properties of quartz are not constant but vary significantly between quartz types and is related to their defect structure as indirectly documented by SEM-CL. This has implications for the way we look upon the deformation of quartz bearing rocks, i.e. quartz in this study features variable rheological behaviour. In addition the fluid flow pattern in shearzones is well expressed by the quartzites and inform about mass transfer processes in the crust. In the next sections the role of fluids and the importance of spatial and temporal fluid availability in quartz deformation and recrystallisation are discussed. Another important aspect of this study is the role of fluids in the formation of high purity quartz through quartz recrystallisation. It is demonstrated that quartz oppose recrystallisation at fluid absent conditions although P and T are changing, whereas quartz subjected to aqueous fluids at the same conditions is chemically altered.

6.1 Textural chronology

Four main types of quartz were documented in quartzites and quartz veins in this study (in chronological order):

Qz1: Bright islands surrounded by narrow darker cracks

Qz2: Light grey quartz with the same grey level as the channels in Qz1. Occasionally with oscillatory zoning.

Qz3: Dark grey diffuse channels intersecting Qz1 and Qz2.

Qz4: Black to very dark grey luminescent.

Additionally, different degrees of luminescence quenching characterise each type. Channels in Qz1 match the luminescence level in Qz2. Thus the textures of Qz1 and Qz2 are related: the Qz1 grains are the altered and brecciated protolith grains and Qz2 the newly formed grains. Qz3 textures always intersect Qz1 and Qz2 textures hence are younger. Luminescence quenching textures related to the Qz3 formation comprise several subtypes:

Luminescence quenching (Qz3) occur along grain boundaries between Qz1 and Qz2, and Qz2 and Qz2. This type of Qz3 occurrence is in optical continuity with the Qz2 grains i.e. on the Qz2 side of the grain boundary suggesting that Qz1 was consumed during this process. However, diffuse channels of Qz3 intersects both Qz1 and Qz2, but are more common in Qz2.

6.2 Patterns of recrystallisation

Regardless of the lithological setting, quartz shows similar textural types. Qz1 has uneven luminescence with dark channels engulfing brighter islands. Less cracked bright quartz is preserved within minerals such as garnet in the garnet-quartz symplectites and dravitic tourmaline in leucosomes in quartz-biotite-tourmaline-

feldspar gneisses. In the following the processes behind the quartz recrystallisation is discussed. At the end the discussion, a model that may explain the observed pattern of recrystallisation is presented (Figure 15).

The presence of aqueous brines in Qz2, the islands texture in Qz1 and the oscillatory zoning in Qz2 imply that brecciation associated with dissolution and re-precipitation is responsible for the formation of Qz2. Experiments demonstrate that only small amounts of water are required to greatly lower the creep strength of quartz (e.g. Kronenberg, 1994; Kronenberg et al., 1984) whereas amounts larger than 0.2 wt% will facilitate brecciation of the quartz (e.g. den Brok and Spiers, 1991; Post and Tullis, 1998). We infer from this that the observed brecciation was the result of the introduction of aqueous fluids to the dry high grade quartz (Figure 15).

The exact micro-nanoscale role of f_{H2O} in quartz deformation is difficult to access, even in experimentally deformed rocks at high and low f_{H2O}. This is because the changes in intragranular water or hydrogen speciation is impossible to detect although the strength of quartz polycrystalline aggregates is lowered at high water pressures (den Brok et al., 1994; den Brok, 1992; Kronenberg and Wolf, 1990). Therefore, the role of water in deformation of quartz aggregates is complex, and not only intragranular water influence the rock strength but also intergranular water. This interpretation is supported by the fact that quartzites deformed without adding water with their original saturated intragranular content they have intermediate strengths whereas they have low strengths with added water (e.g. Kronenberg, 1994 and references herein; Kronenberg and Wolf, 1990). Vacuum dried quartzites are strong and primarily deforms by slip on basal planes with dislocation heterogeneous substructures indicative of low recovery rates (e.g. Kronenberg, 1994 p. 161 and references herein). This agrees with the observed increase in luminescence intensity in Qz1 observed in the vicinity of more deformed areas. An example of this is the coupling between increasing luminescence intensity and changes in subgrain structure from chess board to basal type subgrains in Qz1 grains. This was observed both in quartz veins and quartzites.

In contrast to dry quartzites, dislocation structures in quartz in quartzites that were experimentally deformed under water saturated conditions show homogeneous distributions of both basal and prismatic dislocations and organized dislocation configurations resulting from recovery (e.g. Kronenberg, 1994 p. 161 and references herein). This matches the behaviour of Qz2 and Qz3 which do not show increasing CL-intensity or optical microstructures indicative of strain hardening toward the high strain zones.

Qz3 behaved far different from Qz2 and Qz1 during thrust related deformation. Qz3 formed subgrains with subgrain rotation eventually leading to new grains with a smaller grain size. In contrast, Qz1 and Qz2 mostly behaved brittle or deformed plastically by deformation lamellae. Possibly, the introduction of water in Qz3 not only increased plasticity but also enhanced the local recovery rate (Figure 15) hence facilitating the continuous climb of dislocations during deformation, and lowered work hardening. Initial softening of Qz3 was accomplished by simultaneous cracking and

fluid infiltration. The infiltrating aqueous solutions increased recovery and healing rates. In this process, the quartz was leached of trace elements. We suggest that this process took place in a system of fine scale cracks associated with larger cracks propagating in a horse tail pattern rather than being the result of diffusive processes (Figure 15). Fluid inclusion studies (paper 2, Sørensen and Larsen, 2007) documents that the fluids related to the formation of Qz3 are brines with a salinity of about 30 wt% NaCl equivalents. Such high salinities provides fluids with a very good wetting capability towards quartz (Watson and Brenan, 1987) hence enabling fluid flow even through narrow sub-microscopic cracks. Therefore, the broad channels may be a result of fluids flowing through a main crack dissolving quartz through a system of finer scale cracks splaying off the main crack hence improving the porosity (Figure 15). The smaller grain size in the Qz3 domains increased the permeability of the quartzites during deformation. Therefore, fluids were focused in high strain ductile areas as they percolated through the fault system simultaneously with the cracking process propagating through less ductile Qz1 and Qz2 (Figure 15). Given this scenario, it appears that both intra- and intergranular water participated in the quartz recovery process on a localised scale sustaining the differential behaviour of the quartz types. This is supported by TEM observations of the relations between dislocations and nano-inclusions of H_2O in both natural localised high strain domains and in quartzites deformed experimentally at high P_{H2O} (e.g Kronenberg, 1994 and references therein). Together, they document that water travelling along grain- and subgrain boundaries play an important role in recovery processes in reducing the work hardening (e.g Kronenberg, 1994). In addition fluid inclusion water in shear zones correlates with localised high shear strains (e.g. Kronenberg et al., 1990; Nakashima et al., 1995). Furthermore, the ductility and the recovery rate may be influenced by the presence and speciation of trace elements in the quartz structure. This is because included trace elements may serve as obstacles for propagating dislocation loops during dislocation glide and obstruct climbing dislocations thus making dislocation glide and recovery through dislocation climb less efficient.

Boundaries between grains of Qz2 commonly are straight and have triple point junctions. Boundaries between Qz1 and Qz2, however, are interlobate-lobate. This suggests that two different processes dominated the geometry control and the two types of grain boundaries. The straight Qz2-Qz2 boundaries are obviously explained by energy minimisation by GBAR (grain boundary area reduction) (e.g. Passchier and Trouw, 2005). Pinning, window, dragging and "left over grain" microstructures (see e.g. Jessell, 1987; Passchier and Trouw, 2005 for definitions) documents that Qz2 grains grew at the expense of Qz1 grains during dynamic recrystallisation. According to existing theories on GBM (grain boundary migration) the GBM process is driven by contrasting dislocation densities between grains, i.e. grains with high dislocation densities consume grains with lower dislocation densities in order to minimise the free energy of the system (e.g. Passchier and Trouw, 2005). In our case the high defect concentration in Qz1 is documented by the high and uneven SEM-CL of Qz1 compared to Qz2. The possibility therefore exists that SEM-CL could become an

important tool to improve the understanding of the poorly understood GBM process in quartz tectonites.

The relationship between the formation of Qz2 and the addition of aqueous fluids to the quartzites, in combination with the observation of aqueous fluid inclusions decorating the irregular boundaries between Qz1 and Qz2, suggest that water travelling along grain boundaries assisted the GBM process in our samples.

The textures of Qz3 intersect Qz1 and Qz2. Because the formation of Qz3 relates to the formation of muscovite and decomposition of biotite to poikiloblastic muscovite, it is implied that Mg and Fe was mobilised from the biotites in the quartzites at the same time as quartz recrystallised to form Qz3. This suggests the action of an aqueous fluid capable of mobilising Fe and Mg from the biotite, because no other phases are present next to the muscovite grains that otherwise could have consumed the available Mg and Fe. In addition the geometry of the Qz3 textures resembles a fluid channel texture following grain boundaries or intersecting grains in a fingering pattern. Also the clear relationship between aqueous brines and Qz3 imply that Qz3 must relate to the introduction of an aqueous fluid (Sørensen and Larsen, 2007, paper 2). Apparently these brine fluids were capable of both infiltrating quartz and also of changing the quartz properties. Qz3 channels are more common in Qz2 than in Qz1. This may relate to different fluid propagation properties in the two different quartz types. If the fluid is assumed to propagate through micro-cracks, the different fracturing properties of quartz in relation to the water content may control crack growth and healing (see Kronenberg, 1994 and references herein).

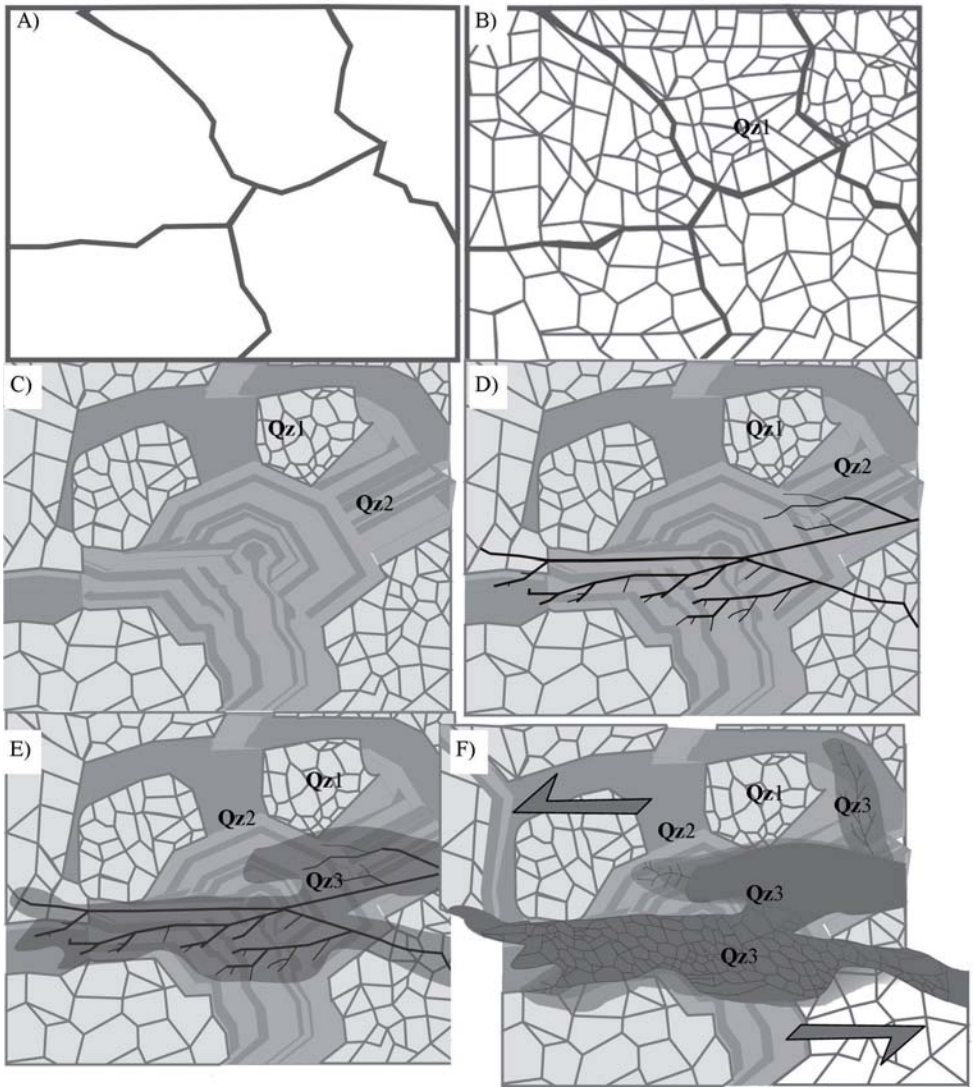

Figure 15: Patterns of recrystallisation as demonstrated by SEM-CL and optical microscopy. A) Homogeneous quartz at high metamorphic grade. B) Introduction of aqueous fluids under differential stress induces brecciation. C) Quartz dissolved during brecciation precipitates as Qz2, Qz1 is the brecciated old grains. D) Repeated deformation induces fracturing. E) Infiltrating aqueous fluids move along the fractures causing recrystallisation (Qz3), but also promoting crack mobility. F) The recrystallised quartz (Qz3) behaves more plastic than Qz1 and Qz2 and deform by SGR (subgrain rotation recrystallisation). Continuous fluid flow through the more fine-grained Qz3 domains increase recovery rates and reduce strain hardening. Crack propagation and recrystallisation still continue and the amount of Qz3 increase.

6.3 Trace element distribution and behaviour

Both Qz1 and Qz2 have strongly variable geochemical signatures. The Ti content is variable, but Qz1 has much higher and more variable Al and B contents. Most of both the Al and B in Qz1 comes from microscopic inclusions of dumortierite, because the B versus Al trend is almost perfectly linear with a coefficient matching the molar B/Al ratio in dumortierite (Figure 14). This is also reflected by the colour variation of Qz1 from blue to pink, with pink quartz being richer in B and Al than blue quartz. Previous studies documented pink coloured dumortierite inclusions in rose quartz (Applin and Hicks, 1987; Goreva et al., 2001). Therefore, it is assumed that mobilisation of B was more intense in relation to the formation of the rose quartz veins. The dumortierite inclusions in quartz grains formed as a result of intergrowth because the strong correlation between B and Al corresponds exactly to that dumortierite (Figure 14).

The difference in SEM-CL between Qz1 and Qz2 probably is a direct or indirect effect of Ti because this element varies most significantly amongst the quartz types (Figure 14). This is also reflected in the SEM-CL spectra of Qz1 and Qz2 that are dominated by possibly Ti-peaks in the quartz lattice, and a peak which probably relates to H_2O and intrinsic defects in the lattice. The "H_2O" peak is more dominant in Qz2 than in Qz1 (Figure 13). This overall correlation is somewhat clouded by variable content of coarse rutile needles in Qz2, causing Ti variations from 20-100 ppm (Figure 14). However, the average Ti content is much lower in Qz2 than in Qz1. Qz1 and Qz2 are also easily distinguished in frequency diagrams (figure 14). The Ti-content in Qz2 in quartzites is much lower than the Ti content in Qz2 in quartz veins in the amphibolites. We suggest that the different Ti contents in these two contrasting chemical environments in combination with the stability of rutile and thus simultaneous growth of rutile and quartz caused this difference. This interpretation is supported by the textural correlation between the formation of Qz2 and breakdown of ilmenite to rutile in sample 03bes32 and with the high abundance of coarse rutile needles in Qz2 in quartz veins in amphibolite.

Qz3 is very low in most trace elements including Al, Ti, and B and has low luminescence. Rutile needles are absent in Qz3, probably because titanite, being abundant in the alteration zone surrounding Qz3, is the stable Ti-mineral.

In contrast to other trace elements, P varies less systematic between the quartz types and show unsystematic variations from 0 ppm to 30 ppm. Either P is very mobile and easily remobilised in and out of the quartz lattice or P is not structurally bound but associated sub-microscopic mineral and fluid inclusions. SEM-CL analysis supports the latter options given that some samples (04bes122) with variable P contents maintain low SEM-Cl signals.

6.4 Implications for mega shearzone fluid migration

The recrystallisation history stored by the quartzites document the fossil plumbing system that accommodated fluid fluxing from deep seated to shallow parts of the Bamble shear zone complex. Judging from the incoherent geochemistry of Qz1 the

quartz bearing rocks probably experienced high grade metamorphism under variable P-T_X_{fluid} conditions. The observed differential behaviour of quartz, induced by an infiltrating fluid into a dry protolith uncovers some important aspects of fluid migration in inter-crustal shearzones. It is confirmed that fluids focused in shearzones is associated with chemical weakening and that large scale mobility of elements occurred. Fe is removed from ilmenite hence facilitating the stability of rutile together with Qz2 and Mg as well as Fe is removed to form muscovite from biotite. These elements are redeposited in other places explaining why ore deposits often occur in the vicinity of shearzones, typically in association with second or third order faults. Therefore, deep crustal shearzones like the Bamble mobile belt serve as fluid conduits providing large scale mass transport. In addition the reduction of grain size in high strain domains increases the number of channels available for fluid transports per volume unit. Once the process of fluid infiltration in localised high strain deformation is initiated, it will probably continue as a self sustained process as long as a fluid supply is available. If however fluid supply ceases, quartz may return to intermediate strength.

6.5 Conclusion and summary

Complex recrystallisation textures in quartz were observed by SEM-CL

- Quartz formed at high metamorphic grades under dry conditions dominated by CO_2-rich fluids, possibly coexisting with brines, underwent localised recrystallisation during cooling and exhumation. Recrystallisation was induced by two main stages of fluid influx.
    - First introduction of aqueous fluids, comprising a mix of CO_2-rich low salinity and CO_2-poor NaCl-KCl-H_2O-CO_2 eutectic salinity brines that provoked brecciation and dissolution re-precipitation of quartz. Quartz types Qz2 and Qz1 bear witness of this process: Qz1 represents relics of old brecciated grains characterised by an uneven luminescence pattern comprising islands with bright luminescence surrounded by darker channels. Qz2 represent quartz that was re-precipitated from the brecciation dissolution process responsible for the formation of Qz1. Luminescence of Qz2 is more even that that of Qz1 but faint oscillatory zoning bear witness to the hydrothermal origin of Qz2. Rutile was the stable Ti-bearing phase when Qz2 formed as documented by the breakdown of ilmenite to rutile in association with Qz2 textures. Coarse rutile needles are common in Qz2 but are more abundant in Qz2 quartz veins in amphibolites than in Qz2 quartzites.
    - Second fluid influx propagated along a feather like system of micro-cracks. Fluids were CO_2 free brines with a good ability to infiltrate the quartz due to low wetting angles of brines against quartz. The brines also had a high transport capacity. Fluid infiltration facilitated recrystallisation of quartz (Qz3) in mm wide fluid channels. Qz3 behaved more plastic than Qz1 and Qz2 during deformation and

experienced SGR (Sub Grain Rotation recrystallisation). Increased SEM-Cl intensity in Qz1 toward zones in which Qz3 experienced SGR testify to increased dislocation densities related to strain hardening processes in Qz1. Qz3 is texturally correlated with the breakdown of rutile to titanite. Qz3 correlate with thrust related microstructures. Fluid inclusion studies document the fluid in equilibrium with Qz3 to be brine with 25 wt% NaCl and 6 wt% $CaCl_2$. Fluid inclusion isochore along with the trust related microstructures in relation Qz3 places Qz3 formation during exhumation at 300-400°C, 3-6 kb.

- Several later fluid influxes caused localised quartz recrystallisation along micron-wide micro-cracks (Qz4).

Trace elements in quartz were gradually removed from the quartz lattice during retrograde recrystallisation correlated with luminescence quenching textures.

Ti along with intrinsic and water related defects is probably responsible for the luminescence observed in our samples and undergoes a progressive depletion during retrograde recrystallisation:

- Qz1 is richest in structurally bound Ti.
- Qz2 is lower in structurally bound Ti but contain numerous rutile needles. They formed as intergrowths because rutile was the stable Ti phase during Qz2 formation. This causes the bulk Ti-content in Qz2 from quartz veins in amphibolite to vary unsystematically because rutile needles were too abundant to be avoided during LA-ICP-MS analyses. Qz2 in quartzite on the contrary gives a constrained average of 32 ppm.
- Qz3 is low in Ti and also in other trace elements. This is partially because of the low abundance of structurally bound trace elements, but the destabilisation of rutile in relation to Qz3 served to produce quartz with a uniform low bulk Ti concentration below 5 ppm.

Our study underlines the importance of fluids on quartz rheology. This is demonstrated by the differential behaviour of Qz1, Qz2 and Qz3 during deformation. During uplift Qz3 deformed plastically and recovered by SGR. At the same time Qz1 experienced strain hardening caused by accumulation of dislocations demonstrated by increased cathodoluminescence intensity. In agreement with experimental studies we infer that the increased plasticity and recovery rate in Qz3 was caused by increased H_2O content in the fluid. This interpretation is substantiated by the record of fluid inclusions in Qz3 by Sørensen and Larsen (2007, paper 2). However, it is also suggested that the trace elements in quartz may affect the rheological properties as trace elements in the quartz lattice may obstruct dislocation glide as well as dislocation climb hence promoting strain hardening.

Grain boundary geometries are also partially controlled by the trace element contents. Qz1-Qz2 grain boundaries are interlobate-lobate with microstructures. Qz2

grew at the expense of Qz1 during GBM, whereas Qz2-Qz2 boundaries are straight with common triple junctions implying static recrystallisation dominated by GBAR.

Our results demonstrate the in the importance of narrow fluid pathways in quartzite lithologies in shearzones. Areas highly affected by metasomatism induced by infiltrating fluid are juxtaposed with apparently unaffected areas millimetres or microns away.

Acknowledgements

Arild Monsøy and Kjetil Eriksen at the thin section laboratory at IGB, NTNU are thanked for patiently having prepared dozens of carefully polished thin sections. Belinda Flem and Øyvin Skår at NGU are acknowledged for their assistance with LA-HR-ICP-MS analyses at NGU. John Rasmus Leinum, Tor Arrild Nilsen, Kari Moen and Jarle Hjelen at NTNU are acknowledged for assisting out with the SEM-equipment at NTNU. This study was financed by the NFR grant to the Strategic University Program entitled "The value chain from mineral deposit to beneficiated product with emphasis on quartz".

References

Applin, K.R. and Hicks, B.D., 1987. Fibers of dumortierite in quartz. American Mineralogist, 71: 786-794.

Cameron, E.M., 1993. Reintroduction of gold, other chalcophile elements and LILE during retrogression of depleted granulite, Tromoy, Norway. Lithos, 29(3-4): 303-309.

Cameron, E.M., Cogulu, E.H. and Stirling, J., 1993. Mobilization of gold in the deep crust - Evidence from mafic intrusions in the Bamble Belt, Norway. Lithos, 30(2): 151-166.

Colivine, A.C. et al., 1984. An intergrated model for the origin of Archean lode gold deposits: Ontario. Geological Survey Open-file Report, 5524, 98 pp.

den Brok, B., Meinecke, J. and Roeller, K., 1994. FTIR determination of intragranular water content in quartzites experimentally deformed with and without added water in the ductile deformation field. Journal of Geophysical Research, B, Solid Earth and Planets, 99: 19821-19828.

den Brok, B. and Spiers, C.J., 1991. Experimental evidence for water weakening of quartzite by microcracking plus solution-precipitation creep. Journal of the Geological Society of London, 148: 541-548.

den Brok, S.W.J., 1992. An experimental investigation into the effect of water on the flow of quartzite. Geologica Ultraiectina, 95. Rijkuniversiteit, Mineralogisch-geologisch Instituut, Utrecht, Netherlands, 177 pp.

Flem, B., Larsen, R.B., Grimstvedt, A. and Mansfeld, J., 2002. In situ analysis of trace elements in quartz by using laser ablation inductively coupled plasma mass spectrometry. Chemical Geology, 182(2-4): 237-247.

Goetze, J., 2000. Cathodoluminescence in applied geosciences. In: M. Pagel, V. Barbin, P. Blanc and D. Ohnenstetter (Editors), Cathodoluminescence in geosciences. Springer. Berlin, Federal Republic of Germany. 2000.

Goetze, J., Ploetze, M., Graupner, T., Hallbauer, D.K. and Bray, C.J., 2004. Trace element incorporation into quartz; a combined study by ICP-MS, electron spin resonance, cathodoluminescence, capillary ion analysis, and gas chromatography. Geochimica et Cosmochimica Acta, 68(18): 3741-3759.

Goetze, J., Ploetze, M. and Trautmann, T., 2005. Structure and luminescence characteristics of quartz from pegmatites. American Mineralogist, 90(1): 13-21.

Goetze, J., Plotze, M. and Habermann, D., 2001. Origin, spectral characteristics and practical applications of the cathodolumimescence (CL) of quartz - a review. Mineralogy and Petrology, 71(3-4): 225-250.

Goreva, J.S., Ma, C. and Rossman, G.R., 2001. Fibrous nanoinclusions in massive rose quartz: The origin of rose coloration. American Mineralogist, 86: 466-472.

Griggs, D.T. and Blacic, J.D., 1965. Quartz; Anomalous weakness of synthetic crystals. Science, 147(3655): 292-295.

Groves, D.I. et al., 1992. Sub-greenshist- to granulite-hosted Archean lode gold deposits of the Yilgarn Craton: A depositional continuum from deep -sourced hydrothermal fluids in crustal-scale plumbing systems. In: J.E. Glover and S.E. Ho (Editors), The Archean: Terrains, processes and metallogeny. Geology Department University Extension 22. University of Western Australia Publication, pp. 325-337.

Harlov, D.E., 2000. Titaniferous magnetite-ilmenite thermometry and titaniferous magnetite-ilmenite-orthopyroxene-quartz oxygen barometry in granulite facies gneisses, Bamble sector, SE Norway; implications for the role of high-grade CO_2-rich fluids during granulite genesis. Contributions to Mineralogy and Petrology 139: 180-197

Jessell, M.W., 1987. Grain-boundary migration microstructures in a naturally deformed quartzite. Journal of Structural Geology, 9(8): 1007-1014.

Knudsen, T.L., 1996. Petrology and geothermobarometry of granulite facies metapelites from the Hisøy-Torungen area, South Norway; new data on the Sveconorvegian P-T-t path of the Bamble sector. Journal of Metamorphic Geology, 14(3): 267-287.

Kohlstedt, D.L., Evans, B. and Mackwell, S.J., 1995. Strength of the lithosphere; constraints imposed by laboratory experiments. Journal of Geophysical Research, B, Solid Earth and Planets, 100(9): 17,587-17,602.

Kronenberg, A.K., 1994. Hydrogen speciation and chemical weakening of quartz. In: P.J. Heaney, C.T. Prewitt and G.V. Gibbs (Editors), Silica; physical behavior, geochemistry and materials applications. Reviews in Mineralogy. Mineralogical Society of America, Washington, DC, United States, pp. 123-176.

Kronenberg, A.K., Kirkby, S.H., Aines, R.D. and Rossman, G.R., 1986. Solubility and diffusional uptake of hydrogen in quartz at high water pressures: implication for hydrolytic weakening Journal of Geophysical Research, B, Solid Earth and Planets, 91: 12723-12744.

Kronenberg, A.K., Segall, P. and Wolf, G.H., 1990. Hydrolytic weakening and penetrative deformation within a natural shear zone. In: A.G. Duba, W.B. Durham, J.W. Handin and F. Wang Herbert (Editors), The brittle-ductile transition in rocks. Geophysical Monograph. American Geophysical Union, Washington, DC, United States, pp. 21-36.

Kronenberg, A.K. and Wolf, G.H., 1990. Fourier transform infrared spectroscopy determinations of intragranular water content in quartz-bearing rocks; implications for hydrolytic weakening in the laboratory and within the Earth. Tectonophysics, 172(3-4): 255-271.

Kronenberg, A.K., Wolf, G.H. and Segall, P., 1984. Variations in intragranular water within a strain gradient; FTIR traverse across a ductile shear zone, AGU 1984 fall meeting. Eos, Transactions, American Geophysical Union. American Geophysical Union, Washington, DC, United States, pp. 1098.

Landtwing, M.R. and Pettke, T., 2005. Relationships between SEM-cathodoluminescence response and trace-element composition of hydrothermal vein quartz. American Mineralogist, 90(1): 122-131.

McCuaig, T.C. and Kerrich, R., 1998. P-T-t-deformation-fluid characteristics of lode gold deposits: Evidence from alteration systematics. Ore Geology reviews, 12: 381-453.

Müller, A., Wiedenbeck, M., Van den Kerkhof, A.M., Kronz, A. and Simon, K., 2003. Trace elements in quartz; a combined electron microprobe, secondary ion mass spectrometry, laser-ablation ICP-MS, and cathodoluminescence study. European Journal of Mineralogy, 15(4): 747-763.

Muto, J., Nagahama, H. and Hashimoto, T., 2004. Microinfrared reflection spectroscopic mapping: application to the detection of hydrogen-related species in natural quartz. Journal of Microscopy, 216: 222-228.

Muto, J., Nagahama, H. and Hashimoto, T., 2005. Water distribution in dynamically recrystallized quartz grains: cathodoluminescence and micro-infrared spectroscopic mappings. In: L. Burlin and D. Bruhn (Editors), Microstructural Evolution and Physical Properties in High-strain Zones. GSL Special Publications. Geological Society of London.

Nakashima, S. et al., 1995. Infrared microspectroscopy analysis of water distribution in deformed and metamorphosed rocks. In: C.J. Spiers and T. Takeshita (Editors),

Influence of fluids on deformation processes in rocks. Tectonophysics. Elsevier, Amsterdam, Netherlands, pp. 263-276.
Nesbit, B.E. and Muehlenbachs, K., 1989. Geology, Geochemistry, and genesis of mesothermal lode gold deposits of the Canadian Cordillera: Evidence for ore formation from evolved meteoric water. In: R.R. Keays, W.R.H. Ramsay and D.I. Groves (Editors), The geology of gold deposits: The perspektive in 1988. Economic Geology Monograph 6, pp. 553-563.
Nesbit, B.E., Murowchcik, J.B. and Muehlenbachs, K., 1986. Dual origins of lode gold deposits in the Canadian Cordillera. Geology, 14: 506-509.
Nijland, T.G., Liauw, F., Visser, D., Maijer, C. and Senior, A., 1993a. Metamorphic petrology of the Froland corundum-bearing rocks; the cooling and uplift history of the Bamble sector, South Norway. Bulletin - Norges Geologiske Undersokelse, 424: 51-63.
Nijland, T.G. and Maijer, C., 1993. The regional amphibolite to granulite facies transition at Arendal, Norway; evidence for a thermal dome. Neues Jahrbuch fuer Mineralogie Abhandlungen, 165: 191-221.
Nijland, T.G., Maijer, C., Senior, A. and Verschure, R.H., 1993b. Primary sedimentary structures and composition of the high-grade metamorphic Nivelda quartzite complex (Bamble, Norway), and the origin of nodular gneisses. Proceedings of the Koninklijke Nederlandse Akademie van Wetenschappen (1990), 96(2): 217-232.
Nijland, T.G. and Touret, J.L.R., 2001. Replacement of graphic pegmatite by graphic albite-actinolite-clinopyroxene intergrowths (Mjavatn, southern Norway). European Journal of Mineralogy, 13(1): 41-50.
Nijland, T.G., Touret, J.L.R. and Visser, D., 1998. Anomalously low temperature orthopyroxene, spinel, and sapphirine occurrences in metasediments from the Bamble amphibolite-to-granulite facies transition zone (South Norway); possible evidence for localized action of saline fluids. Journal of Geology, 106(5): 575-590.
Passchier, C.W. and Trouw, R.A.J., 2005. Microtectonics. 2 ed. Springer. Berlin, Federal Republic of Germany. , 366 pp.
Post, A. and Tullis, J., 1998. The rate of water penetration in experimentally deformed quartzite; implications for hydrolytic weakening. In: M. Chester Fred, T. Engelder and T. Shimamoto (Editors), Rock deformation; the Logan volume. Tectonophysics. Elsevier, Amsterdam, Netherlands, pp. 117-137.
Post, A.D., Tullis, J. and Yund, R.A., 1996. Effects of chemical environment on dislocation creep of quartzite. Journal of Geophysical Research, B, Solid Earth and Planets, 101(10): 22,143-22,155.
Sibson, R.H., Robert, F. and Poulsen, K.H., 1988. High-angle reverse faults, fluid pressure cyckling, and mesothermal gold-quartz deposits. Geology, 16: 551-555.
Sørensen, B.E. and Larsen, R.B., 2007. Paper2: The fluid evolution of the Froland area in the Bamble sector from peak P-T through cooling and uplift: implications

for retrograde mineral paragenesis and PT evolution of the Bamble sector. In: B.E. Sørensen (Editor), Metamorphic refinement of quartz under influence of fluids during exhumation with reference to the metamorphic/metasomatic evolution observed in amphibolites - a detailed field, microtectonic and geochemical study from the Bamble sector, South Norway. PhD Thesis, Department of Geology and Mineral Resources Engineering, NTNU Trondheim.

Sørensen, B.E., Larsen, R.B. and Austrheim, H., 2007. Paper3: Metasomatic evolution of the Froland amphibolites during cooling and uplift - textural observations and geochemical evolution of hydrous minerals. In: B.E. Sørensen (Editor), Metamorphic refinement of quartz under influence of fluids during exhumation with reference to the metamorphic/metasomatic evolution observed in amphibolites - a detailed field, microtectonic and geochemical study from the Bamble sector, South Norway. PhD Thesis, Department of Geology and Mineral Resources Engineering, NTNU Trondheim.

Touret, J., 1968. The Precambrian metamorphic rocks around the Lake Vegår (Aust-Agder, southern Norway). Norges Geologiske Undersøkelse, 257, 45 pp.

Touret, J., 1971. Le faciès granulite en Norvège méridionale II Les inclusions fluides. Lithos, 4: 423-436.

Touret, J., 1985. Fluid regime in southern Norway: the record of fluid inclusions. In: A.C. Tobi and J. Touret (Editors), The deep Proterozoic crust in the North Atlantic Provinces NATO ASI Ser. Ser. C: Math. Phys. Sci., pp. 517-549.

Touret, J. and Olsen, S.N., 1985. Fluid inclusions in migmatites. In: J.R. Ashworth (Editor), Migmatites. Shiva, Glasgow, pp. 265-288.

Tullis, J., 2002. Deformation of Granitic Rocks: Experimental Studies and Natural Examples In: S.-i. Karato and H.-R. Wenk (Editors), Plastic Deformation in Minerals and Rocks. Reviews in MIneralogy. MSA.

Tullis, J. and Yund, R.A., 1989. Hydrolytic weakening of quartz aggregates; the effects of water and pressure on recovery. Geophysical Research Letters, 16(11): 1343-1346.

Van den Kerkhof, A.M., Kronz, A., Simon, K. and Scherer, T., 2004. Fluid-controlled quartz recovery in granulite as revealed by cathodoluminescence and trace element analysis; Bamble sector, Norway. Contributions to Mineralogy and Petrology, 146(5): 637-652.

Wark, D. and Watson, E.B., 2006. TitaniQ: a titanium-in-quartz geothermometer Contributions to Mineralogy and Petrology, 152(6): 743-754.

Watson, E.B. and Brenan, J.M., 1987. Fluids in the Lithosphere, 1. Experimentally determined wetting characteristics of CO_2-H_2O fluids and their implications for fluid transport, host-rock physical properties, and fluid inclusion formation. Earth Planet Scientific Letters, 85: 496-515.

Paper 2: The fluid evolution of the Froland area in the Bamble sector from peak P-T through cooling and uplift: implications for retrograde mineral paragenesis and PT evolution of the Bamble sector

Bjørn Eske Sørensen
Department of Geology and Mineral Resources Engineering, Norwegian University of Science and Technology (NTNU), N7491 Trondheim, Norway
(bjorn.sorensen@ntnu.no)

Rune Berg Larsen
Department of Geology and Mineral Resources Engineering, Norwegian University of Science and Technology (NTNU), N7491 Trondheim, Norway
(rune.larsen@ntnu.no)

Abstract

Microthermometry on fluid inclusions that can be related to specific mineral parageneses constrain the fluid evolution of the Froland area in the Bamble sector to four specific fluid inclusion assemblages (FIA1-4).

FIA1: Pure CO_2 in garnet quartz symplectites that are interpreted as partial melts in amphibolites. FIA1 corresponds to the fluid present during peak metamorphic conditions.

FIA2: Retrograde fluids comprising low CO_2 brines with salinity near the NaCl-KCl-H_2O eutectic and coexisting with CO_2-rich low salinity H_2O-CO_2 mixtures. Found in en-echelon quartz veins, surrounded by biotite-amphibole assemblage.

After FIA2 fluids (FIA3 and FIA4), CO_2 and other carbonic species are not detected.

FIA3: Brines with 25 wt% NaCl and 6wt% $CaCl_2$. FIA3 are hosted by quartz in quartz biotite gneisses. FIA3 relates to scapolitisation and replacement of rutile by titanite and the formation of high purity quartz.

FIA4: Primary inclusions in calcite and epidote cores. Salinities were determined as $CaCl_2$ equivalents by microthermometry and vary between 36 wt% in early FIA4 inclusions and 31 wt% in late FIA4 inclusions. Compositional variation in epidote with $EpCz_{70\text{-}75}$ in cores and $EpCz_{65}$ in rims imply that Fe^{3+} increased over time. This agrees with lowering of the first melting temperatures in late FIA4 inclusions suggesting additional cations in solution.

All together the fluid inclusions document a high salinity averaging 30 wt% throughout cooling and uplift of the Froland area and that the saline fluids partially control the retrograde assemblages. Accordingly, the previously published PT-path of Froland is revaluated with PERPLEX modelling. In addition the well defined isochore

of FIA3 and Ti in quartz thermometry are used to support the new PT-path. Our results confirm the main features of the Nijland et al. (1993) cooling and uplift path. The following stages in the PT-X_{fluid} path could be constrained:

1*:* Simultaneous reactions diopside + phlogopite + quartz = sanidine+tremolite and diopside+H_2O+CO_2 = tremolite + calcite + quartz in calc-silicates fixes PT at a pseuodounivariant point. The presence of rutile together with sanidine and tremolite suggest reduced XH_2O in the fluid caused by the presence of salts and CO_2 in the fluid near the thermal maximum of the tremolite + calcite + quartz assemblage. Accordingly, the PT-conditions were approximately 626°C and 7 kb. The total fluid composition for this stage is estimated to be $XCO_2 = (n_{CO2}/(n_{CO2}+n_{H2O}) = 0.32$, $XH_2O = 0.68$, $wt\%NaCl = wt_{NaCl}/(wt_{H2O}+wt_{NaCl})=0.30$. Because the assemblage sanidine + tremolite is not replaced by phlogopite + calcite + quartz during cooling and uplift we infer that XCO_2 decreased rapidly with falling temperatures.
2: MII (kyanite-chlorite-muscovite veins) and MIII (margarite + corundum) of Nijland et al. (1993) have overlapping PT stability fields. Both are alteration products of an assemblage originally comprising corundum + plagioclase. MII muscovite was stabilised by potassium rich fluids. Decreased potassium content/increased calcium content of the fluid stabilised margarite over muscovite the margarite + corundum assemblage was formed. The stability of margarite + corundum in P-T space is considerably larger than reported by Nijland et al. (1993), who used the anorthite + $H_2O \leftrightarrow$ margarite + zoisite + SiO_2 reaction to define the lower temperature boundary. However, the stability of zoisite is primarily a function of bulk/fluid composition hence zoisite may be stabilised along with margarite in most of the margarite + corundum PT stability field, only by modifying bulk composition. P-T conditions of MII represent a relatively narrow temperature field from 450 to 550°C. Pressure is constrained by the stability of kyanite which defines the lower pressure limit to 4.5 kb.
3: The uplift path is constrained by the isochore of FIA3. The well preserved fluid inclusions suggest an uplift path that was sub parallel with the isochore. Uplift likely occurred at 300 to 400^{o}C. Accordingly, the Froland lithologies experienced a P-drop from 5-7 kb to 2-3 kb at temperatures 100°C lower than the interpretation provided by Nijland et al. (1993).
4: The last stage is defined by coexisting prehnite/pumpellyite and the fluid inclusion studies of Touret and Olsen (1985) to 2-3 kb and 175-280°C.

Our results underline the importance of fluids in interpreting metamorphic mineral assemblages given that the position of the equilibria in P-T space varies considerably with changing fluid composition.
The shift between MII and MIII assemblages marks an important event in the metasomatic evolution of the Bamble sector when alteration shifted from sodic-potassic to sodic-calcic. The same change is recorded by the shift in fluid composition between FIA2 to FIA3.

1 Introduction

The retrograde fluid evolution of the Bamble sector is not well constrained although some studies report on brine fluids associated with alteration processes (e.g. Nijland and Touret, 2001; Nijland et al., 1998; Touret, 1985).

The aim of the current study is to focus on the importance of the fluid composition in regional shear zone complexes, such as the Bamble sector, in partially controlling the mineral assemblages. We aim at reconstructing important stages of the fluid evolution of the Bamble sector from upper amphibolite facies conditions through exhumation to greenshist facies conditions. None of the previous studies were able to constrain the timing, evolution and importance of the fluid phase during exhumation of the Bamble rocks. Particularly, this study demonstrates that the stabilities of the retrograde mineral assemblage are affected by the fluid composition.

The preferred approach is to study fluid inclusion fluids associated with characteristic alteration assemblages. Lack of proper index assemblages in the alteration rocks inhibits precise PT-estimates, however, partially; this inhibition is overcome by thermodynamic modelling of phase diagrams. Partially, the stability of many retrograde mineral assemblages depends on the fluid composition. As a result, many of the previously published PT-paths are uncertain because they do not quantify the role of the fluid composition including the salinity of the fluid.

We demonstrate that high salinity fluids with a high capacity to transport and buffer cations from the host rock lithologies dominated the uplift path.

Our studies document four characteristic stages comprising each their FIA (fluid inclusion assemblages), here presented in chronological order.

FIA1: Partial melting in garnet amphibolite, fluid inclusions from quartz in garnet quartz symplectites. Found at locality 1 (Figure 1).

FIA2: Primary fluid inclusions in en-echelon quartz veins in amphibolite. Found in locality 3 (Figure 1).

FIA3: Inclusions in quartz related to recrystallisation of quartz in a fluid channel pattern and to replacement of plagioclase by scapolite at locality 2 (Figure 1). The quartz formed during infiltration of FIA3 and experienced localised strain softening and the formation of SGR (subgrain rotation recrystallisation) microstructures in quartzites. The geometry of these SGR structures in quartzites suggest that they formed during thrust related deformation in an oblique slip pattern, controlled by the combination of pre-existing weakness planes and a N-S compressive stress field (paper 1, Sørensen and Larsen, 2007). Accordingly, the fluids belonging to FIA3 pose an important control upon the rheological properties of the Bamble rocks during exhumation.

FIA4: Primary inclusions in calcite and in epidote in a calcite-epidote-tremolite-apophyllite calc-silicate assemblage at locality 2 (Figure 1). They are associated with an assemblage that intersects all other observed alteration types. It is barely deformed hence is may have formed late during uplift or even later. The calcite-epidote-tremolite assemblage belongs to a series of complex calc-silicate assemblages formed during

retrogression of a phlogopite-diopside rock. The retrograde assemblages associated with these fluids are the result of hydration and chemical alteration during exhumation. Cation exchange between the fluids and the siliceous gneisses and amphibolites, determines the stable mineral assemblage. The results from the fluid inclusion studies are used to re-evaluate the retrograde PT-path for the Froland area.

2 Geological setting

The Bamble sector comprises exceptionally well preserved Sveconorwegian high grade amphibolite-granulite facies rocks. Most authors agree that peak PT-conditions were c. 850 °C in the HT granulite facies zone at Arendal, and tapering towards lower T in a thermal dome pattern (Figure 1). Peak P was approximately 6-7 kbar.

Fluid inclusion studies document that at peak P-T conditions CO_2 dominated fluids in amphibolite lithologies, and CO_2 + brines in more siliceous gneisses (Touret, 1971). This COH fluid composition is matched by fluid modelling using the iron-titanium oxygen barometer (Harlov, 2000). The conditions during exhumation are far less constrained although the absence of retrograde aluminous silicate assemblages imply high alkali-chloride activities in the retrograde fluids (Touret, 1968). Knudsen (1996) summarise the available retrograde PT-paths of the Bamble sector and conclude that the PT-paths display systematic spatial variations characterised by a steep retrograde path in the southernmost part (Knudsen, 1996), followed by isobaric cooling in the southeast and a slight pressure increase in the north. However, it is also concluded that the P-T estimates are uncertain.

The publication of Nijland and co-workers (1993) is the only study to quantify the retrograde PT-path of the Froland area. Their results imply a 5 stage cooling path: MI (750°C, 7 kb), MII isobaric cooling (600-700°C, 7kb), MIII exhumation and rehydration (500-570°C 3-7 kb), MIV (400°C, 2-4 kb), MV (175-280°C, 2-3 kb). (Cosca et al., 1998) modelled the PT-t path with the Nijland data:

1. Near isobaric cooling at 7 kb and 750-600 °C, dP/dT = 2 bars/°C, DT/dt= 3-8°C/Ma.
2. Exhumation dP/dT = 30 bar/°C, dP(depth)/dt=0.5-1 mm/a, Dt/dt=2-4°C/My.
3. Bamble rocks remained at a depth of approximately 10 km while slowly cooling from 300°C until ~200 Ma (e.g. Nijland et al., 1993).

Intense metasomatic alteration is common along retrograde shear zones and faults following a rhombohedral net work, associated with exhumation and possibly also extensional collapse of the Sveconorwegian mountain range (Touret, 1968). Brine-fluid inclusions are documented together with the alteration assemblages (e.g. Nijland and Touret, 2001; Nijland et al., 1998; Touret, 1985). Aqueous inclusions are interpreted as late, and there is a tendency towards density increase for progressively younger fluid inclusions (Touret and Olsen, 1985). However, aqueous brine inclusions have high densities, but are interpreted as early (Touret and Olsen, 1985). The exact

timing and petrological significance of the retrograde aqueous/aqueous brine inclusions are not resolved (Touret and Olsen, 1985).

Calc-silicate rocks are common in the Bamble sector in both granulite facies areas (Bugge, 1943; Bugge, 1945; Bugge, 1940; Nijland and Maijer, 1993) and amphibolite facies areas (Barth and Dons, 1960).

Studies of amphibolites and quartzites characterises the retrogression as the result of episodic influx of brine fluids in discrete fractures during exhumation (paper 1 and 3, Sørensen and Larsen, 2007; Sørensen et al., 2007).

Furthermore, fluid related quartz recrystallisation textures correlate with thrust related quartz microstructures, testifying to the important role of hydrolytic weakening of quartz in the exhumation process. Similar observations were done in the Modum area (north Bamble sector), where the infiltrating fluids were mixtures of basinal brines and biogenetic carbonic fluids (Gleeson et al., 2003; Munz et al., 1994; Munz et al., 1995; Munz et al., 2002). Gleeson et al. (2003) also underlined the importance of hydrolytic weakening facilitated by retrograde fluids in the exhumation processes in the Modum area.

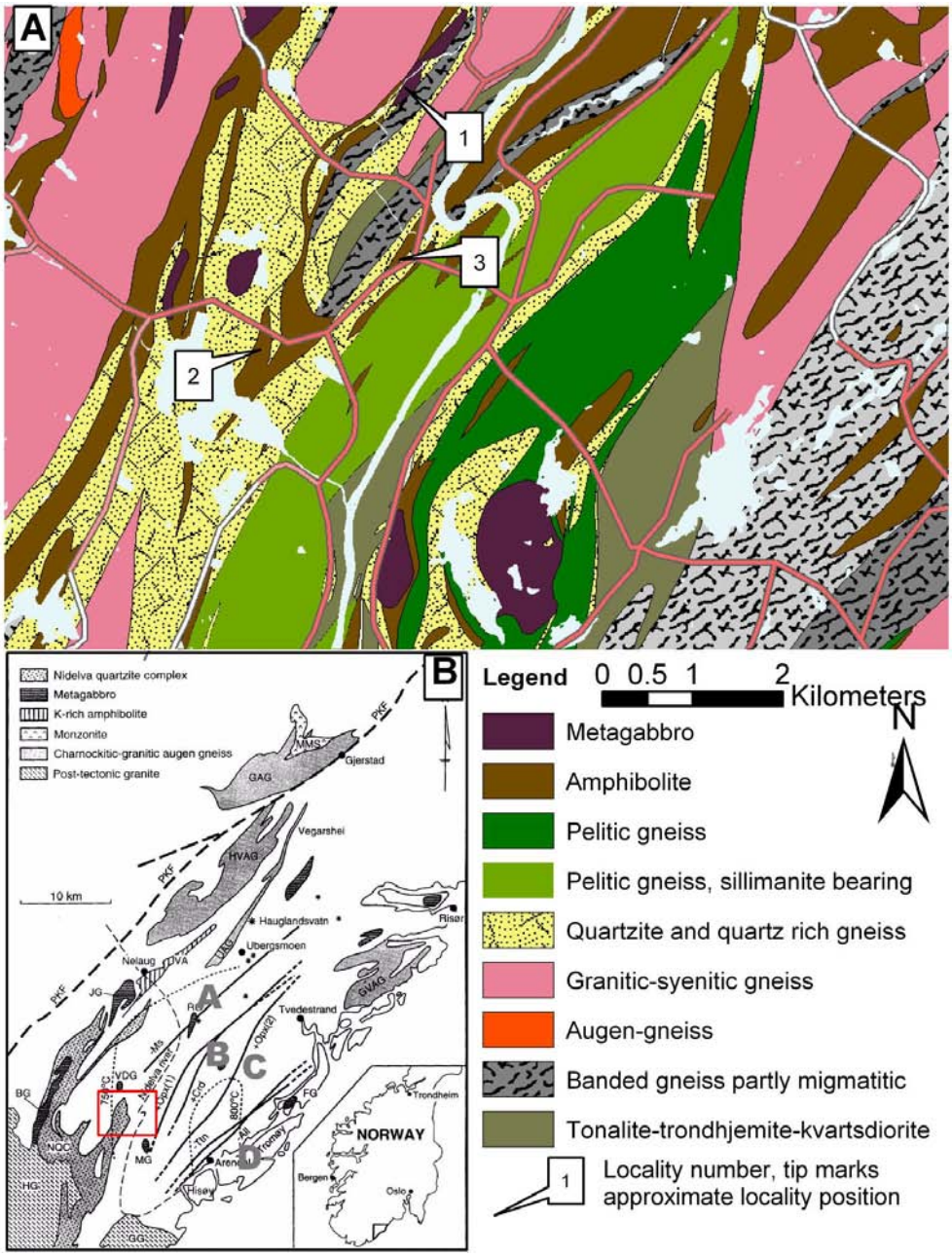

Figure 1: Geological maps. A) Detailed map of the investigated area. Modified from Geological Survey of Norway, N-50 berggrunnskart 16123 Nelaug and 16114 Arendal. Geographic data (roads, lakes and rivers) are added for easy orientation (source: www.geonorge.no). B) Overview map of the Bamble sector displaying the most important

rock units (see legend on map). Insert shows the position of the Bamble sector in South Norway. Red square denotes the position of the study area shown in A. From Nijland et al. (1998). Also shown in A are the metamorphic zones in the Bamble sector.

---

3 Field and petrographic observations

3.1 Calc-silicates

The calc-silicate rocks used in this study comprise a metre thick layer sandwiched between quartz-biotite-plagioclase-microcline gneiss and amphibolite at locality 2 (Figure 1). It is interpreted as a reaction skarn formed at the expense of the host rocks.

The high temperature assemblage comprises diopside + phlogopite+ titanite (Mp1 Table 1). This assemblage is only stable at high P and T, with the lower T stability limit dropping with increasing pressure (see also discussion). The calc-silicates experienced fluid aided retrograde alteration. Mp 1 is preserved in lensoid bodies. Alteration towards the amphibolite comprises biotite and amphibole (Mp2c) giving a gradual transition from the Fe-rich amphibolite to the Mg-rich calc-silicate rock (Figure 3, Table 1). The Alteration product of the Mp1 assemblage against the siliceous gneiss comprises microcline, actinolite and rutile/titanite (Mp2a) (Figure 3, Table 1).

Mp1 is also intersected by two types of vein replacements grouped in Mp2b (Table 1). Mp2b veins exposed toward the amphibolite comprise the assemblage pyrrhotite + calcite + tremolite. Mp2b veins exposed toward the gneiss comprise only calcite + tremolite (Figure 3). This suggests that the Fe in the pyrrhotite bearing veins was supplied by the amphibolite (Figure 3). Both vein types are interpreted as direct replacements of the Mp1 diopside. Quartz is part of the Mp2b assemblage though quartz is not found in the veins but in the metasomatic sides (Table 1). Considerable metasomatic differentiation is observed in relation to the Mp2 assemblage, giving zones comprising pure tremolite.

M2a-b assemblages are intersected by veins comprising new diopside, orthoclase, albite, pyrrhotite and titanite (Mp3, Table 1). The diopside formed in Mp3 is Mg-rich but has a significantly higher Fe content than the Mp1 diopside (Table 2).

Phlogopite is replaced in a later assemblage by clinochlore and muscovite in an assemblage comprising tremolite, pyrrhotite, graphite and minor molybdenite (Mp4). Pyrite is also present in samples dominated by the Mp4 assemblage, but comprises fingering veins intersecting the textures of the Mp4 assemblage.

Mp5 is the last of the calc-silicate assemblages comprising epidote, calcite, tremolite, pyrite and apophyllite (Table 1). Mp5 also occurs in bands intersecting the foliation in the gneiss.

All the Fe-Mg phases except for epidote have compositions close to the Mg-endmembers (Table 2, Figure 2). The amphiboles comprises both edenite and

tschermakite substitutions, with Mg/Fe ratio close to 0.9 (Figure 2). Accordingly it is the Na-Al-Fe proportions that are used in their classification.

Table 1: Alteration stages in calc-silicate rocks.

Name	brief description	mineralogy	Occurrence/paragenises
Mp1	Diopside phlogopite veins	Diopside, phlogopite, minor apatite	Meter thick lensoid bodies/layers at the boundary between quartz biotite-tourmaline-plagioclase gneiss and amphibolite. In some places it occurs together with carbonate bearing rocks
Mp2a	Microcline-tremolite massive metasomatic rock	Microcline, tremolite/actinolite, rutile/titanite and zircon. Calcite occurs with titanite and tremolite but not with rutile. Rutile occurs together with sanidine and tremolite but never with calcite.	Marginal alteration of Mp1 toward the quartz-biotite-plagioclase-tourmaline gneiss. Comprises coarse- and fine-grained parts. Rutile is partly replaced by titanite. Rutile is better preserved in more coarse-grained parts and occurs along with calcite, whereas titanite predominates in the fine-grained parts. The boundary toward Mp1 is smooth whereas the boundary toward the gneiss is serrated
Mp2b	Tremolite-calcite veining intersecting Mp1	Veins: Tremolite, calcite ± pyrrhotite. Metasomatic sides: quartz, titanite, tremolite.	Intersects Mp1 and alters it. Vein thickness varies between cm to mm size and is observed as greenish stripes intersecting the cream coloured Mp1 diopside matrix. Pyrrhotite bearing veins are recognized by rusty stains.
Mp2c	Phlogopite/ biotite-tremolite/magnesiohorblende	Tremolite/-magnesiohornblende, biotite, pyrrhotite and apatite	Not truly calc-silicate but reaction between the calc-silicate and the neighbouring amphibolite.
Mp3	Tremolite-dioside-albite-orthoclase veining	Veins: Tremolite, diopside, albite untwinnned occur intergrown with orthoclase. Calcite also present	Intersects apparently unaffected monomineralic tremolite, belonging to Mp2b. Secondary muscovite is common and clinozoisite commonly forms as rims around pyrrhotite grains. Tremolite grows into the veins, but is chemically similar to the tremolite surrounding the veins.
Mp4	Clinochlor, clinozoisite, graphite bearing assemblage.	Clinozoisite, clinochlore, tremolite, graphite, molybdenite, Pyrrhotite and chalcopyrite	Replacement of Mp1.Field observations testify that it is younger than Mp1, Mp2a, Mp2b and Mp2c.
Mp5	Tremolite-epidote-calcite around calcite-apophyllite vug fillings	Calcite, epidote, tremolite, pyrite and flour apophyllite	Marginal alteration of Mp1+Mp2b toward the quartz-biotite-plagioclase-tourmaline gneiss. Depends on addition of chemical components SiO_2 and Al_2O_3 from the gneiss. Similar assemblages seen in gneiss intersecting all other alterations on the field scale. The Fe needed for epidote formation supplied by replacement of pyrrhotite by pyrite.

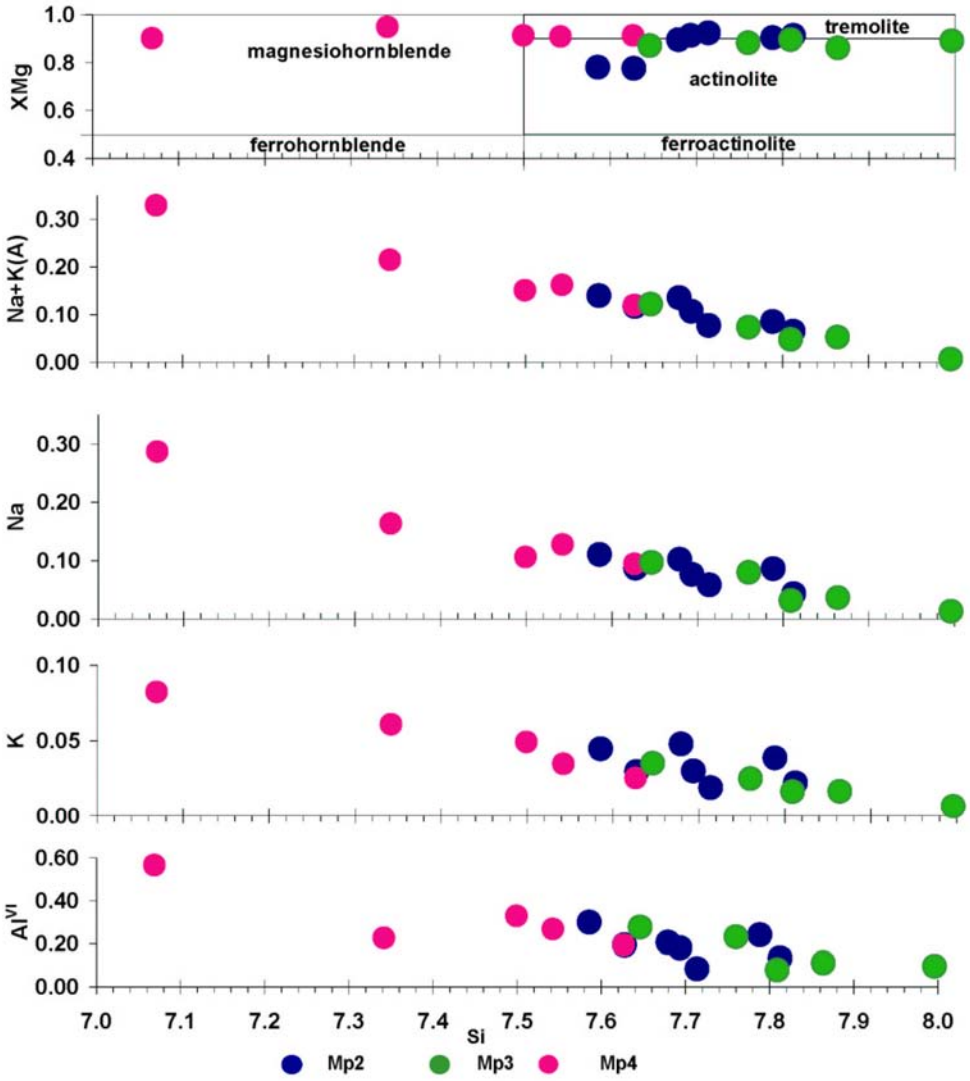

Figure 2 : Amphibole chemistry in calc-silicate rocks. Note the increased edenite ($NaAl^{IV}\square_{-1}Si_{-1}$) and Tschermak ($Al^{IV}Al^{VI}Mg_{-1}Si_{-1}$) substitution in Mp4 amphiboles compared to amphiboles from Mp2 and Mp3.

Table 2: Representative analyses of phases in the calc-silicate assemblages.

	Pyroxene				Phlogopite	Chlorite	Muscovite
	Mp3		Mp1		Mp1	Mp4	Mp4
	average	Std.dev	average	Std.dev			
				Oxide			
SiO_2	54.309	0.603	53.633	0.431	39.268	29.206	45.471
Al_2O_3	0.221	0.083	0.559	0.220	16.667	20.125	36.067
FeO	3.961	0.480	2.458	0.187	6.058	4.829	0.049
MnO	0.211	0.024	0.101	0.016	0.082	0.053	0.000
MgO	15.566	0.293	16.676	0.190	20.719	29.606	0.000
CaO	25.164	0.213	25.453	0.076	0.000	0.007	0.048
Na_2O	0.089	0.037	0.154	0.035	0.129	0.009	0.143
K_2O	0.026	0.020	0.019	0.018	10.128	0	9.983
TOTAL	99.547	0.806	99.054	0.525	93.051	83.835	91.761
H_2O*)	-	-	-	-	4.105	16	4.397
				Calculated formulas			
					22 oxygen	28 oxygen	22 oxygen
Si	2.002	0.007	1.978	0.008	5.736	5.74	6.202
Al^{iv}	0.002	0.003	0.022	0.008	2.264	2.26	1.798
Al^{vi}	0.008	0.005	0.003	0.002	0.606	2.41	3.999
$Fe^{3+*)}$	0.006	0.010	0.047	0.011	no est.	0.08	no est.
Fe^{2+}	0.117	0.017	0.028	0.005	0.740	0.71	0.006
Mn	0.007	0.001	0.003	0.000	0.010	0.01	0.000
Mg	0.855	0.017	0.917	0.007	4.512	8.67	0.000
Ca	0.994	0.009	1.006	0.003	0.000	0.00	0.007
Na	0.006	0.003	0.011	0.002	0.037	0.01	0.038
K	0.001	0.001	0.001	0.001	1.887	0.00	1.737
OH*	-	-	-	-	4.000	16.00	4.000
TOTAL	3.997	0.007	4.016	0.004	19.791	35.90	17.787
XMg	0.874	0.018	0.967	0.005	0.859	0.92416222	-
Wo	50.072	0.196	49.978	0.105	-	-	Y total
En	43.103	0.780	45.564	0.391	-	-	4.005
Fs	6.504	0.768	3.912	0.277	-	-	X total
Ac	0.321	0.132	0.547	0.123	-	-	1.781
*) Fe3+ from Droop (1987) in pyroxene. Fe2+/Fe3+ and OH calculated assuming full site occupancy in phlogopite							Al total 5.798

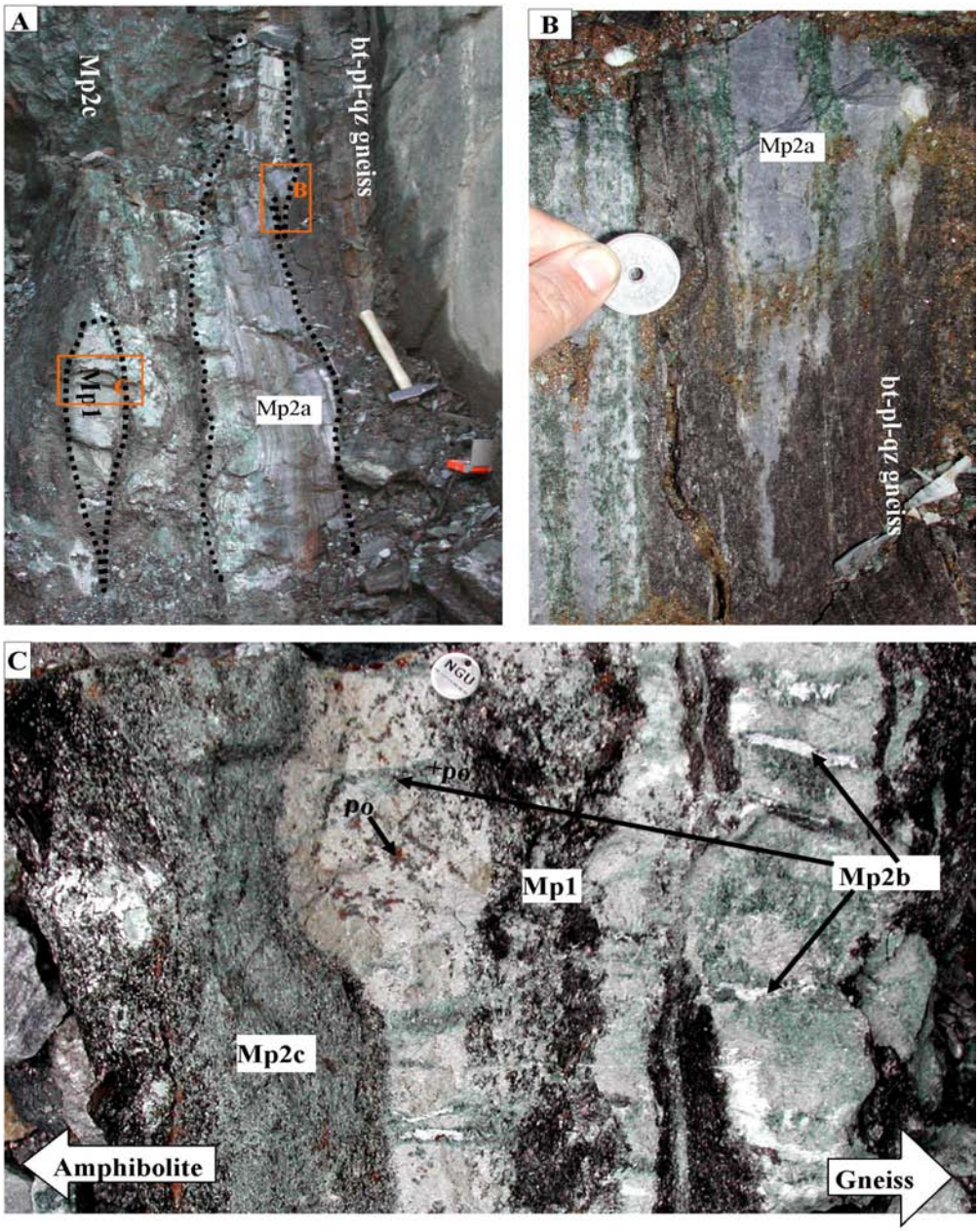

Figure 3: Field image displaying the relation between calc-silicate assemblages Mp1, Mp2a, Mp2b and Mp2c formed in calc-silicate body squeezed between amphibolite (left) and gneiss (right). A) Overview. B) Detail showing Mp2a and gneiss. C) Detail of calc-silicate body, intersected by Mp2b veins, note that pyrrhotite primarily occurs toward the amphibolite, suggesting that Fe was supplied by the amphibolite.

3.2 Amphibolites

The amphibolites experienced a complex metamorphic evolution as discussed in detail by Sørensen et al. (2007, paper 3). The first retrogressive event comprises potassium addition to the amphibolites. This caused the growth of biotite and rims on amphiboles and the formation of decussate textures in reaction zones of magnesiohornblende, biotite, plagioclase and ilmenite bordering en echelon quartz veins and plagioclase-calcite-pyrrhotite veins (Alt1, Table 3). Biotite and plagioclase forming during Alt1 are locally replaced by K-feldspar (Alt2). Late scapolitisation (Alt3) involves replacement of plagioclase by scapolite in the titanite stability field. The amphibolite alteration (Alt1) represent a wide range of amphibole compositions, following the pargasite substitution vector from ferro-tschermakite/(pargasite) (XMg = 0.3) to actinolite (XMg = 0.9) and occurred during falling temperatures (Sørensen et al., 2007, paper 3). A more detailed description of the alteration of the amphibolites is given in Table 3 and in Sørensen et al. (2007, paper 3).

3.3 Quartzites, quartz rich gneisses and quartz veins

Sørensen and Larsen (2007, paper 1) used SEM-CL and LA-ICP-MS to define the recrystallisation path of quartzites along the cooling and uplift path of the Bamble sector. Four main types of quartz are recognised:

Qz1: Bright islands surrounded by narrow darker cracks
Qz2: Light grey quartz with the same grey level as the channels in Qz1. Occasionally with oscillatory zoning.
Qz3: Dark grey diffuse channels intersecting Qz1 and Qz2.
Qz4: Black to very dark grey luminescence.

Qz1 represents relic high grade quartz forming during upper amphibolite facies metamorphism. The cracked texture in Qz1 is linked to introduction of aqueous fluids to a dry protolith causing brecciation, dissolution and precipitation of Qz2. Ti in quartz geothermometry with the Wark et al.(2006) calibration suggests Qz2 formation at c. 626°C. Repetitive pulses of fluids during uplift facilitated quartz recrystallisation and formation of Qz3. Qz3 is more ductile than Qz1 and Qz2 during exhumation and experienced subgrain rotation recrystallisation (SGR) whereas Qz1 and Qz2 were brittle. For more details see Table 4.

Trace element analyses document that quartz was purified through retrograde recrystallisation and Qz3 comprises economically attractive high purity quartz (Sørensen and Larsen, 2007).

Table 3: Alteration types in amphibolites. From Sørensen et al. (2007, paper 3). See text for discussion.

Alt1: Potassic alteration with biotite stable
Alt1a: Alteration of amphiboles associated with introduction of biotite. In thin sections amphibole cores are dark brownish green whereas rims vary from dark bluish green ferropargasite/ferropargasite (Amp3a) through light green magnesiohornblende (Amp3) to almost colourless actinolite (Amp4). **Alt1b:** Veins with a central assemblage comprising plagioclase, calcite, apatite, pyrrhotite, ilmenite/rutile and magnesiohornblende (Amp3). Surrounded by two successive alteration zones, the inner zone comprising amphibole, plagioclase and rutile/ilmenite and the outer zone comprising biotite, plagioclase and ilmenite/rutile. **Alt1c**: Alteration in relation to en-echelon quartz veins intersecting the foliation in the amphibolite. Alteration comprises biotite, amphibole and plagioclase and ilmenite. Alternating zonation with variation in the amount of biotite, plagioclase and amphibole. Ilmenite is partly replaced by titanite. **Alt1d**: biotite amphibole rock. Titanite most common, but ilmenite preserved as cores together with rutile. Similar to the alteration around the en-echelon quartz veins (Alt1c).
Alt2: Potassic alteration K-feldspar replacing plagioclase and biotite
Replacement of biotite by K-feldspar. Final alteration product is a light grey rock consisting of K-feldspar, and light green amphibole (Amp4). Titanite is very abundant in this rock type and almost no ilmenite/rutile is observed. Several types of replacements are seen replacing Alt1 assemblages.
Alt3: scapolitisation
Massive scapolitisation. Quartz veins surrounded by reaction rims of scapolite, but minor amounts of scapolite are also observed in many places in the amphibolite. The quartz veins with the reaction rim of scapolite have a different colouration than quartz veins with less scapolite. The scapolite has a white colour and is only distinguished from commonly occurring white feldspars by its characteristic cleavage.

Table 4: Quartz types documented by SEM-CL in the studied area and their genetic significance. From Sørensen and Larsen (2007, paper 1). See illustration in Figure 4

Quartz type	SEM-CL texture	Genetic interpretation
Qz1	Bright islands surrounded by darker cracks. Typically partially luminescence quenched.	Relic high grade quartz. The island texture testifies to a brecciation and dissolution process and to the formation of Qz2. This related to sudden influx of hydrous fluids under stress in dry protolith quartz.
Qz2	Light grey, sometimes with weak oscillatory zoning. Brighter cores and darker rims, approaching the luminescence of Qz3.	Relates to brecciation and dissolution/re-precipitation of Qz1 and to the first observed influx of hydrous fluids. Qz2 also relate to thrust related dynamic recrystallisation involving high temperature grain boundary migration (GBM) in relation to trusting. Dynamic recrystallisation in Qz2 occur together with plastic deformation of feldspar
Qz3	Dark grey diffuse fluid channel texture, which follows grain boundaries or cut through grains. Qz3 is commonly in optical continuity with Qz2, but is distinguished by the absence of rutile needles and by the SEM-texture.	Relates to influx of aqueous fluids and to SGR (sub grain rotation recrystallisation) in relation to thrusting, which occurs only in Qz3 and in not in juxtaposed Qz2 and Qz1 which commonly shows evidence of brittle deformation at the same time that Qz3 deforms plastically. This is inferred to reflect local variations in the H_2O fugacity. Also associated with breakdown of rutile to titanite.
Qtz4	Narrow cracks and pods of black quartz, crosscutting the other types.	Mostly dissolution textures, comprising two types of cracks: 1: Interconnected network of non-luminescent quartz, following micron thin irregular trans/circum-granular cracks. Texture suggests that pure dissolution dominated dominant and Qz4 thus probably formed in the retrograde dissolution field of quartz. 2: Straight trans-granular cracks intersecting the irregular cracks.

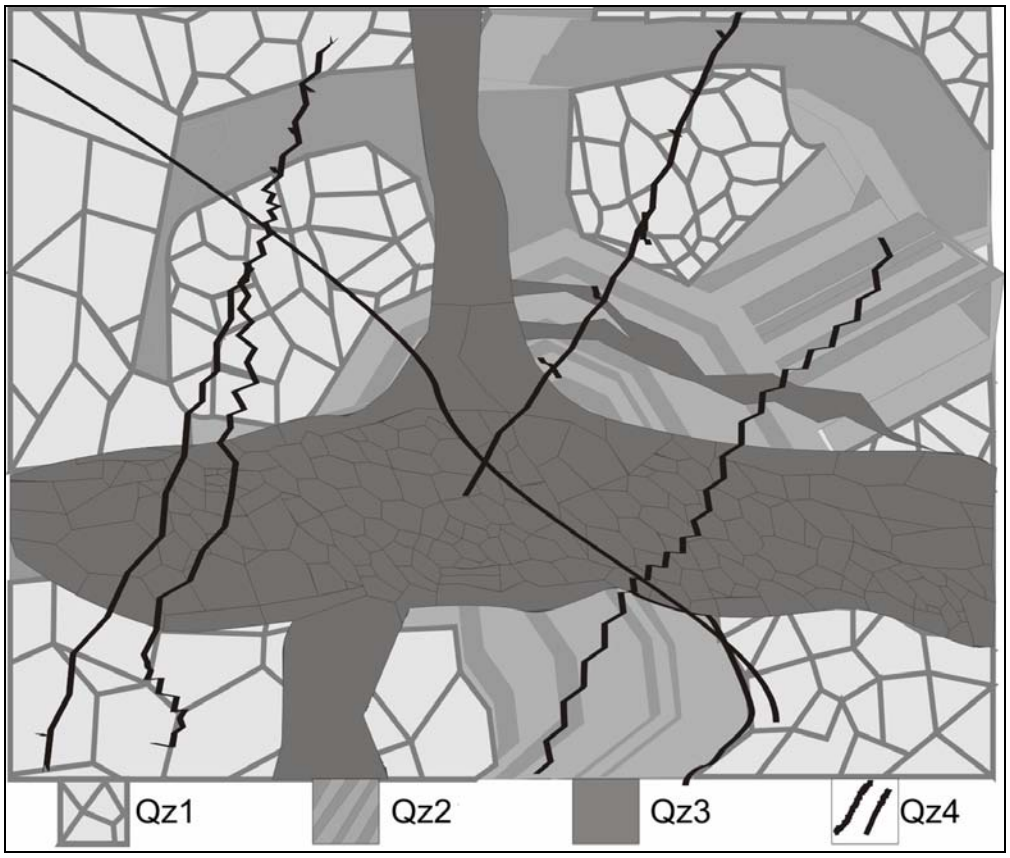

Figure 4: Quartz types as defined by optical microscopy and SEM-CL. Textures are general to quartz veins, quartzites and siliceous gneisses in the investigated area. See Table 4 for description. From Sørensen and Larsen (2007, paper 1).

4 Analytical methods

4.1 Microthermometry

Fluid inclusion microthermometry was accomplished with a Linkam THMSG600 fluid inclusion stage (Linkam Scientific instruments Ltd.), mounted on a Nikon E600 optical microscope, equipped with long distance lenses facilitating magnification to 1000x and a PIXELLINK PL-A662 firewire digital camera. Images and videos were recorded along with the microthermometric experiments on a computer using the Linksys32-DV software (Linkam Scientific instruments Ltd.).

Melting behaviour was studied after cooling to between -100°C and -196°C, followed by heating. Inclusions with simple phase behaviour were measured "live",

using the manual controls in the Linkam software. Phase transitions were first estimated using a high heating rate (20-10°C/min) and then refined using slower heating rates (1-2 °C/min) after keeping the temperature just below the phase transition temperature for 1 or 2 minutes. More complex inclusions were first estimated manually according to the above procedure followed by a refinement using video recording during slow heating experiments. Phase changes that were not observed manually during slow heating were then detected by carefully inspecting the recorded video. This method was particularly strong in estimating eutectic melting temperatures that otherwise may be difficult to distinguish from recrystallisation.

Phase transitions during heating from 20^{o}C, comprising LV-L, LVS-LS; LS-L and LVS-LV, were recorded live, using heating rate of 2°C/min near the transition temperature after the temperature was kept constant for a while. Experiments with slower heating rates confirmed the observed phase transition temperatures.

The fluid inclusion stage was calibrated with a set of synthetic fluid inclusions (fluids Inc.) with 10 measurements on each standard. CO_2 was used for calibration at -56.5°C, an NaCl (25 wt%) was used for calibration at -21.1°C, the eutectic point in the H_2O-NaCl binary, a NaCl (10wt%) standard was used for calibration at –6.646°C. A regression line through the calibration point was strictly linear consistent with a low 0 point offset (- 0.0027 = 0.0) and temperature offset at Tm_CO_2 of -0.91°C. This calibration procedure was far superior of methods using solid standards that failed to give consistent results. However, powder standards were used for high temperature calibration to avoid the subtle volume changes associated with synthetic inclusions.

4.2 Volume fraction estimates

Volume fractions were estimated in a multistage procedure. The bulk inclusion volume was estimated by multiplying the depth (z-axis) of the inclusion with the cross section area (x-, y-axis) of the fluid inclusion. This approach gave good results for regularly shaped inclusions whereas irregularly shaped inclusions gave more uncertain estimates. Relative phase volumes inside the inclusions are now easily obtained, because the phases inside the inclusion have simple shapes. Bubbles of liquid or vapour phases are estimated by measuring two radii and calculating the volume of an ellipsoid body. This ignores the effect of occasional squeezing of the liquid/vapour bubbles against the upper wall of the inclusion. Solids occurring in simple forms were also estimated using simple geometric equations. Phases occupying the rest of the inclusion are calculated by subtraction from the previous volume estimates.

5 Fluid types and textures

5.1 Strategy

Four generations of fluid inclusions are covered by this study: FIA1, FIA2, FIA3 and FIA4.

To establish the fluid chronology, we used the textural chronology of quartz established by Sørensen and Larsen (2007, paper 1) (Table 4, Figure 4) together with the alteration types in amphibolite (Table 3) and calc-silicates (Table 1). A more detailed discussion on the quartz evolution is found in Sørensen and Larsen (2007, paper 1) and a discussion of the metasomatic alteration of amphibolite is found in Sørensen et al. (2007, paper 3).

Samples were collected from three localities: 1: locality representative of the prograde amphibolite evolution 2: locality representative of retrograde evolution of calc-silicates, amphibolite, quartz veins and quartz-biotite-tourmaline gneisses and 3: locality represents potassic alteration in relation to en-echelon quartz veins dominated by quartz type Qz2 intersecting amphibolite (see Figure 1 on page 4 for locations). Samples were first studied texturally and fluid inclusion textures were compared with mineral assemblages and SEM-CL images. Based on this, inclusions that were primary with respect to specific mineral assemblages or to a quartz type were selected for microthermometry analysis. Since inclusions were plentiful, inclusions that could not be texturally correlated with a specific mineral assemblage or quartz type were not measured.

5.2 FIA1: garnet-quartz symplectite in amphibolite

FIA1 comprises isolated primary carbonic inclusions and inclusion clusters in quartz in garnet quartz symplectites. FIA inclusions are interpreted to have formed simultaneously with the symplectites. The symplectites comprise symplectitic garnet and quartz, with minor ilmenite, Cl-apatite and hastingsite. They occur in lenses enclosed by garnet amphibolite, and are interpreted as minimum melts formed by partial melting of the amphibolites (Figure 5a).

The fluid inclusion hosting quartz is bright luminescent with cracked microstructures, comprising bright islands surrounded by duller luminescent channels (Figure 5b). Accordingly, they classify Qz1 that is interpreted as a high temperature quartz type (Sørensen and Larsen, 2007, paper 1). The inclusions are dark pure liquid inclusions at room temperature (Figure 5c). Similar inclusions are found in Cl-apatite and in zircon in the garnet quartz symplectites. FIA1 co-existed with the partial melts forming the garnet quartz symplectites, but probably experienced post entrapment modification due to fracturing of the host quartz grains.

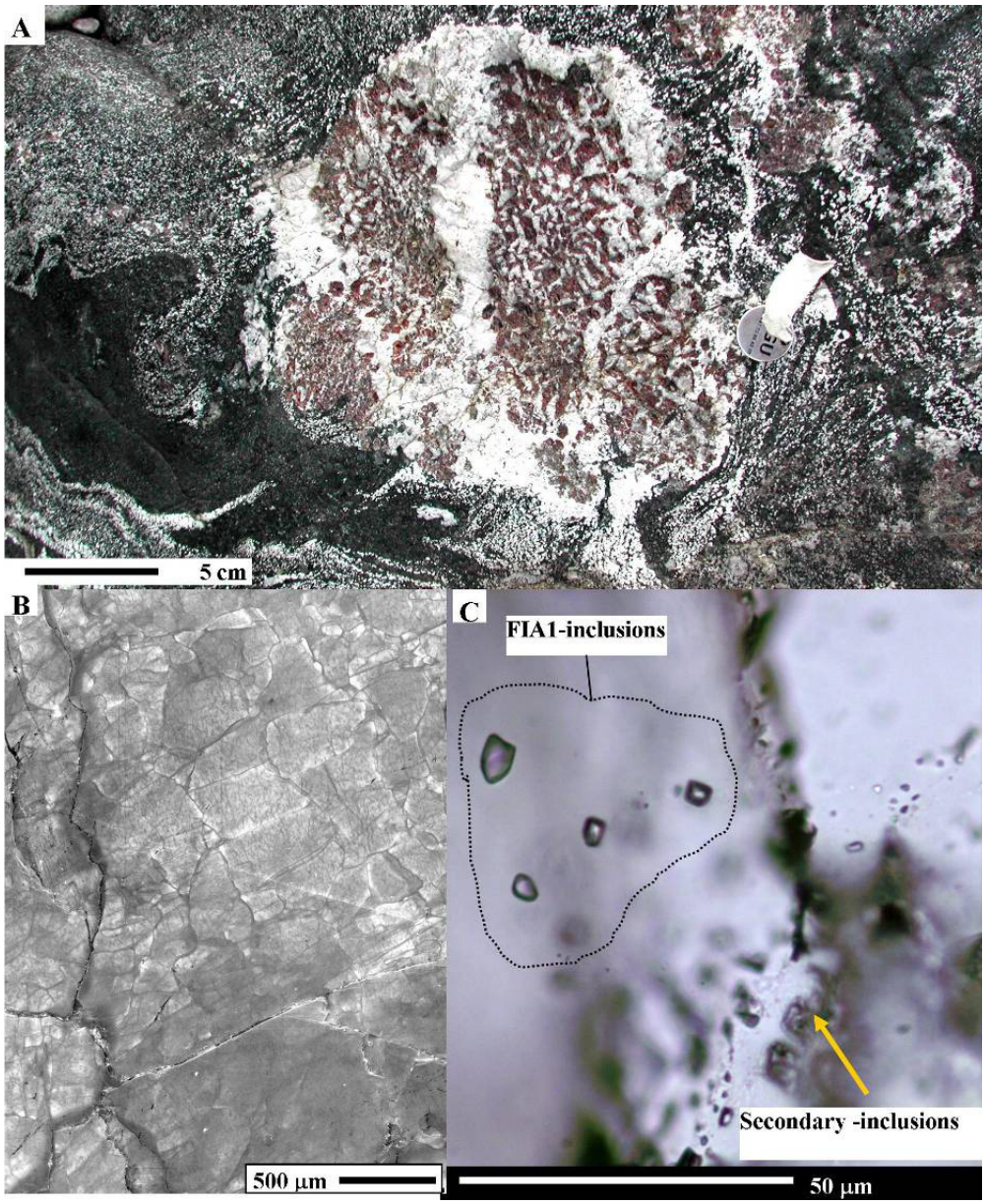

Figure 5: Occurrence of FIA1 in garnet quartz symplectites from locality 1. A) Field picture of garnet quartz symplectite, intersecting garnet amphibolite. B) The cracked texture of the quartz (Qz1) containing inclusion belonging to FIA1. C) Typical cluster of FIA1 carbonic inclusions.

5.3 FIA2: CO_2 and H_2O-rich inclusions in en-echelon quartz veins in amphibolite: related to potassic alteration

FIA2 comprises CO_2-rich and H_2O rich primary inclusions in Qz2, see Sørensen and Larsen (2007, paper 1) and (Figure 4/Table 4). They occur in an amphibolite hosted en echelon quartz vein at locality 3. The vein is bordered by a metasomatic tourmaline, amphibole, biotite, plagioclase and ilmenite alteration zone, Alt1c (Figure 6, Table 3). Amphibole, biotite and plagioclase comprise a decussate texture (Figure 6). The tourmaline is a black schorl rich dravite-schorl solid solution and exclusively occurs in dm-thick layers next to the quartz vein (Figure 6). This is followed by first a dm-thick zone rich in biotite and then a dm-thick zone rich in plagioclase and amphibole (Figure 6). The quartz in the veins is mostly Qz2, however Qz 1 relics are also common (Figure 6). Both Qz1 and Qz2 are intersected by a network of micron-thick cracks of Qz4 (Figure 6d). The quartz vein is deformed and primary inclusions are rare amongst numerous trails of secondary inclusions (not shown).

However, primary inclusions comprising H_2O-rich brines and CO_2-H_2O low saline compositions were positively identified in growth zones in Qz2 by comparison of optical petrography and SEM-CL (Figure 6d). At room temperature the H_2O-rich inclusions comprise liquid water and a liquid CO_2 phase comprising 5 vol%. The CO_2-rich low salinity inclusions comprise liquid H_2O, liquid CO_2 and CO_2 vapour at room temperature (Figure 6d), with variable phase volume proportions (see microthermometry results page 30).

The growth zone related inclusion textures are intersected by Qz4 filled cracks with secondary inclusions and modified primary inclusions (not shown). The biotite-amphibole alteration assemblages, surrounding the quartz veins, are a common assemblage related to fluid related amphibole alteration, formed during exhumation (Sørensen et al., 2007, paper 3) (see Table 3).

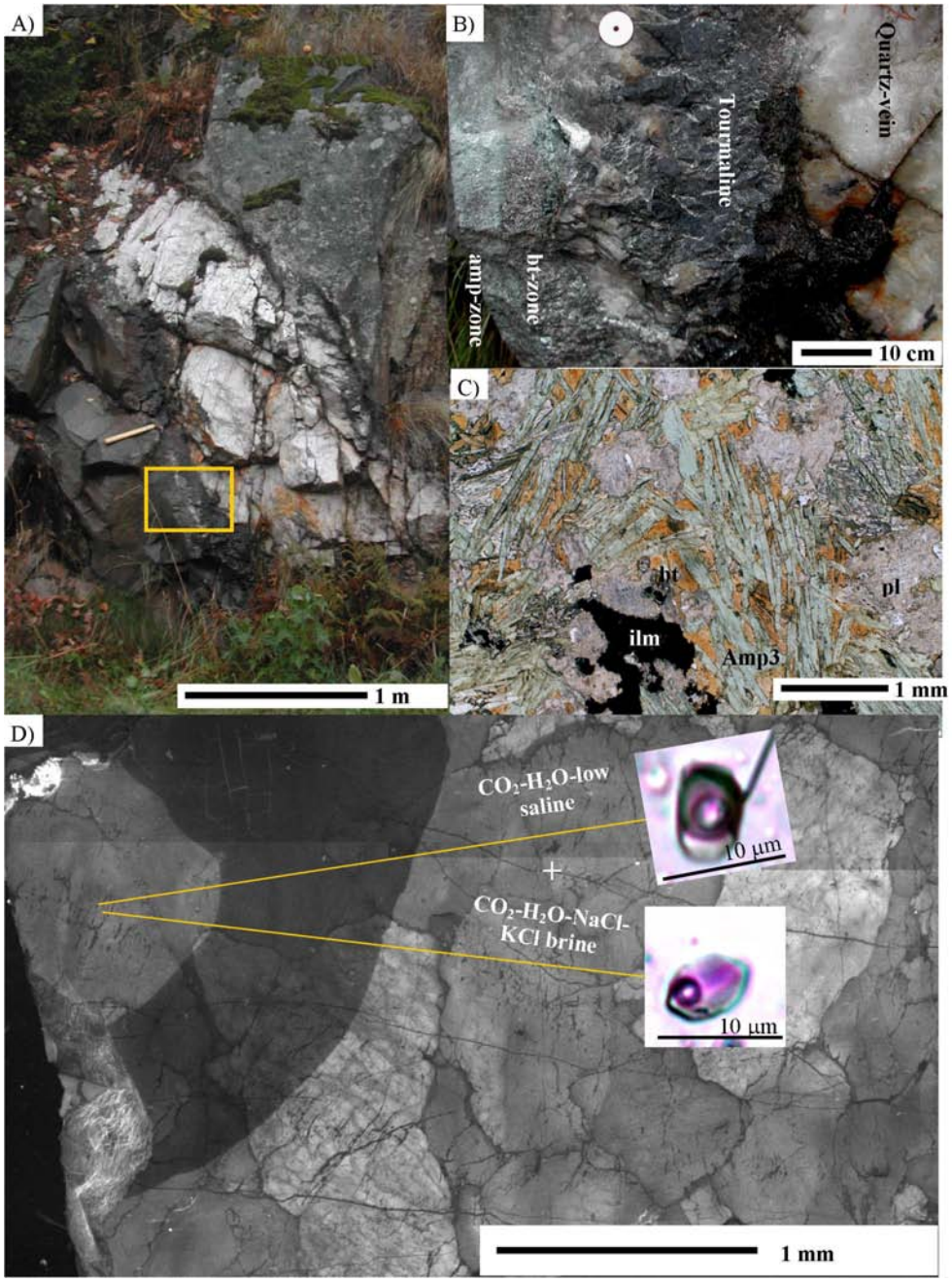

Figure 6: Textures associated with FIA2 inclusions from locality 3. A) Field image of en-echelon quartz vein intersecting amphibolite. B) Zoom on contact between quartz vein and amphibolite showing alternating dm-tick layers in the host rock alteration zones. C)

Typical alteration assemblage, comprising amphibole, biotite plagioclase and ilmenite. D) SEM-CL texture of quartz in the vein comprising relic Qz1 grain and Qz2, which are both intersected by micron thick cracks with Qz4. Also shown is typical fluid inclusions in Qz2, comprising a mixture of H_2O-rich H_2O-CO_2-NaCl-KCl brines and CO_2-rich low salinity H_2O-CO_2-salt inclusions.

5.4 FIA3: LVS primary inclusions in recrystallised quartz, related to scapolitisation and rutile breakdown

FIA3 occurs in recrystallised quartz forming a network of mm-thick fluid channels. These channels correspond to Qz3 of Sørensen and Larsen (2007, paper1) (see Figure 4 and Table 4). Inclusions have a typical diameter of 5-10μm. Inclusions are observed in two settings at locality 2:

1: FIA3 is associated with bleaching zones in quartz-biotite-tourmaline gneiss (Figure 7a). Bleaching is caused by alteration of biotite to muscovite and chlorite and recrystallisation and bleaching of blue quartz to colourless quartz (Figure 7a). Biotite defines the foliation of the non–bleached biotite quartz gneiss, which is intersected by the bleaching zones (Figure 7a). Quartz in the non-bleached quartz biotite mainly comprises Qz1 and Qz2. Qz1 has chessboard subgrain microstructures, suggesting that Qz1 was deformed at high temperatures. The chessboard subgrain pattern is partly overprinted by prismatic subgrains that formed at lower temperatures. Qz2 grains do not show chessboard textures hence must have formed after the initial deformation of the Qz1 grains. On the contrary, deformation lamellae in Qz2 may very well be synchronous with prismatic subgrain formation in Qz1. Similar observations were made by Sørensen & Larsen (2007, paper1) in quartz veins from the same locality. Accordingly, Qz1 and Qz2 could be distinguished by common optical microscopy. Qz3 on the contrary, had to be identified by SEM-CL. However, in thick sections (100 μm), Qz3 may be recognised by the absence of rutile needles, which are common in Qz2 (see below). This difference is not as easily observed in normal thin sections.

Inclusions follow broad channels of Qz3, intersecting Qz1 and Qz2 (Figure 7b and c). The broad channels with Qz 3 are intersected by a network of micron thick cracks with Qz4 (Figure 7b) and calcite bearing fluid inclusions. Qz3 in the fluid channels is in optical continuity with the host Qz2 grains, but they are differentiated optically by the absence of rutile needles (Figure 7e). These observations suggest that rutile was destabilised in relation to the influx of FIA3 fluids. This is confirmed by the breakdown of rutile to titanite in relation to luminescence quenching textures comprising Qz3 and Qz4 (Figure 7d). The absence of calcite in the vicinity of rutile grains infer that calcium required for titanite replacement of rutile was supplied by a fluid phase. Fluid inclusions in Qz3 infiltrate along channels of dull Qz3 intersecting Qz1 and Qz2 (Figure 7b, c and e).

Because FIA3/Qz3 textures are intersected by Qz4 with carbonate mineral inclusions, it is inferred that the fluid evolved to more Ca-rich compositions,

facilitating calcite precipitation. In addition the FIA4 texture indicates that quartz was dissolved and not precipitated during this stage.

Qz3 textures similar to those observed in this study are also found in quartzites where they relate to hydrolytic weakening and localised increased recovery rate facilitating subgrain rotation recrystallisation associated with thrust-related shear deformation (paper 1, Sørensen and Larsen, 2007) and imply that Qz3 formed during exhumation.

2: FIA3 is also associated with quartz in quartz-scapolite veins, related to scapolitisation of plagioclase in amphibolite. Veins are composed of a cm-thick rim of scapolite followed by a cm-thick central zone of quartz (Figure 8). The Cl-intensity of the quartz is generally low and is classified as Qz3 and Qz4. However, in detailed SEM-CL studies a complex fluid migration network is revealed. A broad Qz3 zone is intersected by a micro-thick network of Qz4, comprising micro-inclusions of calcite and calcite bearing fluid inclusions. Qz3 may either be classified as unevenly luminescent and partly recrystallised comprising fluid migration channels or more evenly dull luminescent newly formed Qz3 grains. The new Qz3 grains either occur as inclusions in scapolite grains or in rims enveloping scapolite grains (Figure 8). Fluid inclusions related to Qz3 occur in intragranular trails associated with duller channels. Fluid inclusions are rare in the new Qz3 and were not large enough for microthermometry.

Two generations of later fluid inclusions intersects FIA3. The oldest generation is $LVS_1(S_2)$ inclusions following the Qz4 network (Figure 8). They carry liquid H_2O, vapour, halite (S_1) and commonly also calcite (S_2) (Figure 8). They are fairly similar to FIA3 inclusions but may be differentiated by their direct association with Qz4 in narrow fluid inclusions trails and by the presence of calcite (Figure 8). They are not included in this study because they failed to freeze during microthermometry. However, similar sizes of the halite cubes and the calcite daughter minerals imply an increase in the Ca-content in the fluid from the fluids in Qz3 to the fluids in Qz4.

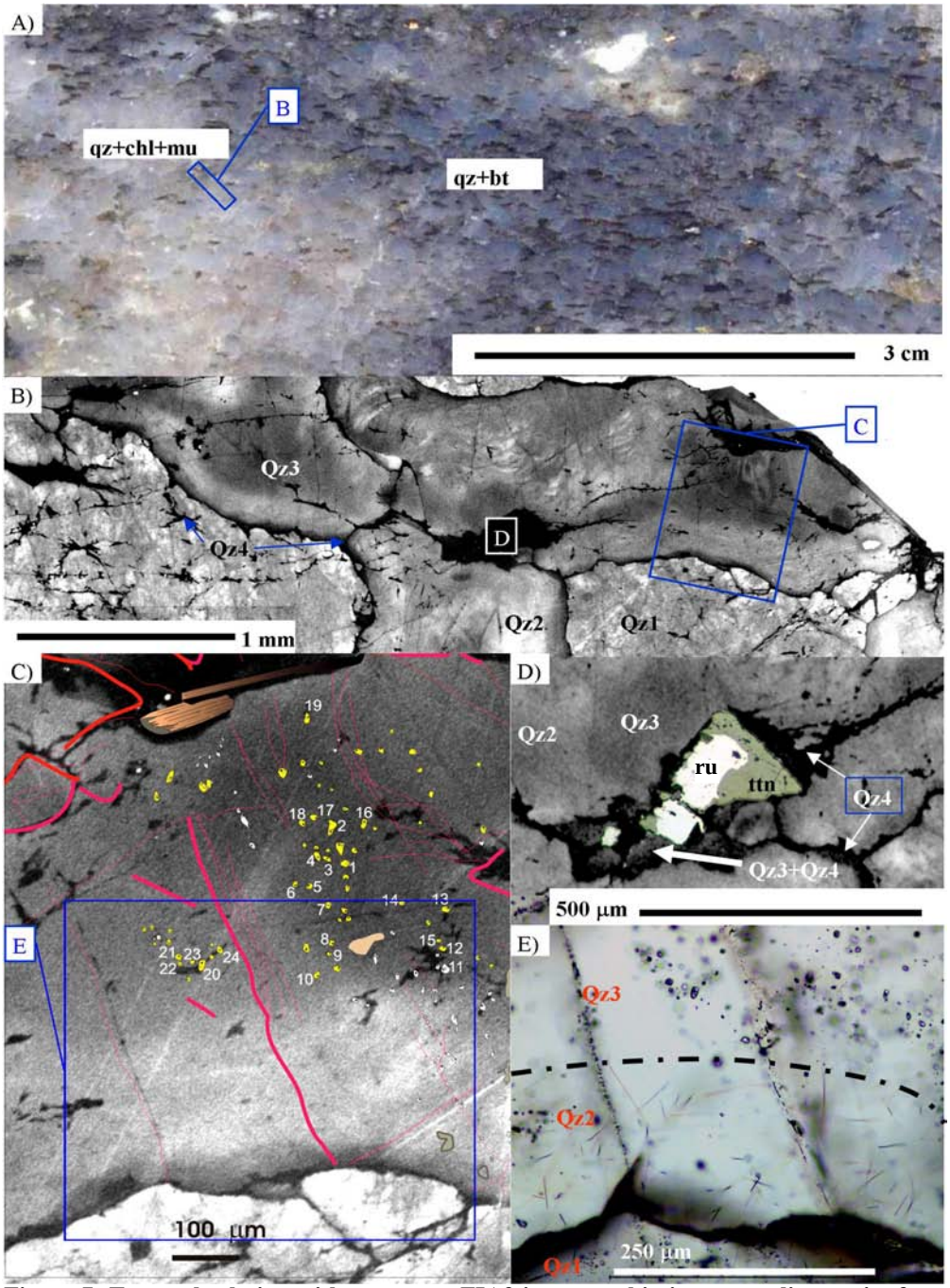

Figure 7: Textural relation with respect to FIA3 in quartz-biotite-tourmaline gneiss from locality 2. A) Field image showing bleaching of the gneiss in relation to fluid infiltration.

Bleaching is an effect of both a colour change in quartz from blue to colourless and due to the breakdown of biotite to a mix of chlorite and muscovite. B) SEM-CL image showing the textural relations involving Qz1, Qz2, Qz3 and Qz4. Qz3 follows broad luminescence quenching channels, intersecting Qz2. C) Zoom on B showing the relation between FIA3 fluid inclusions (yellow) and Qz3 luminescence quenching textures. D) Titanite (ttn) replacing rutile (rt) in relation to luminescence quenching textures. E) Optical image showing the presence of rutile needles in Qz2 and their absence in Qz3.

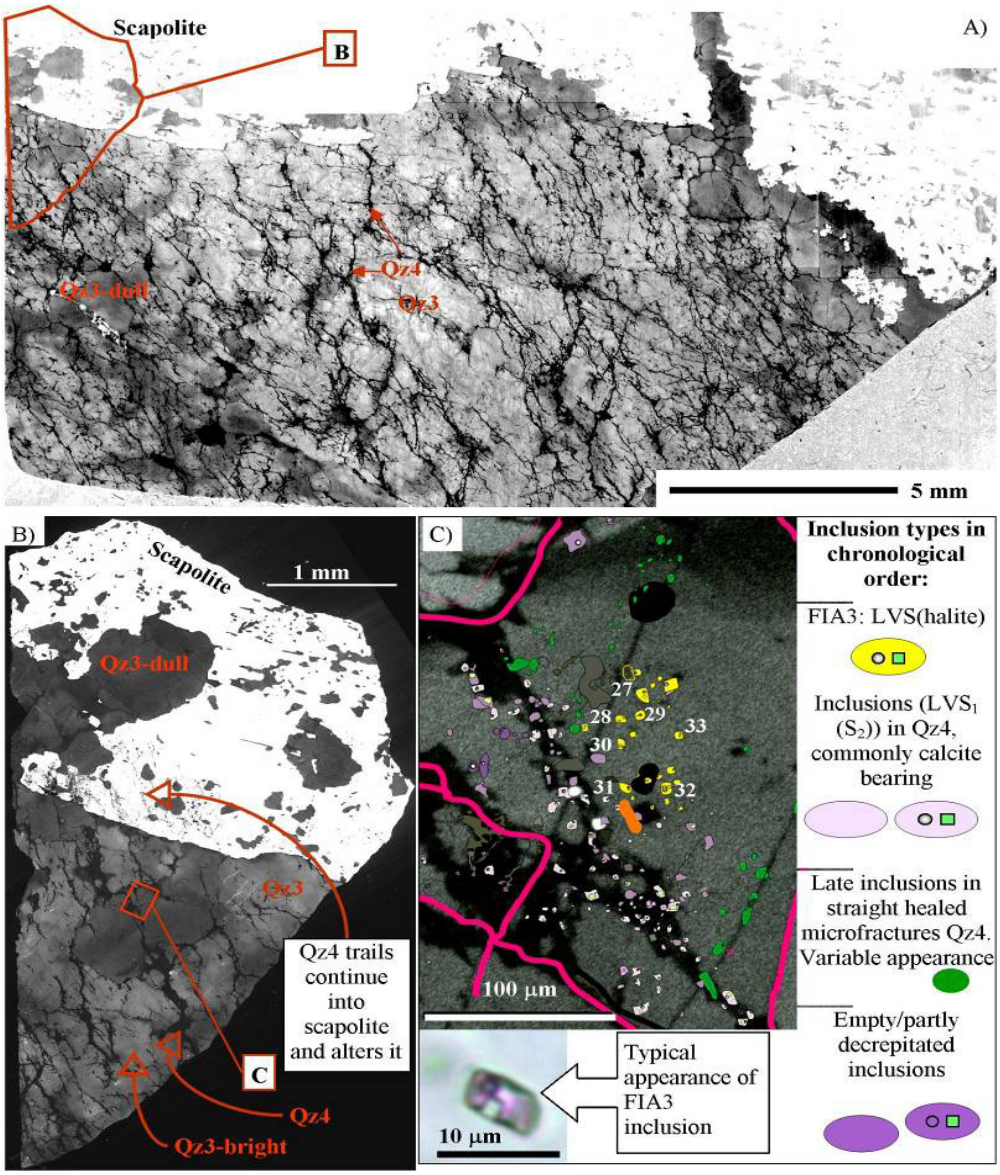

Figure 8: SEM-CL/optical textures in relation to FIA3 in quartz scapolite vein from locality 2. A) Overview showing the relations between Qz3, Qz4 and scapolite. Contrast is enhanced such that differences with quartz type Qz3 are seen. Qz3 may either be classified as (1) unevenly luminescent and partly recrystallised comprising fluid migration channels or (2) more evenly dull luminescent newly formed Qz3 grains commonly as inclusions in scapolite or next to scapolite. B) Detail from (A) showing the location of the fluid inclusions in (C). Note that Qz4 textures intersect scapolite, documenting that Qz4 formed after scapolitisation. C) Detailed view showing the relation between fluid inclusion

assemblages and SEM-CL textures. Inclusions later than FIA3 are distinguished by a combination of optical microscopy and SEM-CL.

5.5 FIA4: LV primary fluid inclusions in calcite and epidote in epidote-actinolite-calcite-pyrite vug fillings.

FIA4 comprises LV inclusions in calcite and epidote in a tremolite-epidote-pyrite-calcite-flour-apophyllite assemblage comprising vug fillings at the boundary between the quartz-biotite-plagioclase-tourmaline gneiss and the diopside rich calc-silicate rocks from locality 2. The vugs comprise an outer zone of mint green tremolite, followed by a cm-thin rim of epidote and pyrite (Figure 9). Calcite is intergranular between epidote and tremolite and also occurs together with flour apophyllite in the central part of the vugs (Figure 9). Epidote is only present together with pyrite (Figure 9). This together with the observation of pyrrhotite relics together with pyrite suggests that excess iron from the alteration of pyrrhotite to pyrite supplied Fe for epidote formation. The epidote-calcite-tremolite-apophyllite assemblage probably formed from the breakdown of a metastable diopside-tremolite-pyrrhotite-phlogopite assemblage, where SiO_2 and Al_2O_3 were supplied from the neighbouring gneiss unit.

Fluid inclusions occur in growth zoned calcite. Epidote grains are zoned with increased pistacite content at their rims and along fractures (Figure 9). Fluid inclusions are also common in epidote cores but not in the rims.

Tremolite grains alter to more Fe-rich compositions (into the actinolite field) along rims and fractures (Figure 10). Along with the increased Fe-content in the amphibole the Al content also drops.

The vug-assemblage (Mp5) is part of a complex alteration sequence observed in calc-silicates comprising clinopyroxene (diopside-(hedenbergite)), phlogopite, tremolitic amphibole, epidote, and titanite (Table 1 on page 9 and section 3.1).

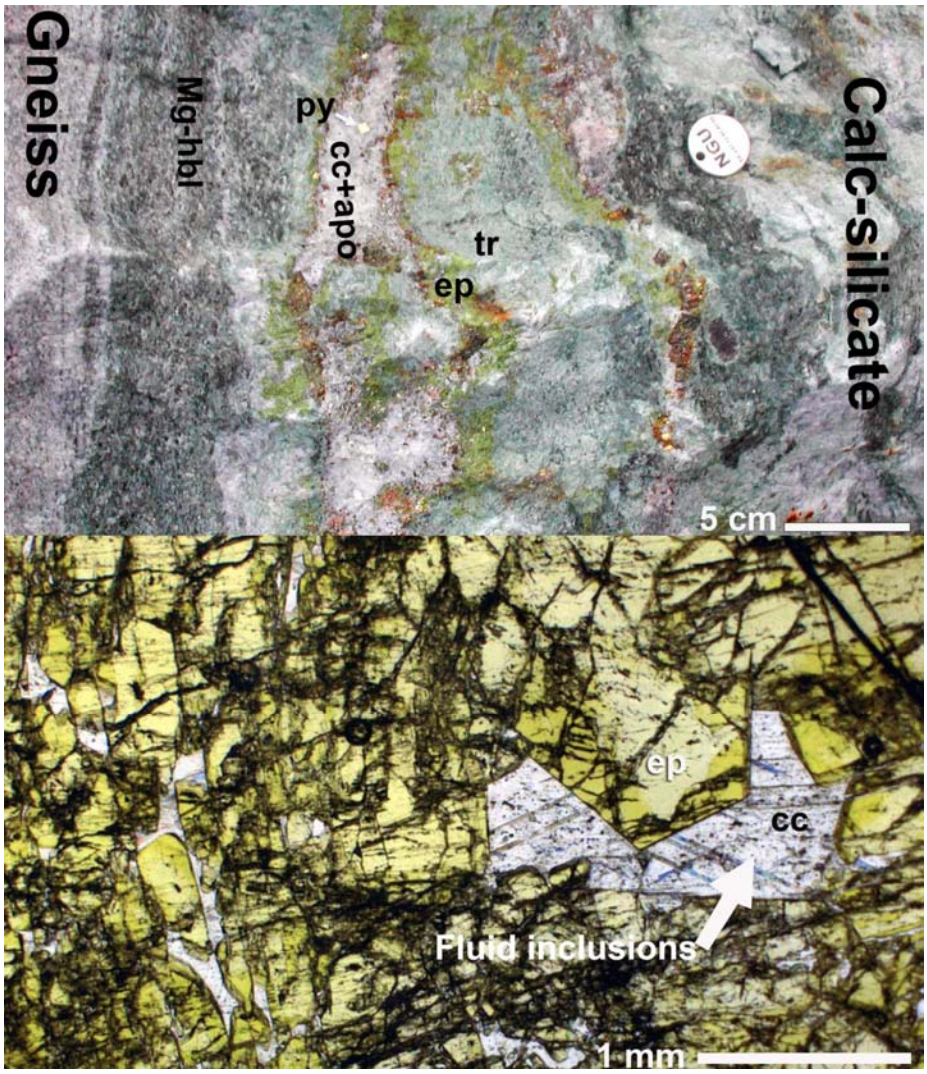

Figure 9: A) Field relations of the tremolite (tr) - epidote (ep) – calcite (cc) - apophyllite (apo) - pyrite (py) assemblage (Mp5) from locality 2. The Mp5 assemblage is squeezed in between the calc-silicates and the gneiss unit. B). Thick section (100μm) image showing epidote calcite assemblage. Large calcite grain contains the primary fluid inclusions included in this study. Note the colour variation in epidote with more intensely coloured rims comprising more Fe-rich epidote.

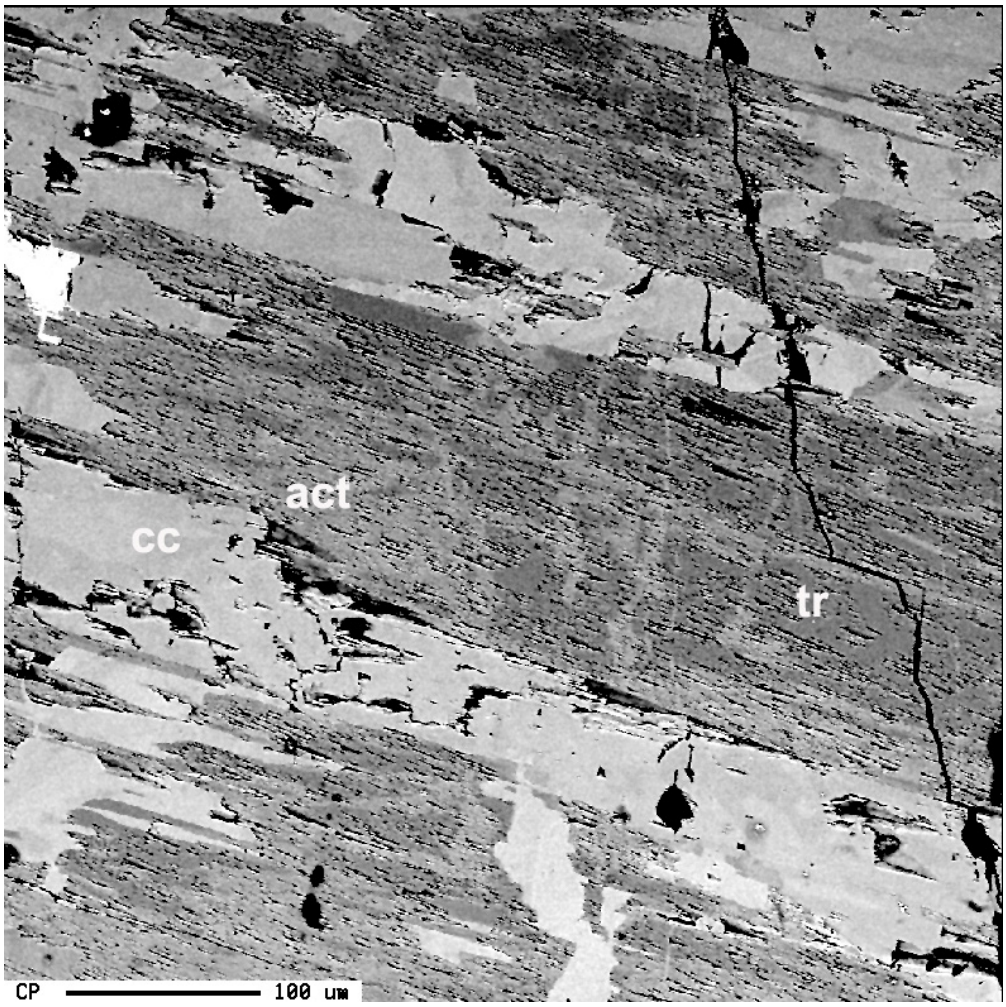

Figure 10: Electron backscatter image displaying calcite (light grey) and amphibole (darker grey) in the Mp5 assemblage from locality 2. Tremolite (tr) is altered to actinolite (act) along fractures.

6 Micro-thermometry results

Most fluid inclusion data were modelled using the FLUIDS1 program suite (Bakker, 2003). However, some inclusion types lack appropriate EOS hence were interpreted with published phase diagrams and extrapolation of EOS expressions.

6.1 FIA1

First melting of the carbonic inclusions occurs at -56.5 to -59 °C, as SV→LV and total homogenisation as LV→L at variable temperatures (Figure 11). H3 phase behaviour (Van den Kerkhof and Thiery, 2001) was followed during heating. This together with the narrow range of melting temperatures imply that the fluids are almost pure CO_2.

The LV→L homogenisation temperatures of the inclusions are scattered from -3.7 to 27.2°C (Figure 11) implying post entrapment modifications, as it was also implied by the cracked CL-texture of the host quartz grains. H_2O is absent, however, preferential H_2O leakage as documented in experiments (Bakker and Jansen, 1990) and by transmission electron microscopy (Bakker and Jansen, 1994) can not be excluded.

Accordingly, the only information available from FIA1 is that CO_2 was the stable carbonic phase during the formation of the garnet-quartz symplectites.

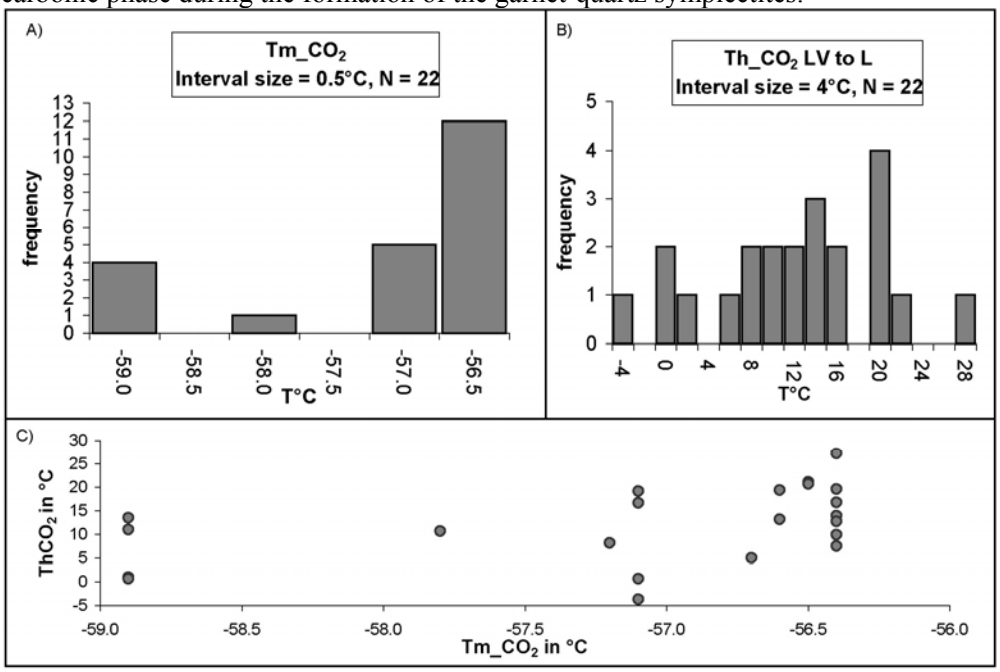

Figure 11: FIA1 microthermometry data. A) Tm_CO_2 displaying a narrow temperature range. B) Homogenisation LV→L (Th_CO_2) showing a wide range of temperatures. C) Plot of Th_CO_2 vs. Tm_CO_2 showing that there is no correlation. Data collected from fluid inclusions in quartz from garnet-quartz symplectites from locality 1.

6.2 FIA2

The FIA2 comprises two groups i.e. CO_2- and H_2O-rich inclusions, which together with textural features imply immiscible fluids. Volume fraction estimates of the CO_2-

rich inclusions show a large scatter (Figure 12). However, the H_2O rich inclusions have a narrow range in volume fraction estimates with 95 % L_{H2O} (+ CO_2 dissolved in the H_2O phase) and 5 % CO_2 (Figure 12).

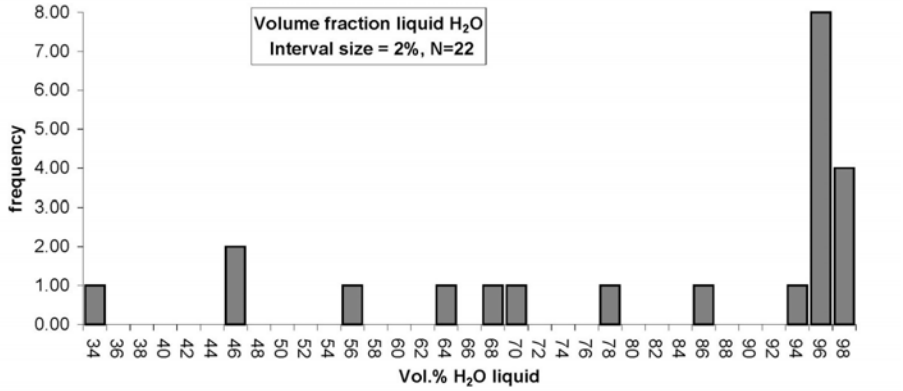

Figure 12: Volume fraction estimates showing that only the H_2O-rich inclusions have constant volume fractions and that the CO_2-rich inclusions have variable volume fractions suggesting that they underwent post-entrapment modifications.

The melting behaviour of the carbonic phase is SG→LG at temperatures close to the melting temperature of pure CO_2 (Figure 13). The clathrate melting temperature is -11 to -2 °C for the H_2O rich inclusion, whereas it is approximately 8 °C for the CO_2-rich inclusions (Figure 13). Both groups fall in narrow ranges of clathrate melting temperatures hence implying that the aqueous phase salinity remained constant. First melting of the aqueous phase could only be determined in the H_2O-rich inclusions and consistently fall at -24.7 °C, i.e. close to eutectic minimum of the H_2O-NaCl-KCl ternary system. The slight offset is probably caused by the presence of CO_2 which is known to systematically lower melting temperatures in aqueous electrolyte inclusions (e.g. Hedenquist and Henley, 1985). This together with the biotite bearing alteration assemblage indicates that the aqueous liquids are best defined by the H_2O-NaCl-KCl ternary system.

The total homogenisation temperature of the H_2O-rich inclusions is about 200°C. The salinity estimates obtained from clathrate melting and melting of ice and hydrohalite show that the salinity was close to the eutectic point i.e X_{NaCl} = 20.2 wt%, X_{KCl} = 5.8wt%. Therefore, the coexisting immiscible fluids probably did not form by phase separation because the H_2O-CO_2 solvus at near eutectic salinities occur at a much higher temperature than the observed total homogenisation temperature of the H_2O-rich inclusions (Bowers and Helgeson, 1983). In conclusion, the H_2O- and CO_2-rich inclusions are not co-genetic but were introduced as separate fluids, during the formation of the en echelon quartz veins and quartz type Qz2.

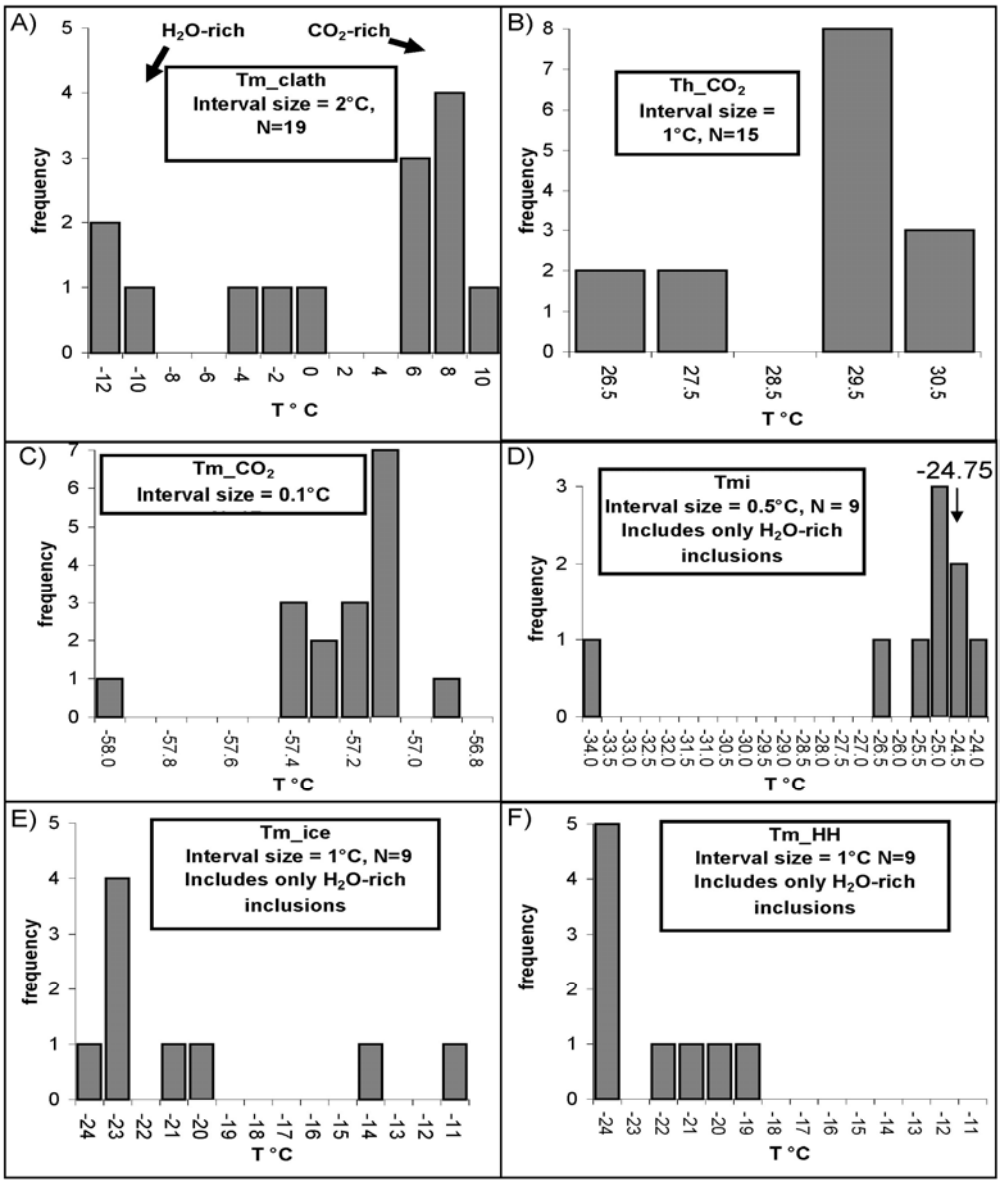

Figure 13: Microthermometry results from FIA2, CO_2-H_2O immiscible fluids. A) Clathrate melting temperatures, not two groups B) Homogenisation of CO_2 C) Tm_CO_2 D) First melting temperatures (Tmi). F) Final melting of hydrohalite (Tm_HH).

6.3 FIA3

FIA3 comprises a narrow range of melting temperatures (Figure 14) with first melting observed at -49 to -45ºC hence supporting an eutectic point around -52°C, given that the first melt fractions are difficult to observe. Thus it is inferred that the inclusions belong to the NaCl-$CaCl_2$-H_2O system.

Final melting of ice occurs at -27 to -25ºC with a few outliers around -40°C (Figure 14). Melting of hydrohalite was uncertain and occurs at different temperatures during sequential heating experiments and hence is not included in the measurements. The LV→L homogenisation temperature (Th) is averaging 126-128°C and mostly occurs before melting of the solid phase (average TmS=150°C). Th and TmS are negatively correlated (Figure 14). Absence of clathrate/hydrate formation implies that H_2O is the only COH fluid.

In the absence of certain hydrohalite measurements, the Ca/Na ratio was estimated from final melting of ice. This introduces errors that are smaller than the error in estimating hydrohalite melting (Williams-Jones and Samson, 1990). The salinity and the Ca/Na ratio was estimated with the method of Vanko et al. (1988), Williams-Jones and Samson (1990) and gave a salinity of 31 wt% with 25 wt% NaCl and 6 wt% $CaCl_2$.

Halite (H) melting generally occurs at higher T than the LV→L phase transition hence differs from the available experimental data where vapour saturated conditions are required during halite melting. In our case the inclusion has left the LVH curve at T1 before LV→L homogenisation. Because the LH liquidus is inclined in PT space an error in the predicted salinity is introduced together with an error in the density and thus also an offset in the isochore (e.g. Bodnar, 2003). Because the conditions of the liquid phase at LVH→LH phase transition is fairly well constrained and because of the nearness to vapour saturation the error was ignored. Hence the mean values of salinity and $Th_{LV\rightarrow L}$(127°C) was used together with the to calculate a fairly well constrained isochoric path with the EOS of Zhang & Frantz (1987).

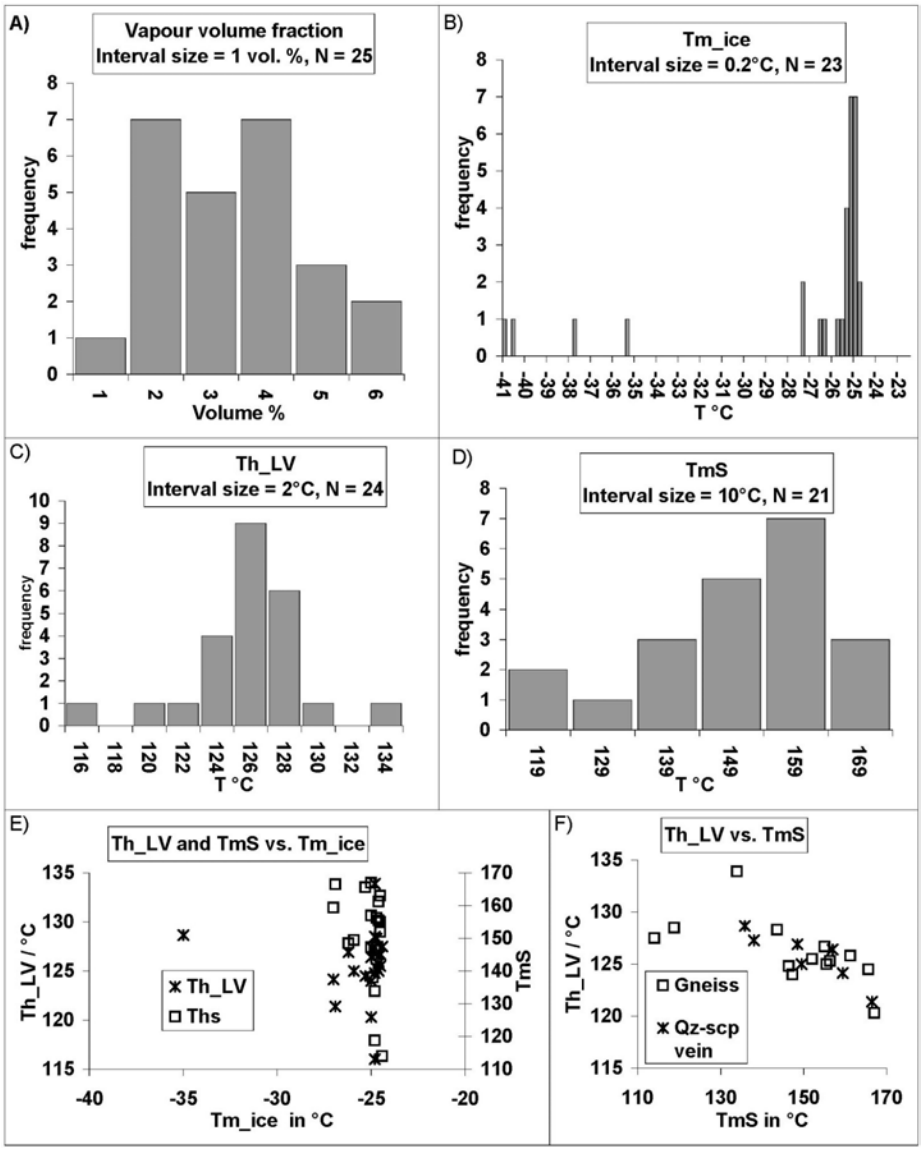

Figure 14: FIA3 microthermometry results. A) Volume fraction estimates B) Final ice melting (Tm_ice) histogram. C) Liquid-vapour homogenisation (Th_LV) histogram. D) Final melting of salt cube (TmS) histogram E) TmS and Th_LV showing no correlation vs. Tm_ice. F) Negative correlation between Th_LV and TmS.

6.4 FIA4

FIA4 fluid inclusions experienced first melting (Tmi) from -74 to -49 °C and the fluid inclusions with Tmi higher than -60°C featured equilibrium behaviour, characteristic of the $CaCl_2$-NaCl-H_2O ternary system (Figure 16).

Fluid inclusions with very low first melting temperatures, however, show significant melting far below the $CaCl_2$-NaCl-H_2O eutectic point suggesting either metastable behaviour or the presence of other cations (Figure 15). Prior to first melting the inclusions become clouded and then speckled as recrystallisation proceeds during heating. The speckled texture is interpreted as a result of hydrohalite formation (Figure 15). At -70 to -80°C individual grains are recognised (Figure 15). First melting commonly occurs at -65°C and at -60°C liquid comprises a significant proportion of the fluid inclusions (Figure 15). At about -55°C, only one solid phase remains in the inclusions (Figure 15). It appears in lensoid bodies like ice but lye at the bottom of the inclusion and, therefore, is interpreted as antarcticite (Figure 15).

Antarcticite is the last phase to disappear in all fluid inclusions. Therefore FIA4 plots in the narrow antarcticite field in the NaCl-$CaCl_2$-H_2O ternary system. The position of the liquidus in this system is not well constrained hence the antarcticite melting temperatures (Tm_ant) were interpreted in the $CaCl_2$-H_2O binary subsystem from phase diagrams in Crawford (1981).

Antarcticite melting occurs within a wide range from -4 to -43 ºC, with peaks at -37 and -26ºC (Figure 16). Because of the steepness of the liquid-antarcticite cotectic curve this translates to a narrow salinity range of 31.7-36 wt % $CaCl_2$ equivalent. Fluid inclusions in epidote cores have a narrow range around -26°C, corresponding to the main peak in calcite hosted fluid inclusions (Figure 16). Similarly the first melting temperatures fall in two clusters; one asymmetrically around -52°C and an other around -65°C. Fluid inclusions in epidote cores are restricted to the narrow range -49 to -51.8°C, suggesting that they are correlated with the inclusions of the -52°C peak of the calcite inclusions (Figure 16). Accordingly, the inclusions with the “normal” first melting temperatures are early and fluid inclusions with the low first melting temperatures are later.

Contoured values of Tm_ant and Tmi, also show a systematic spatial variation (Figure 17). Inclusions with very low first melting temperatures (<-62°C) generally have antarcticite melting temperatures above -30°C (Figure 17). Inclusions with the first melting temperatures above -62°C generally have antarcticite melting temperatures above -30°C (Figure 17). Given the systematic distribution from core to rim of these microthermometric data, it is inferred that the inclusion group with the “normal” first melting temperatures are early and correlates with epidote cores ($EpCz_{70-75}$) and the fluid inclusions with the low eutectics are younger and relates to the alteration rims on the epidote grains ($EpCz_{65}$) (Figure 17).

The density of FIA4 is difficult to pin down as no EOS of calcic brines in this salinity and temperature range exist. Therefore, the density of the inclusion bubble was estimated by extrapolating from values of lower salinity solutions calculated with the Krumgalz et al. (1996) EOS, included in the program Bulk from Fluids package

(Bakker, 2003). Results show that the density of the vapour phase is negligible and that the calculated bulk densities follow a strictly linear trend (Table 5) and are used to calculate densities of the 31.7 and 36 wt% inclusions, respectively (Table 5).

Given that an EOS for these conditions is absent we extrapolated from the "low" salinity EOS of Zhang and Frantz (1987) to estimate the isochore (Table 5). The resulting isochors are fit by a linear equation (Table 5).

Table 5: Density estimates by linear extrapolation from lower salinities calculated with bulk and excel. Also shown are slopes and intercepts of calculated isochores.

Calculated with bulk			
D bulk (g/cc)	D vap (g/cc)	Wt% CaCl2	%vap
1.14377	0.000017	22	4.5
1.16315	0.000017	24	4.5
1.182846	0.000017	26	4.5
1.202834	0.000017	28	4.5
1.223085	0.000017	30	4.5
1.230329	0.000017	30.71	4.5
Estimated with linear extrapolation			
D bulk (g/cc)	D vap (g/cc)	Wt% CaCl2	%vap
1.239899309	0.000017	31.7	4.5
1.282677945	0.000017	36	4.5
Linear :			
D(g/cc) = wt%CaCl2*0,0099 + 0,9245, R^2 = 0,9999			
Calculated homogenisation conditions *			
Th_Calc (31.7wt% $CaCl_2$)		126.715 °C	0.450413 MPa
Th_Calc (36 wt% $CaCl_2$)		148.016 °C	0.482372 MPa
Calculated isochores P(bar) = aT(°C) + c **			
	slope(a)	intercept(c)	R^2
31.7 wt% CaCl2	22.67	-2868.56	1
36 wt% CaCl2	22.63	-3344.45	1

*) calculated with Zhang & Frantz (1987) EOS, loner38 (Bakker, 2003)

**) calculated with Zhang & Frantz (1987) EOS included in isoc (Bakker, 2003))

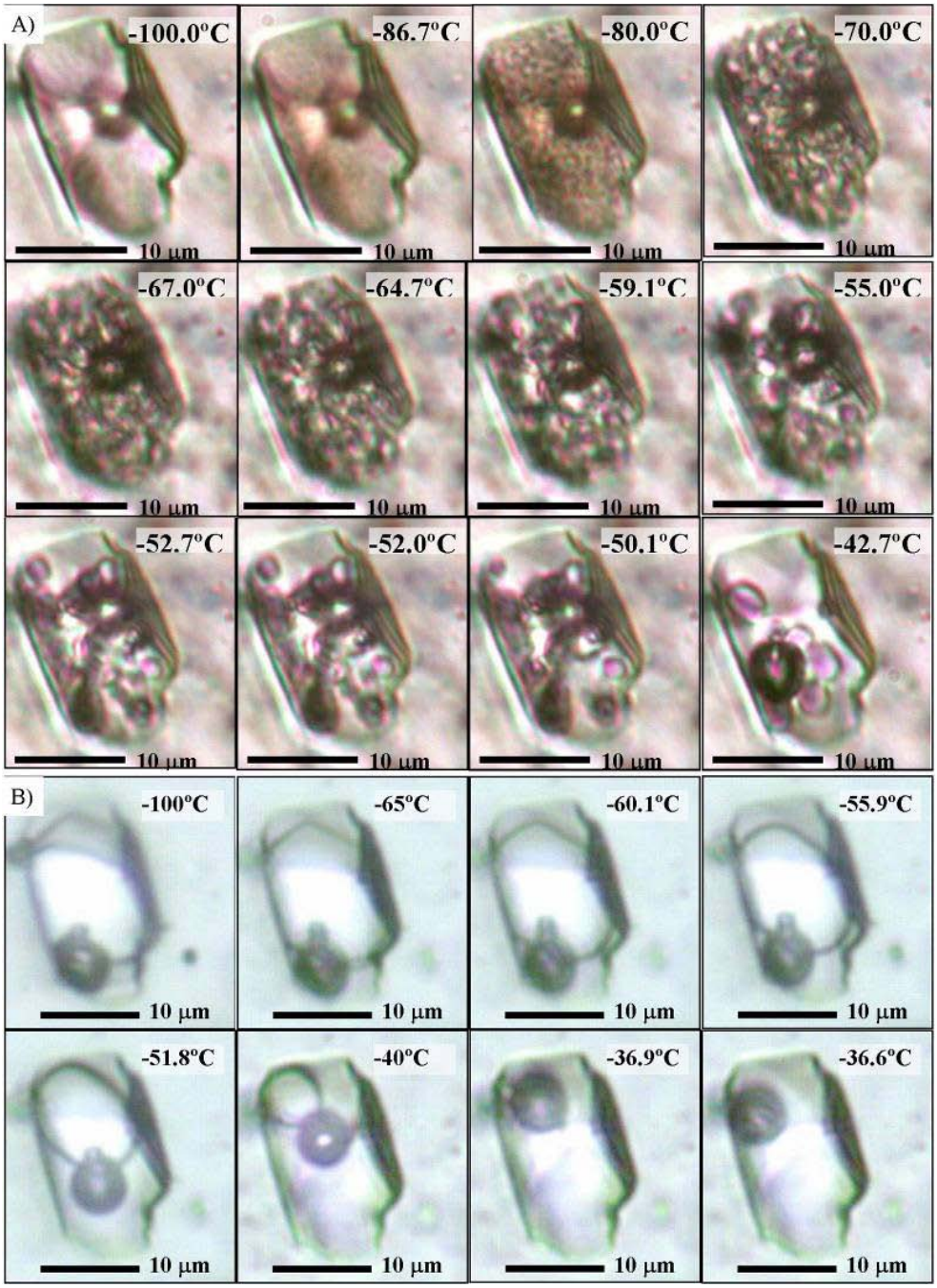

Figure 15: Melting behaviour of inclusions belonging to FIA4 with very low first melting temperatures. A) Single cooling and heating path with cooling 20ºC/min. At –100ºC the

inclusion is frozen and glass and relic vapour bubble is observed. During heating the inclusion gradually recrystallises. This is commonly observed around –90 to –85ºC by a darkening of the inclusion and by a speckled appearance caused by tiny crystals of solid phases forming. As heating proceeds the tiny crystals gradually coarsen and at around –70°C individual grains are recognised. First melting is difficult to observe but appears around –65ºC, identified by careful video inspection. Around –60ºC the liquid phase becomes clearly visible and near –52° a large proportion of the inclusion is liquid. Two types of solids are seen: one forming relatively large crystals with low relief and tiny crystals of a greenish appearing phase with higher relief/birefringence. At around –50ºC only the low relief persists. This phase continues to melt and at –40ºC only a few crystal s remain. These crystals are denser than water as they are situated at the bottom of the inclusion. B) Sequential heating/freezing close to the melting temperature of this phase reduces the number of crystals to 1. During freezing to –100°C the crystal adopts a subhedral shape, with a 120 degrees angle between crystallographic surfaces, meeting in a sharp corner. Around –65 this corner roundens, indicating that the crystal melting initiates. As melting proceed the crystal becomes increasingly rounded and has adopted a lensoid shape at about –55.9ºC. At –36.9ºC the solid is almost melted with only a tiny crystal left which finally melts at –36.6ºC.

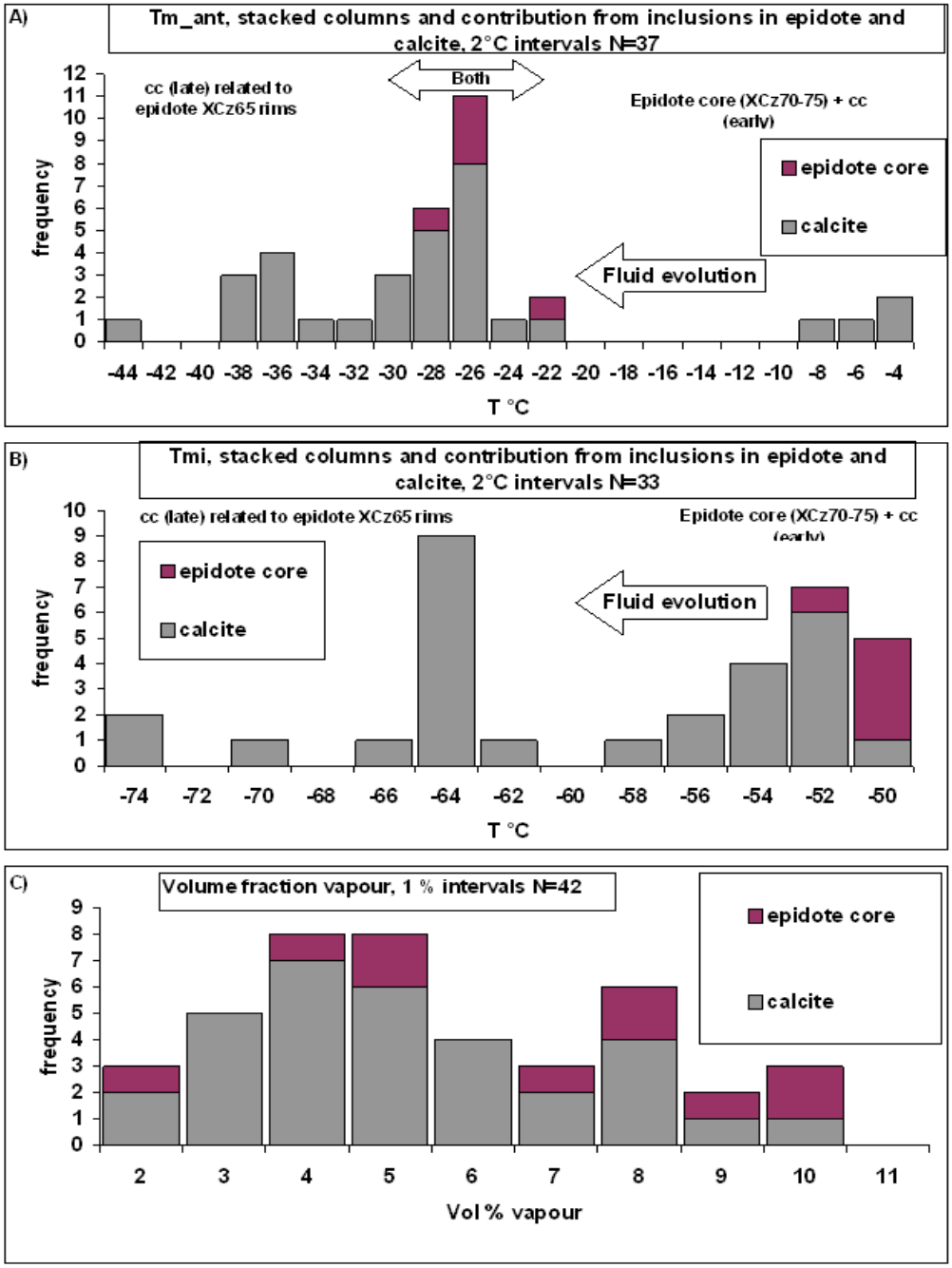

Figure 16: Microthermometry results FIA4. A) Final melting of antarcticite B) First melting C) Volume fraction estimates. Stacked columns of data from epidote and calcite. See text for discussion.

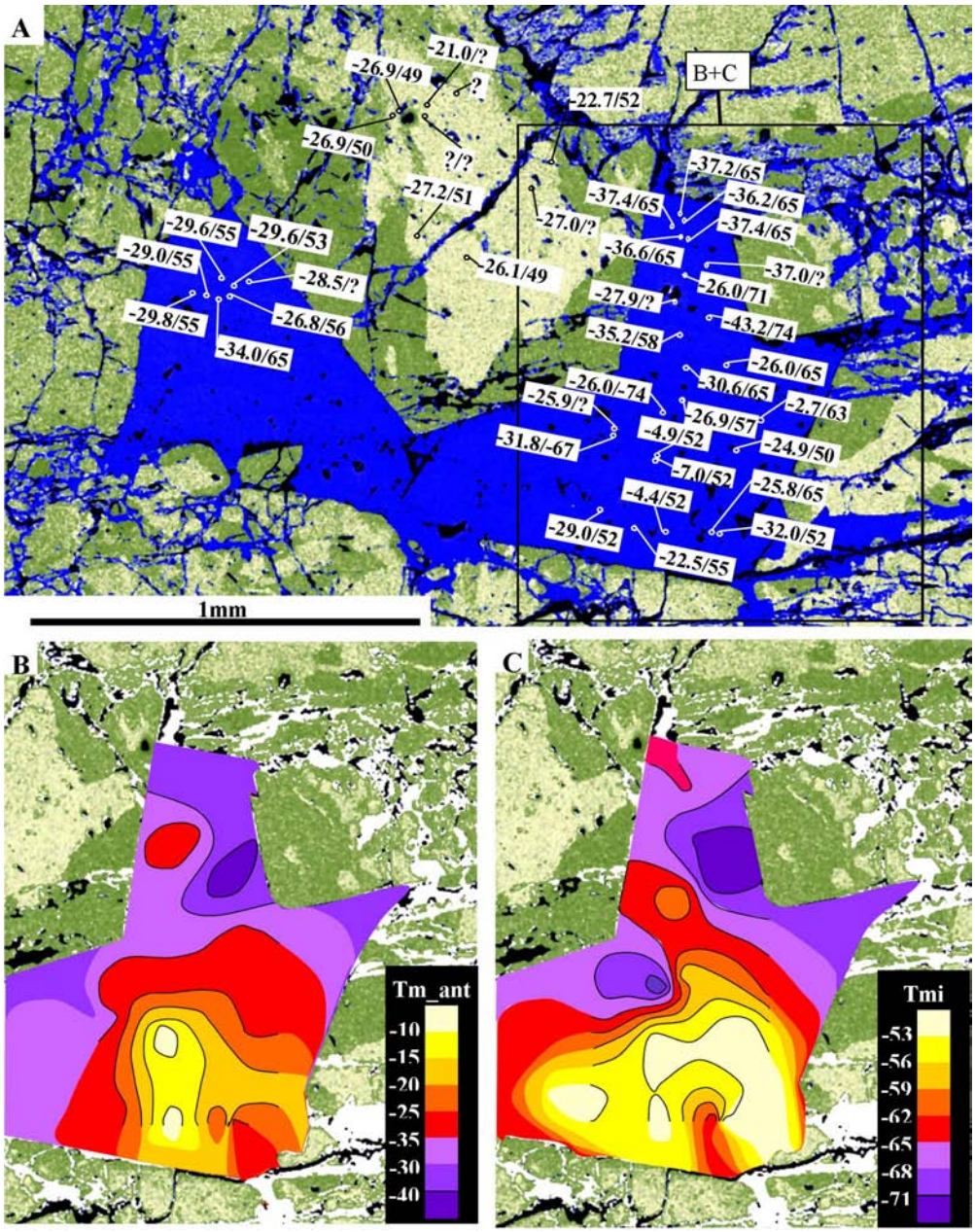

Figure 17: Spatial distribution of antarcticite and initial melting temperatures in inclusions in epidote ($EpCz_{70-75}$) shown as overlay on colourised backscatter image. Blue is calcite, light greenish yellow epidote ($EpCz_{70-75}$), and green epidote ($EpCz_{65}$). A) Individually plotted values of Tm-antarcticite/Tmi in calcite and epidote cores, note the

variable values in calcite compared to the more constant values in epidote. Note also the increasing abundance of $EpCz_{65}$ toward the top of the image B) Contour plot with 5ºC intervals of tm-antarcticite. Note the general bottom to top decreasing values and the decreasing values toward epidote $EpCz_{65}$. C) Contour plot of Tmi with 3ºC intervals. Note that Tmi decreases toward the top and toward epidote ($EpCz_{65}$). Note also the correspondence between the yellow-red contour of Tm-antarcticite and yellow-orange, indicating a group of inclusions with Tm-antarcticite above –30ºC and Tmi above –62°C. This group is similar to the inclusions in the epidote cores. Areas with solid lines in the contour plots are contoured based on the fluid inclusion data. Areas that only shaded are inferred.

7 Discussion

7.1 Summary of the observed fluid evolution

FIA1 is texturally correlated with high grade metamorphism of the area and comprises virtually pure CO_2-fluids co-existing with eutectic melts formed by partial melting of amphibolite. In agreement with studies of Fe-Ti oxides in the granulite facies area around Tromøy (2000), CO_2 is the stable carbonic species at the ambient oxygen fugacities.

FIA2 is the earliest retrograde fluid and comprises mixtures of two fluid types: 1) low salinity CO_2-rich H_2O-CO_2 inclusions, 2) H_2O-CO_2-NaCl-KCl brines with near eutectic compositions and low in CO_2. Thermodynamic modelling does not allow type 1 and 2 inclusions to be the result of in situ phase separation. Rather they represent fluid mixing of fluids derived from separate sources.

FIA3 comprises LVS inclusions of aqueous brines and no carbonic fluid. The most important salts are NaCl (average 25 wt %) and $CaCl_2$ (average 6 wt%). The salinity is near constant and LV to L homogenisation occurs in a narrow range around 126-128°C Altogether giving dense brines following a steeply inclined isochore.

FIA4 is LV inclusions representing aqueous $CaCl_2$ (31-36 wt%) brines with no carbonic fluids. The degree of fill is high giving dense fluids following a steeply inclined isochore in P-T space. The final melting of antarcticite varies systematically along growth zones in calcite. Epidote grains are zoned with $EpCz_{70\text{-}75}$ in cores and $EpCz_{65}$ in rims. Amphibole displays similar evolution with actinolite replacing tremolite in a fracture pattern recognised in backscatter images. FIA4 Fluid inclusions are only found in epidote cores. Fluid inclusions in the epidote cores correlate with fluid inclusions with the higher antarcticite melting temperatures in calcite, and with higher initial melting temperatures.

7.2 Fluid evolution in relation to cooling and uplift of the Bamble sector

The FIA3 isochors intersects the PT-path of Nijland et al. (1993) at low T and P after uplift (not shown). However, the low T and P intersection does not agree with the observation that FIA3 formed close to the brittle-ductile transition during thrust related deformation. Previous studies of the retrograde assemblages ignore the effect of salts and CO_2 although, as previously demonstrated for the Bamble fluids salt and CO_2 contents are considerable. Accordingly, we will here attempt to re-evaluate the P-T evolution taking in to consideration, the fluid evolution.
The peak T conditions are well constrained to 6-7 kb, 700-750°C (Nijland and Maijer, 1993) and corresponds to the stage when the FIA1 fluids (pure CO_2), co-existed with partial melts forming the quartz-garnet symplectites.

In order to unravel the poorly constrained retrograde evolution, we designed phase diagrams with the PERPLEX programming package (Connolly, 1990; Connolly, 1995; Connolly, 2005; Connolly and Petrini, 2002) and an updated version of the HP98 thermodynamic dataset (Holland and Powell, 1998) for the PTX_{fluid}-estimations. This combination facilitated the construction of phase diagrams including fluids of variable composition. We implemented our own data in combination with the mineral data and petrographic observations of Nijland et al. (1993). A common problem, also experienced in the current study, is to simplify the chemical complexity in terms of chemical components, mineral solid solution models, and overlapping phase stability fields. Accordingly, to recognise the correct equilibria is complicated by the fact that phase stabilities of complex systems are determined by high-variance equilibria rather than the more simple univariant equilibria of the conventional petrogenetic grids (Connolly and Petrini, 2002). Commonly this challenge is partially solved by fixing the bulk composition and to calculate ($PT\text{-}X_{fluid}$) pseudosections. Here, the obstacle is to define a so-called thermodynamically effective bulk composition (e.g. Stuwe, 1997). Not least, because the thermodynamic bulk composition may change during cooling as a result of metamorphic differentiation and mineral zonation. The degree of changes in the thermodynamically effective bulk composition during cooling also increases with grain size, because successively larger parts of the grains are removed from the reactive volume of the rock (Stuwe, 1997). Apparently, this scenario is illustrated by the zoned amphiboles described in Sørensen et al. (2007, paper 3) where the strong zoning pattern is maintained as a result of progressively shortening the diffusion distances during exhumation and cooling. However, temporal and spatial variations in fluid availability are also factors controlling the amphibole zonation.

In conclusion, the PT-conditions can not be modelled on the assumption that the retrograde mineral assemblages are products of equilibrium solid-solid net reactions with higher grade minerals as reactants and with the thermodynamic composition comprised by the bulk rock volume. A more reasonable approach is to test the stability of the product phases (retrograde assemblages). For the chemically more complex phases the bulk composition was normally fixed, although, in some cases, this

approach was inhibited by the pronounced mineral zonation. Rather, it is preferred to use the modal proportions of retrograde minerals to estimate a hypothetical bulk composition.

The retrograde reactions include mixed volatile reactions that are difficult to portray in traditional PT phase diagrams because the phase boundaries varies as a function of fluid composition. Traditionally such systems are expressed as P- or T-XCO_2 Schreinemakers projections. This method is only applicable to mixed volatile system if one parameter may be independently constrained and it is difficult to trace limiting reactions if this is not the case (Connolly and Trommsdorff, 1991). In an alternative method, the fluid is defined as a solution phase using a pseudocompound approximation (Connolly and Kerrick, 1987) for the fluid to calculate a P-T Schreinemakers projection including a fluid of variable composition (Connolly and Trommsdorff, 1991). Three types of univariant curves can be traced in such a diagram; (1) true univariant volatile neutral, (2) true univariant volatile dependant, (3) P, T or Xfluid extrema (Table 6).

Table 6: Main reaction types in mixed volatile P-T Schreinemakers projections used to interpret phase boundaries in PT-X_{fluid} phase diagrams. "c" denotes the number of components in the system.

Reaction type	Description
1: True univariant volatile neutral	The simplest reactions are reactions that involve c+ 1 phases the same proportion of volatile component on both sides of the reaction. The position of these reactions is fixed in PT-space independently of fluid composition. The stabilities of the assemblages on either side of the reaction boundary however are truncated by volatile components, limiting the stability in PT-Xfluid space.
2: True univariant volatile dependant	Involves c+1 phases including the fluid of variable composition. The fluid composition varies along the reaction curve i.e. the PT-conditions are fixed as a function of P *or* T. Corresponds to pseudoinvariant points in P or T Xfluid (fixed either P or T) Schreinemakers projections.
3. P, T or Xfluid extrema of reactions involving C-phases.	Minima/maxima in T-Xfluid or P-Xfluid of volatile dependant c-phase reactions. In addition fluid end member positions of reactions can also be plotted (i.e. pure H_2O or CO_2). The position of the reaction curve for intermediate fluid compositions are termed pseoudounivariant curves and will plot between the end member curves and the curves of the minima/maxima as isopleths of fixed fluid composition in PT-diagrams.

The calc-silicate assemblages observed in the current study involve equilibria that depend not only on P and T but also on fluid availability and composition. An early retrograde replacement was replacement of the diopside-phlogopite assemblage (Mp1) by tremolite-sanidine-rutile assemblage (Mp2a), tremolite, calcite quartz (Mp2b) and biotite-amphibole (Mp2c). Field and microscopic observations imply that these assemblages formed simultaneously as a function of chemical (i.e. protholith) variations. Mp2a formed in reaction of the Mp1 assemblage with the quartz-biotite-plagioclase gneiss providing excess SiO_2 and K_2O. Mp2b is replacement of diopside. Mp2c formation is more complex as it involves interaction with the chemically complex amphibolite adding Fe to the Fe-Mg phases hence adding the effect of solid-

solutions. Mp2a and Mp2b on the contrary involve only almost pure phases and are more easily interpreted in PT-Xfluid space. The chemical system comprising Mp1, Mp2a and Mp2b is K_2O-MgO-CaO-Al_2O_3-SiO_2-TiO_2-COH (KMCAS-Ti-COH). Two observations were used to simplify the system: 1. the only carbonic fluid encountered is CO_2, limiting the fluid to the binary H_2O-CO_2 COH-subsystem 2. K_2O and Al_2O_3 are linked in the observed phases and can be joined in one chemical component similar to sanidine/microcline: $KAlSi_3O_8$. As a result, the muscovite bearing reactions, for example, is not shown. The simplified chemical system comprises $KAlSi_3O_8$-MgO-CaO-SiO_2-TiO_2-H_2O-CO_2. We used the method of Connolly and Trommsdorff (1991) to model the fluid as a binary H_2O-CO_2 fluid. All other phases were considered as pure end members, because Fe-Mg substitution was limited. A simplified version of the results is illustrated in Figure 18, and relevant calc-silicate reactions are summarised in Table 7 with full reaction stoichiometry which is not stated in the text or the figures.

The upper P stability of tremolite + sanidine is limited by the fluid independent univariant reaction 1 (tr + san ↔ di + phl + qz) toward the assemblage phlogopite + diopside + quartz (Table 7). In addition the assemblage tremolite +sanidine+ calcite is limited by reaction 2 (tr + san + cc ↔ phl +di + H_2O + CO_2) with a thermal maximum at XCO_2 = 0.75 and its minimum stability at XCO_2 = 0 (Figure 18). This is approximately equal to the maximum stability of the assemblage tremolite + quartz + calcite limited by reaction 3 (Table 7), also at XCO_2 = 0.75 (Figure 18). Therefore, it is implied that Mp2a and Mp2b formed simultaneously at the same XCO_2-PT conditions. Local presence of calcite in Mp2a is controlled by excess Ca where SiO_2 is scarce. Given that Mp2a and Mp2b formed simultaneously, the assemblages must have formed at the pseudoinvariant point comprising the intersection between reaction 1 and reaction 3 (Table 7, Figure 18). The maximum T conditions corresponds to the intersection of the thermal extremity of reaction 3 with reaction 1 at T=636°C, 7070 bar, XCO_2 = 0.75. The observation of sanidine gives a minimum T, P of 456°C and 8417 bar.

Reaction 7 (phl + ttn + qz ↔ H_2O + ru + tr + san) defines the stability of the rutile together with sanidine and tremolite (Figure 18). The position of reaction 7 in P-T space depends on XCO_2 in that at fixed T the sanidine + rutile + tremolite assemblage is stabilised at higher P by increasing XCO_2 (Figure 18, Table 7). However, at high XCO_2, reaction 7 is pinched against reaction 8 (Table 7, Figure 18)

Reaction 8 (phl + ttn + qz + dol ↔ CO_2 + H_2O + ru + tr + san) occurs at a higher temperature than reaction 2 and 3 along the reaction 1 curve (Figure 18, Table 7). Thus the rutile + sanidine + tremolite assemblage is not entirely compatible with the Mp2a and Mp2b assemblages. The stability field is however close at XCO_2 = 0.75.

The edenite + tschermakite substitution was active in the amphiboles (Sørensen et al., 2007, and this paper). Therefore, amphibole-bearing assemblages are stable at higher temperatures hence explaining the unexpected stability of rutile. The exact effect of this is difficult to quantify as the observed edenite and tschermakite substitutions vary within the amphiboles in the assemblages. We infer this to be the result of local chemical variations i.e. the Na-content of the rock will control the amount of Al in

amphibole at a given temperature. The effects of amphibole solid solutions can only be explored in fixed bulk composition pseudosections. We believe that the corrections made by such pseudosections will only have an illustrative function because the amphibole stability is sensitive to the thermodynamically effective bulk composition. In conclusion the first retrogression occurred near the maximum thermal stability of the tremolite + quartz + calcite assemblage with a significant CO_2 fraction in the coexisting fluid.

Fluid inclusion studies documents salts in all the retrograde fluids. Salt is decreasing the a_{H2O} and, therefore, an estimated XCO_2 at 0.75 for the onset of retrogression is too high. With a total salinity of 30 wt% NaCl, the true XCO_2 value would only be about 0.23 (Y (CO_2)* on Figure 19). Because this is the salinity in the total fluid and we measured 30wt% NaCl equivalent in the aqueous phase both CO_2 and the salinity must be adjusted. Because of the construction of the H_2O-CO_2-NaCl EOS in PERPLEX wt% NaCl is expressed as total wt% in the fluid i.e. wt% NaCl = Xsalt = $wt_{NaCl}/(wt_{NaCl}+wt_{CO2}+wt_{H2O})$, $y(CO_2)^* = nCO_2/(nH_2O+nCO_2)$. In our fluid inclusion studies we indicate the wt% of NaCl in the aqueous phase i.e. wt% NaCl = Ysalt = $wt_{NaCl}/(wt_{NaCl}+Wt_{H2O})$. The two methods of calculating salinity are related through mass balance considerations. The problem is that the fluid composition is determined by the position of the pseudoinvariant point Mp2 as a function of Xsalt and that the relation between Xsalt and Ysalt depends on YCO_2*. This was solved by calculating several T-YCO_2* sections, such as the one in Figure 19, at different Xsalt values. Subsequently, the Xsalt and YCO2* of the pseudoinvariant point were plotted on a diagram. Calculated values of Xsalt as a function of YCO2* at fixed Ysalt= 30 wt% were plotted on the same diagram. The intersection between the curve defined by the pseudoinvariant points and the curve of Xsalt at Ysalt = 30 wt% defined the fluid composition at $XCO_2 = (n_{CO2}/(n_{CO2}+n_{H2O}) = 0.32$, $XH_2O = 0.68$, wt%NaCl = $wt_{NaCl}/(wt_{H2O}+wt_{NaCl})$=30wt%. In mole fractions of the total fluid this corresponds to $XCO_2 = 0.30$, $XH_2O = 0.62$ and XNaCl = 0.08.

The phase diagram in Figure 18 shows both the probable path of initial retrogression and subsequent retrogression history toward lower T. The stability of the assemblage tremolite + sanidine is limited by both the univariant reaction 1 and the pseoudounivariant reaction 4 (phl + cc + qz $\leftrightarrow$ tr + san). Phlogopite + calcite + quartz is stabilised over sanidine + tremolite at higher T by high XCO_2. The XCO_2 isopleths of reaction 4 are closely spaced at high XCO_2 (Figure 18). Replacement of sanidine + tremolite by quartz + calcite + phlogopite was not observed. Accordingly, either the XCO_2 decreased rapidly as the temperatures fell or the PT path followed the slope of the reaction 4 isopleths (Figure 18). The fluid inclusions data support that a rapid fall in XCO_2 is the best approximation.

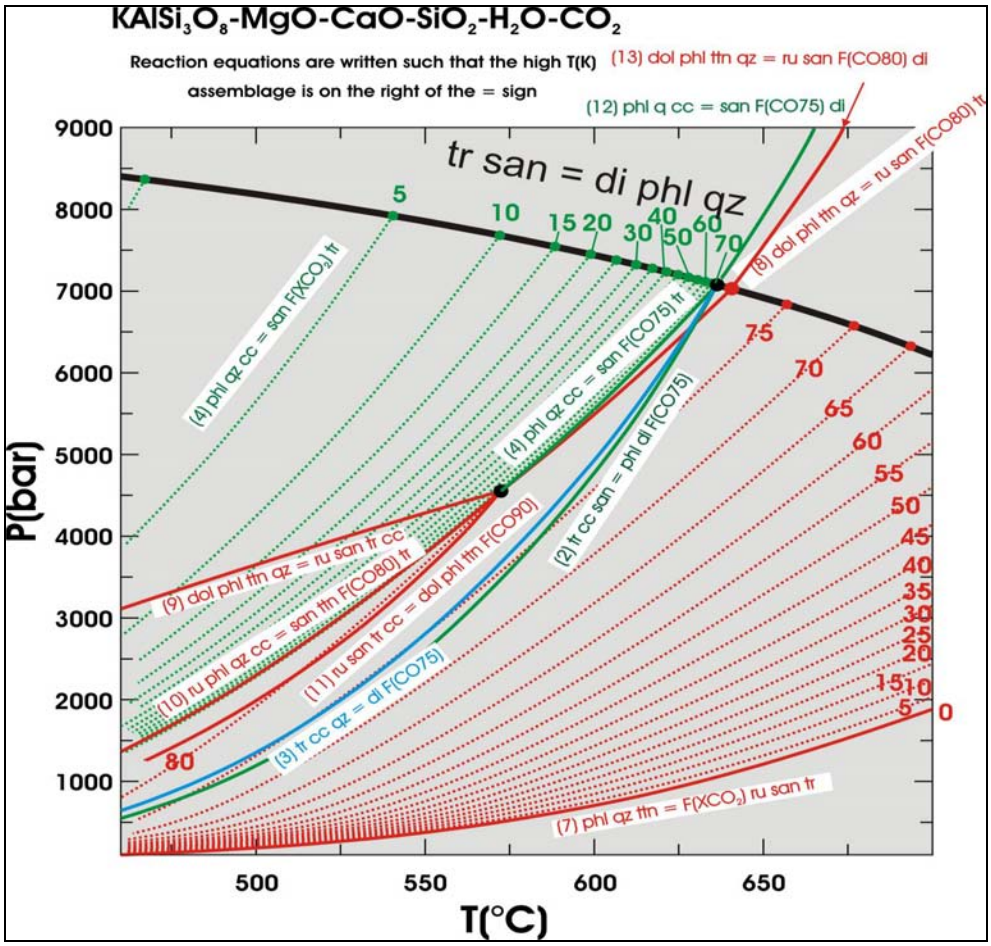

Figure 18: Relevant phase equilibria for Mp1, and Mp2. PT-XCO_2 conditions for the formation of the Mp2 assemblages are defined by univariant, singular (extrema) and pseoudounivariant mineral reactions. Stability of assemblages tr + san and ru + tr + san is partly limited by pseudoinvariant equilibria, which are only univariant PT-curves for fixed fluid composition. Reaction equations do not include stoichiometry. Numbering of reactions is the same here as in the text and Table 7 where full reaction equations are found. Calculated with PERPLEX (Connolly, 1990) and an updated version of HP98 thermodynamic dataset (Holland and Powell, 1998). The true univariant reaction governing the overall stability of Mp1 over Mp2a is given a thick black line, red lines are reactions involving rutile bearing assemblages, green tr + san ± cc, and blue is the maximum thermal stability limit of Mp2b. Stippled lines are isopleths for a specific fluid composition, whereas solid lines are singular or true univariant. The XCO_2 in the reactions is stated in two ways: 1. as COX meaning XCO_2 = X% 2. F(XCO_2) is stated as percentage where isopleths are plotted, here the XCO_2 value is written as a number on each isopleth.

Table 7: Relevant mineral reactions in the $KAlSi_3O_8$-MgO-CaO-SiO_2-TiO_2-H_2O-CO_2 system. The reaction type refers to the terminology in Table 6. Note that muscovite bearing equilibria are not considered in this system. Reactions are written such that the high temperature assemblage is on the right of the ↔ sign.

1	Type 1	tr +san ↔2di+phl+4qz
2	Type 3	2tr+san+3cc ↔ phl+7di+H_2O+3CO_2
3	Type 3	tr+3cc+2qz ↔ 5di+H_2O+3CO_2
4	Type 3	12qz+3cc+2.5phl↔2.5san+1.5tr+3CO_2+H_2O
5	Type 3	tr+3cc↔dol+4di+H_2O+CO_2
6	Type 3	5dol+8qz+H_2O↔3cc+tr+7CO_2
7	Type 3	5phl+6ttn+18qz↔2H_2O+3ru+3tr+5san
8	Type 2	(10/4-9/4X)phl+(3-3X)ttn+(9-7X)qz+1/2Xdol ↔ XCO_2+(1-X)H_2O+(3-3X)ru+(6/4-5/4X)tr+(10/4-9/4X)san
9	Type1	2dol+phl+4ttn+4qz↔4ru+san+tr+4cc
10	Type2	ru+phl+qz+Xcc↔san+ttn+tr+XCO_2+(1-X)H_2O, Full reaction equation is with fluid dependent stoichiometry: (4X-3)ru+(2.5-2.5X)phl+(9-8X)qz+Xcc↔ (2.5-2.5X)san+(4X-3)ttn+(1.5-1.5X)tr+XCO_2+(1-X)H_2O,
11	Type2	ru+san+tr+cc↔dol+phl+ttn+(1-X)H_2O+XCO_2 Full reaction equation is with fluid dependent stoichiometry: (6-4X)ru+(1/2X-1/4)san+(3/4-1/2X)tr+(9-7X)cc ↔(9/2-4X)dol+(1/2X-1/4)phl+(6-4X)ttn+(1-X)H_2O+XCO_2
12	Type 3	6qz+3cc+phl↔3di+san+3CO_2+H_2O
13	Type 2	(1-X)phl+(3-3X)ttn+(3-2X)qz+ ½Xdol↔ (3-3X)ru+(1-X)san+(3-2½X)di+XCO_2+(1-X)H_2O

None of the assemblages in Mp3, Mp4 or Mp5 are limited by true univariant reactions and progressive fluid aided metasomatosis during the addition of Na, further complicates the interpretation. However, PT-X_{fluid} extrema along with pseoudounivariant volatile dependant reactions allow for a tentative interpretation. Mp3 comprise the diopside + tremolite+ calcite assemblage whereas quartz is absent. Therefore, Mp3 was stable above reaction 3 but below reactions 2 and 5 (Table 7, Figure 19). Quartz is not in excess because the tremolite diopside assemblage otherwise would have decomposed by reaction 3. The stability field of the Mp3 assemblage in the K_2O-Al_2O_3-MgO-CaO-SiO_2-TiO_2-H_2O-CO_2 system at 7 kbar is shown in Figure 19. The stability of the Mp3 is narrow in this system (Figure 19). However, the presence of Na, Al and Fe in amphibole would increase the stability and hence the shown stability field is smaller than in reality. Because XCO_2 is decreasing during retrogression, it is implied that the Mp3 assemblage is locally stabilised by decreasing the XCO_2. Figure 19 also illustrates that the isobaric cooling path is only realised if XCO_2 continuously decreased during cooling. The phase diagram (Figure 19) also imply that the diopside bearing assemblages may only survive retrogression

at silica undersaturated conditions hence explaining why the diopside bearing Mp1 assemblage commonly is preserved in a protective shell of Mp2a.

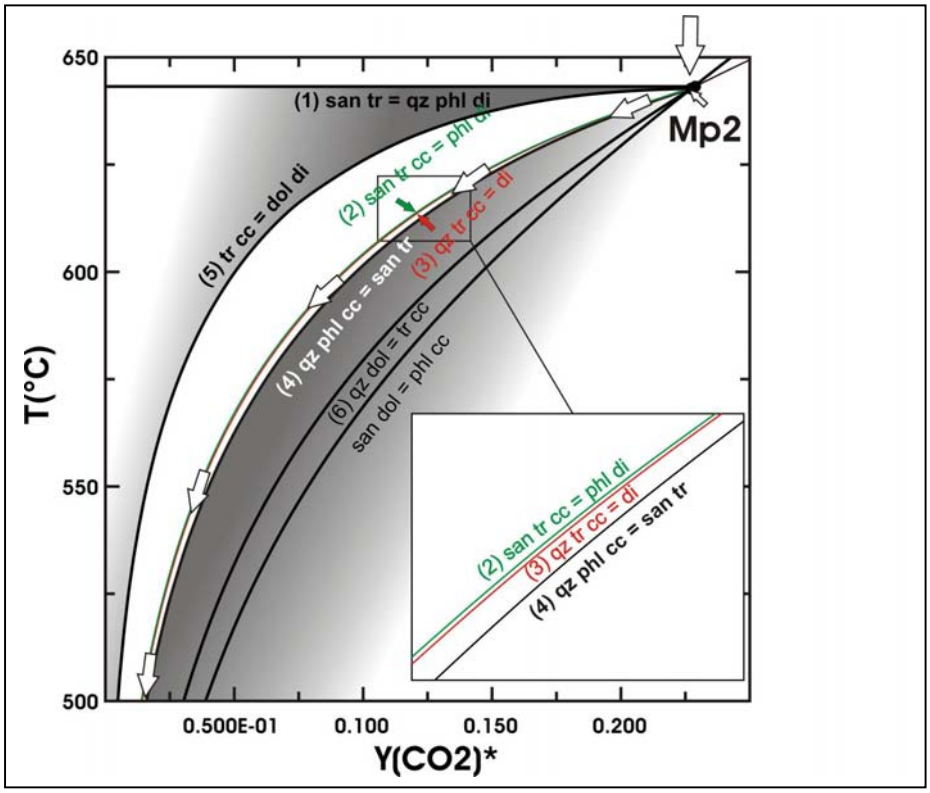

Figure 19: Isobaric T-XCO_2 section at $P=P_{fluid}$=7000 bar for the K_2O-Al_2O_3-MgO-CaO-SiO_2-TiO_2-H_2O-CO_2-NaCl system showing the stability field of Mp3 between the red and green reaction curves. White arrows illustrate possible fluid evolution during cooling. The grey shading show the limits of the T-fluid space constrained by reactions quartz + dolomite +phlogopite and tr + cc = dol +di. It should be kept in mind that the section is only illustrative and that the narrow stability field of Mp3 is probably larger because of solid solution in amphibole. Mp3 stability can only be constrained if one thermodynamic parameter may be independently fixed. In addition the diagram uses Mg-endmembers and does not take into account the edenite and tschermakite substitution in amphibole. Reaction equations are written such that the high temperature assemblage is to the right of the = sign. Calculated with PERPLEX and an updated version of the HP98 dataset. $YCO_2^*=n_{CO2}/(n_{H2O}+n_{CO2})$.

Amphiboles of the Mp4 assemblage are more Al, K and Na rich than other amphiboles in the calc-silicates. Therefore, both edenite and tschermakite substitution was important in the Mp4 amphiboles and Na was an important component that stabilised the Mp4 assemblage. The Mp4 assemblage could not form from the Mp1

assemblage, without adding Na to the bulk composition. Given the flexibility of the amphiboles in P-T-X space they can not be used to constrain PT-X_{fluid} conditions in this case.

The stability of the Mp5 assemblage (epidote-calcite-tremolite/actinolite-pyrite assemblage related to FIA4) is probably a greenshist-subgreenshist facies assemblage. The stability of this assemblage depends on activity-activity relations in the coexisting fluid phase (Bird and Spieler, 2004). Core to rim increase in the Fe-content of both epidote and amphibole could be an effect of both PT-changes and small variations in fluid composition. Figure 20 outline the effects of variations of cation to hydrogen ratios in the coexisting fluid on phase equilibria in the CaO-Al_2O_3-Fe_2O_3-SiO_2-H_2O-HCl system at fixed P and T. From this it appears that compositional changes of epidote may be controlled by the fluid composition. For example, calcite dissolution change the cation speciation and increase pH hence increasing the Fe-content of epidote from X_{Ps} = 0.15 to 0.27 (Bird and Spieler, 2004). However, the decreasing $CaCl_2$ content in the fluid inclusions associated with the increased pistacite content in epidote, contradicts this explanation. Rather, the increasing pistacite is due to increased Fe^{3+}/Ca ratio of the fluid. This interpretation is supported by the lowering of the first melting temperatures observed parallel with the increased Fe content in the epidote grains. Accordingly, lowering of the first melting is enhanced by increasing the complexity of the fluid system. However, Figure 20 is only a principal sketch and is only partially explaining the evolution.

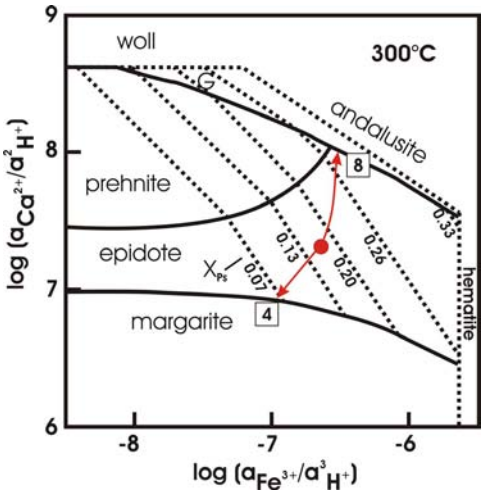

Figure 20: Activity-Activity diagram showing the phase relations in the system CaO-Al_2O_3-Fe_2O_3-SiO_2-H_2O-HCl as a function of cation to hydrogen ion activity at P=86 bar in the presence of quartz and fluid with unit activity of water. Stability fields of phases in the system are shown by solid lines. Prehnite, epidote and garnet (G) all involve solid solution between Fe^{3+} and Al. Stippled lines show isopleths of constant Fe-content with labels denoting the equivalent Xps content in the epidote field. Arrows represent changes in epidote predicted by theoretical irreversible reaction path models of anorthite and calcite reactions with aqueous solution, labelled 4 and 8 respectively in the diagram. From Bird and Spieler (2004). More information on sources of thermodynamic data is found therein. The diagram is purely illustrative in our case but demonstrates the high variance of epidote bearing assemblages, which are sensitive to small changes in fluid composition.

Nijland et al. (1993) provide excellent field and petrographic documentation of the paragenetic evolution during cooling and uplift observed in corundum bearing rocks from Kleggåsen in near vicinity of our study area. Their study includes parageneses formed during retrogression of a rock originally comprising corundum + plagioclase + biotite + rutile + sillimanite (MI). Nijland et al. (1993) define three main retrograde stages:

MII: Kyanite-muscovite chlorite veins intersecting MI

MIII: Assemblage corundum + margarite replacing kyanite in MII and corundum + plagioclase in MI.

MIV+MV: a mixture of late alterations.

In the following discussion we provide a detailed revaluation of their interpretation, based on phase diagram calculations.

Nijland et al. (1993) interpreted the formation of the MII veins to be the result of a fluid interacting with the host rock according to the following reaction:

reaction I: The formation of ky-mu-chl veins

$$MII: 3sil + bt + 0.5\,pl + 4H_2O \leftrightarrow mu + 0.5chl + ky + (0.1Ti, 0.08Mg, 0.2Ca + 0.1Na)$$

The reaction is slightly metasomatic because the composition of the products and reactants deviate. Nijland et al. (1993) used the presence of kyanite over sillimanite in conjunction with the textural observation that margaritisation occurred at a later stage, to infer that the reaction occurred at P = 7 kb and T = 600-700°C. However, we argue that the reaction must occur in the kyanite field at lower T because chlorite and not biotite was the stable Fe-Mg phase. We used three solution models for the solids: muscovite model Mica(CH2) (Coggon and Holland, 2002), chlorite model Chl(HP) (Holland et al., 1998) and biotite model Bio(HP)(Powell and Holland, 1999) and calculated pseudosections for variable XCO_2. The salinity of H_2O was kept constant at 30wt% using an internal fluid EOS in PERPLEX which is calibrated with devolatisation/decarbonation reactions (Aranovich et al., 2005). Nijland (pers. comm., 2007) confirms that he observed brines in MII kyanite as fluid inclusions containing halite; however, he did not study the inclusions in details. The bulk composition was estimated using the stoichiometry of the kyanite forming reaction (reaction I) and the average mineral compositions from Nijland et al. (1993). The resulting pseudosection is shown in Figure 21a. The stability range of the MII assemblage is well constrained in temperature but not in pressure and also depends on the fluid composition (Figure 21a). The stability limits shifts to lower temperatures and pressures with increasing XCO_2 (Figure 21a). According to Nijland et al. (1993) the low temperature limit of the MII is defined by the stability of corundum and plagioclase over margarite i.e. the onset of margaritisation. However, as documented below, this assumption is contradicted by the fact that MIII and MII have overlapping stability fields. Note that the MII stability field is not univariant but has a variance of 5, meaning that 4 thermodynamic parameters must be fixed to constrain the MII field.

The MIII comprises margarite + corundum (Nijland et al., 1993) and formed from metasomatic replacement of kyanite. This replacement reaction must involve a Ca^{2+} + Na^{+} bearing fluid. A number of reactions were suggested for this replacement. In common, they all involve cation exchange with a fluid phase (see Nijland et al., 1993 for references). Stabilisation of the margarite + corundum requires the decomposition of quartz and removal of SiO_2 (Nijland et al., 1993, by for example reaction II):

Reaction II: Reaction suggested by Nijland et al. (1993) to be responsible of the metasomatic replacement of kyanite (ky) by margarite (mrg) plus corundum (cor):

$$3\mathrm{ky} + \mathrm{Ca}_{(aq)} + 3\,\mathrm{H_2O} + 0.5\,\mathrm{O_2} = \mathrm{mrg} + \mathrm{cor} + \mathrm{Si(OH)_4}$$

Bucher et al. (2005) use thermodynamic modelling to demonstrate that removal of SiO_2 generates excess Al_2O_3 in a mica schist, stabilising corundum + margarite. SiO_2 is removed in a chemical gradient, because the chemical potential of SiO_2 is lower in a forsterite + talc assemblage in surrounding ultramafic rocks.

In Froland, this is not applicable because the corundum-bearing rocks are surrounded by granitic gneisses with excess SiO_2.

Accordingly, kyanite decomposition must be re-evaluated. It is suggested that the following reaction was responsible for the replacement of kyanite by margarite + corundum:

Reaction III: Our model for metasomatic replacement of kyanite by margarite-paragonite solid solution (MaPa) and corundum (cor). Note that reaction stoichiometry depends on margarite composition and that for pure endmember margarite no corundum would form as the result of kyanite breakdown:

$$(3 - \mathrm{X})\mathrm{ky} + (1 - \mathrm{X})\mathrm{Na}_{(aq)} + \mathrm{XCa}_{(aq)} + \mathrm{H_2O} + (0.25 + 0.25\mathrm{X})\mathrm{O_2} =$$
$$(1.5 - 1.5\mathrm{X})\,\mathrm{cor} + \mathrm{MaPa}(\mathrm{Xma}, (1 - \mathrm{X})\mathrm{pa})$$

Accordingly, the margarite + corundum formation is a function of cation activities in the fluid phase as well as of P and T. As a result the margarite forming reaction is difficult to portray in PT-diagrams.

To characterise the P-T-X properties of the margarite + corundum assemblage it is easier to assume solid-solid reactions. This approach requires the hypothetical modelling of the assemblages that would have formed instead of corundum + margarite given different PT-conditions for the same bulk composition (Reaction III). Given that only one silicate-reactant is present (ky) (1 mole p.f.u.) and Al_2O_3 (1 mole p.f.u.) the bulk Al/Si ratio is locked at 1. In addition the Ca/Na ratio is fixed by the margarite composition, which again fixes the Si content and hence the Al content of the products. Using these constraints on the bulk composition we calculated pseudosections to test the stability of the margarite + corundum assemblage. As above, the salinity is fixed at 30 wt% using the same fluid EOS as for MII and solution models Pl(h) (Newton et al., 1980) for plagioclase and Mica(CH2) for margarite. The results document that the

stability field of the MIII assemblage is considerably larger than that reported by Nijland et al (1993) (Figure 21b). The upper limit is quite similar, but the lower limit is expanded. Similar results were found by constructing pseudosections for the replacement of the MI assemblage by margarite + corundum. Because the results are similar only one diagram is present here. The difference in the lower T limit of MIII between our estimate and the Nijland et al. (1993) is caused by the fact that Nijland et al. (1993) defines the lower limit of MIII by the absence of zoisite/clinozoisite and the reaction:

reaction IV: Low temperature ilmit of MIII according to Nijland et al. (1993)

$$5an + 2H_2O \leftrightarrow mrg + 2zo + 2SiO_2$$

However, there are two observations that rule out reaction IV. First, the reaction will, as also noted by Nijland et al. (1993), shift to lower T with increasing Xab in plagioclase. Second, and most important, the stability of zoisite in the CNASHC system depends on the bulk composition and/or cation composition of the coexisting fluid (Rosing et al., 1987). In conclusion, the reaction suggested by Nijland et al. (1993) is contradicted by the bulk composition which prohibits the stabilisation of zoisite/clinoziosite, which would need higher Ca-content of the system. Most importantly, the PT-stabilities of MII and MIII are coinciding (Figure 21). Therefore, the paragenetic change from MII to MIII is not related to PT changes.

Studies of the hydration of corundum + plagioclase imply that the fluid cation composition controls the hydrated assemblages (Rosing et al., 1987). Activity diagrams show that the stability of margarite + corundum at 550°C and 5 Kb is possible in fluids with a SiO_2 activity of about 0.1, log (aCa^{2+}/a^2H^+) of about 6 and low log (aK^+/aH^+) (Rosing et al., 1987). Increased K^+ contents of the fluid relative to H^+ and Ca^{2+}, stabilise muscovite over margarite. Therefore, the change from MII to MIII probably reflects increased Ca^{2+} relative to K^+ in the fluid phase. This scenario agrees with the fluid inclusion observations that record changes in the cation composition from the NaCl-KCl-H_2O-CO_2 (FIA2) to NaCl-$CaCl_2$–H_2O (FIA3) fluids. In conclusion, the shift from MII to MIII marks the transition from potassic to sodic alteration and is constrained to the MIII stability field in the Froland area, at about 550 to 450 °C, and P > 4500 bar.

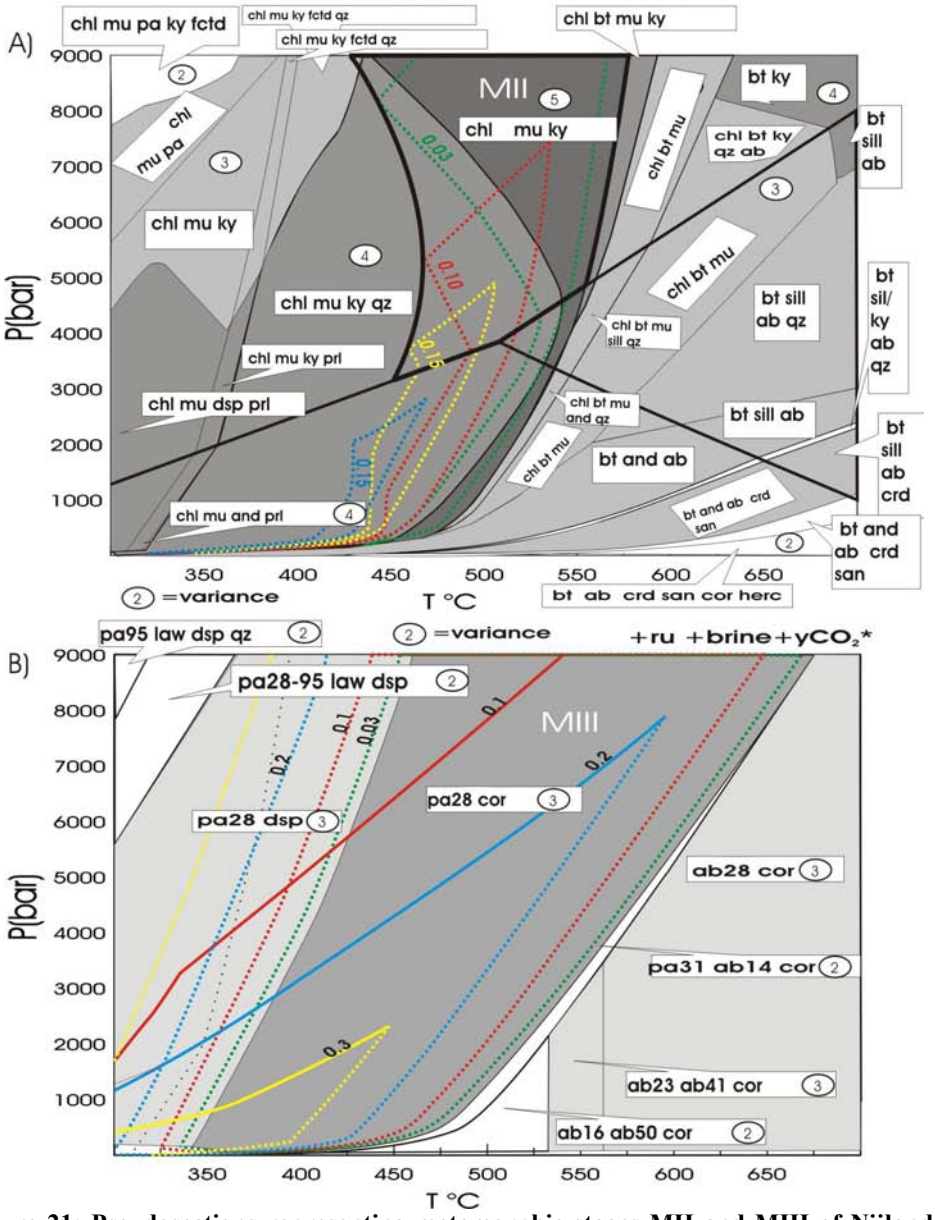

Figure 21: Pseudosections representing metamorphic stages MII and MIII of Nijland et al. (1993). A) MII comprising the assemblage Kyanite (ky), chlorite (chl), and muscovite (Mica(CH2)). The stability field is dependant on fluid composition and shifts to lower pressure with increasing XCO_2 in the coexisting fluid (coloured lines with label indicating

XCO_2). The pressure is broadly constrained by the stability of kyanite. B) MIII comprising Margarite and corundum has a larger stability field than MII. Isopleths show change in the stability fields for various XCO_2 values. Both assemblages are less stable in CO_2-rich than in H_2O rich fluids. The stability fields of MII and MIII overlap but the MIII assemblage has a larger stability field and would have stabilised before MII if only P and T were changed at constant fluid compositons. Pseudosections were calculated with PERPLEX (Connolly, 1990; Connolly and Petrini, 2002) and an updated version of the HP98 dataset (Holland and Powell, 1998).

7.3 Tentative PT-fluid path

The aim of this section is to propose a tentative PT-for the Froland area (Figure 22).

The first retrograde assemblage that may be used for the P-T path is the tremolite + sanidine assemblage (Mp2a). The stability of the Mp2a assemblage is limited by the univariant reaction diopside + phlogopite + quartz (Figure 22). As previously discussed the Mp2a and Mp2b assemblages probably formed simultaneously hence the PT-condition lie on a pseudoinvariant point. This interpretation is supported by the assemblage tremolite + calcite + sanidine in Mp2a, which has similar stability field as Mp2b (Figure 22). The stability of rutile + sanidine + tremolite/actinolite within Mp2a is not compatible with the model system, where the Fe, Al, Na and K content of amphibole was not considered. However the stability of the rutile bearing assemblage increases at high XCO_2 in the fluid. Thus we make the semi-quantitative interpretation that XCO_2 in the fluid was high when Mp2a and Mp2b formed and that they formed near their maximum thermal stability in the model system.

Mp2c, comprising amphibole + biotite, forms from the Mp1 diopside + phlogopite assemblage toward amphibolite. Field observations suggest that Mp2c is related to the biotite-amphibole assemblages in the amphibolite. Thus the semi-quantitative estimate provided by the calc-silicate assemblages Mp2a and Mp2b probably serves as an estimate of the initial PT-X fluid conditions for the first introduction of biotite in the amphibolites and the quartz type named Qz2. Qz2 in quartzites coexists with rutile hence the Ti in quartz geothermometer of Wark and Watson (2006) is applicable giving a temperature of 626°C. This agrees well with the paragenetic data of the calc-silicates and suggests that Qz2, introduction of biotite in amphibolites, and formation of the tremolite + sanidine assemblage were all related to the same early retrograde stage (Figure 22). The fluid inclusions in FIA2 comprise brine fluids. The presence of brines in the fluid would serve to reduce the activity of H_2O and hence the XCO_2 predicted by the model system with binary H_2O-CO_2 fluid. In conclusion we infer that Mp2 formed at c. 626-640°C and 7000 bar with a fluid with about 30 wt% salts and $XCO_2 = n_{CO2}/(n_{CO2}+n_{H2O}) = 0.32$(Figure 19).

The tremolite-sanidine assemblage (Mp2a) is well preserved suggesting that the assemblage phlogopite + calcite + quartz was not introduced during cooling by reaction 4 (Table 7). Isopleths of reaction 4 are closely spaced (Figure 18 and Figure

19) suggesting either that the PT-path followed the isopleths or that the fluid composition changed towards much more H_2O rich compositions during early cooling.

Later mineral parageneses in the calc-silicates are constrained by high variance equilibria that depend on both the fluid composition and the chemical complexity sustained by increasing the amount of Al and Na in amphibole and by increasing the Fe content in amphibole.

The next stage in the fluid and PT evolution is better characterised by Nijland et al. (1993). MII and MIII are interpreted to comprise two separate PT-events (Nijland et al. 1993) however; they probably formed at similar PT-conditions, but with different cation composition of the coexisting fluid. MII is characterised by activity-activity diagrams in Rosing et al. (1987). MII formed with a KCl bearing fluid, whereas MIII formed with a $CaCl_2$ bearing fluid. This transition is preserved in the FIA2 to FIA3 transition and marks a change from potassic/sodic to sodic/calcic alteration. This event occurred at 425-575 °C, minimum pressure of 4500 bar given the stability of kyanite.

The only data that are available for the uplift path is the isochore of FIA 3, which formed during exhumation near the brittle-ductile transition of quartz. In addition the lack of decrepitation textures in relation to FIA3 suggests that the pressure difference between the uplift path and the FIA3 isochore was smaller than the decrepitation strength of fluid inclusions in quartz. Bodnar et al. (1989) determined an empirical relation between inclusion size and decrepitation strength in quartz:

$P(kbar)=4.26\ D^{-0.423}$ where D is the inclusion diameter in microns

With an inclusion size ranging from 5 to 10 μm this gives strength between 1608 and 2156 bar.

The last part of the retrograde path is constrained by coexisting prehnite and pumpellyite and fluid inclusions at 175-280 °C and 2-3 kb (Nijland et al., 1993; Touret, 1985). We infer an uplift path through the isochore of FIA3 down to this point, between 300-400°C, from 5-7kb and down to 2-3 kb. Isopleths of the reaction, calcite + rutile +quartz $\leftrightarrow$ titanite, indicates that XCO_2 was lower than 0.001. This strengthens the validity of our inferred PT-X fluid uplift path. Our inferred PT-path is presented in Figure 22. It is shifted towards considerably lower temperature than the PT path of Nijland et al. (1993), in agreement with our fluid inclusion data. The PT-path suggested here implies fast uplift at a low temperature. This agrees with the partly brittle partly plastic behaviour of the Bamble rocks during uplift.

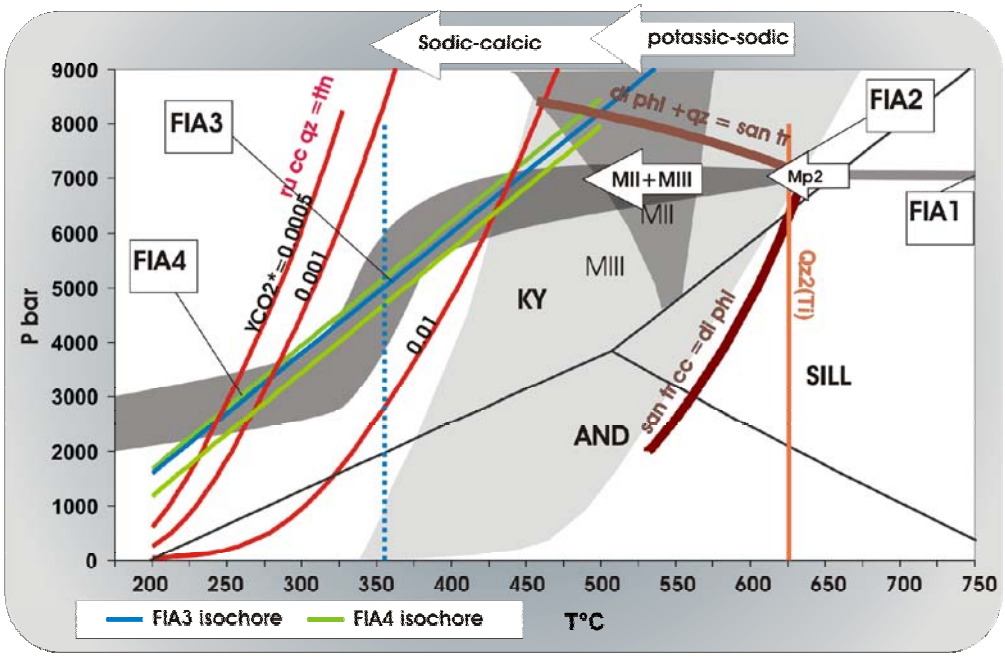

Figure 22: Tentative PT-Xfluid path of the study area, with possible implication for the uplift path of the Bamble sector. The PT-X_{fluid} path is assembled using a combination of mineral paragenetic and fluid inclusions data. Because fluid inclusions and mineral paragenesis that are simple enough to be portrayed quantitatively in PT-space the correctness of the PT-path rely on textural correlations between assemblages in one rock type and fluid inclusions found in other rock types. Arrows on the top of the diagram indicate condition when alteration changed from potassic-sodic to sodic-calcic.

7.4 Quartz recrystallisation and purification, the role of the fluid

High purity quartz, the Qz3 of Sørensen and Larsen (2007, paper 1), formed when the fluids were dominated by NaCl with minor $CaCl_2$. These fluids form quartz with mm-scale recrystallisation textures in a channel like pattern, not only lowering the luminescence of the quartz but also removing most impurities including the rutile needles.

The solubility of quartz in pure water displays a general increase with P and T. However, the solubility is also a function of the fluid composition. Except for an initial salting in effect at low salinity and pressure, the presence of salts has a negative effect on the quartz solubility. Similarly the presence of non-polar dissolved species like CO_2 will have a stronger effect (e.g. Newton and Manning, 2000; Shmulovich et al., 2006).

Aqueous brines have lower wetting angles against quartz than low salinity fluids (e.g. Watson and Brenan, 1987). This enables brines to infiltrate quartz on a fine scale via micro-pores. CO_2 or other non-polar dissolved species will have the opposite effect (Watson and Brenan, 1987). The increased infiltration capability of brines counteracts the effect of the lower solubility of quartz in brine, because the high degree of infiltration increases the surface area of quartz which is exposed to the fluid. We also suspect that the quartz recrystallisation observed is not simply a process of dissolution and re-precipitation, but also a process of minimising the free energy of quartz at the given PT-X_{fluid} condition, i.e. quartz with specific trace element configurations will be stable. However it is inferred from our study that a fluid phase is needed for reaction to occur.

The type of recrystallisation depends also on the PT path and the gradients in the quartz solubility. If the solubility is increased along the PT-path then narrow dissolution textures will be dominant. On the contrary, if the solubility decrease along the PT-path, it is more likely that the dissolved quartz will be redistributed locally.

Therefore, we believe variation in quartz solubility gradients is the background for the difference between the Qz3 and Qz4 textures i.e. Qz3 formed in a PT-envelope where the quartz solubility decreases with temperature, whereas Qz4 formed with increasing quartz solubility with temperature. $CaCl_2$ in fluids decrease the quartz solubility more than NaCl (Shmulovich et al., 2006), suggesting the change in fluid cation speciation from Na dominated to Ca dominated also served to decrease the quartz solubility. Furthermore, the presence of carbonates in fluid inclusions in Qz4 document that CO_2 was present hence reducing the infiltrating capability of the fluids.

7.5 The fluid evolution as a result of fluid rock interaction

The retrograde fluids maintain a high salinity throughout the retrograde uplift path. However, the cation speciation is changing. The first retrograde fluids are mixtures of NaCl-KCl-H_2O-CO_2 with eutectic salinity and introduced together with low salinity H_2O-CO_2 mixtures. CO_2 is absent in the subsequent fluids and their cation composition changes. The evolution in cation composition can be described in the H_2O-NaCl-KCl-$CaCl_2$ tetrahedron (Figure 23). The cation composition experience significant changes at constant salinities in going from:

NaCl-KCl → NaCl-$CaCl_2$ → $CaCl_2$ (Figure 23)

Probably this evolutionary path is the result of fluid rock interactions at variable P and T during the formation of various mineral assemblages (Table 8).

The aqueous phase in FIA2 comprises near eutectic NaCl-KCl-H_2O mixtures. This agrees with the observation that potassium required for biotite formation was introduced to the amphibolites by a fluid phase. Beach (1980) suggested the following reaction for the formation of biotite in retrograde shear zones in amphibolites in the Lewsian complex:

$2Na_{0.5}Ca_2(Mg, Fe)_{4.5}Al_{0.5}Si_7AlO_{22}(OH)_2 + 2K+ + 16H^+ \leftrightarrow$
$K_2(Mg,Fe)_{4.5}AlSi_6Al_2O_{20}(OH)_4 + 8SiO_2 + 4.5(Mg,Fe^{2+}) + 4Ca^{2+} + Na^+ + 8H_2O$

This is a reaction consuming K and producing H_2O, Mg, Fe, Ca and Na. In the study area, however, the formation of biotite coincides with the formation of a new amphibole which is chemically different from the old amphibole. The composition of the newly formed amphibole and biotite varies, but the distribution of octahedral Mg and Fe between biotite and amphibole follows an univariant trend (Sørensen et al., 2007, paper 3). This suggests that biotite and amphibole in the area formed under similar conditions and that the observed compositional variations in both minerals is caused by variations in the temperature (Sørensen et al., 2007, paper 3). An interesting aspect is that the compositions of the overgrowth rims follow the same trend throughout area whereas amphibole cores follow different trends. Sørensen et al. (2007, paper 3) infer this to be the result of a change in the rock/fluid system from being internally buffered to being externally buffered. The implication is that the retrograde fluids throughout the area have an external source that, after a brief period with internal buffering changed fluid composition from a low salinity H_2O-CO_2 mixture to a H_2O rich brine. This is mirrored by univariant trends of amphiboles and the linear correlations between X_{Fe} in coexisting amphiboles and biotites. These trends imply that the equilibrium between amphibole and biotite is controlled by an externally derived fluid that stabilises progressively more Mg-rich biotite and amphibole due to exhumation and cooling.

Although an external fluid was supplied, the fluid cation speciation continuously equilibrated with the ambient mineral assemblages. The formation of biotite from amphibole leads to a K-loss and Na-gain in the fluid. This was partially balanced by increased albite contents of plagioclase. However the consumption of K by the formation of biotite and by replacement of plagioclase by K-feldspar lead to a loss of K and a gain of Na and Ca in the fluid hence shifting the composition towards the NaCl-$CaCl_2$-H_2O ternary and FIA3 (Figure 23, Table 8). CO_2 is absent in FIA3. Four factors may influence the loss of CO_2:

1. Stabilisation of carbonates under the consumption of CO_2 from a limited CO_2 reservoir. However, having an open system this is hardly the case
2. The high salinity of the aqueous phase increases the liquid immiscibility of H_2O and CO_2 (e.g. Bowers and Helgeson, 1983). As FIA2 comprises two separate fluid types, one CO_2-rich low salinity fluid and brine with low CO_2, it is likely that the two fluid types were not miscible at the entrapment conditions. As concluded before however it is not possible to determine if the fluid inclusions formed by phase separation or they are the result of partial fluid mixing.
3. Brine fluids migrate more easily in silicate rocks than CO_2 rich fluids because of their lower wetting angles (e.g Watson and Brenan, 1987). Thus brine and CO_2 rich fluids probably differentiate along the transport pathway after phase separation.

4. Because of the high salinity of the observed salinity of the fluids, CO_2 is not likely to have infiltrated on along the grain boundaries like the brines. Thus CO_2 may have been restricted to wide channels in the shear-zone system and escaped.

The increased Ca/Na ratio that followed FIA3 may relate to the Na consumption of plagioclase and addition of Ca to the fluid.

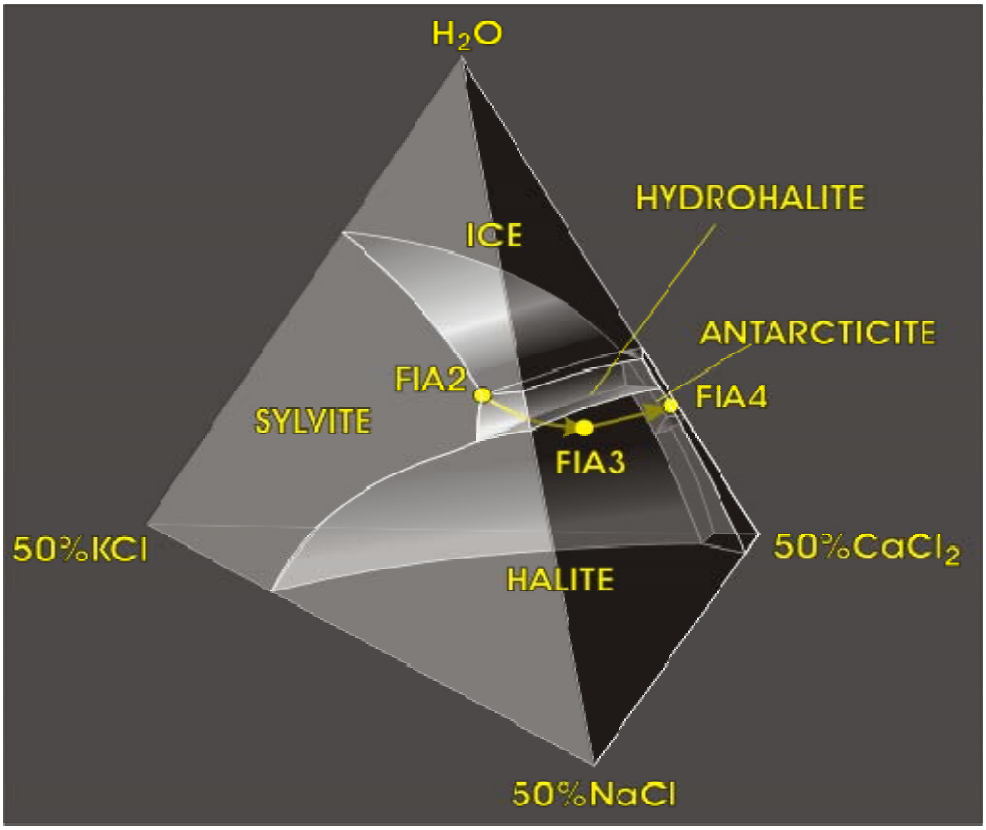

Figure 23: Partly schematic polythermal projection of the H_2O rich part of the H_2O-NaCl-KCl-$CaCl_2$ system after Kornerup-Madsen (1979) showing a three-dimensional impression of the observed cation and salinity evolution of the fluid in relation to the low temperature phase relations observed in microthermometry experiments.

Table 8: The fluid evolution interpreted as a result of fluid-rock interaction. See text for discussion.

Occurrence	Type	Petrologic significance
FIA1		
Qz1 Garnet quartz symplectite and partial melting	CO_2 dominated fluid. Internally buffered (closed system)	Variable high grade conditions and partial melting in amphibolite
Influx of aqueous brines mixing with CO_2-rich fluids, open system		
FIA2		
Qz2 in en echelon quartz veins intersecting amphibolite	Juxtaposed 1: H_2O -NaCl-(KCl) - CO_2 H_2O rich eutectic brine 2: H_2O-CO_2 CO_2-rich low salinity fluid	K-metasomatism causing growth of biotite and alteration of amphibole. Around qz-veins equilibrium decussate biotite and amphibole forms, but inside the amphibolite, amphibole grains are only partly altered with rim-core variations
K supplied to rock by fluid and Na exchanged into fluid, from replacement of plagioclase by K-feldspar and formation of biotite from fluid components + amphibole components.		
FIA3		
Qz3 in quartz-scapolite veins in quartz-biotite gneiss	LVS NaCl-$CaCl_2$-H_2O 25wt% NaCl 6wt% $CaCl_2$	Breakdown of rutile and calcite and growth of scapolite from plagioclase, though coupled mineral reactions: ru+cc+qz↔ttn, ru+Ca(aq)+qz↔ttn pl+cc+Na(aq)+Cl(aq)↔scp
Continuous reaction between plagioclase and fluid exchanging Na from fluid into plagioclase and Ca into fluid as plagioclase becomes more albite rich during cooling		
FIA4		
Fluid inclusions in calcite and epidote in tremolite-epidote-calcite apophyllite vug-assemblages	LV inclusions with 31-36 wt% $CaCl_2$ equivalent, the presence of Fe^{3+} suggested by changes in Fe content of epidote and lowering of first melting temperatures	Stabilisation of pyrite over pyrrhotite adds Fe to the silicate assemblages in the calc-silicate. This stabilises epidote. As significant amounts of calcite is found and no CO_2 detected in the fluid inclusions implies a large fluid/rock ratio.

7.6 Other studies of the retrograde fluids and alteration assemblages in the Bamble sector

Several studies now document the occurrence of brines in the Bamble sector and their effects on mineral equilibria. Nijland and Touret (2001) documented how a graphic pegmatite was replaced by albite-actinolite-clinopyroxene intergrowths, involving considerable modification of the bulk composition via mobilisation of Al_2O_3 and K_2O and addition of Na_2O. Their fluid salinities are comparable to our study, but they do not report the cation composition of the fluids.

Brine fluids facilitate both mass transport and chemical modification of the rocks they are infiltrating. They also affect volatile bearing metamorphic equilibrium reactions in two ways:

1: The presence of salts reduces the activity of water. This shifts the hydration reactions to a lower temperature compared to the $P = P_{H_2O}$ models used in many petrogenetic grids.
2: Hydrous silicates such as amphiboles, biotite and scapolite contain halogens. Several studies imply that halogens in hydrous minerals affect both the SRO (short range order) and LRO (long range order) between elements in the mineral structure. Such effects may be different between different mineral species, and may effect exchange reactions commonly used in geothermobarometry like the garnet biotite exchange thermometer (e.g. Kullerud, 1995).

Nijland et al. (1998) suggested that localised formation of orthopyroxene outside the granulite facies area of the Bamble sector was induced by the local action of brine fluids, which reduced the activity of H_2O, hence shifting dehydration equilibria to lower temperatures.

Alteration assemblages revealing evidence of significant mass transfer are frequently reported from the Bamble sector. Although we only report data from a geographically limited area we hold that brines are the prime suspect of the mass transfer in the Bamble Sector as a whole. Although no other systematic studies of the retrograde fluids exist, several papers report brines with salinities comparable to those reported here. Several studies also document the chemical alteration experienced by the Bamble rocks (Brøgger, 1934; Bugge, 1965; Elliott, 1966; Frodesen, 1968; Jøsang, 1966; Munz et al., 1994; Munz et al., 1995).

Sørensen et al. (2007, paper 3) suggested that the interaction between the brines and hydrous silicates facilitated Fe depletion in the amphibolites and in addition documented direct association between Fe-Cu sulphide formations and alteration of amphibole. Increased understanding of the interaction between hydrous minerals and Cl-bearing fluids, detailed petrographic, geochemical, mineralogical and fluid inclusion studies are needed in order to fully understand the alteration processes in the Bamble sector.

8 Conclusions

1. Brines dominated the fluid phase throughout the cooling and uplift path. CO_2 was quickly expelled during initial stages of retrogression. Salinities in the aqueous phase comprised approximate 30 wt% NaCl equivalents throughout cooling and uplift.
2. A revised retrograde PT-path is suggested based on phase diagram modelling including the effect of the high salinity on retrograde mineral reactions.
3. First introduction of aqueous brines coincides with the brecciation of quartz and dissolution reprecipitation leading to the Qz1 and Qz2 quartz SEM-CL textures and with the first retrograde stage observed in calc-silicates. Ti in quartz thermometry and PT-conditions constrained by phase diagrams agree on formation conditions of T = 626-640°C and P = 7000 bar and a fluid with the approximate composition $XCO_2 = n_{CO2}/(n_{CO2}+n_{H2O}) = 0.32$, $XH_2O = 0.68$, $wt\%NaCl = wt_{NaCl}/(wt_{H2O}+wt_{NaCl})=0.30$ wt%. In mole fractions of the total fluid this corresponds to $XCO_2 = 0.30$, $XH_2O = 0.62$ and XNaCl = 0.08.
4. A second stage of fluid infiltration is characterised by H_2O-rich brines in the greenshist facies. Fluid infiltration during exhumation caused recrystallisation of quartz and formation of high purity quartz (Qz3) and reaction with plagioclase and calcite to form scapolite.
5. Late post kinematic fluids found in vug assemblages are also brines, testifying that a high salinity was maintained throughout the uplift history.
6. The high salinity of the fluid facilitated small and large scale mass transfer in the Bamble sector.

References

Aranovich, L.Y., Haefner, A., Connolly, J.A.D., Gerya, T.V. and Ulmer, P., 2005. Experimental determination of H_2O and CO_2 activity-composition relations in the H_2O-CO_2-NaCl fluids by reversed dehydration and decarbonation reaction, manuscript, pp. 822-828.

Bakker, R.J., 2003. Package FLUIDS 1. Computer programs for analysis of fluid inclusion data and for modelling bulk fluid properties. Chemical Geology, 194(1-3): 3-23.

Bakker, R.J. and Jansen, J.B., 1990. Preferential water leakage from fluid Inclusions by means of mobile dislocations. Nature, 345(6270): 58-60.

Bakker, R.J. and Jansen, J.B., 1994. A Mechanism for Preferential H_2O Leakage from Fluid Inclusions in Quartz, Based on Tem Observations. Contributions to Mineralogy and Petrology, 116(1-2): 7-20.

Barth, T.F.W. and Dons, J.A., 1960. Precambrian of southern Norway. Norges Geologiske Undersøkelse, 208: 6-67.

Beach, A., 1980. Retrogressive metamorphic processes in shear zones with special reference to the Lewisian Complex. Journal of Structural Geology, 2(1-2): 257-263.

Bird, D.K. and Spieler, A.R., 2004. Epidote in geothermal systems, Epidotes. Reviews in Mineralogy & Geochemistry, pp. 235-300.

Bodnar, R.J., 2003. Interpretation of data from aqueous-electrolyte fluid inclusions. In: I.M. Samson, A. Anderson and L.J. Marshall (Editors), Fluid inclusions: analysis and interpretation. Short course. MAC.

Bodnar, R.J., Binns, P.R. and Hall, D.L., 1989. Synthetic fluid Inclusions. 6. Quantitative-evaluation of the decrepitation behavior of fluid inclusions in quartz at one atmosphere confining pressure. Journal of Metamorphic Geology, 7(2): 229-242.

Bowers, T.S. and Helgeson, H.C., 1983. Calculation of the thermodynamic and geochemical consequences of nonideal mixing in the system H_2O-CO_2-NaCl on phase-relations in geologic systems - Equation of state for H_2O-CO_2-NaCl fluids at high-pressures and temperatures. Geochimica Et Cosmochimica Acta, 47(7): 1247-1275.

Brøgger, W.C., 1934. On several Archean rocks from the south coast of Norway; II, The south Norwegian hyperites and their metamorphism. 1; 1, 421 pp.

Bucher, K., De Capitani, C. and Grapes, R., 2005. The development of a margarite-corundum blackwall by metasomatic alteration of a slice of mica schist in ultramific rock, Kvesjoen, Norwegian Caledonides. Canadian Mineralogist, 43: 129-156.

Bugge, A., 1943. Geological and petrological investigations in the Kongsberg-Bamble formations Norges Geologiske Undersøkelse, 160: 1-150.

Bugge, A., 1945. Löddesöl skarn forekomst. Norsk Geologisk Tidsskrift, 25: 35-47.

Bugge, A., 1965. Iakttagelser fra rektangelbladet Kragerø og den store grunnfjellsbreksje. Norges Geologiske Undersøkelse, 229: 115p.

Bugge, J.A.W., 1940. Geological and petrological investigations of the Arendal district. Norsk Geologisk Tidsskrift, 20: 71-112.

Coggon, R. and Holland, T.J.B., 2002. Mixing properties of phengitic micas and revised garnet-phengite thermobarometers. Journal of Metamorphic Geology, 20(7): 683-696.

Connolly, J.A.D., 1990. Multivariable phase-diagrams - An algorithm based on generalized thermodynamics. American Journal of Science, 290(6): 666-718.

Connolly, J.A.D., 1995. Phase-diagram methods for graphitic rocks and application to the system C-O-H-FeO-TiO_2-SiO_2. Contributions to Mineralogy and Petrology, 119(1): 94-116.

Connolly, J.A.D., 2005. Computation of phase equilibria by linear programming: A tool for geodynamic modeling and its application to subduction zone decarbonation. Earth and Planetary Science Letters, 236(1-2): 524-541.

Connolly, J.A.D. and Kerrick, D.M., 1987. An algorithm and computer-program for calculating composition phase-diagrams. Calphad-computer coupling of phase diagrams and thermochemistry, 11(1): 1-55.

Connolly, J.A.D. and Petrini, K., 2002. An automated strategy for calculation of phase diagram sections and retrieval of rock properties as a function of physical conditions. Journal of Metamorphic Geology, 20(7): 697-708.

Connolly, J.A.D. and Trommsdorff, V., 1991. Petrogenetic grids for metacarbonate rocks - pressure-temperature phase-diagram projection for mixed-volatile systems. Contributions to Mineralogy and Petrology, 108(1-2): 93-105.

Cosca, M.A., Mezger, K. and Essene, E.J., 1998. The Baltica-Laurentia connection Sveconorwegian (Grenvillian) metamorphism, cooling, and unroofing in the Bamble sector, Norway. Journal of Geology, 106: 539-552.

Crawford, M.L., 1981. Phase equilibria in aqueous fluid inclusions. In: L.S. Hollister and M.L. Crawford (Editors), Fluid inclusions: Applications to Petrology. Mineralogical Society of Canada Short course Handbook. MAC.

Droop, G.T.R., 1987. A general equation for estimating Fe^{3+} concentrations in ferromagnesian silicates and oxides from microprobe analyses, using stoichiometric criteria. Mineralogical Magazine, 51(361): 431-435.

Elliott, R.B., 1966. Association of amphibolite and albitite, Kragero South Norway. Geological Magazine, 103(1): 1-7.

Frodesen, S., 1968. Petrographical and chemical investigations of a precambrian gabbro intrusion, Hiåsen, Bamble area, south Norway. Norsk Geologisk Tidsskrift, 48: 281-306.

Gleeson, S.A., Yardley, B.W.D., Munz, I.A. and Boyce, A.J., 2003. Infiltration of basinal fluids into high-grade basement, South Norway: sources and behaviour of waters and brines. Geofluids, 3(1): 33-48.

Harlov, D.E., 2000. Titaniferous magnetite-ilmenite thermometry and titaniferous magnetite-ilmenite-orthopyroxene-quartz oxygen barometry in granulite facies gneisses, Bamble sector, SE Norway; implications for the role of high-grade CO_2-rich fluids during granulite genesis. Contributions to Mineralogy and Petrology 139: 180-197

Hedenquist, J.W. and Henley, R.W., 1985. The importance of CO_2 on freezing point measurements of fluid: evidence from active geothermal systems and implications for epithermal ore deposition. Economic Geology, 80(5): 1379-1406.

Holland, T., Baker, J. and Powell, R., 1998. Mixing properties and activity-composition relationships of chlorites in the system MgO-FeO-Al2O_3-SiO_2-H_2O. European Journal of Mineralogy, 10(3): 395-406.

Holland, T.J.B. and Powell, R., 1998. An internally consistent thermodynamic data set for phases of petrological interest. Journal of Metamorphic Geology, 16(3): 309-343.

Jøsang, O., 1966. Geologiske og petrografiske undersøkelser i Modumfeltet. Norges Geologiske Undersøkelse, 235: 148p.

Knudsen, T.L., 1996. Petrology and geothermobarometry of granulite facies metapelites from the Hisøy-Torungen area, South Norway; new data on the Sveconorvegian P-T-t path of the Bamble sector. Journal of Metamorphic Geology, 14(3): 267-287.

Konnerup-Madsen, J., 1979. Fluid Inclusions in Quartz from Deep-Seated Granitic Intrusions, South-Norway. Lithos, 12(1): 13-23.

Krumgalz, B.S., Pogorelsky, R. and Pitzer, K.S., 1996. Volumetric properties of single aqueous electrolytes from zero to saturation concentration at 298.15 degrees K represented by Pitzer's ion-interaction equations. Journal of Physical and Chemical Reference Data, 25(2): 663-689.

Kullerud, K., 1995. Chlorine, titanium and barium-rich biotites - Factors controlling biotite composition and the Implications for garnet-biotite geothermometry. Contributions to Mineralogy and Petrology, 120(1): 42-59.

Munz, I.A., Wayne, D. and Austrheim, H., 1994. Retrograde fluid infiltration in the high-grade Modum Complex, South Norway - Evidence for age, source and REE mobility. Contributions to Mineralogy and Petrology, 116(1-2): 32-46.

Munz, I.A., Yardley, B.W.D., Banks, D.A. and Wayne, D., 1995. Deep penetration of sedimentary fluids in basement rocks from Southern Norway - Evidence from hydrocarbon and brine inclusions in quartz veins. Geochimica Et Cosmochimica Acta, 59(2): 239-254.

Munz, I.A., Yardley, B.W.D. and Gleeson, S.A., 2002. Petroleum infiltration of high-grade basement, South Norway: Pressure-temperature-time-composition (P-T-t-X) constraints. Geofluids, 2(1): 41-53.

Newton, R.C., Charlu, T.V. and Kleppa, O.J., 1980. Thermochemistry of the high structural state plagioclases. Geochimica Et Cosmochimica Acta, 44(7): 933-941.

Newton, R.C. and Manning, C.E., 2000. Quartz solubility in H_2O-NaCl and H_2O-CO_2 solutions at deep crust-upper mantle pressures and temperatures: 2-15 kbar and 500-900 degrees C. Geochimica Et Cosmochimica Acta, 64(17): 2993-3005.

Nijland, T.G., Liauw, F., Visser, D., Maijer, C. and Senior, A., 1993. Metamorphic petrology of the Froland corundum-bearing rocks; the cooling and uplift history of the Bamble sector, South Norway. Bulletin - Norges Geologiske Undersokelse, 424: 51-63.

Nijland, T.G. and Maijer, C., 1993. The regional amphibolite to granulite facies transition at Arendal, Norway; evidence for a thermal dome. Neues Jahrbuch fuer Mineralogie Abhandlungen, 165: 191-221.

Nijland, T.G. and Touret, J.L.R., 2001. Replacement of graphic pegmatite by graphic albite-actinolite-clinopyroxene intergrowths (Mjavatn, southern Norway). European Journal of Mineralogy, 13(1): 41-50.

Nijland, T.G., Touret, J.L.R. and Visser, D., 1998. Anomalously low temperature orthopyroxene, spinel, and sapphirine occurrences in metasediments from the Bamble amphibolite-to-granulite facies transition zone (South Norway); possible evidence for localized action of saline fluids. Journal of Geology, 106(5): 575-590.

Powell, R. and Holland, T., 1999. Relating formulations of the thermodynamics of mineral solid solutions: Activity modeling of pyroxenes, amphiboles, and micas. American Mineralogist, 84(1-2): 1-14.

Rosing, M.T., Bird, D.K. and Dymek, R.F., 1987. Hydration of Corundum-Bearing Xenoliths in the Qorqut Granite Complex, Godthabsfjord, West Greenland. American Mineralogist, 72(1-2): 29-38.

Shmulovich, K.I., Yardley, B.W.D. and Graham, C.M., 2006. Solubility of quartz in crustal fluids: experiments and general equations for salt solutions and H_2O-CO_2 mixtures at 400-800 degrees C and 0.1-0.9 GPa. Geofluids, 6(2): 154-167.

Sørensen, B.E. and Larsen, R.B., 2007. Paper1: Fluid induced multistage recrystallisation microstructures in quartzites and quartz veins from the Bamble shear zone complex. In: B.E. Sørensen (Editor), Metamorphic refinement of quartz under influence of fluids during exhumation with

reference to the metamorphic/metasomatic evolution observed in amphibolites - a detailed field, microtectonic and geochemical study from the Bamble sector, South Norway. PhD Thesis, Department of Geology and Mineral Resources Engineering, NTNU Trondheim.

Sørensen, B.E., Larsen, R.B. and Austrheim, H., 2007. Paper3: Metasomatic evolution of the Froland amphibolites during cooling and uplift - textural observations and geochemical evolution of hydrous minerals. In: B.E. Sørensen (Editor), Metamorphic refinement of quartz under influence of fluids during exhumation with reference to the metamorphic/metasomatic evolution observed in amphibolites - a detailed field, microtectonic and geochemical study from the Bamble sector, South Norway. PhD Thesis, Department of Geology and Mineral Resources Engineering, NTNU Trondheim.

Stuwe, K., 1997. Effective bulk composition changes due to cooling: a model predicting complexities in retrograde reaction textures. Contributions to Mineralogy and Petrology, 129(1): 43-52.

Touret, J., 1968. The Precambrian metamorphic rocks around the Lake Vegår (Aust-Agder, southern Norway). Norges Geologiske Undersøkelse, 257, 45 pp.

Touret, J., 1971. Le faciès granulite en Norvège méridionale II Les inclusions fluides. Lithos, 4: 423-436.

Touret, J., 1985. Fluid regime in southern Norway: the record of fluid inclusions. In: A.C. Tobi and J. Touret (Editors), The deep Proterozoic crust in the North Atlantic Provinces NATO ASI Ser. Ser. C: Math. Phys. Sci., pp. 517-549.

Touret, J. and Olsen, S.N., 1985. Fluid inclusions in migmatites. In: J.R. Ashworth (Editor), Migmatites. Shiva, Glasgow, pp. 265-288.

Van den Kerkhof, A. and Thiery, R., 2001. Carbonic inclusions. Lithos, 55(1-4): 49-68.

Vanko, D.A., Bodnar, R.J. and Sterner, S.M., 1988. Synthetic fluid inclusions: VIII. Vapor-saturated halite solubility in part of the system NaCl-CaCl2-H2O, with application to fluid inclusions from oceanic hydrothermal systems. Geochimica et Cosmochimica Acta, 52(10): 2451-2456.

Wark, D. and Watson, E.B., 2006. TitaniQ: a titanium-in-quartz geothermometer Contributions to Mineralogy and Petrology, 152(6): 743-754.

Watson, E.B. and Brenan, J.M., 1987. Fluids in the Lithosphere, 1. Experimentally determined wetting characteristics of CO_2-H_2O fluids

and their implications for fluid transport, host-rock physical properties, and fluid inclusion formation. Earth Planet Scientific Letters, 85: 496-515.

Williams-Jones, A.E. and Samson, I.M., 1990. Theoretical estimation of halite solubility in the system NaCl-$CaCl_2$-H_2O; applications to fluid inclusions. The Canadian Mineralogist, 28(2): 299-304.

Zhang, Y.G. and Frantz, J.D., 1987. Determination of the Homogenization Temperatures and Densities of Supercritical Fluids in the System NaCl-KCl-$CaCl_2$-H_2O Using Synthetic Fluid Inclusions. Chemical Geology, 64(3-4): 335-350.

Paper 3: Metasomatic evolution of the Froland amphibolites during cooling and uplift – textural observations and geochemical evolution of hydrous minerals

Bjørn Eske Sørensen
Department of Geology and Mineral Resources Engineering, Norwegian University of Science and Technology (NTNU), N-7491 Trondheim, Norway
(bjorn.sorensen@ntnu.no)

Rune Berg Larsen
Department of Geology and Mineral Resources Engineering, Norwegian University of Science and Technology (NTNU), N-7491 Trondheim, Norway
(rune.larsen@ntnu.no)

Håkon Austrheim
Department of Earth Sciences, University of Oslo, N-0316 Oslo, Norway
(h.o.austrheim@geo.uio.no)

Abstract

This study addresses the metasomatic alteration of ortho-amphibolites, in the Froland area in the Bamble sector, South Norway. High salinity brines with near constant salinities of c. 30 wt% solvents, infiltrated and metasomatised the amphibolites throughout cooling and uplift. Potassic alteration and biotite formation comprise the earliest deducible alteration event and is seen as overgrowth on amphiboles. Alteration begins by formation of ferrotschermakite/ferropargasite rims on the amphibole cores. Rims gradually becomes richer in Mg and depleted in Fe, K, Na, Al and Cl and, finally, terminates with Cl poor actinolite (XMg ≈ 0.9). Simultaneously biotite experiences metasomatic alteration that is strongly correlated with the coexisting calcic amphibole.

The compositional changes reflect the complex interaction between brine fluids and hydrous minerals during cooling and uplift. Accordingly, the brine fluids fully control the composition of Fe-Mg silicates by metasomatosis. Therefore the models arguing that the Cl content of biotite is a function of the original Fe/Mg ratio of the mineral, fluid composition and PT-conditions (Munoz, 1992; Munoz and Swenson, 1981) can not explain the Froland amphiboles and biotites because silicate and whole rock chemistries are changed by interaction with the fluid. The composition of the halogen

bearing Fe-Mg silicates is partially controlled by the aqueous fluid composition along with P and T. Two models may explain the biotite and amphibole chemical zonation.

Model 1: zoning reflects interactions with a fluid of varying composition at fixed P and T. This model explains the compositional zoning observed by Kullerud (1995; 1996).

Model 2: compositional zoning reflects interaction with a fluid having constant halogen contents during gradually changing PT-conditions.

Model 2 is preferred in the current study because biotites and amphiboles in our study formed during cooling and exhumation with constant salinities of the coexisting fluid thus eliminating Model 1.

In intensively altered areas the original amphibolite mineralogy is entirely replaced. Here we observe the large-scale metasomatic processes in a small scale version, for example following this pattern toward the centre of a vein: Amphibolite with small amount of biotite (host rock)→ Zone1: biotite-plagioclase zone → Zone2: amphibole-plagioclase zone → Zone3: Plagioclase + calcite + apatite zone → Zone3a: pyrrhotite + ilmenite (rutile +titanite) ± amphibole + calcite+ chalcopyrite + apatite. This small scale observation reflects how ore forming elements, such as Cu, Mo, Au and Fe, are mobilised from the one part to an other part of the Bamble shear zone complex at a larger scale (see also Cameron et al., 1993).

1 Outline and summary

The Bamble sector is renowned for its fluid-related metasomatic rocks. However, systematic studies of the retrograde evolution of the volatile fluids are rare and fragmentary.

The aim of this study is to identify the parameters that control the metasomatic evolution in the Froland area of the Bamble sector. Halogen-bearing minerals document fluid/rock interaction during metamorphism and metasomatism. This paper includes mineral chemistry data from amphibolites on amphibole, biotite, apatite and scapolite including the F, OH and Cl contents. Results are related to fluid inclusion studies reported elsewhere (Sørensen and Larsen, 2007b, paper 2). The main focus is on the evolution of amphiboles. One reason for this choice is that amphiboles are stable in a wide temperature interval, from upper amphibolite facies to greenshist/subgreenshist facies. Equally important is the fact that changes in the amphibole chemistry are easily distinguished by the thin section colours. This allows for simple optical correlation between amphibole chemical evolution and the chronology of metasomatic events. The metasomatic evolution of the amphibolites is also described in detail. Contrary to earlier studies, the metasomatic evolution reported here is dominated by potassic alteration commonly expressed by the introduction of biotite to the amphibolite assemblage associated with the formation of rims on the amphiboles. Therefore, the chemical evolution of amphibole rims carries important information on the alteration process. This alteration process is observed throughout the area where amphibole rims feature a significant colour variation from deep blue-

green ferropargasite/ferrotschermakite to pale green actinolite. These variations are also observed in single samples. Amphibole rims, biotite and biotite-amphibole pairs follow univariant trends.

Geochemical trends are combined with textural studies to establish a chronological scenario. Timing of alteration in the Froland area partially differs from previous studies elsewhere in the Bamble sector. For example, contrary to other studies, the early stages of potassic alteration precede the sodic-calcic alteration reported from the eastern Bamble (e.g. Brøgger, 1934) (see background). In the Froland area fluid inclusion studies document that brine fluids of near constant salinities dominated throughout cooling and exhumation (Sørensen and Larsen, 2007b, paper 2). We therefore suggest that most alteration occurred at constant Cl/H_2O ratio. We also suggest that the high salinity of the fluids controls the metasomatic processes and the ore formation in the Bamble sector with PT-conditions imposing changes in the cation exchange between fluid and rock. Accordingly, we argue that the univariant trends of amphibole and biotite reflects the interaction with an externally derived fluid with near constant salinity during falling P-T conditions.

Ultimately, this study support that the Mg-Cl avoidance model, stating that energetic interaction between octahedral cations Mg and Fe is controlling the $Cl \leftrightarrow OH$ exchange for amphibole and biotite, is not applicable and may actually be void as it was also suggested by Kullerud (2000).

In future thermodynamic modelling, we suggest that coexisting biotite and amphibole is used in order to avoid the effects caused by the bulk rock Fe/Mg ratio. A full thermodynamic model should include not only the chemical potentials of Fe, Mg, Cl and OH species in the solids, but also aqueous species because of Fe and Mg exchange between biotite/amphibole and a fluid phase. The presence of other complexing ions in the fluid may also play an important role in the exchange of metal ions between silicates and a fluid. Until better calibrations are available, Cl in amphibole or biotite cannot be used as a quantitative assessment of fluid composition. Fluid inclusions are the most reliable source on the composition of paleo-fluids.

2 Fluid alteration in the Bamble sector

Metasomatic processes are common in the Bamble sector and encompasses scapolitisation, albitisation, abundant apatite and more rare dolomite veining (Dahlgren et al., 1993). Amphibole-scapolite rocks are known from several localities (Korneliussen et al., 2000) and they are commonly associated with enstatite-phlogopite rocks and albitites of controversial origin. Metasomatism is restricted to diffuse, but mapable associated with faults, joints and lithological contacts between metagabbros and metasedimentary units (Nijland and Touret, 2001). Alteration zones comprise a network that may be characterised as a regional plumbing network (Nijland and Touret, 2001). Commonly, fluid alteration facilitates large scale mass transfer. This is supported by the spatial relation between ore deposits and zones of massive alteration.

Sodic alteration is most conspicuous in comprising long known albitites - scapolite - hornblende rocks (Brøgger, 1934; Bugge, 1965; Elliott, 1966; Jøsang, 1966; Munz et al., 1994; Munz et al., 1995). Structurally controlled apatite bearing Fe/Cu sulfide/oxide deposits and rutile deposits structurally related to the scapolitisation zones (Korneliussen et al., 2000). Brøgger (1934) suggested that the breccia-related iron ores at Langøy were products of leaching processes involving metagabbros and Korneliussen et al. (2000) suggest that similar models may as well account for other ore deposits.

Nijland et al. (1993a) studied the geochemistry of hydrous minerals in amphibolites from localities in the Bamble sector in an approach to understand the fluid evolution in the Bamble sector during prograde as well as retrograde PT-t paths. They conclude that systematic variations of the fluid composition from granulite to amphibolite facies areas are absent. Compositional variations are encountered on a much more localised scale (e.g. Nijland et al., 1993a).

Scapolite commonly occurs as replacement of plagioclase along grain boundaries, indicating that it is a late phase (Nijland et al., 1993a) in the Froland area, whereas it seem to be an earlier phase in more intensely scapolitised rocks in the eastern part of the Bamble sector. The formation of scapolite in the Froland area relates to introduction of saline aqueous fluids during retrogression (Sørensen and Larsen, 2007b, paper 2).

More intense scapolitisation is observed at Ødegårdens Verk where scapolitisation of metagabbro formed a rock composed of scapolite-phlogopite-rutile rocks intersected by phlogopite-enstatite-apatite veins and albitites (Elliott, 1966). Scapolite in the hornblende-scapolite rock is a chlorine rich marialite with the A site fully occupied by Cl and 3.7 atoms Al p.f.u. (per formula unit), rather than the 3.0 allocation suggested by plagioclase substitution (Lieftink et al., 1993). The hornblendes at Ødegårdens Verk also display rimward zoning from Cl, Al and alkali rich cores, to Al and Cl poor rims that also are enriched in Mg (Lieftink et al., 1994). Veins comprising Cl-apatite, enstatite and phlogopite are also common at Ødegårdens Verk. Alteration of the veins during scapolitisation resulted in partial replacement of Cl-apatite and enstatite by hydroxyl-flour apatite and hornblende respectively (Lieftink et al., 1994). The Cl-apatite carry trails and patches of monazite and xenotime in areas altered to hydroxyl-flour apatite during amphibolite facies alteration (Lieftink et al., 1994). This observation was matched by experiments with fluids of variable composition on Cl-apatite from Ødegårdens Verk by Harlov et al. (2002). Their experiments also demonstrated that fluid composition is more important than P and T for the formation of hydroxyl/flour apatite during alteration of Cl-apatite. The hydroxyl-flour apatite with trails and patches was reproduced by H_2O and F bearing fluids.

Albitites are also a common result of sodic alteration in the Bamble sector, and comprise a wide range of expressions (Nijland and Touret, 2001). Albitisation was later than the scapolitisation given that scapolite is replaced by albite (Brøgger, 1934).

On the contrary, potassic alteration are not previously reported from the Bamble sector, although biotite is common in the more altered parts of the metagabbro at

Langøy, eastern Bamble (Unpublished data: Håkon Austrheim, 2006) and Cameron (1993b) reported reintroduction of LILE including K and chalcophile elements that were leached during granulite and amphibolite facies metamorphism, during retrogression on Tromøy. In the studied area potassic alteration is much more pronounced than sodic alteration types. The most common expression of potassic alteration is the introduction of biotite into the amphibolites. However, potassic alteration also includes grey K-feldspar together with actinolite-titanite rocks in the most intensively altered parts. Because these rocks were not described before in the Bamble sector we will discuss their petrography and outcrop textures in detail in section 4.1.

The alteration processes are strongly influenced by fluid composition, P and T. In the only systematic study of the retrograde fluid evolution (paper 2, Sørensen and Larsen, 2007b) it is documented that the fluid composition in the Froland area comprise brines with 30 wt% salts throughout cooling and uplift of the area. Three crucial fluid evolutionary stages could be unravelled:

FIA2. Early retrograde fluids in vein quartz comprising a mixture low salinity CO_2-rich fluids and H_2O-rich eutectic salinity NaCl-KCl-H_2O-CO_2 brines associated with biotite-amphibole assemblages bordering en echelon quartz veins in amphibolite.

FIA3. H_2O-NaCl-$CaCl_2$ brines with 25 wt% NaCl and 6 wt% $CaCl_2$, involved in localised scapolitisation and replacement of rutile by titanite in siliceous gneisses and replacement of ilmenite by titanite in amphibolites.

FIA4. $CaCl_2$-rich aqueous fluids in late vug assemblages comprising tremolite, epidote, calcite, pyrite and apophyllite. Inclusions are found in calcite and in cores of epidote grains. FIA4 was modelled in the binary $CaCl_2$-H_2O system. Variations in final melting of antarcticite suggest a decreasing $CaCl_2$ salinity over time from 36 wt% in early inclusions to 31 wt% in late inclusions. Late inclusions relates to increased Fe-content in epidote and it is suggested that the Fe^{3+} content in the fluid increased over time in agreement with the lowering of the eutectic melting temperature from the ideal of -52°C in the binary $CaCl_2$-H_2O system.

Sørensen and Larsen (2007b, paper 2) used observations of fluid inclusions and calc-silicate assemblages in combination with a re-interpretation of the mineral paragenetic data presented by Nijland et al. (1993b) to re-evaluate the cooling and exhumation path of the Bamble sector (Figure 1). The retrograde fluids may partially be superimposed upon the PT-evolution of the Froland area (Figure 1). More details in are given in Sørensen and Larsen (2007b, paper 2). In summary, the cooling and uplift path begins by the simultaneous formation of tremolite + sanidine and tremolite + sanidine + calcite assemblages at c. 626-636°C and 7 kb. The next stage agrees with MII (ky + chl + ms) and MIII (ma +crn) of (Nijland et al., 1993b). The pressure is uncertain although a path may be extended from this stage to the isochore of FIA3. Because the fluid inclusions in FIA3 are well preserved showing no evidence of post entrapment modification the exhumation path could not have deviated more than 2 kb from the FIA3 isochore. The last part of the cooling and exhumation path is constrained by MV at 2-3 kb and 175-280°C (Nijland et al., 1993b; Touret, 1985) The PT-path preserves the main characteristics of the path published by Nijland et al. (1993b), but the uplift is

shifted 100°C toward lower temperatures and is in better agreement with the dominance of cataclastic microstructures in thrust related structures. A shift between potassic and sodic-calcic alteration occurred between FIA2 and FIA3. The Shift between MII and MIII probably correlates with the shift in alteration types (Figure 1).

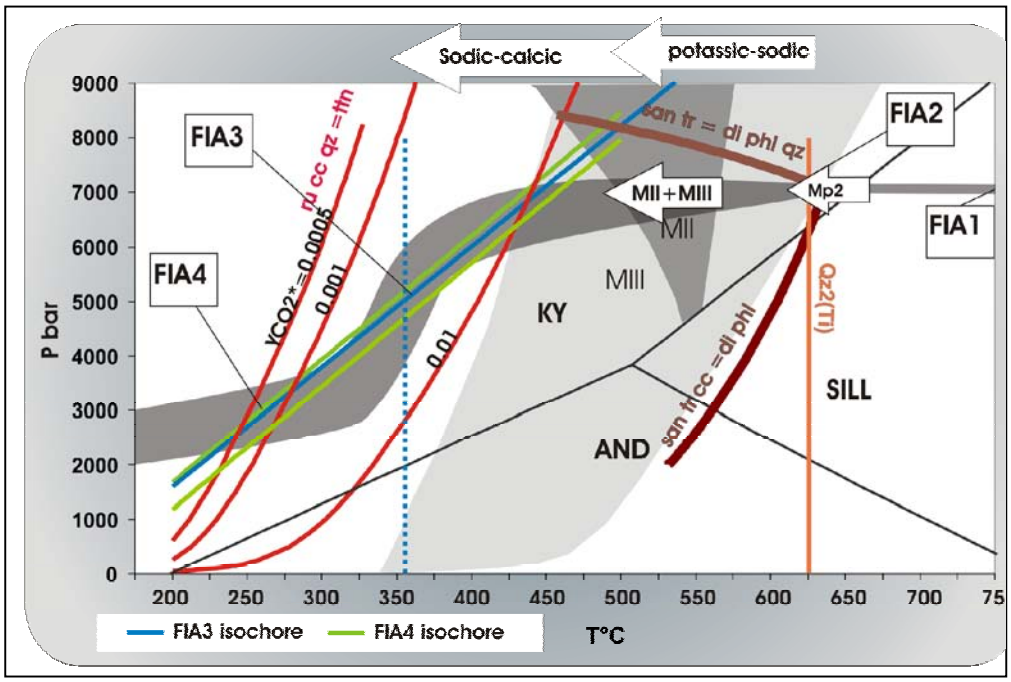

Figure 1: Tentative PT-Xfluid path of the study area, with possible implication for the cooling and uplift path of the Bamble sector. The PT-Xfluid path is assembled using a combination of mineral paragenetic and fluid inclusion data. Because fluid inclusions and mineral parageneses that are simple enough to be portrayed quantitatively in PT-space are not always present the correctness of the PT-path relies on textural correlations between assemblages in one rock type and fluid inclusions found in other rock types. Arrows on the top of the diagram indicate condition when alteration changed from potassic-sodic to sodic calcic. From Sørensen and Larsen (2007b, paper 2). For a more detailed discussion of the derivation of the PT-path see Sørensen and Larsen (2007b, paper 2). Reactions are written such that the high temperature assemblage is to the right of the = sign.

3 Geological setting

The rocks included in this study comprise quartzites, amphibolites and calc-silicate lithologies from the Froland area, Bamble sector, South Norway (Figure 2). The Bamble sector is part of the South West Scandinavian domain (SSD) that is divided

into a number of segments bounded by regional shear zones and thrusts that formed during the Sveconorwegian orogeny (Ahall and Gower, 1997; Bingen et al., 2002). The Bamble sector is interpreted as the mid-crustal part of a volcanic arc complex (Knudsen and Andersen, 1999). The Bamble sector was accreted to the Telemark terrain during an early Sveconorwegian (1,15-1,10 Ga) event (Bingen et al., 2002; 2001).

Structurally, the Bamble sector comprises a SW to NE linear deformation belt with onshore dimensions of 20-40 km times 140-150 km (Figure 2).

Supracrustal lithologies of amphibolite to granulite facies metasedimentary and metavolcanic rocks dominate the belt and is intruded by numerous mafic stocks and dykes as well as granitiod plutons and pegmatites (Starmer, 1991; Starmer, 1993; Starmer, 1996). The Supracrustal suite was deposited in two inter-orogenic periods of the Gothian orogeny at 1,85-1,7 Ga (Knudsen et al., 1997) and 1,5-1,2 Ga (Bingen et al., 1998) respectively. Recent studies confirmed Sveconorwegian high-grade metamorphic overprinting throughout the Bamble sector (Bingen et al., 1998; Bingen and Van-Breemen, 1998; Cosca et al., 1998; Johansson and Kullerud, 1993; Knudsen, 1996; Kullerud and Dahlgren, 1993; Kullerud and Machado, 1991).

Generally, the foliation trends NE-SW in the Bamble belt (Falkum and Petersen, 1980). Based on structural trends, the Bamble sector is divided in two domains (Falkum and Petersen, 1980):

-*The eastern sub-region* (main zone) in the coastal area is dominated by intense shear folding with a NE-orientation, most other directions being rotated into parallelism by a dextral strike slip regime. The structural pattern is dominated by tight isoclinal folds and well developed mineral lineations. Older structures are preserved in rigid bodies.

- *The Northern border* constituting a transitional zone 10-15 km wide, is characterized by moderate shear folding where NE-SW trending structures of the Bamble sector are superimposed on former NW-SE trending folds of the Setesdal gneisses. The transition zone commonly shows interference between the two structural events.

The Bamble sector features well preserved granulite facies rocks and distinctive metamorphic zones gradually going from amphibolite facies in north to granulite facies along the coast. Peak metamorphic conditions are well constrained, both in terms of P, T and fluid evolution.

Traditionally the Bamble sector is divided into four coast parallel regions labelled A-D (Field et al., 1980; Lamb et al., 1986; Smalley et al., 1983):

A: Amphibolite facies, as defined by absence of metamorphic orthopyroxene in metabasite.

B: Granulite facies; primarily comprising acid to intermediate host gneisses with a broadly granitic mineralogy, separated from A by an orthopyroxene isograde in metabasites.

C: First occurrence of charnokitic gneiss (K-feldspar, plagioclase, orthopyroxene and quartz).

D: Region within the granulite facies area with low concentrations of potassium and low concentration of LILE, REE and chalcophile elements, especially Au, Sb, As and S.

Earlier studies of the Bamble sector placed the area of highest temperature in the coastal region near Arendal and Tromøy in region D which was thought to be LILE depleted during peak metamorphism. However recent studies imply that low LILE concentration reflects the origin of the mafic gneisses rather than granulite facies depletion (Knudsen and Andersen, 1999). Furthermore, geothermobarometry show that the temperature in zones C and D are comparable (Harlov, 1992; Harlov, 2000a; Knudsen and Lidwin, 1996; Nijland and Maijer, 1993). Accordingly, zone D is not a separate metamorphic zone (Harlov, 2000b). Geothermobarometry of mineral equilibria imply that the highest temperatures probably were situated inland in a NW-SE oriented thermal dome with peak T at 830°C in the granulite facies area (Zones B and C) and peak T=750-700°C in the so called amphibolite facies area (zone A) (Nijland and Maijer, 1993). I.e. the entire region was actually exposed to granulite facies metamorphism.

Metamorphic fluids developed from pure CO_2 +N_2 ±CH_4 inclusions in the granulite facies to mixed H_2O-CO_2 fluids in the amphibolite facies (Touret, 1971; Touret, 1972; Touret, 1985). Some authors suggest a magmatic origin of the CO_2 rich fluids (Knudsen and Lidwin, 1996; Van den Kerkhof et al., 1994). The presence of CO_2 rich fluids during peak granulite facies metamorphism is confirmed by titaniferous magnetite-ilmenite thermometry and titaniferous magnetite–ilmenite-orthopyroxene-quartz oxygen barometry, implying that the stable COH-fluid phase at $LOGfO_2$ = -11 to -14 estimated for the peak PT-conditions (800°C and 7.5 kbar) is CO_2 for both region C and D (Harlov, 2000b).

Given that the structures of the Setesdal district are rotated into the foliations of the Bamble belt, it is inferred that the structures in the Bamble belt comprise the youngest structural event in the evolution of the South Norwegian basement. Following the strike-slip deformation, the Bamble sector was thrust on top of the Setesdal sector. In many places, the main thrust zone follows the Porsgrund Kristiansand fault, but thrusts are also identified to the east of the fault (e.g Touret, 1968). Thrusting probably began in epidote-amphibolite facies and progressed through lower greenshist facies as exhumation proceeded (e.g Touret, 1968). Finally extensional tectonics depressed the SE Bamble block. Evidence of thrusting is indisputable, although the kinematic evolution during thrusting is poorly understood and mostly inferred from, mapping and large scale observations by Starmer (1987; 1991; 1993; 1996) and Henderson and Ihlen (2004).

Thrust related greenshist facies deformation generated quartz mylonites (Morton et al., 1970), mainly comprising quartz and muscovite (Morton et al., 1970). Grain size reduction in the mylonites is considerable i.e. from cm-size to microns-size. Thrust related deformation terminated with brittle deformation, cataclasites and brecciation as exhumation proceeded and the temperatures lowered (e.g Touret, 1968).

Recently, Henderson & Ihlen (2004) documented ductile deformation of synkinematic pegmatites. They infer that thrust related deformation in the Bamble sector was incremental with long periods of ductile deformation interrupted by short periods of high strain rate leading to fracturing and injection of the syntectonic pegmatites.

Using the retrograde P-T path of Nijland et al. (1993b) the uplift and cooling rates were constrained to ~3°-8°C/Ma at 725-550°C, and cooling rates of ~2°-4°C/Ma in the interval 550-300°C (Cosca et al., 1998). Initial cooling of the Bamble sector approached isobaric conditions (dP/dT=2bars/°C) from 725-550°C, but was followed by near isothermal uplift (dP/dT=30bars/°C) in the temperature interval 550-300°C (Cosca et al., 1998). Following the relatively fast exhumation path, the Bamble sector experienced near isobaric cooling from 300°C and onwards (Cosca et al., 1998). The very low temperature (<300°C) path is constrained by late prehnite and pumpelyite together with fluid inclusion data (Touret and Olsen, 1985).

Amphibolites are common in the Bamble sector, featuring three expressions (Nijland et al., 1993a):

1. Concordant amphibolite bands intercalated with gneisses (Brøgger, 1934; Starmer, 1985).
2. Entirely metamorphosed but discordant plutons like the Vimme amphibolite (Nijland, 1989)
3. Partly amphibolitised “hyperites” with cores of coronitic gabro, which are increasingly amphibolitised towards their margins (Brickwood and Craig, 1987; Brøgger, 1934; Bugge, 1940).

Nijland (1995) studied the geochemistry of the amphibolites in the Bamble sector and documented that the majority are of an igneous origin. The amphibolites are commonly subjected to significant metasomatic processes affecting the mineralogy (Brøgger, 1934; Frodesen, 1968).

4 Results

4.1 Field and petrographic observations

4.1.1 Introduction

Five main localities were used in this study, all situated within a 5 square kilometre area (Figure 2).

Locality 1 represents the best preserved high grade evolution and provides detailed information on the formation of garnet amphibolite from coronitic gabbro.

Locality 2 and 3 features well preserved garnet amphibolite, but does not preserve any coronitic gabbro.

Locality 4 shows en echelon quartz veins in amphibolite bordered by zones of potassic alteration of amphibolite. Veins vary in thickness from dm to m thickness. En echelon veins belonging to this type are common in the Froland area.

Locality 5 displays the most pronounced amphibolite alteration. A vertical section through a zone of intensive alteration of amphibolite is exposed at a quarry. The orientation of the hydrothermal alteration zone and the local foliation is almost perpendicular to the regional foliation trend, but parallel to the orientation of splay offs of thrust related mylonites in the area (see map in Touret, 1968). The SE and NW facing walls are most informative concerning the architecture of the alteration zone. Three rock types are recognized in the quarry; amphibolite and quartz-biotite-microcline-plagioclase-tourmaline gneiss. Furthest to the east is gneiss, followed by amphibolite and then more gneiss. Calc-silicate rock is sandwiched between gneiss and amphibolite. Details on the calcsilicates may be found elsewhere (Sørensen and Larsen, 2007b, paper 2).

East of the main alteration zone the gneiss is bleached and deformed to mylonitic gneiss with grey stripes marking the presence of graphite. Flakes of graphite define the foliation together with biotite and red-brown tourmaline. The quartz texture is typical of mylonitic gneiss with quartz grain boundaries showing evidence of high temperature grain boundary migration recrystallisation (GBM). Plagioclase and feldspar grains vary in shape from irregular to lens shaped. The lens shaped feldspar show variable degrees of asymmetry, with asymmetric feldspars defining a shear sense in agreement with an upward movement of the SW block. Partly bleached leucosomes of dravitic tourmaline and slightly bluish quartz are preserved as relics in the deformed and bleached gneiss. West of the alteration zone, the gneiss is darker and does not carry graphite. Bluish quartz in the quartz-dravite leucosomes gives a distinctive dark colour. Alteration occur as localised fracture related veins, related to introduction of aqueous brines (see Sørensen and Larsen, 2007b, paper 2). In spite of the different appearance of the two gneiss units we suggest that they were formed from the same protolith due to many similarities in the mineralogy. Because of the alteration pattern it is evident that main fluid alteration occurred in the hanging wall rocks, to the east.

Main types of calcic amphiboles

Six main types of amphibole were observed in the studied area, hereafter denoted **Amp1, Amp1a, Amp2, Amp3, Amp3a** and **Amp4** (Table 1). **Amp1, Amp1a and Amp2** comprises the likely high metamorphic grade amphiboles (amphibole cores), whereas **Amp3, Amp3a and Amp4** (amphibole rims) formed during exhumation. The distinction between amphibole types 3 and 4 is purely descriptive as they represent a continuous series from magnesiohornblende to actinolite**.** The different amphibole types are not observed at all localities (Table 1). The types of occurrence of the amphiboles and at which localities the different amphibole types were observed at are stated in Table 1.

Table 1: Amphibole types, description and mode of occurrence

	Type	Classification	Type of occurrence	locality
cores	Amp1	Ferri/ferrotschermakite	Garnet amphibolite.	1, 2 and 3
	Amp1a	Hastingsite/ferropargasite	Garnet-quartz symplectite	1, 2
	Amp2	Ferropargasite	Amphibolite, not garnet bearing.	5
rims	Amp3	Magnesiohornblende	Overgrowth rims and in decussate textures together with biotite and plagioclase	5
	Amp3a	Ferropargasite/ferrotschermakite	Overgrowth rims on amphiboles in association with biotite	1, 2 and 3
	Amp4	Actinolite-magnesiohornblende	Same as Amp3	5

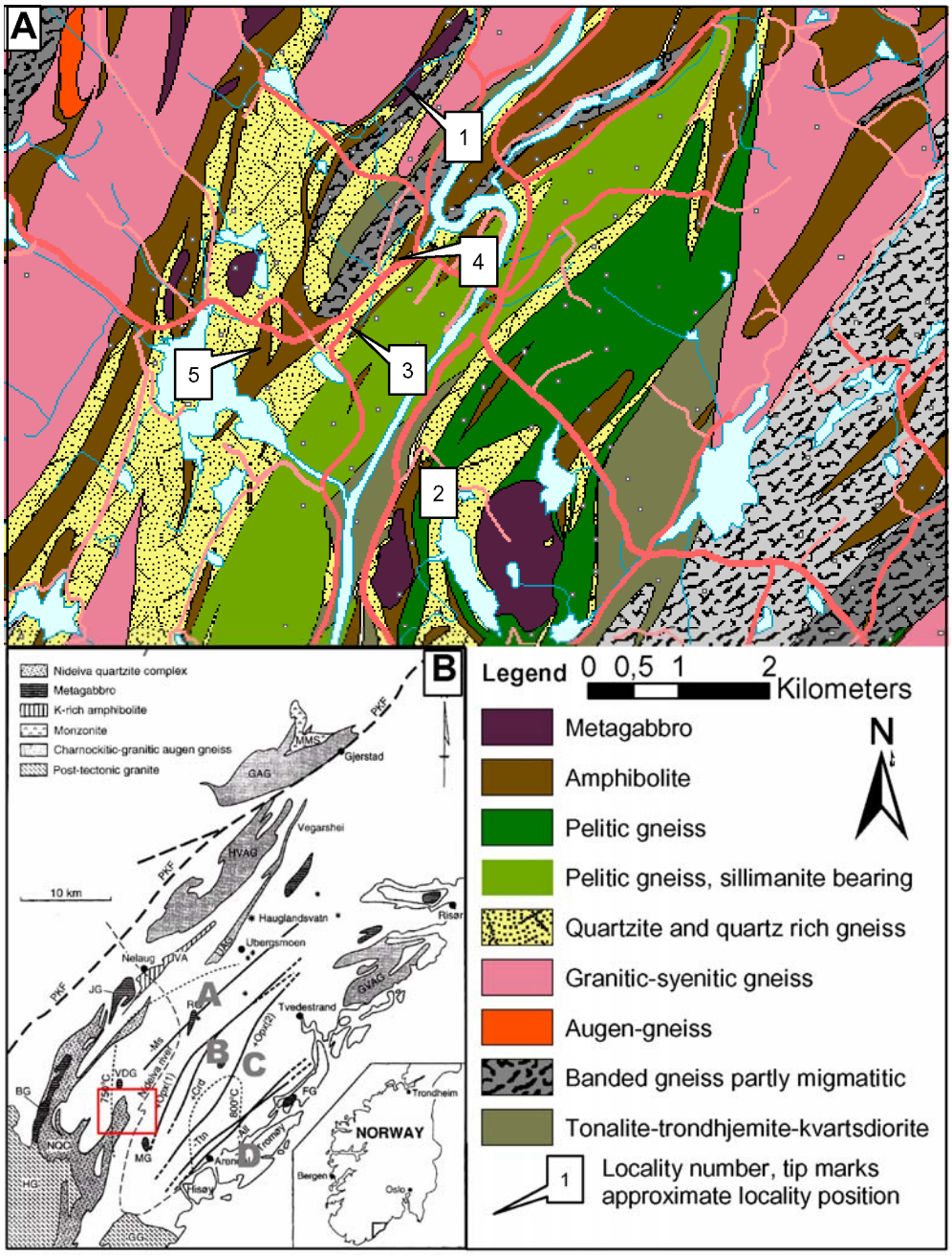

Figure 2: Geological maps. A) Detailed map of the investigated area. Modified from Geological Survey of Norway N-50 berggrunnskart 16123 Nelaug and 16114 Arendal. Geographic data (roads, lakes and rivers) are added for easy orientation (source:

www.geonorge.no). B) Overview map of the Bamble sector displaying the most important rock units (see legend on map). Insert shows the position of the Bamble sector in South Norway. Red square denotes the position of the study area shown in A. From Nijland et al. (1998). Also shown in B are the metamorphic zones in the Bamble sector.

4.1.2 Amphibolitisation during prograde metamorphism (type locality: locality 1)

The transition from a coronitic gabbro to garnet-amphibolite with cm-dm-sized garnet and black amphibole is observed macroscopically in the field (Figure 3). Field observations define the following units:

1. Coronitic gabbro
2. Garnet-amphibolite with small garnet and preservation of subophitic texture.
3. Banded garnet-amphibolite with cm-dm sized garnets, and banding between dark amphibole rich layers and light plagioclase rich layers. Garnets are in the dark layers and are surrounded by black amphibole rims.
4. Garnet-quartz and quartz-plagioclase symplectites.
5. Mixture of Gneiss/quartzite/amphibolite.
6. Extremely coarse-grained quartzite with blue quartz.
7. Pegmatites intersecting all the other units.
8. Rose quartz veins.

The magmatic ophitic texture is well preserved with lath shaped plagioclase crystals surrounding grains of pyroxene (Figure 5). Plagioclase and pyroxene are never in contact but separated by rims of amphibole ± garnet. The interiors of pyroxene grains are cut by numerous cracks with alteration to amphibole in a mesh texture.

The change from coronitic gabbro to the garnet amphibolite is gradual and can be followed on the map scale (Figure 3). Over half a meter, pyroxene-gabbro (Figure 4a) is entirely altered to a garnet-amphibolite (1) (Figure 4b). Garnet-amphibolite (1) grades into garnet-amphibolite (2) (Figure 4c) over a distance of about two meters. Garnet-amphibolite (2) follows garnet-amphibolite (1) and is distributed as a 6 m thick layer. Garnets are always partially altered to chlorite along joints.

While fresh looking garnets are irregular in shape altered garnets are rounded (Figure 4c). This observation documents that the garnets grew in a low strain environment and that deformation began after the growth of the garnets, resulting in partial breakdown. Towards the boundary to unit (5) the amount of garnet gradually decreases, but the black amphibole rich layers persists as dark schlieren. Unit (5) is a mixture of gneiss, amphibolite and quartzite. The widespread occurrence of green amphibole (field colour) in this unit indicates that it was subjected to more retrogression than the other units. Sigmoidal bodies featuring deformed quartz schlieren imply a dextral sense of

shear during retrogression, as also suggested by NNE striking foliation being rotated into NE striking foliations (Figure 3).

In the completely amphibolitised area the garnet amphibolite consist of amphibole, plagioclase, garnet and minor ilmenite. The texture is granoblastic with interlocking amphibole and plagioclase grains surrounding large garnets (Figure 5). The Amphibole is brown tschermakite commonly displaying twins. Generally the amphiboles are homogeneous. However, they have overgrowth rims of more greenish blue amphibole, commonly associated with biotite (se next section). Amphibole commonly occurs as inclusions in poikiloblastic garnets. Plagioclase contains both polysynthetic twinning and commonly also twins tapering towards pointed end that are interpreted as deformation twins (Figure 5). The deformation twin cuts through earlier through the polysynthetic twinning.

The garnet-quartz and quartz-plagioclase symplectites are not evenly distributed in the amphibolite, but mostly occur in two areas (see Figure 3). When properly exposed, they occur as lensoid bodies connected by dark amphibole rich bands intersecting the garnet amphibolite (Figure 4d). The intergrowth texture between garnet and quartz suggest that they grew simultaneously (Figure 4d). The texture and the distribution of symplectites in lenses and zones imply an igneous origin, perhaps as partial migmatitic melts.

The mineralogy of the garnet-quartz symplectitic intergrowth is amphibole, biotite, feldspar and garnet and an opaque assemblage of ilmenite, pyrrhotite, chalcopyrite and minor rutile on the edges of ilmenite grains. Amphiboles in the garnet-quartz symplectites are considerably darker than in the garnet amphibolite. As ilmenite occurs as inclusions within the garnet, it is interpreted as primary with regard to the formation of the garnet quartz symplectites. Ilmenite also occurs as rounded blebs, perhaps an indication of melt immiscibility. Biotite, epidote and pyrrhotite are secondary and relate to the formation of blue-green rims on the dark olive green amphibole cores (see next section).

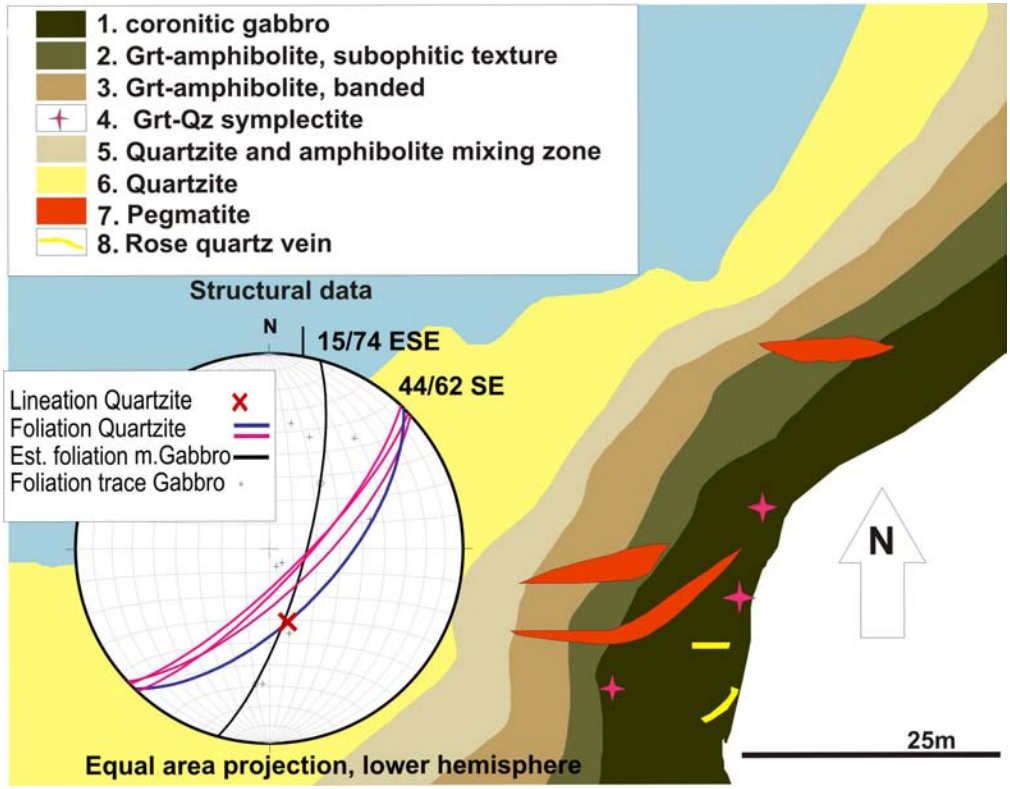

Figure 3: Detailed map of locality 1, showing the transition from gabbro to garnet amphibolite. Insert displays the structural observation from the locality; foliations are stated as direction/dip. NNE striking foliations inferred to be early are partly rotated in NE striking structures during dextral shear strike-slip deformation. Lineation observed in quartzite reflects the intersection between the old and the new foliation. See text for discussion.

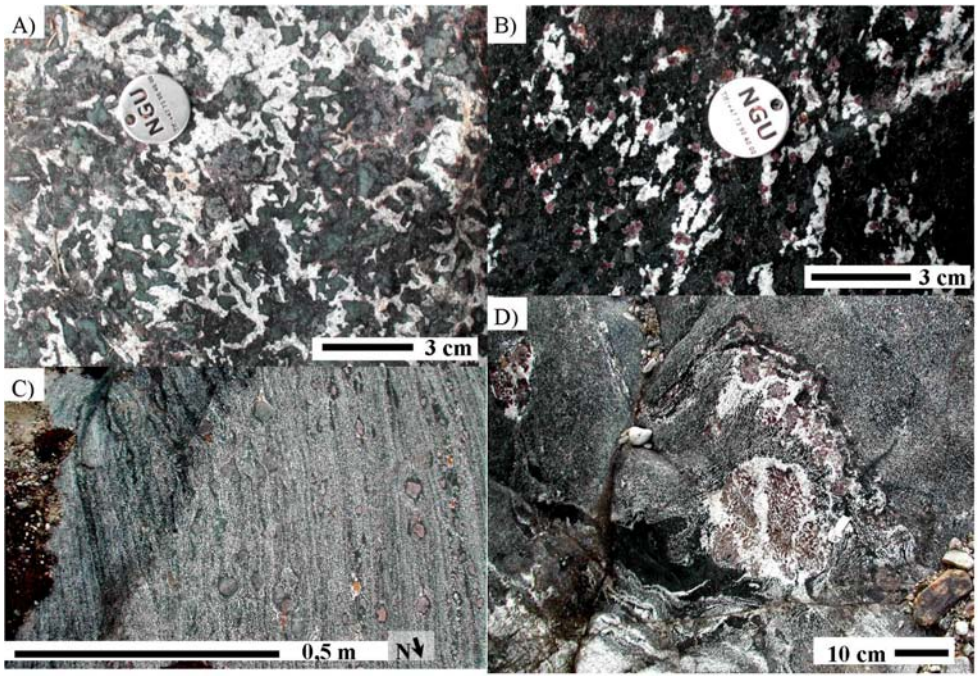

Figure 4: Field observations related to amphibolitisation of gabbro and garnet quartz symplectites at locality 1. A) Coronitic gabbro with subophitic texture. B) Completely amphibolitised gabbro with preserved subophitic texture and a static appearance. C) Completely evolved deformed garnet amphibolite, subophitic texture not recognisable. D) Garnet quartz symplectite in garnet amphibolite.

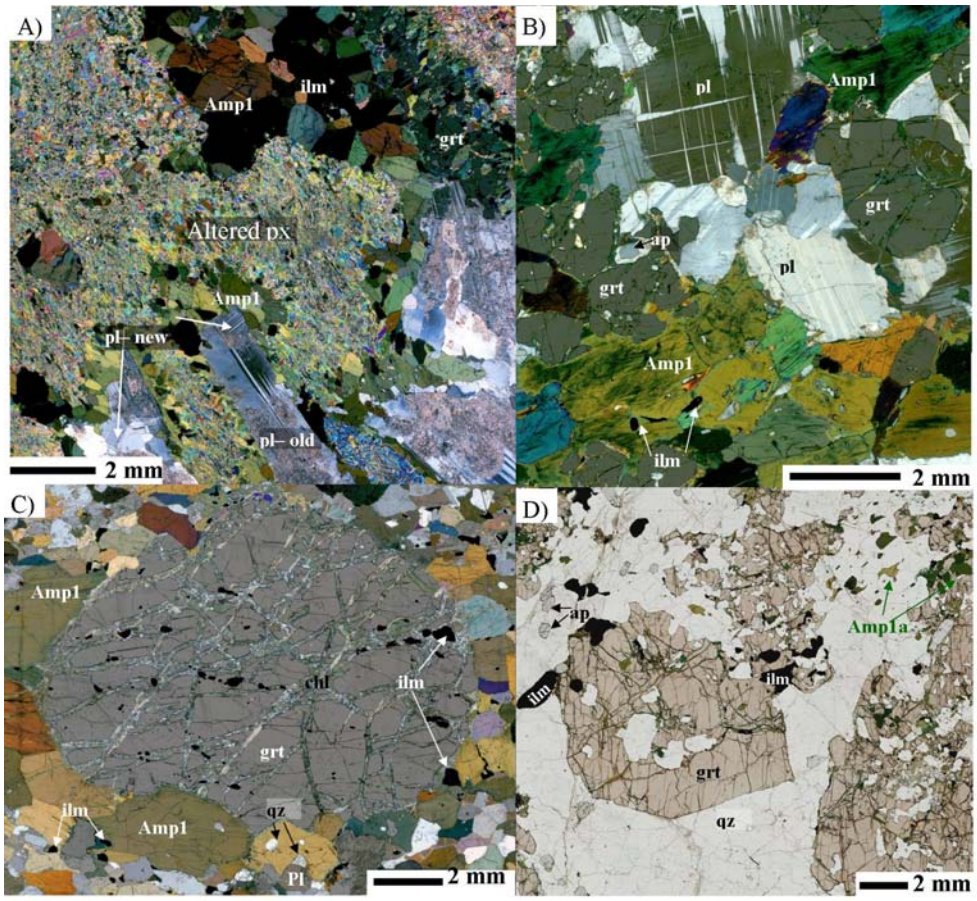

Figure 5: Petrographic observations related to the formation of garnet amphibolite and garnet-quartz symplectites at locality 1. A) Coronitic gabbro displaying relic pyroxene overgrown by hornblende against plagioclase. Garnet is formed between ilmenite and plagioclase. B) Completely amphibolitised gabbro comprising plagioclase, amphibole, garnet and minor ilmenite. C) Granoblastic banded garnet amphibolite with cm-sized garnet in matrix of tschermakitic amphibole and plagioclase. Ilmenite present inside garnet as well as in the matrix. D) Garnet-quartz symplectite, mainly comprisng garnet and quartz. Ilmentite, Cl-apatite and hastingsite (Amp1a) are also common.

4.1.3 Retrograde alteration of amphibolite

Retrograde alteration shows considerable spatial variation. The most common alteration is potassic-sodic. Sodic-calcic alteration is later and more local. The alteration events comprise three main groups, i.e. potassic alteration with biotite (Alt1),

potassic alteration with K-feldspar (Alt2) and sodic-calcic alteration with scapolitisation (Alt3) (Table 2).

Alt1 and subtypes

Potassic alteration with biotite is the earliest observed alteration type (Alt1) and is divided into four main groups (Alt1a-d) (Table 2). Altered amphibole rims associated with biotite (Alt1a) are observed at all localities.

The cores of the amphiboles (Amp1-2, Table 1) are commonly dark green, brownish green or brown in thin section. They are overgrown by distinctive amphibole rims (Figure 6). This is interpreted as reaction rims related to the formation of the biotite grains. The amphibole rims vary in colour from dark blue-green (Amp3a) to green (Amp3) and almost colourless (Amp4) (Figure 6). This colour variation marks the transition from ferropargasite/ferrotschermakite through magnesiohornblende to actinolite with large compositional variations within a single locality and even a single sample. In parallel with the amphibole evolution, biotite also change colour. Dark blue green overgrowths on amphibole (Amp3a) are common at localities 1, 2 and 3, whereas lighter coloured amphiboles (Amp3 and Amp4) are more common at localities 4 and 5. More extreme potassic alteration involving complete replacement of the original amphibolite mineralogy is also common (see below).

Alteration associated with en-echelon quartz veins at locality 4 (Alt1c) follows a characteristic pattern (Figure 7 and Table 2). A dm-thick rim of black tourmaline is bordering quartz veins (Figure 7b). This is followed by alternating dm-thick layers rich in amphibole and biotite respectively (Figure 7b). Within these layers magnesiohornblende (Amp3) together with biotite, plagioclase form a decussate texture (Figure 7c). Apatite and ilmenite also belongs to the Alt1c assemblage (Figure 7c). Plagioclase is almost completely altered, whereas biotite and particularly amphibole is well preserved. Biotite is partially replaced by K-feldspar and ilmenite is partly replaced by titanite. Small amounts of pyrrhotite occur in the Alt1c alteration zones in the plagioclase and amphibole rich and biotite poor domains. Similar textures are also seen in amphibolite without quartz veining (next).

Zonation from biotite- to amphibole rich domains as in Alt1c is common. This is particularly obvious around sub horizontal sulphide-bearing plagioclase-calcite (Alt1b), intersecting the amphibolite foliation at locality 5 (Table 2 and Figure 8). The following mineralogical zonation is developed towards the sulphide bearing Alt1b plagioclase-calcite veins (Figure 8):

Amphibolite with small amount of biotite (host rock)→ Zone1: biotite-plagioclase zone → Zone2: amphibole-plagioclase zone → Zone3: Plagioclase + calcite + apatite zone → Zone3a: pyrrhotite + ilmenite (rutile +titanite) + calcite+ chalcopyrite + apatite ± amphibole in the core of the plagioclase rich Zone3 (Figure 8). A distinctive transition in Ti-bearing phases from ilmenite/ rutile to titanite is observed in the veins (Figure 8). Titanite is the latest Ti-phase given that it always occurs as rims on rutile

and Ilmenite. Pyrrhotite and ilmenite formed simultaneously. Ilmenite grew at the expense of rutile because rutile is found as relics included in ilmenite grains (Figure 8).

Biotite-bearing alteration rocks comparable to those surrounding quartz veins at locality 4 is also common at locality 5 (Alt1d, Table 2). In some cases the amphibolite mineralogy is completely replaced by decussate biotite, amphibole, (K-feldspar) and Fe-Ti oxides (Alt1d, Figure 9).

Alt2

K-feldspar has partially replaced biotite (Alt2). In the field this is observed as lighter grey stripes intersecting the dark brown biotite-amphibole Alt1d rock (Figure 9a). Biotite is never completely absent but persists as atoll texture in K-feldspar (Figure 9c-d). Relics of plagioclase occur as cores in K-feldspar or biotite grains (Figure 9d).

Alt3

Local scapolitisation is common, normally as replacement of plagioclase by scapolite. It is challenging to decide which one of the amphibole types that associates with scapolitisation and because amphibole grains in scapolitised areas appear corroded probably none of them associates with the scapolite (Figure 10). Given that the amphibole, plagioclase ($Ab_{65-70}An_{30-33}$), biotite assemblage is replaced by scapolite; the scapolitisation must be younger than the biotite, amphibole, and plagioclase alteration (Alt1). Timing of biotite after K-feldspar replacement is hard to decipher, and they may possibly be simultaneous with the scapolitisation. Large grains of fresh looking biotite are observed in contact with scapolite perhaps implying that biotite and scapolite were in equilibrium (Figure 10). This conclusion is however challenged by grain impingement of scapolite on biotite (Figure 10b). Furthermore, country rock amphibolite preserves its dark colour. The scapolite has much higher meionite content than scapolites from elsewhere in the Bamble sector. Relics of rutile and ilmenite are preserved within coronas of titanite, which was probably the stable Ti-bearing phase during the scapolitisation. Quartz and calcite are observed in connection with the coronas which thus probably formed by the reaction cc + ru + qz → ttn + CO_2 in conjunction with the scapolitisation (Figure 10d). Scapolite is only observed in places where both calcite and plagioclase are common phases, for example replacing the Alt1b paragenesis.

Quartz veins in relation to amphibolite alteration

Quartz veins display a district colour variation which is readily observed in the field and can be correlated with decreasing colour intensity in biotite and amphibole surrounding the veins. Bleached quartz veins are spatially related with zones rich in light green amphibole (field colour, Amp4); whereas darker and more bluish/pinkish quartz veins are associated with less retrogressed amphibolite. Investigations by

Sørensen and Larsen (2007a, paper 1) document, however, that quartz in the quartz veins is related to several stages of dissolution/reprecipitation, meaning that not all quartz in the veins correlate with the surrounding alteration assemblage. Rather quartz in the quartz veins is partly altered or recrystallised.

Table 2: Main alteration types in amphibolite. See text for discussion.

Alt1: Potassic alteration with biotite stable
Alt1a (Figure 6**)**: Alteration of amphiboles associated with introduction of biotite. In thin sections amphibole cores are dark brownish green whereas rims vary from dark bluish green ferro-pargasite (Amp3a) through light green magnesiohornblende (Amp3) to almost colourless actinolite (Amp4). **Alt1b (**Figure 8**):** Veins with a central assemblage comprising plagioclase, calcite, apatite, pyrrhotite, ilmenite/rutile and magnesiohornblende (Amp3). Surrounded by two successive alteration zones, the inner zone comprising amphibole, plagioclase and rutile/ilmenite and the outer zone comprising biotite, plagioclase and ilmenite/rutile. **Alt1c (**Figure 7**)**: Alteration in relation to en-echelon quartz veins intersecting the foliation in the amphibolite. Alteration comprises biotite, amphibole and plagioclase and ilmenite. Alternating zonation with variation in the amount of biotite, plagioclase and amphibole. Ilmenite is partly replaced by titanite. **Alt1d (**Figure 9**)**: biotite amphibole rock. Titanite most common, but ilmenite preserved as cores together with rutile. Similar to the alteration around the en-echelon quartz veins (Alt1c).
Alt2: Potassic alteration K-feldspar replacing plagioclase and biotite (Figure 9)
Replacement of biotite by K-feldspar. Final alteration product is a light grey rock consisting of K-feldspar, and light green amphibole (Amp4). Titanite is very abundant in this rock type and almost no ilmenite/rutile is observed. Several types of replacements are seen replacing Alt1 assemblages.
Alt3: scapolitisation (Figure 10)
Massive scapolitisation. Quartz veins surrounded by reaction rims of scapolite, but minor amounts of scapolite are also observed in many places in the amphibolite. The quartz veins with the reaction rim of scapolite have a different colouration than quartz veins with less scapolite. The scapolite has a white colour and is only distinguished from commonly occurring white feldspars by its characteristic cleavage.

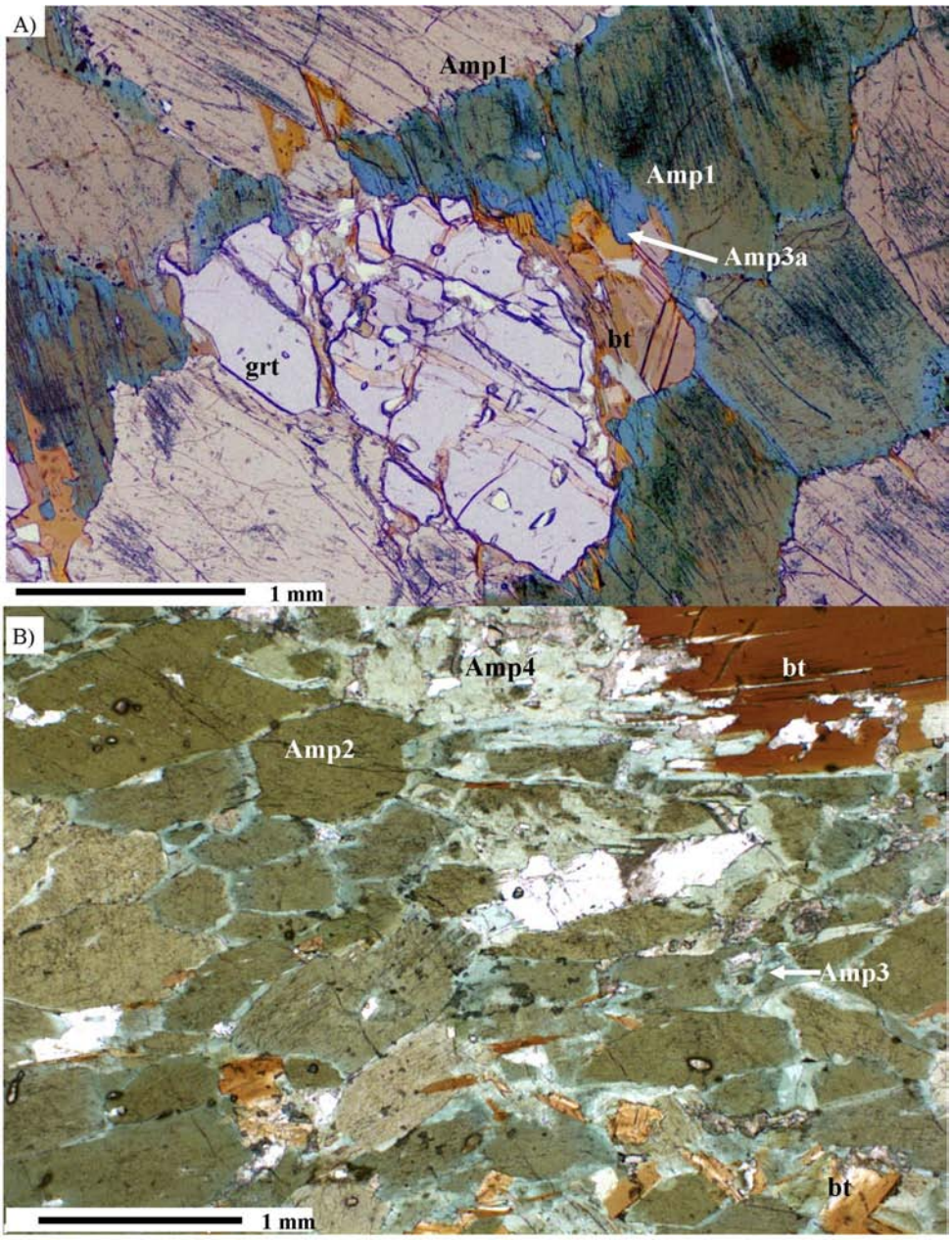

Figure 6: Alteration rims on amphiboles next to biotite grains. A) Amp1 in garnet amphibolite partly altered to Amp3a along cracks and grain boundaries in association with the introduction of biotite. From locality 1. B) Amp2 partly altered to amphiboles types Amp3 and Amp4 along with the formation of biotite. From locality 5.

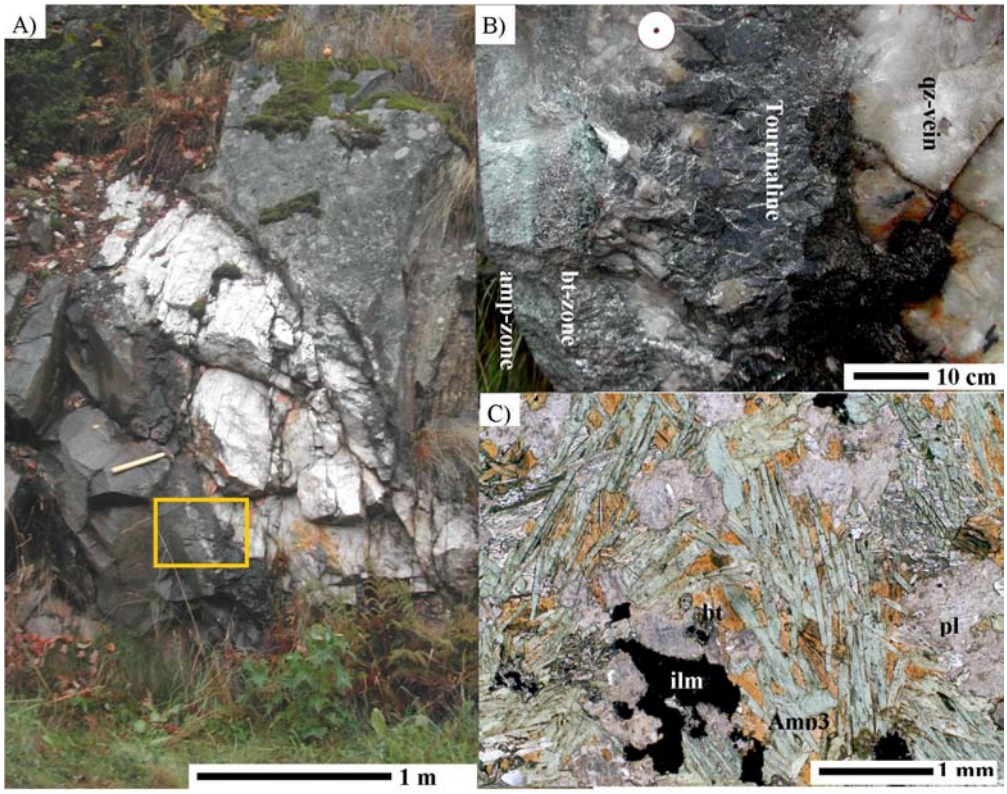

Figure 7: Field appearance and reaction textures around en-echelon quartz veins in amphibolite at locality 4. A) Field image displaying meter thick en echelon quartz vein intersecting amphibolite, yellow box denotes the position of image in B. B) Zoom on the alteration bordering the en echelon veins against the amphibolite. See text for discussion. C) Thin section image showing decussate texture of amphibole and biotite together with ilmenite and dusty plagioclase.

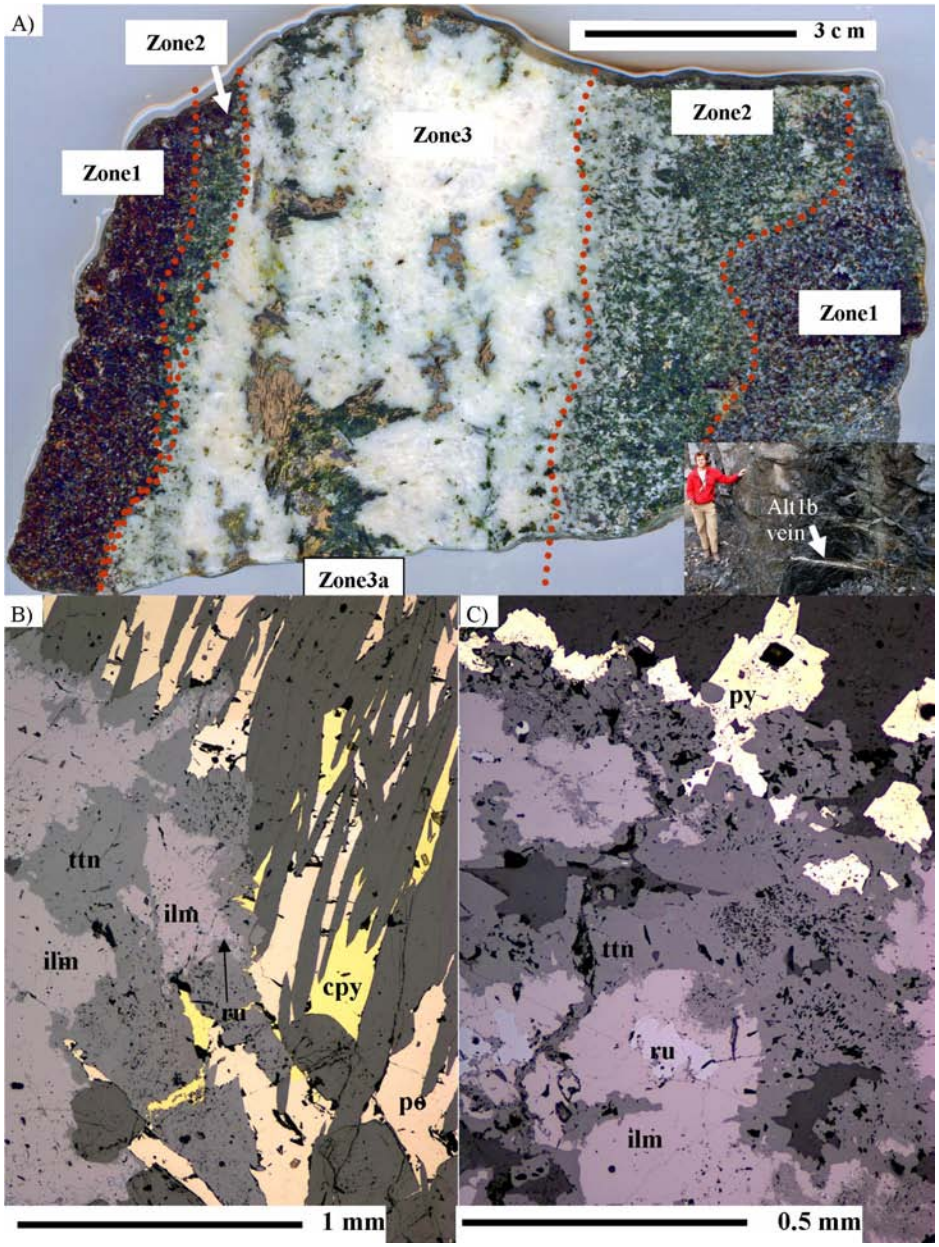

Figure 8: Amphibole plagioclase veins from locality 5 and their textural evolution. A) Note the distinct potassium depletion in the proximal (Zone 2 and 3) and enrichment in the distal part (Zone 1) of the alteration system (see text). B) Ore mineral assemblage in amphibole Amp3 (dark grey). C) Successive changes in Ti-phase stability.

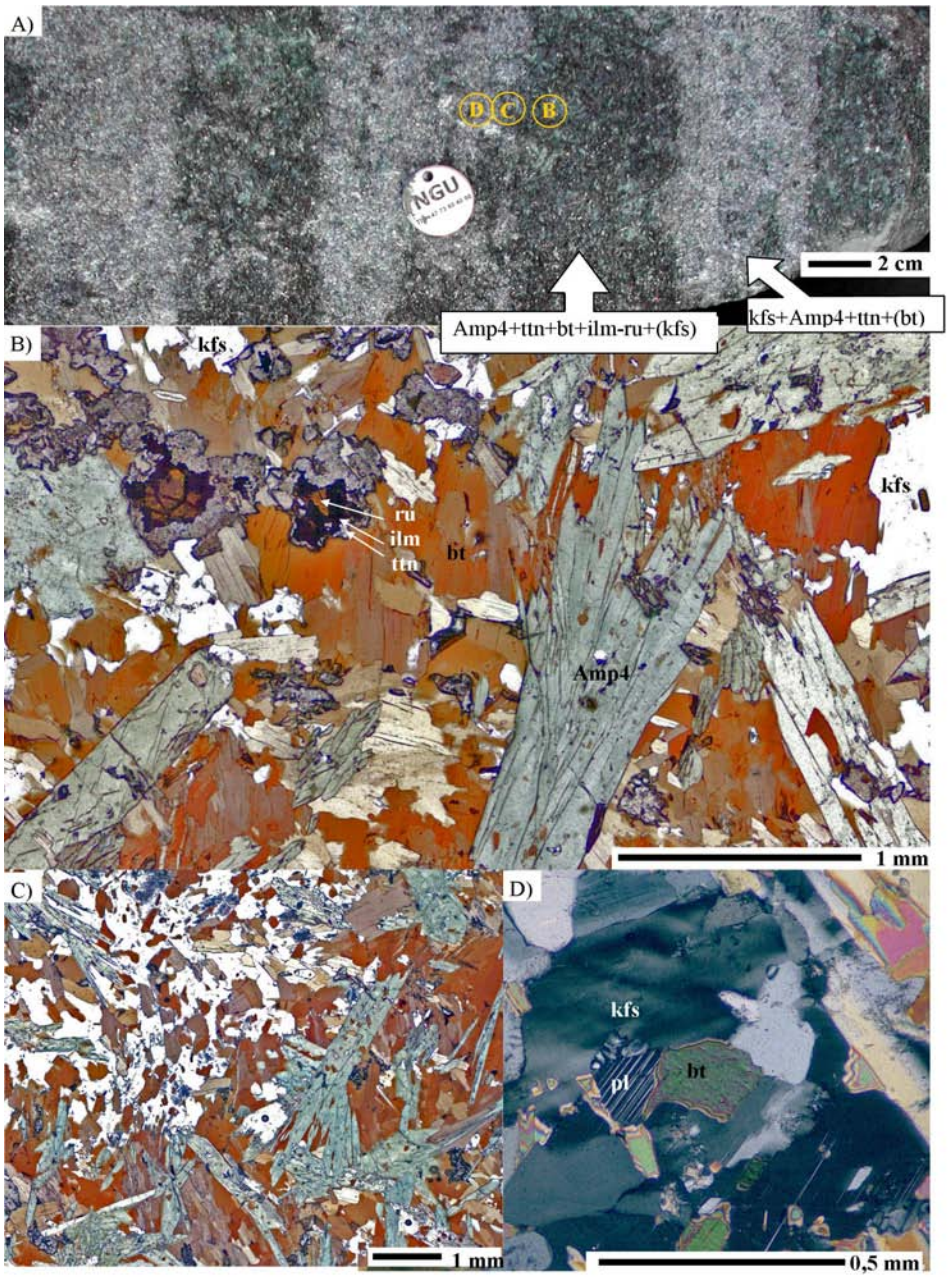

Figure 9: Decussate texture of biotite, amphiboles and Fe-Ti phases partly replaced by K-feldspar, amphibole titanite assemblage, from locality 5. A) Field image of fingering replacement pattern of the grey K-feldspar bearing rock on the Amphibole biotite rock. B) Decussate texture of amphibole, and minor K-feldspar. Note the successive change in

Ti-bearing from cores of rutile through ilmenite to titanite. C) K-feldspar replacing biotite, with left over grains of biotite inside the K-feldspar grains giving an atoll texture. Note that there is no ilmenite in the K-feldspar rich domain D) Remnants of plagioclase inside K-feldspar grain.

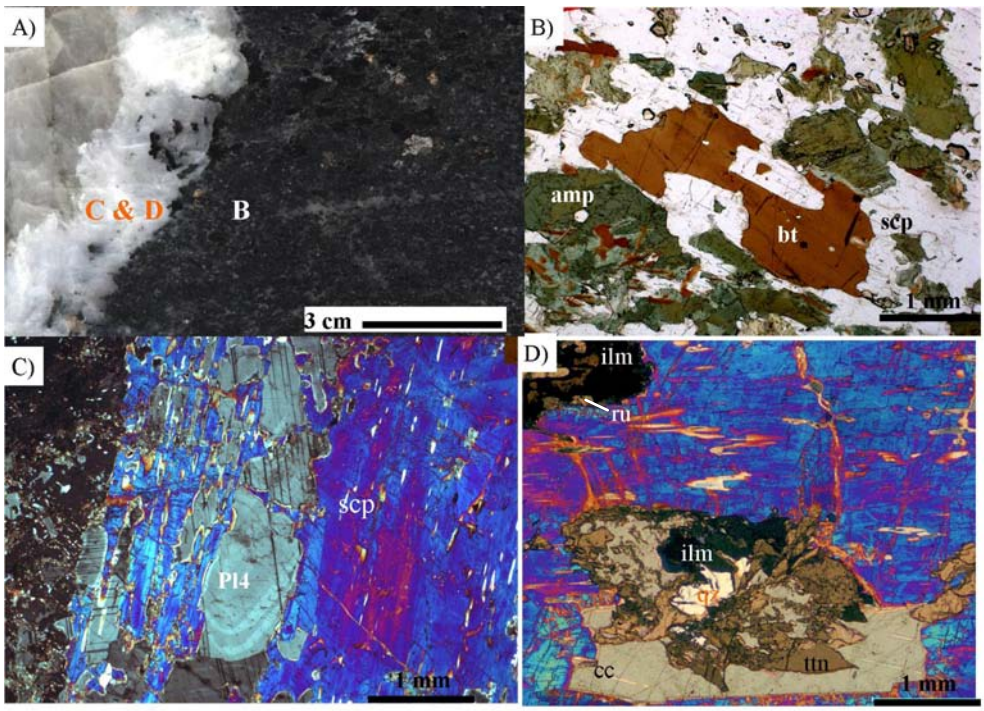

Figure 10: Scapolitisation observed around quartz-scapolite vein. A) Polished slab with indication of thin section images. From right to left is first grey quartz, followed by white scapolite and then scapolitised amphibolite. B) Scapolitised amphibolite. C) Scapolite replacing plagioclase intersecting growth zoning and deformation twins. D) Calcite ilmenite, rutile and quartz reacting to form titanite.

4.2 Mineral chemistry by EPMA analysis

Representative samples from localities 1, 4 and 5 were analysed by EPMA with a JEOL JXA-8900 combined WDS-EDS microprobe at the department of Materials Science NTNU. Results were standardised using a ZAF correction for matrix effects. Biotite, muscovite, amphibole, plagioclase and epidote data were collected using the same standard setup (Table 3). Apatite analyses were calibrated with an apatite standard, except for F and Cl where fluorite and tugtupite standards respectively were used because F and Cl may migrate through the atomic lattice of apatite as a result of

electron bombardment (Table 3). Amphibole formulae were calculated $^{+}$ on the basis of total cations – (Ca + Na + K) = with 13 (13eCNK method) with Fe^{3+} estimation by charge balance. Accordingly, Fe^{3+} value of the calcic amphiboles is a stoichiometric estimate and not a measured value. However, comparisons of measured and calculated Fe^{3+} in calcic amphiboles show that the 13eCNK method is the most accurate (e.g. Cosca et al., 1991; Gualda and Vlach, 2005). Scapolite formulas were recalculated with the procedure of Teertstra and co-workers (1997), with an additional iterative procedure to make a stoichiometric HCO_3 and CO_3 estimate (see section 4.2.2). Biotite formulas was normalised to 22 oxygen with all Fe assumed to be Fe^{2+}. Apatite formulas was normalised to 25 oxygen, feldspar formulas to 32 oxygen. The quality of Na, Ca and Al analyses was attained by comparing calculated feldspar formulas with the ideal stoichiometry of feldspar using the relation , NaK(1-Ca)Ca(Ca)Al(1+Ca)Si(3-Ca)O8. This gave satisfying results with deviations within 0-2 % of the ideal values.

Table 3: Standards used in calibration of EPMA analysis

element	Silicate setup	Apatite setup
Si	Wollastonite	Wollastonite
Al	Spessartine garnet	Spessartine garnet
Ti	Titanite	Titanite
Fe	Olivine	Olivine
Mg	Olivine	Olivine
Mn	Spessartine garnet	Spessartine garnet
Ca	Wollastonite	Apatite
Na	Albite	Albite
K	Orthoclase	Orthoclase
P	Apatite	Apatite
Cr	Chromite	Chromite
V	Element standard	Element standard
F	CaF	CaF
Cl	Tugtupite	Tugtupite

4.2.1 Amphiboles and biotites

Figure 11 shows the general geochemical evolution of the amphiboles vs. their Si content. Geochemical trends of amphibole cores and rims are strongly contrasting (Figure 11). Amphibole cores follow their own trend whereas the amphibole rims are aligned along a single geochemical trend (Figure 11). Particularly, this is evident in the plot displaying $Al^{VI} + Fe^{3+} + Ti$ vs. Si (Figure 11).

The prograde evolution of amphibole in garnet amphibolite follows trends from ferri-tschermakitic toward hastingsitic to ferropargasitic compositions (Figure 11). The main exchange vector during prograde conditions is substitution of Fe^{2+} for Fe^{3+}. The total amount of Fe recorded by zonings in amphibole cores (Amp1, 1a, and 2) is constant

within each amphibole type and changes in Fe^{3+} and Fe^{2+} only reflects the $Fe^{2+} \Leftrightarrow Fe^{3+}$ substitution (Figure 12). In a Fe^{2+} vs. Fe^{3+} diagram a set of lines with inclinations of -1 arise but with differing intercepts (Figure 12a). A main charge compensating substitution is Na for Ca at the M4-site and (Na,K) for vacancy (□) in A, which have a linear correlation with the Fe^{3+} content (Figure 12b). Although compensating substitutions have good linear correlations they are not explaining the total charge balance given that substituting mole fraction is 0.62 and not 1 as required. Probably, the missing charges may be accounted for by oxy-substitution, i.e. the amphiboles were partially oxidized with O_2^- substituting for OH^- as also documented in experiments under H^+ deficient conditions (Clowe et al., 1988; Popp et al., 1995). However, given the stoichiometric approach to the Fe^{3+} estimate, this conclusion is uncertain. Only tschermakitic amphiboles in the garnet amphibolite (Amp1) have considerable Fe^{3+} contents whereas amphibole cores in the garnet-free amphibolite (Amp2) has low Fe^{3+} contents and high Fe^{2+} contents (Figure 12). Amp1 shows coupled increase in A-site occupancy and decreasing X_{Mg} (Figure 11). The other core type amphiboles (Amp1a and Amp2) are relatively enriched in Cl and (Na, K) in the A-site compared to the retrograde overgrowth rims (Figure 11).

Retrograde overgrowths rims on amphiboles (Amp3, 3a and 4) show a wide range of compositions, from ferrotschermakite/ferropargasite towards actinolite along the ferropargasite exchange vector toward actinolite with XMg ≈ 0.9 (Figure 11). With increasing X_{Mg} and Si content they are progressively depleted in Cl and (Na, K) in A (Figure 11). The relation between Fe^{2+} and Fe^{3+} is less systematic (Figure 12). This reflects variations in the Fe_{tot} and the Fe^{2+}/Fe^{3+} ratio. The main factor in this trend is a drop in Fe_{tot}, whereas the Fe^{3+} contents generally are low (Figure 12).

Along with the increasing X_{Mg} and Si contents the total amount of tetra- and trivalent ions in the M sites of the amphibole rims also decreases along linear trends, which are not followed by amphibole cores (Figure 11). A plot of Al^{VI} against Si does not show as strong a correlation as the former, and additionally show disarrays for the core type amphiboles (not shown). This imply that even low concentrations of Fe^{3+} influence the Al^{VI} substitution mechanisms in the retrograde overgrowth rims and retrograde amphiboles.

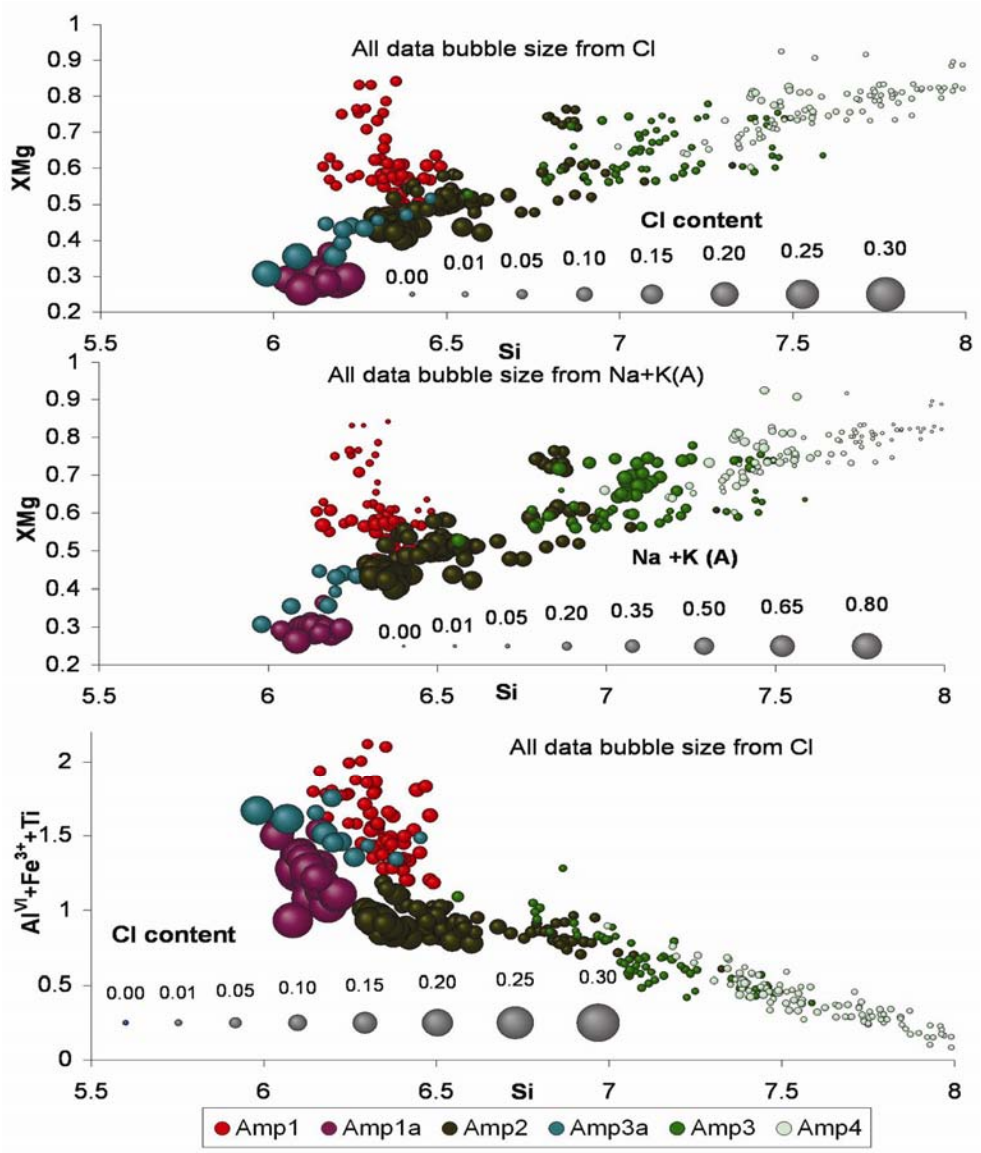

Figure 11: General amphibole evolution. Upper two diagrams display the evolution in X_{Mg} versus Si plot, documenting the interdependence between X_{Mg} (Mg/(Mg+Fe^{2+})), Si, (Na, K) in A and Cl. Note that this plot corresponds to the plotting scheme of Leake et al. (1997). Lowermost diagram shows the evolution in terms of octahedral Al, Fe^{3+} and Ti and Cl vs. Si. Amp1, 1a and 3a analyses from samples from locality 1. Amp3 and Am4 analyses from localities 4 and 5. See text for discussion

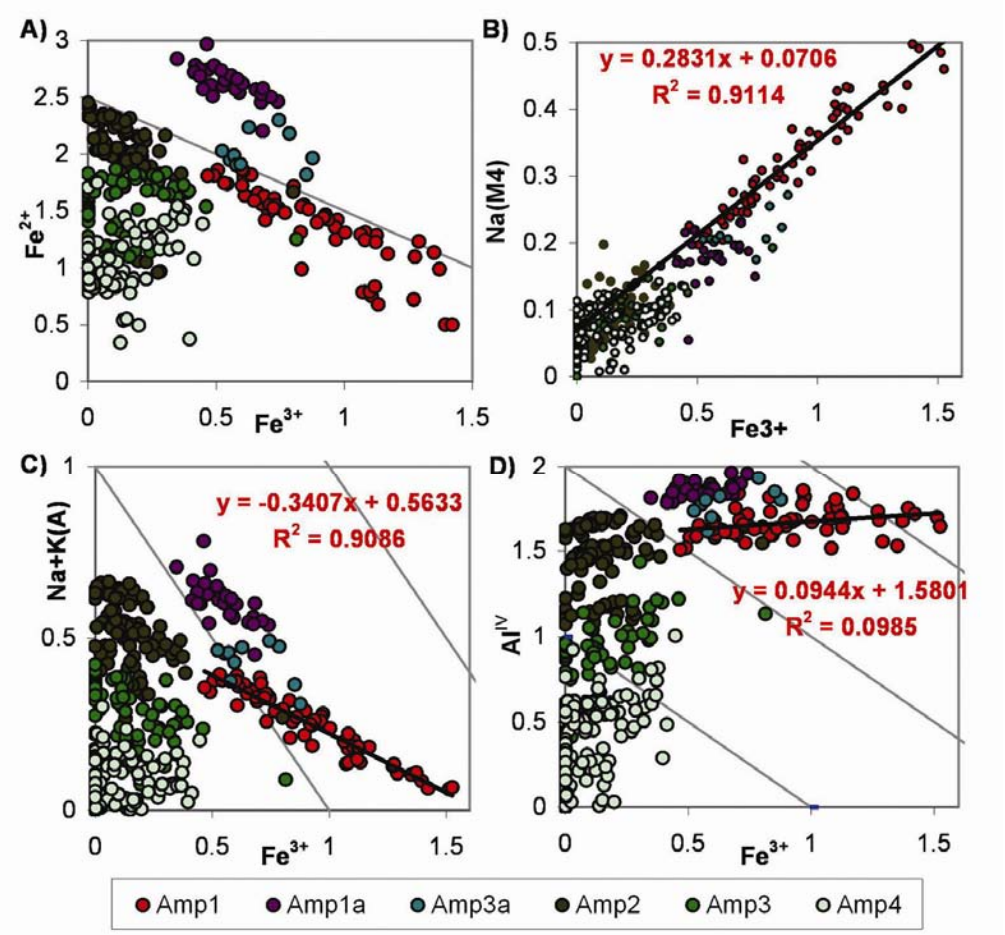

Figure 12: Trends with Fe^{3+}, regression lines based on amp1 data only. A) Fe^{2+} vs. Fe^{3+}. B) Na (M4) vs. Fe^{3+}. C) Na +K (A) vs. Fe^{3+}. D) Al^{IV} vs. Fe^{3+}. Note grey lines marking 1:1 negative correlations for comparison. Amp1, 1a and 3a analyses from samples from locality 1. Amp3 and Am4 analyses are from localities 4 and 5. See text for discussion.

All amphiboles except Amp1 show correlations of several other elements with their Cl-content (Figure 13). In Amp1 the only correlation is a positive correlation between Fe^{2+} and Cl (Figure 13). The trends vary between the amphibole types in both inclination and intercepts (Figure 13). Trends between K and Cl display different linear correlations for the individual amphibole groups (Figure 13a). The inclination of trends of K vs. Cl in Amp1a and Amp2 are similar but they have different intercepts (Figure 13a). With respect to the amphiboles that coexist with biotite (Amp3 and Amp4), trends vary between locality 1 and 5. The blue-green amphibole rims (Amp3a) show a

flat trend whereas the retrograde overgrowths at locality 5 show a step trend for both Amp3 and Amp4 (Figure 13a).

Mg and Fe contents also correlate with Cl (Figure 13b-d). The X_{Mg} for all data, except Amp1 fits on a linear trend with an inclination of -2. Amp1, however, follows a steep trend with an inclination of about -7 (Figure 13d). In approaching the detection limit for Cl Amp3 and Amp4 should not follow distinctive trends for this element. However a zoom on the plot suggest that the low Cl concentration data separates into two strictly linear and parallel trends (Figure 13a-e). Possibly, this difference in intercept reflects contrasting Fe_{tot} in the geochemical system (i.e. the protholith). This is reflected by the two groups of the core amphiboles Amp2, with different Fe_{tot} (Figure 13c). Similar effects are also observed with respect to X_{Mg}.

Fe_{tot} in Amp1, Amp1a and Amp2 varies independently of their Cl contents (Figure 13c). The Fe_{tot} within amphibole types Amp1, Amp1a and Amp2 is not affected by the Cl incorporation although there is a general grouping with high Fe_{tot} amphiboles having higher Cl (Figure 13c). Contrary to Fe_{tot}, both Fe^{2+} and hence also X_{Mg} correlates with Cl in Amp1, whereas there is no correlation in Amp1a and Amp2 (Figure 13b-d). Accordingly, in Amp1a and Amp2 the incorporation of Cl mostly affect the K content (Figure 13a), whereas high Fe-contents probably promotes Cl incorporation (Figure 13b-d). A similar effect is seen in the Al^{IV}/Si content for Amp1, Amp1a and Amp2 although it is more clear with respect to Fe_{tot} (Figure 13e).

The overall Froland trends in the amphiboles are realised in single grains (Figure 14). Overgrowths of Amp3 and Amp4 are observed on Amp2 and overgrowths of Amp4 on Amp3 are commonly observed. In all cases the chemical change from core to rim is the same, following the general trends with increasing Mg and Si and decreasing Fe, Al^{IV}, Al^{VI}, Cl., Ti, K and Cl (Figure 14).

Amphibole chemistry in the other characteristic alteration types also follows the systematic evolution demonstrated by the biotite-related amphibole rims. Amphiboles in early biotite potassic alteration types Alt11b-c are magnesiohornblende-actinolite (Amp3-4), whereas amphiboles in the K-feldspar bearing potassic alteration assemblages are more actinolitic and belong to the Amp4 group.

Because Amp3, Amp3a and Amp4 are mostly correlated petrographically with biotite it is useful to compare coexisting amphibole and biotite. As for the amphiboles, the Cl content of biotite correlates negatively with X_{Mg} and positively with the Fe content (Figure 15). There are curvilinear correlations between the X_{Mg} and Fe, Mg and Cl contents of coexisting amphibole and biotite (Figure 15). The Cl content of biotite is mostly higher than that of coexisting amphibole, but at high Cl contents, the Cl-contents of amphibole and biotite are similar (Figure 15). Only poor correlations are found between Al^{IV} and Cl content of biotite and between the Al^{IV} of biotite/amphibole pairs (Figure 15).

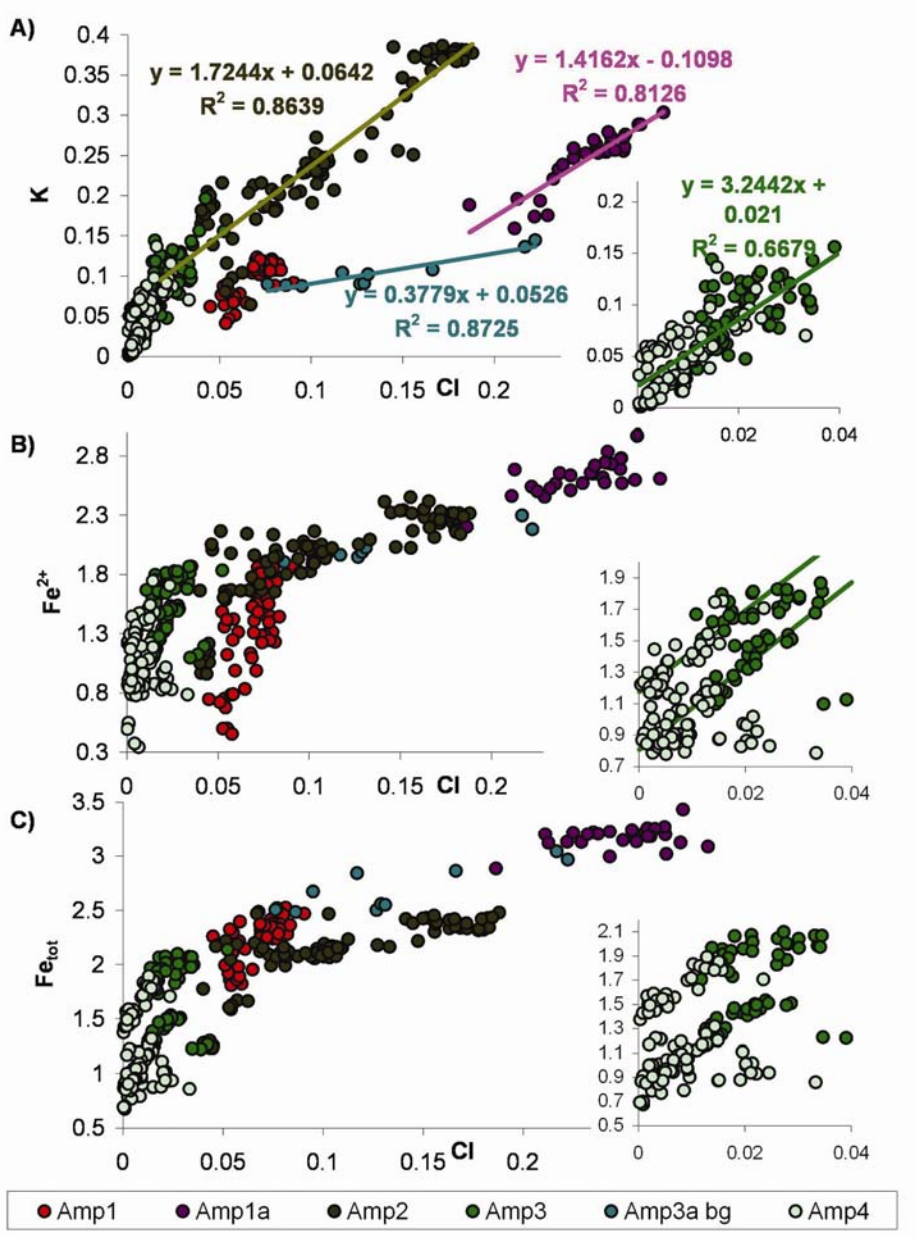

Figure 13: See caption on next page.

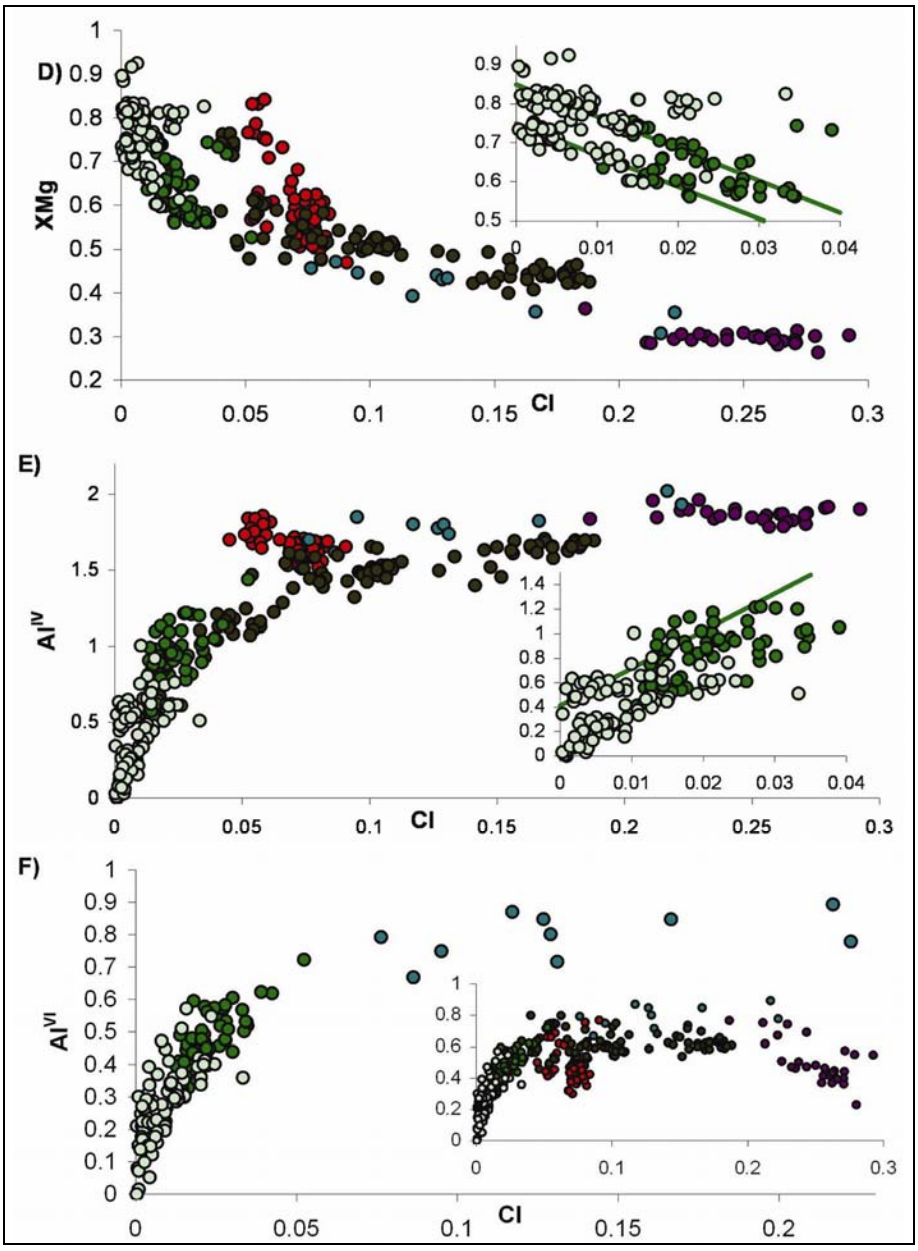

Figure 13 (continued): Composition of amphibole as a function of Cl-content. Amp1, 1a and 3a analyses from samples from locality 1. Analyses of Amp3 and Am4 from localities 4 and 5. A) K vs. Cl B) Fe2+ vs. Cl C) Fe_{tot} vs. Cl. D) XMg vs. Cl. E) Al^{IV} See text for discussion. F) Al^{VI} vs. Cl. See text for discussion.

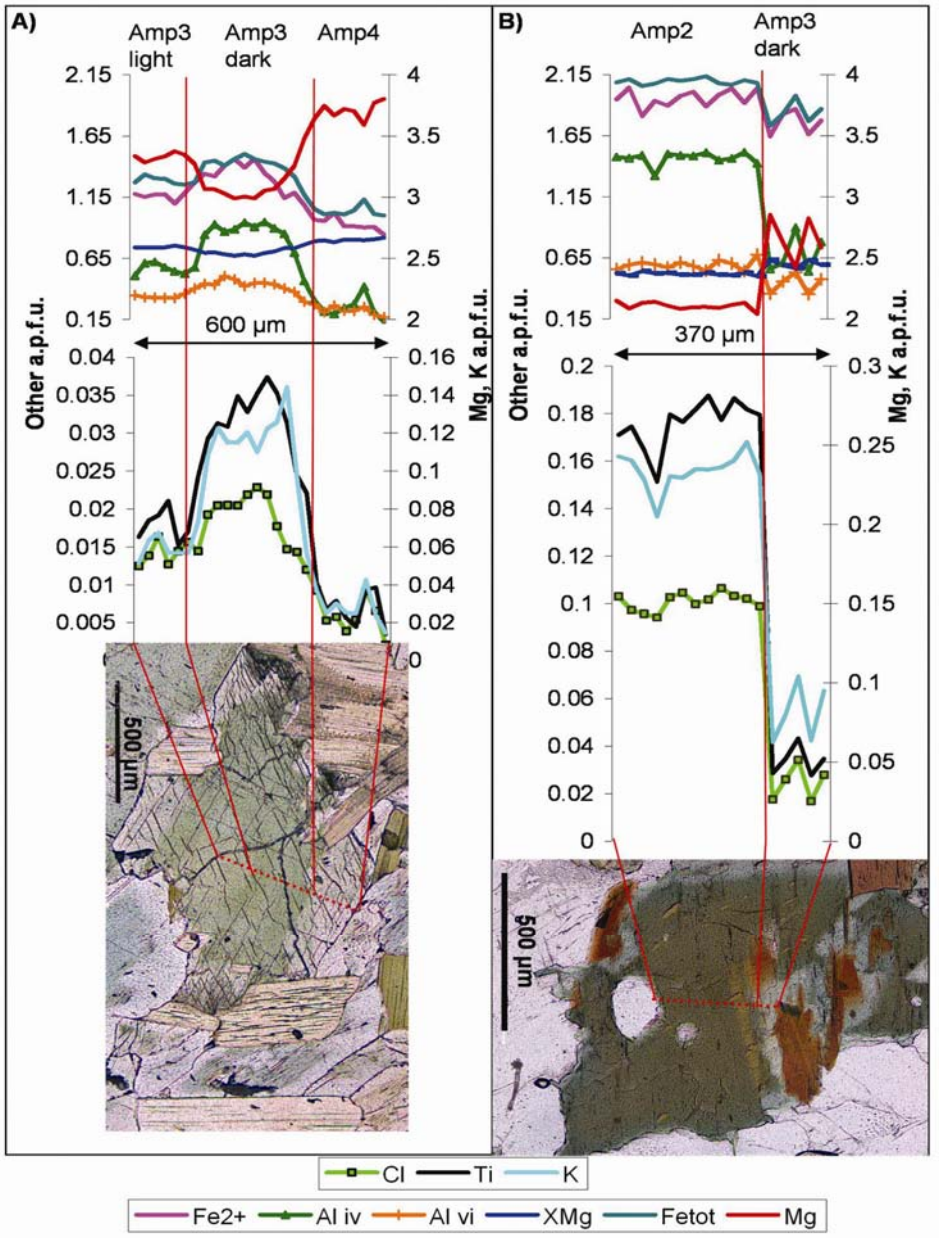

Figure 14: Line scans across amphibole grains showing the stages in the progressive amphibole alteration. A) Amp3 partly altered to Amp4. Note that biotite is in contact with both types. B) Overgrowth of Amp3 on Amp2. Note the sharp alteration boundary when compared to A., Both amphiboles are from locality 5.

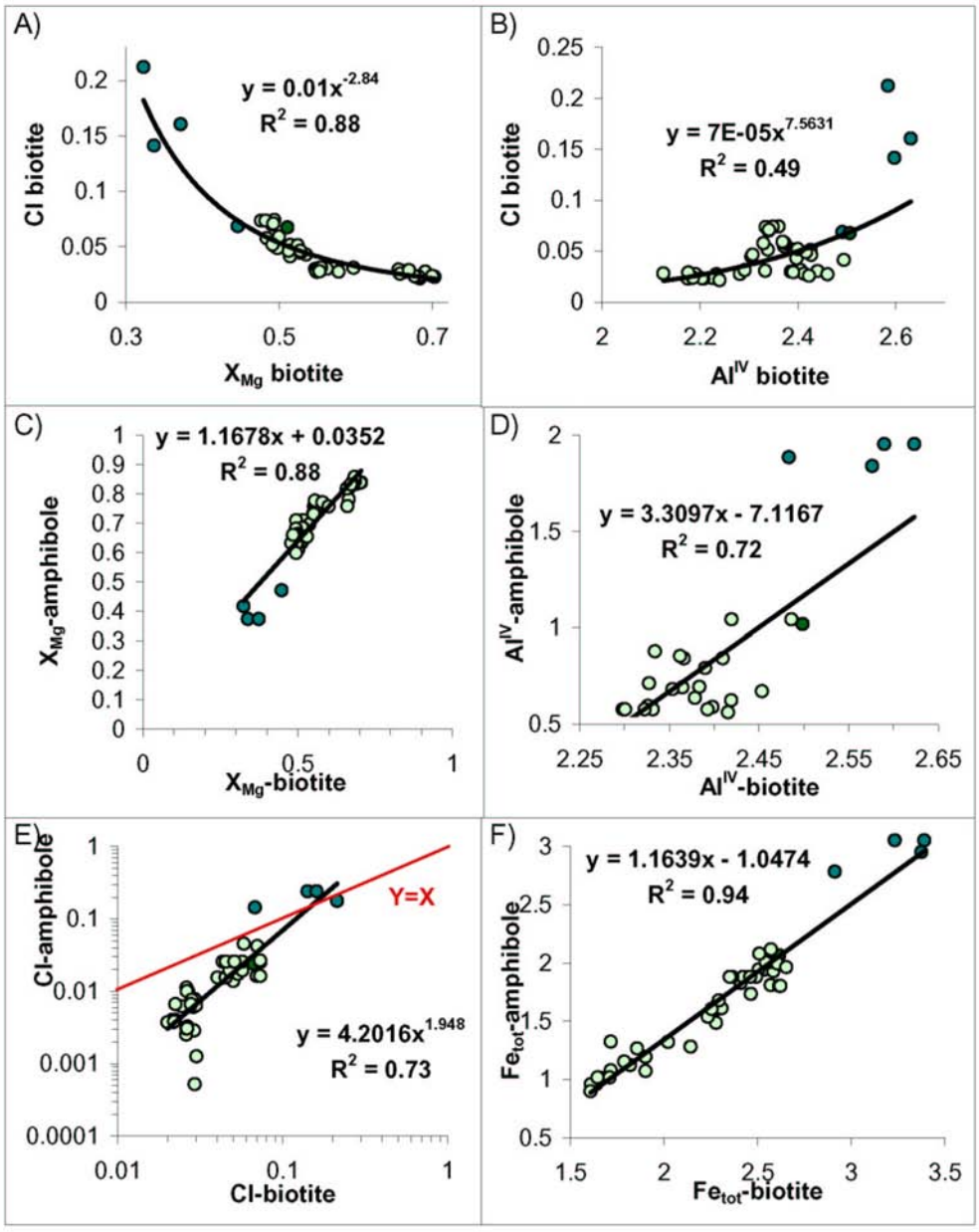

Figure 15: Comparison of biotite and amphibole evolution. Analyses of Amp3a and coexisting biotite from locality 1. Amp3, Amp4 and coexisting biotite analyses from localities 4 and 5. A) The Cl content of biotite against the XMg of biotite, with a power law correlation. B) Al^{VI} content and Cl of biotite only display a weak correlation. C) Correlation between X_{Mg} of coexisting amphibole and biotite. D) Al^{VI} of coexisting

amphibole and biotite only display a weak correlation. E) Correlation between Cl-contents of coexisting amphibole and biotite. F) Correlations between Fe_{tot} in coexisting amphibole and biotite. Colour labelling of amphibole same as in Figure 11, 12 and 13.

4.2.2 Plagioclase and scapolite

The composition of plagioclase varies amongst the localities and plagioclase also evolves toward higher albite contents as amphibolite alteration proceeds. Plagioclase in garnet amphibolite (Pl1) has a restricted compositional range (average = $An_{39.4}Ab_{60.4}Or_{0.2}$). Pl1 is unzoned, however, is overgrown by albite rich plagioclase (Pl1-rim $An_{30,1}Ab_{69,8}Or_{0,1}$). The garnet quartz symplectites have one group of plagioclases having the same composition as Pl1(Pl3) in the garnet amphibolite and also comprise an albite rich plagioclase (Pl3a).

Plagioclase texturally correlated with amphibole cores in the garnet free amphibolite (locality 5), is considerably more anorthite rich ($An_{51,4}Ab_{47,9}Or_{0,8}$) than plagioclase in the garnet amphibolite. Secondary plagioclase is more albite rich, but divides in two main groups i.e. Pl3 ($An_{37,3\text{-}45,3}Ab_{53,9\text{-}61,9}Or_{0,2\text{-}1,4}$) and Pl4 ($An_{28,9\text{-}33,4}Ab_{65,7\text{-}70,3}Or_{0,6\text{-}1,0}$). Pl3 is associated with Alt4, whereas plagioclase Pl4 replaces Pl3, but probably also coexist with the amphibole-biotite assemblages.

Table 4: Representative plagioclase analyses. Note to few analyse of pl1-rims for statistics

Type	averaged values			range		
	An	Ab	Or	An	Ab	Or
Pl1	39,4±0,8	60,3±0,8	0,3±0,1	37,6-40,9	58,8-62,2	0,2-0,4
Pl2	51,4±0,7	47,9±0,8	0,8±0,1	50,5-53,3	46,0-48,8	0,6-0,9
Pl3	40,4±2,3	58,8±2,2	0,8±0,2	37,3-45,3	53,9-61,9	0,2-1,4
Pl4	30,5±1,3	68,6±1,3	0,8±0,1	28,9-33,4	65,7-70,3	0,6-1,0
Pl1-rims	30,1	69,8	0,1	?	?	?
Pl3a	20,0±3,2	79,6±3,3	0,4±0,2	16,3-23,3	76,1-83,4	0,2-0,7

Scapolite was only documented in samples from locality 5. It replaces both the primary and the secondary plagioclases. The stoichiometric formula of scapolite is of the form (e.g. Teertstra and Sheriff, 1997):

$M_4T_{12}O_{24}A$, where M= Ca, Na, K; T= Si, Al; A= Cl, CO_3, SO_4, HCO_3 and OH

All analyses are close to ideal stoichiometry with 12 Si and Al and approximately 4 cations in the M site. Scapolite in the area shows considerable compositional variation

(EqAn=100*(Al-3)/3=41.3-59.5). The scapolite has a significant Cl content, whereas S and F only occur in minor amounts. The Cl and Na content have negative linear correlations with EqAn, whereas the sum of divalent cations (≈ Ca) has a positive correlation (Figure 16). The K content on the contrary, shows a positive although poor correlation with EqAn (Figure 16).

CO_3^{2-} was estimated using 3 model calculations: 1. Charge balance optimisation using $\Sigma M+=\Sigma A^-+\Sigma TO2^-$ (see Teertstra and Sheriff, 1997) 2: A-site occupancy (CO_3=1-S-Cl-F) 3. Combined charge balance and A-site occupancy by an iterative method, gives a result that can be caused by both OH^- and HCO_3^-. Method 2 gives a systematic correlation between A-site occupancy and EqAn (Figure 17). The correlation with EqAn is inherited from the correlation between Cl and EqAn, and this model satisfies charge balance constraints but not site occupancy. Method 1 gives a poor correlation between EqAn and the CO_3 content (Figure 17). Model 3 provides the best fit as it charge balance A-site occupancy and is correlated with EqAn (Figure 17). The modelling suggests that other species than CO_3^{2-} and Cl^- is present in the scapolite. We suggest that they are water related species i.e. OH^- and HCO_3^-, but cannot prove it because this would require a quantitative estimate of the water content.

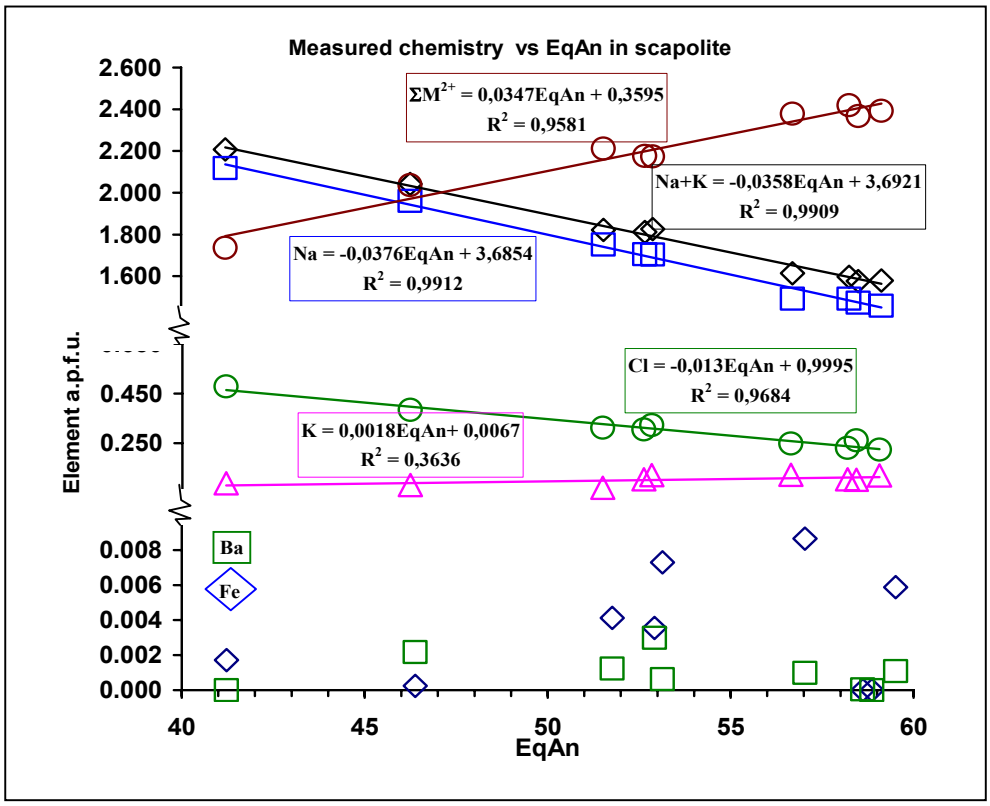

Figure 16: Scapolite chemistry in element a.p.f.u. vs. EqAn (100*(Al-3)/3). See text for discussion.

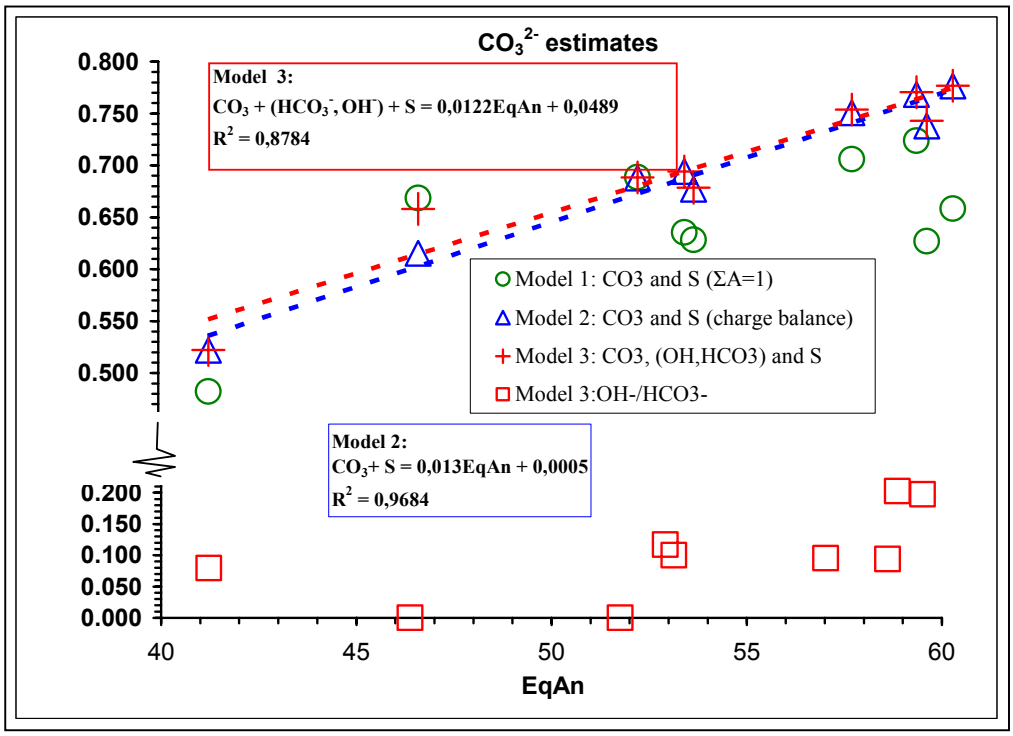

Figure 17: The three models of CO_3 estimation, only model 2 and 3 give reasonable correlations between CO_3 and EqAn. Model 3 is preferable for calculations of endmembers and exchange vectors because it satisfies both charge balance and site occupancy. See text for discussion

4.2.3 Apatite

Apatites also follow a systematic evolution in their halogen geochemistry. The evolution path of apatite, however, deviates significantly from the paths of biotites and amphiboles. Apatite contains considerable amounts of F not detected in amphibole and biotite. Apatite in garnet quartz symplectites is Cl-apatite. Apatite coexisting with the alteration assemblages show rising F with increasing degrees of alteration in samples where amphibole and biotite are more Mg-rich and poor in Cl, Al and Fe (Figure 18). Early apatite in garnet quartz symplectites is relatively enriched in Ce, which is incorporated in monazite next to altered Cl-apatite grains (Figure 18). Late F-apatite coexisting with Amp4 display enrichment in Ce and Y, whereas intermediate apatite coexisting with Amp3 is enriched in neither Ce nor Y (Figure 18).

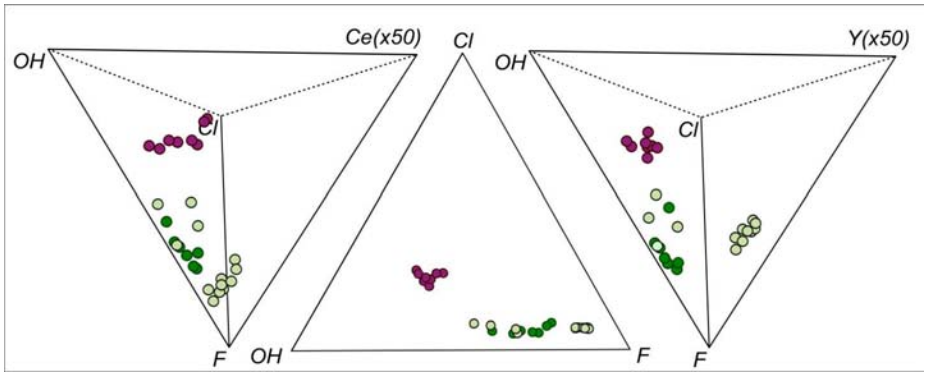

Figure 18: Halogens in apatite. Dark red brown is apatite in garnet quartz symplectites co-existing with Amp1a. Green symbols represent apatite occurring together with Amp3 and light green occurring together with amp 4. Middle diagram display the halogen evolution, diagram to the left the coupling with the Ce-content and the diagram to the right the Y- content. See text for discussion.

5 Discussion

This paper documents a well defined retrogression path for the amphiboles. The aim of this discussion is to relate the amphibole evolutions to the fluid evolution of the Bamble shear zone. The chemical evolutions of the hydrous phases confirm and complement the results of fluid inclusion analysis by Sørensen and Larsen (2007b, paper 2).

The chemical evolution of amphibole relates to its halogen content. In the following sections we will document how halogen chemistry changes in the amphiboles relates to the fluid properties and metamorphic conditions. The aim is also to approach the source and regional origin of metasomatism in the Froland area as well as the Bamble zone.

5.1 Prograde-retrograde evolution of amphibolite

The garnet amphibolite amphiboles (Amp1) follow a different chemical trend when compared to other amphibole types in this study when looking at variations in Fe^{3+}, Na(M4) and (Na,K) in A. Furthermore, charge balance constraints suggest that the amphiboles were oxidised during a period of low fH^{+}. However, field evidence show that the garnet amphibolite formed as a result of hydration of the hyperite with a gradual transition from coronitic gabbro to pyroxene free garnet amphibolite. As this hydration process is not in agreement with low fH^{+} (e.g. Clowe et al., 1988) we infer that the garnet amphibolite was subjected to oxidation after initial amphibolitisation. The correlation between decreasing XMg, Fe^{3+} and increasing Cl suggests that amphiboles in the garnet amphibolite partially equilibrated to the fugacity conditions

of an infiltrating chloride bearing fluid. This may reflect the conditions at which Amp2 in the garnet free amphibolite formed.

To summarise, the amphibolites went through the following evolutionary stages:

1. Amphibolitisation of gabbro, as documented by field and petrographic evidence at locality 1.
2. Cessation in amphibolitisation and oxidation of amphiboles in garnet amphibolite during H^+ deficient conditions.
3. High-grade amphibolite facies alteration and amphibolitisation under the influence of chloride bearing solutions.
4. Biotite stabilised in the amphibolites (Alt1), due to infiltrating K-bearing brines with near constant salinity. Amphiboles react with the infiltrating fluid causing changes in amphibole composition. The most common expression of the fluid infiltration is overgrowth rims on amphiboles against introduced biotite grains. In zones of more intense alteration more complex alteration develops.
5. Stabilisation of K-feldspar at the expense of biotite and plagioclase (Alt2).
6. High fH_2O destabilises calcite and the assemblage calcite+ (ilmenite)/rutile + quartz which is replaced by the assemblage titanite + CO_2. This leaves CO_2 available for the formation of rather meionite rich scapolite according to the simple reaction; plagioclase + CO_2 + brine → scapolite+ quartz (Alt3). As no trace of CO_2 was detected in the coexisting fluid inclusions (paper 2, Sørensen and Larsen, 2007b), it is assumed that the CO_2 in the scapolite must be locally derived i.e. from decomposition of calcite and that the CO_2 did not mix into the aqueous brine. This also document that scapolite formed below the PT conditions of the solvus in the H_2O-CO_2-salt system hence also why scapolite is only observed in association with calcite.

5.2 Cl-OH in amphibole and biotite during retrogression

The Cl content of amphibole and biotite is a function of several factors including pressure, temperature, fluid composition and the actual composition of the amphibole that is a partial function of the host rock chemistry. These effects are probably reflected in our data. The effect of the amphibole chemistry is reflected by the shift in K vs. Cl content trends of amphiboles with different Fe_{tot} content. Cores of amphiboles follow individual trends at each locality whereas rims follow a general trend. In both retrograde amphiboles and in biotite there is a negative correlation between X_{Mg} and Cl.

Biotite features a linear correlation between X_{Mg} and $\log(OH_{biotite}/Cl_{biotite})$. Munoz (1992) and Munoz and Swenson (1981) suggested that the Cl-content of biotite is a function of the Mg-Cl avoidance effect and the original Fe/Mg ratio at given PT-Xfluid

condition. However, calculated f_{H_2O}/f_{HCl} using Munoz (1992) equations produces a linear correlation with X_{Mg} in biotite irrespective of the temperature, thus suggesting that the fluid composition varied (not shown). Contrary to this conclusion, the studies of Sørensen and Larsen (2007b) suggests near constant salinity in the fluid and show that potassic alteration took place in the temperature interval c. 625-450°C. Biotite also formed in this T-interval. It is not possible to obtain the observed variation in biotite Cl content using a constant fluid Cl/OH ratio and the Mg-Cl avoidance model suggested by (Munoz, 1992; Munoz and Swenson, 1981).

In agreement with Kullerud (2000) we suggest that the disagreement is a result of uncertainties in the assumptions made by Munoz and co-workers in their Mg-Cl avoidance models. The Cl-Mg avoidance model rests on the argument that linear trends between log(XF/XCl) and XMg in biotite imply constant PT-X_{fluid} conditions and that the Cl-content was controlled by the Mg-Fe ratio of biotite. This is a strongly biased opinion given that, thermodynamically, there may be several other explanations for univariant trends. The controlling parameter can not be decided alone from the univariant trend. Many parameters could be involved including the PT-conditions, fluid composition, chemical potentials and internal chemical constraints.

Also opposing the Mg-Cl avoidance model of Munoz and co-workers is that both the Froland amphiboles and biotites feature rimward increase in XMg. This suggests that XMg in both minerals was controlled by an external parameter, because no other minerals in the assemblages can account for the progressive loss of Fe by biotite and amphibole. As other phases also become lower in Fe, the only interpretation is metasomatism, i.e. Fe was mobilised and depleted from the amphibolites. The question is what induces this metasomatism. Zoned amphiboles in other studies have been related to changes in fluid composition at fixed PT in both metamorphic (e.g. Kullerud, 1995; Kullerud, 1996; Kullerud, 2000; Kullerud and Erambert, 1999; Xiao et al., 2005) and magmatic (Sato et al., 2005) environments. However, in Froland the fluids maintained constant Cl/H_2O ratios throughout cooling and uplift (Sørensen and Larsen, 2007b, paper 2). Accordingly, this is not the underlying cause of Mg-zonation.

Kullerud (2000) argue that gradual changes in PT conditions with fluids of fixed Cl/H_2O ratios would produce similar trends. That is also the most likely explanation for the Froland amphiboles. The key to understand the linear trends lies in the relation between coexisting biotite and amphibole, which are also univariantly correlated along logarithmic trends. The K_DFe between biotite and amphibole may be expressed in the following way (e.g. Cooper, 1972):

$$K_D Fe(amp-bt) = e^{-\Delta F/2RT} = \frac{\frac{X_{Fe}^{Amp}}{1-X_{Fe}^{Amp}}}{\frac{1-X_{Fe}^{Bt}}{X_{Fe}^{Bt}}},$$

$$where\ X_{Fe} = Fe^{2+} / \sum octahedral\ sites.$$

Accordingly, if biotite and amphibole formed at the same temperature and if the Fe content was not affected by the brine fluids, then, according to this expression, plots of XFe/(1-XFe) of amphibole vs. that of biotite would give linear trends with zero intercept at a given temperature and increasing inclination with increasing temperature (Cooper, 1972). Increased incorporation of Fe over Mg in amphibole with increasing temperature is clearly expressed in the following citation from Ramberg (1952):
"*The problem of how Al in 4-coordination affects the valency property of oxygen and thus the Mg-Fe distribution can now be considered. When the electropositive Al is placed in the site of the more electronegative Si, the bonds to the neighboring oxygen atoms become ionic and, in particular, of less double-bond character, and, as a consequence, the bonds from the neighboring non bridging oxygen toward metal ions become more covalent (see fig. 9 [here* Figure 19 *]). We can therefore conclude that, by substituting Al for Si in the silicate structure, the electronegativity of the oxygen decreases and* ***the Fe/Mg ratio is likely to increase, all other conditions being equal***."

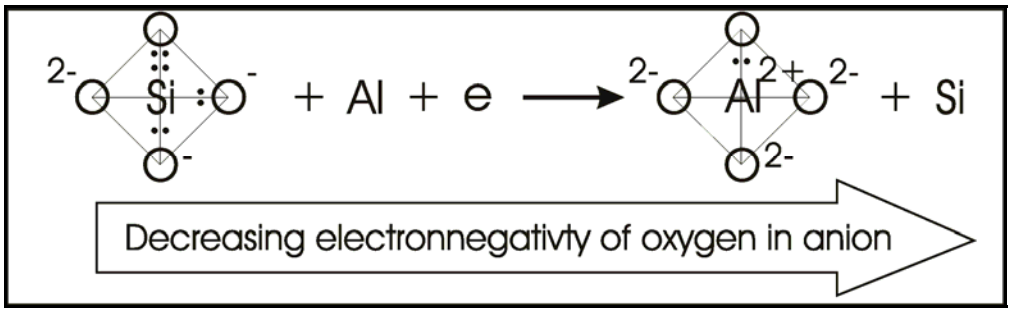

Figure 19: The change in electronegativity of oxygen in AO_4^{x-} when Si is replaced by Al. Redrawn from Ramberg (1952).

Because tetradrally coordinated Al (Al^{IV}) increases in amphibole with increasing metamorphic grade then according to the above statement, the Fe/Mg ratio in amphibole will increase as an effect of the Al substitution. The increase in Al^{IV} in biotite is less than that of amphibole. As a direct consequence of this, K_DFe (amp-bt) increases with temperature. Cooper (1972) tested this theory by plotting values of K_DFe (amp-bt) against amphibole Al^{IV} and found a general correlation although many outliers were attributed to other factors also being important. Figure 20 displays a plot of KdFe for the Froland data. There is a convincing linear correlation, which, however has a non-zero intercept. Utilizing the principle of Ramberg this is inferred as the result of different temperature at each data point. It may also be reasoned that the linear correlation reflect that amphibole and biotite were buffered by a fluid with constant salinity during cooling and exhumation and that equilibrium was achieved because of the linearity of the K_DFe(amp-bt) plot.

Given this scenario the variation between the Cl-contents of coexisting amphibole and biotite may also be interpreted. The observed complexity of the amphibole and biotite relates to the way that Cl affects the lattice and SRO (short range order in the minerals). If Fe-F and Mg-Cl avoidance was the governing factor of Cl incorporation in amphibole, one might expect LRO between Fe and Cl and that the incorporation of Fe would change the amphibole structure in order to make space for the large Cl ion in the A site. This is not confirmed by X-ray structural refinement analysis of Cl-bearing amphiboles (Makino et al., 1993; Oberti et al., 1993). Here, it is documented that the introduction of Cl in the amphibole lattice induces local deformation of the lattice structure and increasing cell volume. The Fe enrichment in Cl-rich amphibole is due to SRO (short range order) between Fe and Cl (Oberti et al., 1993). Oberti et al (1993) also suggested that the incorporation of Cl in amphibole promotes incorporation of K in the A site and substitution of Al^{IV} for Si in the tetrahedral sites. This is in good agreement with the general compositional variations in amphibole (Kullerud, 2000, and references therein) and also the trends observed in our study. Because Cl-incorporation increases the cell volume of amphibole (Oberti et al., 1993) it is expected that the Cl incorporation depends positively on temperature. In addition Oberti et al. (1993) suggested that increased size of the octahedral sites forced an increased size of the tetrahedral sites, hence favouring Al over Si. On the contrary, if the cell volume of the mineral increases during rising T is associated with more Al^{IV} then Cl is more easily incorporated into the amphibole lattice at high than at low temperatures. Given that Al^{IV} and hence also Fe and Cl increase at a lower rate with T in biotite than in amphibole it is expected that the Cl exchange between biotite and amphibole will be temperature dependant, and proportionally more Cl is incorporated in amphibole when compared to biotite at higher temperatures than at lower temperatures. In addition the increased A site occupancy (edenite component) and K content of amphibole with increasing temperature will also promote Cl-incorporation because of the SRO between Cl and K observed by Oberti (1993). The variation in the range of edenite like substitution in biotite is less than in amphibole hence this effect is expected to be less pronounced in biotite than in amphibole. All together this agrees with our conclusions because the inferred high temperature amphiboles have higher Cl contents than co-existing biotite whereas the more evolved amphibole and biotite pairs that formed at lower T do not show this bias.

Cl-data reported in the literature of coexisting biotite and amphibole support our conclusions. In some cases the Cl-content in amphibole is higher than in coexisting biotite (e.g. Leelanandem, 1969; Leger et al., 1996; Markl et al., 1998; Zhu et al., 1994) but higher Cl content in biotite is also common (Ekstrom, 1972; Zhu et al., 1994). From the above discussion we conclude that T is the most important parameter in controlling the Cl-content. Accordingly, upper amphibolite to granulite facies amphiboles are often more Cl and Fe rich than coexisting biotite (Kullerud, 1996; Leelanandem, 1969; Leger et al., 1996; Markl et al., 1998) whereas amphiboles from lower grade contain less Cl and Fe than coexisting biotite (e.g. Ekstrom, 1972; Zhu et al., 1994). Similar to our findings, Nijland et al. (1993a) found that coexisting biotites

and amphiboles display varying Cl-ratios with biotite mostly being more Cl-rich than amphibole, but with the opposite also being common.

Our results show that there may be many explanations of univariant Cl-element trends in amphibole and biotite. In our study the univariant trends are caused by gradual changes in P and T in amphibolites interacting with fluids of constant salinity, whereas other studies document changes in the fluid composition at fixed PT.

It should be emphasised that not all elements composing the amphibole rims are aligned along the same univariant trends. One of the most important observations is that the trends with Mg, Fe and Cl feature several parallel but vertically offset trends. This is attributed to variations in the bulk chemical environment, i.e. the protholith.

So far the qualities of natural and experimental calibrations do not allow for the use of Cl in amphibole or biotite in a direct quantitative assessment of the fluid composition. Until better data are available, fluid inclusions by far is the most reliable tool in quantifying the fluid composition in magmatic and metamorphic environments.

One of the most important issues to keep in mind is that Cl and F-bearing fluids influence the chemistry of hydrous silicates. Accordingly, this is an important factor in ore genesis. Furthermore it may influence exchange equilibria between silicates used for thermobarometric calculations. As an example garnet biotite Fe-Mg exchange is strongly affected. Kullerud (1995) found that Cl affected the Fe-Mg exchange vector between garnet and biotite and that a correction of K_DFe-Mg (bt-grt) could be made for the biotite garnet pairs using X_{Ti}^{bt} and X_{Cl}^{bt}:

$$\ln K_D(corrected) = \ln\left[(X_{Fe}^{bt} / X_{Mg}^{bt})/(X_{Fe}^{grt} / X_{Mg}^{grt})\right] - 2.60X_{Ti}^{bt} - 5.67X_{Cl}^{bt}$$

This correction, however, is probably not generally applicable to garnet-biotite thermometry because the expression of lnK_DFe-Mg as a function of X_{Ti}^{bt} and X_{Cl}^{bt} is applicable only at specific temperature conditions (Kullerud, 1995). Zhu and Sverjensky (1992) suggested an alternative correction for the effect of Cl in biotite on lnK_DFe-Mg based on the activity of Cl-annite which they retrieved from the experiments of Munoz and Swenson (1981). This model however underestimate the effect of Cl in the study of Kullerud (1995), probably because of the uncertainties in the Munoz and Swenson (1981) data but also because of the ideal and random mixing models used for Mg, Fe, OH and Cl used in their retrieval (Kullerud, 1995). In conclusion no thermodynamic expression may fully compensate for the effect of Cl upon the Fe-Mg exchange between biotite and other Fe-Mg silicates.

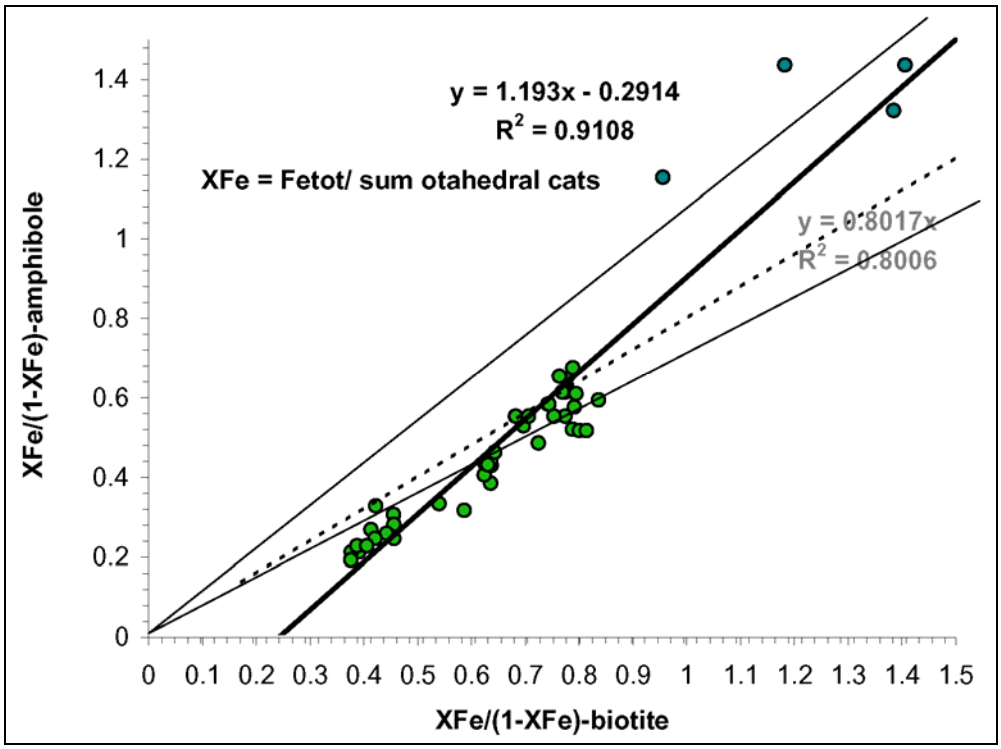

Figure 20: Comparison of KdFe of amphibole-biotite pairs. Note that there is a linear collation with a non-zero intercept. See text for discussion.

5.3 Cl-OH-F in apatite and scapolite

Whereas F was not detected in the studied amphibole and biotite, apatite features an evolution from Cl-OH apatite in the garnet quartz symplectites toward increasingly F-rich apatite parallel with the amphiboles and biotites becoming Mg-rich and Cl poor. However, most hydrothermal apatite is F-rich due to the high partitioning of F into apatite compared to the fluid. The $\log(aHCl/aH_2O)/\log(aHF/aH_2O)$ of Zhu and Sverjensky (1991) show that only small amounts of F ($\log(aF/aH_2O = 10^{-6})$ in the fluid would suffice to give F-apatite fractions of 0.9 in a 5 molal Cl- solution at 300°C. The stability field of F-apatite increases with decreasing temperature (Zhu and Sverjensky, 1991) hence F-enrichment in the Froland-apatite probably reflect dropping temperature and not F-enrichment in the fluid.

Y and Ce are relatively enriched in early apatites in garnet-quartz symplectites whereas intermediate OH-F apatite coexisting with Amp3 is low in both Y and Ce. Late F-apatite coexisting with Amp4 is relatively enriched in Y. Harlov and co-workers (2003; 2002) studied the alteration of Cl-apatite from Ødegårdens Verk, Bamble sector and replicated observed chemical evolution by hydrothermal alteration

experiments. Their results imply that, mostly, the alteration of Cl-apatite is a function of fluid composition and that P and T are less significant. Hydrothermal alteration with H_2O-rich fluids is more effective in removing Y+REE from Cl-apatite than F-rich aqueous fluids, probably because F stabilises Y in the apatite lattice (Harlov et al., 2002). The depletion of Ce and Y in the intermediate apatite in our study agrees with the depletion observed by Harlov and co-workers (2002) by alteration with a H_2O-rich fluid. In agreement with the observation by Harlov and co-workers (2002) the enrichment of Y in late F-rich apatite is a product of the F-enrichment.

We only studied a limited number of apatite samples in our study and focussed mainly on the retrograde evolution of apatite. Nijland and co-workers (1993a) studied halogen zonation patterns in apatite from amphibolite samples scattered across the Bamble sector, which they related to the prograde fluid evolution. They conclude that systematic spatial variations across the metamorphic zones of the Bamble sector are absent. They observe three main types of F-zonation patterns; (1) W-shaped, (2) Rimward increasing and (3) Rimward decreasing. They infer that the patterns reflect the fluid environment, with most features belonging to the prograde evolution. However, Nijland et al. (1993a) do suggest that the rimward increasing F-content (3) could have formed during either prograde or retrograde conditions due to increasing F-content in the fluid. However the rimward F-increase reported by Nijland et al. (1993a) is more likely to be due to cooling because F-apatite is stable even with a low F fluid at low temperatures (Zhu and Sverjensky, 1991). The variable patterns observed in apatite probably tell the same story as our amphibole cores that also show variable trends. Probably, this is an effect of local buffering during peak PT conditions.

From our textural observations, we infer that scapolite was formed late in the mineral assemblage. Although scapolite coexisted with CO_2-free fluids, scapolite formula recalculation implies that scapolite probably contain significant CO_3 and HCO_3. Accordingly, CO_2 did not come from the fluid. Textural observations imply that scapolitisation depended on the presence of both calcite and plagioclase. Similar observations were made by Visser and co-workers (1999). Therefore, we suggest that scapolite formed by a reaction involving calcite as also suggested by Visser et al. (1999):

cc + brine+ pl = scp

The strongly variable composition is mostly a function of local chemical variations, particularly in the amount of calcite, the composition of the replaced plagioclases and the Ca/Na ratio of the coexisting fluid. Given that the fluids maintained constant compositions (paper 2, Sørensen and Larsen, 2007b) it was primarily the local rock composition governed by plagioclase and calcite that buffered the scapolite composition.

5.4 Genetic interpretation of the textural evolution

The principles derived from the mineral chemistries of biotite and amphibole respectively provide a model in combination with our fluid inclusion observations. This model may be used to understand the complex alteration textures observed on field as well as thin section scale. The amphibole trends confirm the interaction with brines of more ore less constant salinity during cooling and exhumation.

The first alteration type are potassic and occur as the introduction of Fe-rich biotite and amphibole overgrowths comprising the blue green ferrotschermakites observed at locality 1 (Amp3a). The Al^{IV} and Fe content of these rims are higher than in the amphibole cores. However, as the temperature decreased the amphibole rims became more Mg-rich and Al poor than the cores, comprising magnesiohornblende-actinolite. Early alteration assemblages contain calcite, suggesting that the fluid contained CO_2. This is confirmed by the FIA2 fluid inclusions (see Sørensen and Larsen, 2007b, paper 2).

Elements were redistributed on both hand specimen and field scale in the amphibolites. The most prominent example of this process is the conspicuous modal differentiation characterising the amphibolite in generating areas dominated by biotite and amphibole, biotite and plagioclase, biotite and plagioclase etc. The zoning observed around the plagioclase veins at locality 5 and the border zones around the en echelon veins at locality 4 are good examples of this effect. This principle is most easily illustrated by the mineralogical zonation in the alteration zones associated with the plagioclase-calcite veins (Alt1b) at locality 5:

The central zone1 is enriched in ilmenite, Ca, CO_2, Fe and sulphur; this is followed by a zone free of biotite mainly comprising plagioclase and amphibole, followed by an amphibole free zone mainly comprising biotite and plagioclase. This local scale observation may possibly mirror the metasomatic processes at a much larger scale throughout the Bamble sector. I.e. Fe and other elements are removed from the amphibolites and redeposited elsewhere giving rise to the numerous Fe-deposits as well as Fe-Cu oxide/sulphide deposits across the Bamble sector. This is also suggested by Brøgger (1934) for the breccia related deposits at Langøy, that formed when mafic rocks were altered by scapolitisation and albitisation processes. Korneliussen et al. (2000) suggest this as a general genetic model for the Fe-Cu deposits in the Bamble sector.

Genetic models of ore deposits would benefit from an increased understanding of the interaction of fluids with silicates in the wall rocks because fluid-rock interactions in the wall rock probably explain many element enrichments leading to ore formation. Bearing this in mind, we find it peculiar that many studies of ore deposits use the model proposed by Munoz (1992) and Munoz and Swenson (1981) to calculate halogen activities in ore forming fluids because the model assumes that crystal chemical constraints are in control of the halogen contents of biotite and amphibole. Rather we suggest that the fluid phase pose a partial control on the mineral chemistry and that fluid rock interaction leads to changes in mineral and fluid composition in

order to obtain equilibrium conditions. As parameters such as pressure, temperature, fluid composition and fluid-rock ratios changes the equilibria also changes.

In our study the mineralogical changes are facilitated by fluid rock interaction with a fluid of constant salinity during cooling and exhumation. The understanding of the architecture and tectono-metamorphic evolution of the Bamble sector remain fragmentary. Partially because the importance of massive pulses of highly saline fluids were not fully appreciated. Our study concerns a rather limited portion of the Bamble sector, however, it is one of the few studies that documents the importance of highly saline aqueous fluids and demonstrates the implications for the mineralogy and metasomatic processes on micro as well as macro scale. Studies by Cameron (1993a; 1993b) and Cameron and co-workers (1993) document the mobilisation of Au and other chalcophile elements during high grade metamorphism and retrogression in the Bamble sector through analysis of the whole rock chemistry. Their results document how chalcophile elements are depleted through amphibolitisation of coronitic gabbro at high fO_2 (Cameron et al., 1993) and reintroduced in retrograde veins focussed at higher crustal levels near the brittle-ductile transition (Cameron, 1993b).

Ti-phases experience a gradual evolution as exemplified by cores of rutile that are overgrown/replaced by rims of ilmenite which again are overgrown/replaced by titanite. The replacement of rutile by ilmenite is easily explained by the gradual loss of Fe from the Fe-Mg silicates biotite and amphibole.

On the contrary, the replacement of ilmenite by titanite is more difficult to explain. Harlov et al. (2006) suggests that the titanite rims formed due to the reactions:

$$\text{cpx} + \text{ilm} + \text{quartz} + H_2O = \text{amphibole} + \text{titanite (hydration)}$$

or

$$\text{amphibole} + \text{ilmenite} + O_2 = \text{titanite} + \text{magnetite} + \text{quartz} + H_2O$$

The general absence of clinopyroxene and magnetite in our samples, however, precludes the above reactions. Rather, it is inferred that metasomatism is involved. Calcite is commonly observed in vicinity of the replacement rims hence may be the source of Ca in titanite together with plagioclase that also becomes more albite rich as metasomatic alteration proceeds. The Fe lost by the ilmenite is likely to have formed sulphides as petrographic observations suggest that pyrite in some cases formed together with the titanite rims.

Potassic alteration with biotite formation was followed by potassic alteration where biotite was replaced by K-feldspar. No Fe/Mg phase seem to increase during this stage hence suggesting that the replacement involved mobilisation of Fe. In relation to this replacement, ilmenite is almost completely replaced with titanite, suggesting that the replacement of ilmenite by titanite belongs to the same metasomatic event as the Fe-depletion of amphibole and replacement of biotite by K-feldspar.

Scapolitisation involves the replacement of plagioclase + calcite by scapolite and ilmenite and rutile by titanite.

5.5 The metamorphic evolution of the area as experienced by amphibolites

Based on this discussion we summarise the metamorphic evolution as experienced by the amphibolites as follows:

1. Amphibolitisation of gabbro: Field and petrographic evidence document the gradual amphibolitisation of gabbro. This relates to the formation of garnet bearing amphibolites. Notably the chemistry of amphiboles in the garnet bearing amphibolites is dissociated from the evolution in non-garnet bearing amphibolites. This is especially clear when it comes to Cl and Fe.
2. Oxidation of garnet amphibolite. The amphiboles in the garnet amphibolites show high estimated Fe^{3+}. This may reflect oxidation because charge compensation is not completely obtained by the measured elements.
3. Formation of partial melts (the garnet quartz symplectites).
4. Formation of garnet free amphibolites
5. Retrogression and metasomatism of amphibolite during exhumation.
    a. Introduction of K-bearing CO_2-H_2O solutions and formation of biotite, amphibole overgrowth rims and en echelon quartz veins, gradual loss of CO_2 from the fluid phase
    b. Formation of K-feldspar at the expense of biotite and plagioclase. Change in fluid composition due to loss of K in the fluid-rock interaction related to mineral reactions.
    c. Scapolitisation, characterised by replacement of plagioclase by scapolite (EqAn = 41.3-59.5). Apparently this reaction correlates with CO_2 free fluid inclusions in nearby quartz.

Our results underline the importance of highly saline aqueous fluids in the retrogression of amphibolites. Unaltered high-grade amphibolite is juxtaposed with completely altered and chemically transformed rock that once was amphibolite. The most prominent chemical alteration experienced by the amphibolites is the enrichment in potassium, marked by the introduction of biotite and K-feldspar.

In addition our results confirm the ore formation models suggested by (Brøgger, 1934; Korneliussen et al., 2000) in which the ore deposits situated proximally and distally to the altered amphibolites are the ultimate results of the depletion processes in the amphibolites. Mass transfer was controlled by equilibria between brines of almost constant salinity and mineral assemblages during cooling and uplift.

6 References

Ahall, K.I. and Gower, C.F., 1997. The Gothian and Labradorian orogens; variations in accretionary tectonism along a late Paleoproterozoic Laurentia-Baltica margin. GFF, 119(2): 181-191.

Bingen, B., Boven, A., Punzalan, L., Wijbrans, J.R. and Demaiffe, D., 1998. Hornblende (super 40) Ar/ (super 39) Ar geochronology across terrane boundaries in the Sveconorwegian Province of S. Norway. Precambrian Research, 90: 159-185.

Bingen, B., Mansfeld, J., Sigmond, E.M.O. and Stein, H., 2002. Baltica-Laurentia link during the Mesoproterozoic; 1.27 Ga development of continental basins in the Sveconorwegian Orogen, southern Norway. Canadian Journal of Earth Sciences = Revue Canadienne des Sciences de la Terre, 39(9): 1425-1440.

Bingen, B., Nordgulen, Ø. and Sigmond, E.M.O., 2001. Correlation of supracrustal sequences and origin of terranes in the Sveconorwegian orogen of SW Scandinavia: SIMS data on zircon in clastic metasediments. Precambran Research 108: 293-318.

Bingen, B. and Van-Breemen, O., 1998. Tectonic regimes and terrane boundaries in the high-grade Sveconorwegian Belt of SW Norway, inferred from U-Pb zircon geochronology and geochemical signature of augen gneiss suites. J. Geol. Soc. Lond. , 155: 143-154.

Brickwood, J.D. and Craig, J.W., 1987. Primary and reequilibrated mineral assemblages from the Kongsberg and Bamble areas, Norway. Norges Geologiske Undersøkelse, 410: 1-23.

Brøgger, W.C., 1934. On several Archean rocks from the south coast of Norway; II, The south Norwegian hyperites and their metamorphism. 1; 1, 421 pp.

Bugge, A., 1965. Iakttagelser fra rektangelbladet Kragerø og den store grunnfjellsbreksje. Norges Geologiske Undersøkelse, 229: 115p.

Bugge, J.A.W., 1940. Geological and petrological investigations of the Arendal district. Norsk Geologisk Tidsskrift, 20: 71-112.

Cameron, E.M., 1993a. Precambrian gold - perspectives from the top and bottom of shear zones. Canadian Mineralogist, 31: 917-944.

Cameron, E.M., 1993b. Reintroduction of gold, other chalcophile elements and LILE during retrogression of depleted granulite, Tromoy, Norway. Lithos, 29(3-4): 303-309.

Cameron, E.M., Cogulu, E.H. and Stirling, J., 1993. Mobilization of gold in the deep crust - Evidence from mafic intrusions in the Bamble Belt, Norway. Lithos, 30(2): 151-166.

Clowe, C.A., Popp, R.K. and Fritz, S.J., 1988. Experimental investigation of the effect of oxygen fugacity on ferric-ferrous ratios and unit-cell parameters of 4 natural clinoamphiboles. American Mineralogist, 73(5-6): 487-499.

Cooper, A.F., 1972. Progressive metamorphism of metabasic rocks from Haast Schist Group of Southern New Zealand. Journal of Petrology, 13(3): 457-492.

Cosca, M.A., Essene, E.J. and Bowman, J.R., 1991. Complete chemical-analyses of metamorphic hornblendes - Implications for normalizations, calculated H_2O activities, and thermobarometry. Contributions to Mineralogy and Petrology, 108(4): 472-484.

Cosca, M.A., Mezger, K. and Essene, E.J., 1998. The Baltica-Laurentia connection Sveconorwegian (Grenvillian) metamorphism, cooling, and unroofing in the Bamble sector, Norway. Journal of Geology, 106: 539-552.

Dahlgren, S., Bogoch, R., Magaritz, M. and Michard, A., 1993. Hydrothermal dolomite marbles associated with charnockitic magmatism in the Proterozoic Bamble Shear Belt, South Norway. Contributions to Mineralogy and Petrology, 113(3): 394-409.

Ekstrom, T.K., 1972. Coexisting scapolite and plagioclase from two iron formations in northern Sweden. Lithos, 5: 175-185.

Elliott, R.B., 1966. Association of amphibolite and albitite, Kragero South Norway. Geological Magazine, 103(1): 1-7.

Falkum, T. and Petersen, J.S., 1980. The Sveconorwegian orogenic belt, a case of late-Proterozoic plate-collision. Geologische Rundshcau, 69: 622-647.

Field, D., Drury, S. and Cooper, D.C., 1980. Rare-earth and LIL element fractionation in high-grade charnockitic gneisses, South Norway. Lithos 13: 281-289.

Frodesen, S., 1968. Petrographical and chemical investigations of a precambrian gabbro intrusion, Hiåsen, Bamble area, south Norway. Norsk Geologisk Tidsskrift, 48: 281-306.

Gualda, G.A.R. and Vlach, S.R.F., 2005. Stoichiometry-based estimates of ferric iron in calcic, sodic-calcic and sodic amphiboles: A comparison of various methods. Anais Da Academia Brasileira De Ciencias, 77(3): 521-534.

Harlov, D., Tropper, P., Seifert, W., Nijland, T. and Forster, H.J., 2006. Formation of Al-rich titanite ($CaTiSiO_4O$-$CaAlSiO_4OH$) reaction rims on ilmenite in metamorphic rocks as a function of fH_2O and fO_2. Lithos, 88(1-4): 72-84.

Harlov, D.E., 1992. Comparative oxygen barometry in granulites, Bamble sector, SE Norway. Journal of Geology, 100: 447-464

Harlov, D.E., 2000a. Pressure-temperature estimation in orthopyroxene-garnet bearing granulite facies rocks, Bamble sector, Norway. Mineralogy and Petrology, 69: 11-33.

Harlov, D.E., 2000b. Titaniferous magnetite-ilmenite thermometry and titaniferous magnetite-ilmenite-orthopyroxene-quartz oxygen barometry in granulite facies gneisses, Bamble sector, SE Norway; implications for the role of high-grade CO_2-rich fluids during granulite genesis. Contributions to Mineralogy and Petrology 139: 180-197

Harlov, D.E. and Foerster, H.J., 2003. Fluid-induced nucleation of (Y+REE)-phosphate minerals within apatite; nature and experiment; Part II, Fluorapatite. American Mineralogist, 88(8-9): 1209-1229.

Harlov, D.E., Foerster, H.J. and Nijland, T.G., 2002. Fluid-induced nucleation of (Y + REE)-phosphate minerals within apatite; nature and experiment; Part I, Chlorapatite. American Mineralogist, 87(2-3): 245-261.

Henderson, I.H.C. and Ihlen, P.M., 2004. Emplacement of polygeneration pegmatites in relation to Sveco-Norwegian contractional tectonics; examples from southern Norway. Precambrian Research, 133(3-4): 207-222.

Johansson, L. and Kullerud, L., 1993. Late Sveconorwegian metamorphism and defromation in southwestern Sweden. Precambrain Research, 64: 347-360.

Jøsang, O., 1966. Geologiske og petrografiske undersøkelser i Modumfeltet. Norges Geologiske Undersøkelse, 235: 148p.

Knudsen, T.L., 1996. Petrology and geothermobarometry of granulite facies metapelites from the Hisøy-Torungen area, South Norway; new data on the Sveconorvegian P-T-t path of the Bamble sector. Journal of Metamorphic Geology, 14(3): 267-287.

Knudsen, T.L. and Andersen, T., 1999. Petrology and geochemistry of the Tromøy gneiss complex, South Norway; an alleged example of

Proterozoic depleted lower continental crust. Journal of Petrology 40: 909-933.

Knudsen, T.L., Andersen, T., Maijer, C. and Verschure, R.H., 1997. Trace-element characteristics and Pb isotopic evolution of metasediments and associated Proterozoic rocks from the amphibolite- to granulite-facies Bamble sector, Southern Norway. Chemical Geology, 143(3-4): 145-169.

Knudsen, T.L. and Lidwin, A., 1996. Magmatic CO_2, brine and nitrogen inclusions in Sveconorwegian enderbitic dehydration veins and a gabbro from the Bamble sector, southern Norway. European Journal of Mineralogy, 8: 1041-1063.

Korneliussen, A., Dahlgren, S., Ihlen, P.M. and Sandstad, J.S., 2000. On the relationships between metasomatic processes (scapolitisation) at deep crustal levels and fracture-bound ore deposits in the Bamble sector of the Fennoscandian Shield, S. Norway. In: P. Weihed and O. Martinsson (Editors), 2nd annual GEODE-Fennoscandian shield workshop on Paleoproterozoic and Archean greenstone belts and VMS districts in the Fennoscandian Shield Luleå University of Technology Research Report Gällivare-Kiruna, Sweden, pp. 22-25.

Kullerud, K., 1995. Chlorine, titanium and barium-rich biotites - Factors controlling biotite composition and the Implications for garnet-biotite geothermometry. Contributions to Mineralogy and Petrology, 120(1): 42-59.

Kullerud, K., 1996. Chlorine-rich amphiboles: Interplay between amphibole composition and an evolving fluid. European Journal of Mineralogy, 8(2): 355-370.

Kullerud, K., 2000. Occurrence and origin of Cl-rich amphibole and biotite in the Earth's crust - implications for fluid composition and evolution. In: I. Stober and K. Bucher (Editors), Hydrogeology of crystalline rocks. Kluwer Academic Publishers, Netherlands, pp. 205-225.

Kullerud, K. and Erambert, M., 1999. Cl-scapolite, Cl-amphibole, and plagioclase equilibria in ductile shear zones at Nusfjord, Lofoten, Norway: Implications for fluid compositional evolution during fluid-mineral interaction in the deep crust. Geochimica et Cosmochimica Acta, 63: 3829-3844.

Kullerud, L. and Dahlgren, S., 1993. Sm-Nd geochronology of Sveconorwegian granulite facies mineral assemblages in the Bamble shear belt, South Norway. Precambrian Ressearch 64: 389-402.

Kullerud, L. and Machado, N., 1991. End of a controversy; U-Pb geochronological geochronological evidence for significant Grenvillian activity in the Bamble area, Norway., Sixth Meeting of the European Union of Geosciences. Terra Abstracts, pp. 504.

Lamb, R.C., Smalley, P.C. and Field, D., 1986. P-T conditions for the Arendal granulites, southern Norway; implications for the roles of P, T and CO_2 in deep crustal LILE-depletion. Journal of Metamorphic Geology 4: 143-160.

Leelanandem, C., 1969. Electron microprobe analyses of chlorine in hornblendes and biotites from charnockitic rocks of Kondapall, India. Mineralogical Magazine, 37(287): 362-365.

Leger, A., Rebbert, C. and Webster, J., 1996. Cl-rich biotite and amphibole from Black Rock Forest, Cornwall, New York. American Mineralogist, 81(3-4): 495-504.

Lieftink, D.J., Nijland, T.G. and Maijer, C., 1993. Cl-rich scapolite from Ødegardens Verk, Bamble, Norway. Norsk Geologisk Tidsskrift, 73(1): 55-57.

Lieftink, D.J., Nijland, T.G. and Maijer, C., 1994. The behavior of rare-earth elements in high-temperature Cl-bearing aqueous fluids; results from the Ødegardens Verk natural laboratory. The Canadian Mineralogist, 32 Part 1: 149-158.

Makino, K., Tomita, K. and Suwa, K., 1993. Effect of chlorine on the crystal-structure of a chlorine-rich hastingsite. Mineralogical Magazine, 57(389): 677-685.

Markl, G., Ferry, J. and Bucher, K., 1998. Formation of saline brines and salt in the lower crust by hydration reactions in partially retrogressed granulites from the Lofoten Islands, Norway. American Journal of Science, 298(9): 705-757.

Morton, R.D., Batey, R. and O'Nions, R.K., 1970. Geological investigations in the Bamble sector of the Fennoscandian Shield south Norway. 1. The geology of eastern Bamble. Norges Geologiske Undersøkelse, 263, 61 pp.

Munoz, J.L., 1992. Calculation of HF and HCl fugacites from biotite compositions; revised equations. Geological Society of America Abstracts with Programs, 24: 221.

Munoz, J.L. and Swenson, A., 1981. Chloride-hydroxyl exchange in biotite and estimation of relative HCl/HF activities in hydrothermal fluids. Economic Geology, 76(8): 2212-2221.

Munz, I.A., Wayne, D. and Austrheim, H., 1994. Retrograde fluid infiltration in the high-grade Modum Complex, South Norway - Evidence for age, source and REE mobility. Contributions to Mineralogy and Petrology, 116(1-2): 32-46.

Munz, I.A., Yardley, B.W.D., Banks, D.A. and Wayne, D., 1995. Deep penetration of sedimentary fluids in basement rocks from Southern Norway - Evidence from hydrocarbon and brine inclusions in quartz veins. Geochimica Et Cosmochimica Acta, 59(2): 239-254.

Nijland, T.G., 1989. De Geologie van het Nelaug gebeid, Bamble sector, Zuid Noorwegen. Unpublished Masters Degree Thesis, Utrecht university, Utrecht, 85 pp.

Nijland, T.G., Jansen, J.B.H. and Maijer, C., 1993a. Halogen geochemistry of fluid during amphibolite-granulite metamorphism as indicated by apatite and hydrous silicates in basic rocks from the Bamble sector, South Norway. Lithos, 30(2): 167-189.

Nijland, T.G., Liauw, F., Visser, D., Maijer, C. and Senior, A., 1993b. Metamorphic petrology of the Froland corundum-bearing rocks; the cooling and uplift history of the Bamble sector, South Norway. Bulletin - Norges Geologiske Undersokelse, 424: 51-63.

Nijland, T.G. and Maijer, C., 1993. The regional amphibolite to granulite facies transition at Arendal, Norway; evidence for a thermal dome. Neues Jahrbuch fuer Mineralogie Abhandlungen, 165: 191-221.

Nijland, T.G. and Touret, J.L.R., 2001. Replacement of graphic pegmatite by graphic albite-actinolite-clinopyroxene intergrowths (Mjavatn, southern Norway). European Journal of Mineralogy, 13(1): 41-50.

Nijland, T.G., Touret, J.L.R. and Visser, D., 1998. Anomalously low temperature orthopyroxene, spinel, and sapphirine occurrences in metasediments from the Bamble amphibolite-to-granulite facies transition zone (South Norway); possible evidence for localized action of saline fluids. Journal of Geology, 106(5): 575-590.

Nijland, T.G. and Visser, D., 1995. The provenance of Bamble amphibolites, Norway. Proceedings of the Koninklijke Nederlandse Akademie Van Wetenschappen-Biological Chemical Geological Physical and Medical Sciences, 98(1): 69-88.

Oberti, R., Ungaretti, L., Cannillo, E. and Hawthorne, F.C., 1993. The mechanism of Cl incorporation in amphibole. American Mineralogist, 78(7-8): 746-752.

Popp, R.K., Virgo, D. and Phillips, M.W., 1995. H deficiency in kaersutitic amphiboles: Experimental verification. American Mineralogist, 80(11-12): 1347-1350.

Ramberg, H., 1952. Chemical bonds and distribution of cations in silicates. Journal of Geology, 60(4): 331-355.

Sato, H., Holtz, F., Behrens, H., Botcharnikov, R. and Nakada, S., 2005. Experimental petrology of the 1991-1995 Unzen dacite, Japan. Part II: Cl/OH partitioning between hornblende and melt and its implications for the origin of oscillatory zoning of hornblende phenocrysts. Journal of Petrology, 46(2): 339-354.

Smalley, P.C., Field, D., Lamb, R.C. and Clough, P.W.L., 1983. Rare earth, Th-Hf-Ta and large-ion lithophile element variations in metabasites from the Proterozoic amphibolite-granulite transition zone at Arendal, South Norway. Earth Planet Scientiffic Letters, 63: 446-458.

Sørensen, B.E. and Larsen, R.B., 2007a. Paper1: Fluid induced multistage recrystallisation microstructures in quartzites and quartz veins from the Bamble shear zone complex. In: B.E. Sørensen (Editor), Metamorphic refinement of quartz under influence of fluids during exhumation with reference to the metamorphic/metasomatic evolution observed in amphibolites - a detailed field, microtectonic and geochemical study from the Bamble sector, South Norway. PhD Thesis, Department of Geology and Mineral Resources Engineering, NTNU Trondheim.

Sørensen, B.E. and Larsen, R.B., 2007b. Paper2: The fluid evolution of the Froland area in the Bamble sector from peak P-T through cooling and uplift: implications for retrograde mineral paragenesis and PT evolution of the Bamble sector. In: B.E. Sørensen (Editor), Metamorphic refinement of quartz under influence of fluids during exhumation with reference to the metamorphic/metasomatic evolution observed in amphibolites - a detailed field, microtectonic and geochemical study from the Bamble sector, South Norway. PhD Thesis, Department of Geology and Mineral Resources Engineering, NTNU Trondheim.

Starmer, I.C., 1985. The evolution of the South Norwegian Proterozoic as revealed by major and mega-tectonics of the Kongsberg and Bamble sectors. In: J.L.R. Touret and A.C. Tobi (Editors), The deep Proterozoic crust of the North Atlantic Provinces. Reidel, Dordrecht, pp. 259-290.

Starmer, I.C., 1987. The geological map of the Bamble sector, South Norway, The geology of southernmost Norway: A geological excursion guide with thematic articles prepared for the NATO advanced study institute. Special Publication Geological Survey of Norway, pp. 25.

Starmer, I.C., 1991. The proterozoic evolution of the Bamble sector, Southern Norway; correlation across southern Scandinavia and the Grenvillian controversy. Precambrain Research, 49: 107-139.
Starmer, I.C., 1993. The Sweconorwegian orogeny in southern Norway, relative to deep crustal structures and events in the North Atlantic Proterozoic supercontinent. Norsk Geologisk Tidsskrift, 73: 109-132.
Starmer, I.C., 1996. Accretion, rifting, rotation and collision in the North Atlantic supercontinent, 1700-950 Ma. In: Precambrain crustal evolution in the North Atlantic Region. Geological Society of London Special Publications, 112: 219-248.
Teertstra, D.K. and Sheriff, B.L., 1997. Substitutional mechanisms, compositional trends and end member formulae of scapolite. Chemical Geology, 136: 233-260.
Touret, J., 1968. The Precambrian metamorphic rocks around the Lake Vegår (Aust-Agder, southern Norway). Norges Geologiske Undersøkelse, 257, 45 pp.
Touret, J., 1971. Le faciès granulite en Norvège méridionale II Les inclusions fluides. Lithos, 4: 423-436.
Touret, J., 1972. Le faciès granulite en Norvège méridionale et Les inclusions fluides. . Sci. Terre 17: 179-193.
Touret, J., 1985. Fluid regime in southern Norway: the record of fluid inclusions. In: A.C. Tobi and J. Touret (Editors), The deep Proterozoic crust in the North Atlantic Provinces NATO ASI Ser. Ser. C: Math. Phys. Sci., pp. 517-549.
Touret, J. and Olsen, S.N., 1985. Fluid inclusions in migmatites. In: J.R. Ashworth (Editor), Migmatites. Shiva, Glasgow, pp. 265-288.
Van den Kerkhof, A.M., Kreulen, R. and Touret, J.L.R., 1994. Juvenile CO_2 in enderbites of Tromøy near Arendal, southern Norway: a fluid inclusion and stable isotope study. Journal of Metamorphic Geology, 12: 301-310.
Visser, D., Nijland, T.G., Lieftink, D.J. and Maijer, C., 1999. The occurrence of preiswerkite in a tourmaline-biotite-scapolite rock from Blengsvatn, Norway. American Mineralogist, 84(5-6): 977-982.
Xiao, Y.L., Hoefs, J. and Kronz, A., 2005. Compositionally zoned Cl-rich amphiboles from North Dabie Shan, China: Monitor of high-pressure metamorphic fluid/rock interaction processes. Lithos, 81(1-4): 279-295.
Zhu, C. et al., 1994. Tem-Aem observations of Cl-rich amphibole and biotite and possible petrologic implications. American Mineralogist, 79(9-10): 909-920.

Zhu, C. and Sverjensky, D.A., 1991. Partitioning of F-Cl-OH between minerals and hydrothermal fluids. Geochimica Et Cosmochimica Acta, 55(7): 1837-1858.
Zhu, C. and Sverjensky, D.A., 1992. F-Cl-OH Partitioning between biotite and apatite. Geochimica Et Cosmochimica Acta, 56(9): 3435-3467.